NATIONAL TECHNICAL UNIVERISTY OF ATHENS (NTUA)
SCHOOL OF CIVIL ENGINEERING
INSTITUTE OF STRUCTURAL ANALYSIS AND ANTISEISMIC RESEARCH

Limit State Numerical Procedures for Cyclically Loaded Elastoplastic Structures

PhD Dissertation

by

Konstantinos D. Panagiotou

Supervisor: Prof. K.V. Spiliopoulos

Athens, February 2015

ΕΘΝΙΚΟ ΜΕΤΣΟΒΙΟ ΠΟΛΥΤΕΧΝΕΙΟ (ΕΜΠ)

ΣΧΟΛΗ ΠΟΛΙΤΙΚΩΝ ΜΗΧΑΝΙΚΩΝ

ΕΡΓΑΣΤΗΡΙΟ ΣΤΑΤΙΚΗΣ ΚΑΙ ΑΝΤΙΣΕΙΣΜΙΚΩΝ ΕΡΕΥΝΩΝ

Αριθμητικές Διαδικασίες Εκτίμησης Οριακών Καταστάσεων Ελαστοπλαστικών Κατασκευών υπό Ανακυκλιζόμενη Φόρτιση

Διδακτορική Διατριβή

ΤΟΥ

Κωνσταντίνου Δ. Παναγιώτου

Επιβλέπων: Καθηγητής Κ.Β. Σπηλιόπουλος

Αθήνα, Φεβρουάριος 2015

PhD Examination Committee

I certify that I have read this dissertation and that in my opinion it is fully adequate, in scope and quality, as a dissertation for the degree of Doctor of Philosophy.

Konstantinos Spiliopoulos
Professor
(Supervisor)
School of Civil Engineering
National Technical University of Athens

Manolis Papadrakakis
Professor
(Member of advisory committee)
School of Civil Engineering
National Technical University of Athens

Yiannis Dafalias
Emeritus Professor
(Member of advisory committee)
School of Applied Mathematical and Physical Science
National Technical University of Athens

Christos Bisbos
Professor
School of Civil Engineering
Aristotle University of Thessaloniki

Efstathios Theotokoglou
Professor
School of Applied Mathematical and Physical Science
National Technical University of Athens

Spyros Karamanos
Professor
Department of Mechanical Engineering
University of Thessaly

Vissarion Papadopoulos
Assistant Professor
School of Civil Engineering
National Technical University of Athens

Dedicated to my parents

Konstantinos D. Panagiotou
Civil Engineer NTUA, MSc
PhD candidate of National Technical University of Athens
Author e-mail: kdpanag@gmail.com

© 2015 Konstantinos D. Panagiotou

All rights reserved. No part of the material protected by this copyright notice may be reproduced or utilized in any form or by any means, electronic or mechanical, including photocopying, recording or by any information storage and retrieval system, without the prior permission of the author.

Summary

Civil and mechanical engineering structures are generally subjected to high levels of loading. Heavy traffic, earthquake loading or waves are the main source of cyclic loading on civil engineering structures, like bridges, pavements, buildings, and offshore structures. On the other hand, mechanical engineering structures like nuclear reactors, aircraft gas turbine propulsion engines also operate under high levels of cyclic mechanical and temperature loads. Under all these kinds of loading, these structures are forced to develop plastic strains.

The asymptotic steady state behavior of an elastic-perfectly plastic structure under cyclic loading may be determined by time consuming incremental time-stepping calculations. Direct methods, alternatively, have a big computational advantage as they attempt to find the characteristics of the cyclic state right from the start of the calculations. Moreover, it very often happens that the complete time history of loading is not known, but only its variation intervals. In these cases, direct methods are the only way to establish safety margins. Typical examples of direct methods are the limit and the shakedown analysis.

Thus, the current PhD thesis initially aimed at developing a modern direct method to determine the long-term effects of an elastoplastic structure subjected to a given cyclic loading time history. Any steady state, like elastic shakedown (safe state) or alternating plasticity or ratcheting (unsafe states) may be predicted. The developed direct method has been called Residual Stress Decomposition Method (RSDM).

The method focuses on the expected cyclic nature of the residual stresses at the steady state. Thus, the unknown residual stresses are decomposed into Fourier series that have the same period as the cyclic loading. It is the coefficients of these series that are estimated through an iterative procedure. It is proved that an update of these coefficients may be found with the aid of the integral of the cycle time derivatives of these residual stresses inside a loading cycle. These derivatives may be estimated at discrete cycle points by enforcing equilibrium and compatibility at these points. The procedure converges uniformly to the actual cyclic residual stress for a loading below the elastic shakedown limit or to unsafe cyclic total stress, which

may be used to mark the regions that develop plastic strains. The method then continues to determine whether the applied loading would lead the structure to incremental collapse or to low-cycle fatigue.

Furthermore, the RSDM was used to manufacture a more general method the RSDM-S, which may be used to determine the load bearing capacity of cyclically loaded elastoplastic structures by producing safety margins against excessive inelastic deformations. The developed RSDM-S procedure constitutes a new upper bound approach to provide the elastic shakedown factor for structures under any combination of cyclic thermo-mechanical loadings. The procedure generates a descending sequence of loading factors, through the use of RSDM, which shrinks the load domain until the residual stresses become constant in time.

Both the two methods were formulated within the finite element (FE) method. The efficiency of the approaches is shown through examples of application.

Keywords: Direct methods, Cyclic loading, Plasticity, Fourier series, Shakedown, Alternating plasticity, Ratcheting.

Acknowledgments

I would like to express my special appreciation and thanks to my supervisor Professor Konstantinos Spiliopoulos, he has been a tremendous mentor for me. I would like to thank him for encouraging my research and for allowing me to grow as a research scientist.

Additionally, I thank my committee members, Professor Manolis Papadrakakis and Professor Yiannis Dafalias, for reviewing this thesis.

Furthermore, I would like to express my gratefulness to:

a) the “Alexander S. Onassis” public benefit foundation
b) the “Propondis” public welfare foundation,

for their contributions towards my financial support.

Finally, there are no words to express my gratitude to my parents, who always believed in me and were patiently supportive. Thank you.

Konstantinos Panagiotou

Εκτεταμένη περίληψη στην ελληνική γλώσσα

1. Εισαγωγή

Ένα από τα πλέον σημαντικά προβλήματα στην επιστήμη του μηχανικού αποτελεί η πρόβλεψη εάν μία κατασκευή μπορεί να αναλάβει τα επιβαλλόμενα χρονικά επαναλαμβανόμενα φορτία και με ποια περιθώρια ασφαλείας, ή εάν θα χάσει τη λειτουργικότητά της ένεκα κατάρρευσης, κόπωσης ή μεγάλων ανελαστικών παραμορφώσεων. Φόρτιση οδοστρωμάτων από κίνηση οχημάτων, σεισμική δράση ή κύματα είναι η κύρια πηγή ανακυκλιζόμενης φόρτισης σε κατασκευές πολιτικού μηχανικού. Από την άλλη μηχανολογικές κατασκευές όπως μηχανές, τουρμπίνες και πυρηνικοί αντιδραστήρες υπόκεινται σε υψηλής στάθμης ανακυκλιζόμενα φορτία είτε μηχανικά είτε θερμικά.

Ο μόνος τρόπος πρόβλεψης εάν μία κατασκευή, ή ένα τμήμα αυτής, μπορεί να αναλάβει τα επιβαλλόμενα φορτία, είναι, κυρίως, μέσω των «βήμα προς βήμα» μεθόδων (step by step method). Για τη διεξαγωγή τέτοιων αναλύσεων χρειάζονται προγράμματα πεπερασμένων στοιχείων (π.χ. Abaqus) που απαιτούν ιδιαιτέρως επαχθείς και χρονοβόρους υπολογισμούς αφού πρέπει να ακολουθηθεί επακριβώς το πρόγραμμα φόρτισης και να κατατμηθεί σε πολύ μικρά χρονικά διαστήματα, ώστε η διαδικασία επίλυσης να είναι αριθμητικά ευσταθής. Όταν η φόρτιση είναι σε κάποιο βαθμό ανακυκλιζόμενη, μία πολύ καλύτερη προσέγγιση του προβλήματος έγκειται στην ανάπτυξη μεθόδων που λέγονται «άμεσες» (direct methods) οι οποίες έχουν τη δυνατότητα να προσεγγίζουν το πρόβλημα με απευθείας υπολογισμούς. Επιπλέον, τις περισσότερες φορές, η ακριβής ιστορία της φόρτισης δεν είναι γνωστή παρά μόνο κάποια όρια εντός των οποίων η φόρτιση μπορεί να μεταβάλλεται αυθαίρετα. Σε αυτές τις περιπτώσεις, οι άμεσες μέθοδοι αποτελούν τη μόνη λύση για να υπολογίσει κανείς όρια ασφαλείας.

Η κλασσική οριακή ανάλυση οριακών καταστάσεων προϋποθέτει μονότονη, αναλογικά αυξανόμενη φόρτιση και στοχεύει στον υπολογισμό του φορτίου πλαστικής

κατάρρευσης. Ωστόσο, για ανακυκλιζόμενη φόρτιση με άγνωστη την ιστορία της και γνωστά μόνο τα όρια μεταβολής, η κατάρρευση μπορεί να συμβεί για στάθμες φορτίου μικρότερες του φορτίου πλαστικής κατάρρευσης. Κι αυτό διότι υπάρχουν δύο νέες μορφές αστοχίας, η αστοχία λόγω εναλλαγής του προσήμου της μεταβολής των πλαστικών παραμορφώσεων και η αστοχία λόγω της διαρκής συσσώρευσης των πλαστικών παραμορφώσεων δηλαδή λόγω επαυξητικής κατάρρευσης. Για να εξασφαλιστεί η κατασκευή υπό ανακυκλιζόμενα φορτία πρέπει μετά από μια αρχική παροδική φάση να παρουσιάσει ελαστική συμπεριφορά ακόμα και αν υπάρχει τοπική διαρροή. Το φαινόμενο αυτό ονομάζεται προσαρμογή και μπορεί να μας προσδιορίσει κάποιας όρια ασφαλείας για την κατασκευή.

Βασιζόμενοι στο γεγονός ότι για κατασκευές από ευσταθή υλικά, υποκείμενες σε ανακυκλιζόμενες φορτίσεις, υπάρχει μία ασυμπτωτική σταθεροποιημένη κατάσταση (asymptotic steady state), οι άμεσες μέθοδοι στοχεύουν στον προσδιορισμό αυτής της κατάστασης από την αρχή των υπολογισμών. Τυπικά παραδείγματα άμεσων μεθόδων είναι η οριακή ανάλυση (limit analysis) για μονοτονικά φορτία και η ανάλυση προσαρμογής (shakedown analysis) για ανακυκλιζόμενα φορτία.

Οι περισσότερες άμεσες μέθοδοι στη βιβλιογραφία αντιμετωπίζουν το πρόβλημα της προσαρμογής των κατασκευών μέσω του είτε του στατικού είτε του κινηματικού θεωρήματος. Έτσι λοιπόν καταλήγουν σε προβλήματα μαθηματικού προγραμματισμού προσπαθώντας να μεγιστοποιήσουν ή να ελαχιστοποιήσουν μία αντικειμενική συνάρτηση που συνήθως αναπαριστά το συντελεστή φόρτισης. Ένα μειονέκτημα αυτών των μεθόδων είναι ότι οδηγούν συνήθως σε ένα πρόβλημα βελτιστοποίησης το όποιο χρειάζεται ιδιαίτερα σύνθετους αλγόριθμους για να επιλυθεί. Αυτό λοιπόν τις καθιστά δυσχερής στο να ενσωματωθούν σε υπάρχοντες κώδικες πεπερασμένων στοιχείων.

Κύριος στόχος λοιπόν της παρούσας διατριβής είναι να αναπτυχθούν κάποιες σύγχρονες άμεσες μέθοδοι που θα αντιμετωπίζουν το πρόβλημα της ελαστοπλαστικής συμπεριφοράς των κατασκευών υπό ανακυκλιζόμενα φορτία. Ειδικότερα έχουν αναπτυχθεί δύο αριθμητικές διαδικασίες. Μία πρώτη, που αφορά το είδος της ασυμπτωτικής κυκλικής συμπεριφοράς που θα οδηγηθεί μία κατασκευή υπό

δοσμένες ανακυκλιζόμενες φορτίσεις, και μία δεύτερη η οποία θα υπολογίζει όρια ασφαλείας για κατασκευές υπό ανακυκλιζόμενα φορτία.

2. Βασικές έννοιες στην ασυμπτωτική συμπεριφορά κατασκευών υπό ανακυκλιζόμενη φόρτιση

Ας θεωρήσουμε ένα σώμα με όγκο V και επιφάνεια S. Το σώμα αυτό υπόκειται σε κάποια φορτία σε ένα τμήμα της επιφάνειας S ενώ σε κάποιο άλλο τμήμα της επιφάνειας υποβάλλονται μηδενικές μετατοπίσεις (σχήμα 1α). Ας θεωρήσουμε τώρα, ότι το εφαρμοζόμενο φορτίο έχει τη μορφή:

$$\mathbf{P}(t) = \mathbf{P}(t + nT) \tag{1}$$

όπου με έντονα γράμματα συμβολίζονται διανύσματα και μητρώα.

Στην παραπάνω εξίσωση το $\mathbf{P}(t) = \left\{P_1(t), P_2(t), ..., P_q(t)\right\}$ είναι ένα διάνυσμα στήλη, όπου με q συμβολίζεται ο αριθμός των διαφόρων φορτίων (για παράδειγμα στο σχήμα 1β, $q = 2$). Μία φόρτιση τέτοιας μορφής συνιστά μία *κυκλική φόρτιση* με περίοδο T, όπου το t συμβολίζει ένα χρονικό σημείο μέσα στον κύκλο φόρτισης και το n αποτελεί τον αριθμό των πλήρων κύκλων φόρτισης. Μία τυπική μορφή ανακυκλιζόμενης φόρτισης και η τροχιά της σε ένα δισδιάστατο χώρο φόρτισης φαίνεται στο σχήμα 1β.

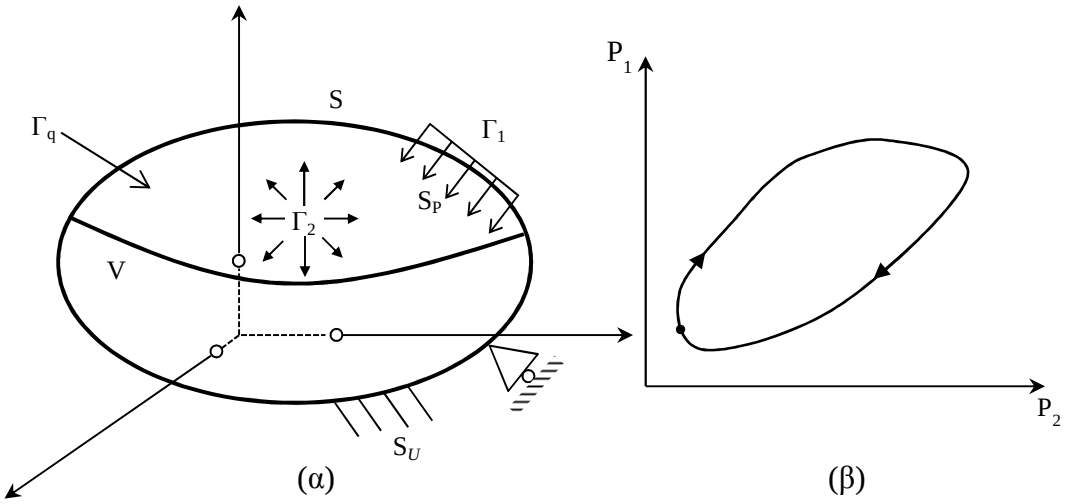

Σχήμα 1 α) Κατασκευή υπό επιβαλλόμενα φορτία, β) κυκλική φόρτιση

Ας υποθέσουμε ότι η κατασκευή αποτελείται από ελαστοπλαστικό υλικό. Σε οποιοδήποτε χρονικό σημείο $\tau = \frac{t}{T}$ το πεδίο των συνολικών τάσεων στην κατασκευή μπορεί να χωρισθεί σε δύο όρους: έναν πρώτο όρο $\boldsymbol{\sigma}^{el}(\tau)$ ο οποίος εξισορροπεί τα εξωτερικά φορτία, υποθέτοντας πλήρως ελαστική συμπεριφορά, και έναν δεύτερο όρο $\boldsymbol{\rho}(\tau)$ που αποτελεί τις αυτοϊσορροπούμενες τάσεις στην κατασκευή λόγω ανελαστικότητας. Έτσι, μπορούμε να γράψουμε:

$$\boldsymbol{\sigma}(\tau) = \boldsymbol{\sigma}^{el}(\tau) + \boldsymbol{\rho}(\tau) \tag{2}$$

Όμοια μπορούμε να γράψουμε και για το ρυθμό μεταβολής των παραμορφώσεων:

$$\dot{\boldsymbol{\varepsilon}}(\tau) = \dot{\mathbf{e}}^{el}(\tau) + \dot{\boldsymbol{\varepsilon}}_r(\tau) \tag{3}$$

Ο ρυθμός μεταβολής της παραμένουσας παραμόρφωσης $\dot{\boldsymbol{\varepsilon}}_r(\tau)$ κατά τον ίδιο τρόπο χωρίζεται σε έναν ελαστικό και ένα πλαστικό όρο. Άρα μπορούμε να γράψουμε την πιο πάνω εξίσωση ως:

$$\dot{\boldsymbol{\varepsilon}}(\tau) = \dot{\mathbf{e}}^{el}(\tau) + \dot{\boldsymbol{\varepsilon}}_r^{el}(\tau) + \dot{\boldsymbol{\varepsilon}}^{pl}(\tau) \tag{4}$$

Κατά τα γνωστά ισχύουν οι πιο κάτω εξισώσεις που συνδέουν τις επιμέρους τάσεις και παραμορφώσεις:

$$\begin{aligned} \dot{\boldsymbol{\sigma}}^{el}(\tau) &= \mathbf{D} \cdot \dot{\mathbf{e}}^{el} \\ \dot{\boldsymbol{\rho}}(\tau) &= \mathbf{D} \cdot \dot{\boldsymbol{\varepsilon}}_r^{el} \\ \dot{\boldsymbol{\varepsilon}}^{pl} &= \lambda \cdot \frac{\partial f}{\partial \boldsymbol{\sigma}} \end{aligned} \tag{5}$$

όπου $\mathbf{D}$ είναι το μητρώο ελαστικότητας. Η τελευταία σχέση εκφράζει το συσχετισμένο νόμο ροής (associated flow rule), όπου το πεδίο $\boldsymbol{\sigma}$ εκφράζει μία εντατική κατάσταση στην επιφάνεια διαρροής, δηλαδή $f(\boldsymbol{\sigma}) = 0$. Η ακόλουθη ανισότητα, που σχετίζεται με την κυρτότητα της επιφάνειας διαρροής, είναι γνωστή ως αξίωμα του Drucker και είναι μείζονος σημασίας στην πλαστικότητα:

$$(\boldsymbol{\sigma} - \boldsymbol{\sigma}_*) \cdot \dot{\boldsymbol{\varepsilon}}^{pl} \geq 0 \tag{6}$$

Αποδεικνύεται ότι μία κατασκευή, που αποτελείται από ένα ευσταθές υλικό που υπακούει το αξίωμα του Drucker, μετά από πολλούς κύκλους φόρτισης θα φτάσει,

ασυμπτωτικά, σε ένα κύκλο σταθεροποιημένης εντατικής κατάστασης (steady state) στον οποίο οι τάσεις καθώς και ο ρυθμός μεταβολής των παραμορφώσεων σταθεροποιούνται και παραμένουν αμετάβλητοι σε κάθε επόμενο κύκλο φόρτισης. Άρα λοιπόν, οι τάσεις και ο ρυθμός μεταβολής των πλαστικών παραμορφώσεων γίνονται περιοδικοί, έχοντας την ίδια περίοδο με την ανακυκλιζόμενη φόρτιση.

Ο σταθεροποιημένος κύκλος εντατικής κατάστασης (steady stress cycle), σε κινηματικούς όρους, χαρακτηρίζεται από το γεγονός ότι η επαύξηση των πλαστικών παραμορφώσεων ανά κύκλο:

$$\Delta\boldsymbol{\varepsilon}^{pl} = \int_0^1 \dot{\boldsymbol{\varepsilon}}^{pl} d\tau \tag{7}$$

συνιστά ένα συμβιβαστό πεδίο παραμορφώσεων με μηδενικές μετατοπίσεις στο κινηματικά δεσμευμένο τμήμα της επιφάνειας του σώματος.

Υπάρχουν λοιπόν οι ακόλουθοι διαφορετικοί τύποι σταθεροποιημένων κύκλων εντατικής κατάστασης, ή αλλιώς μία κατασκευή υπό ανακυκλιζόμενη φόρτιση μπορεί να συμπεριφερθεί με έναν από τους εξής τρόπους:

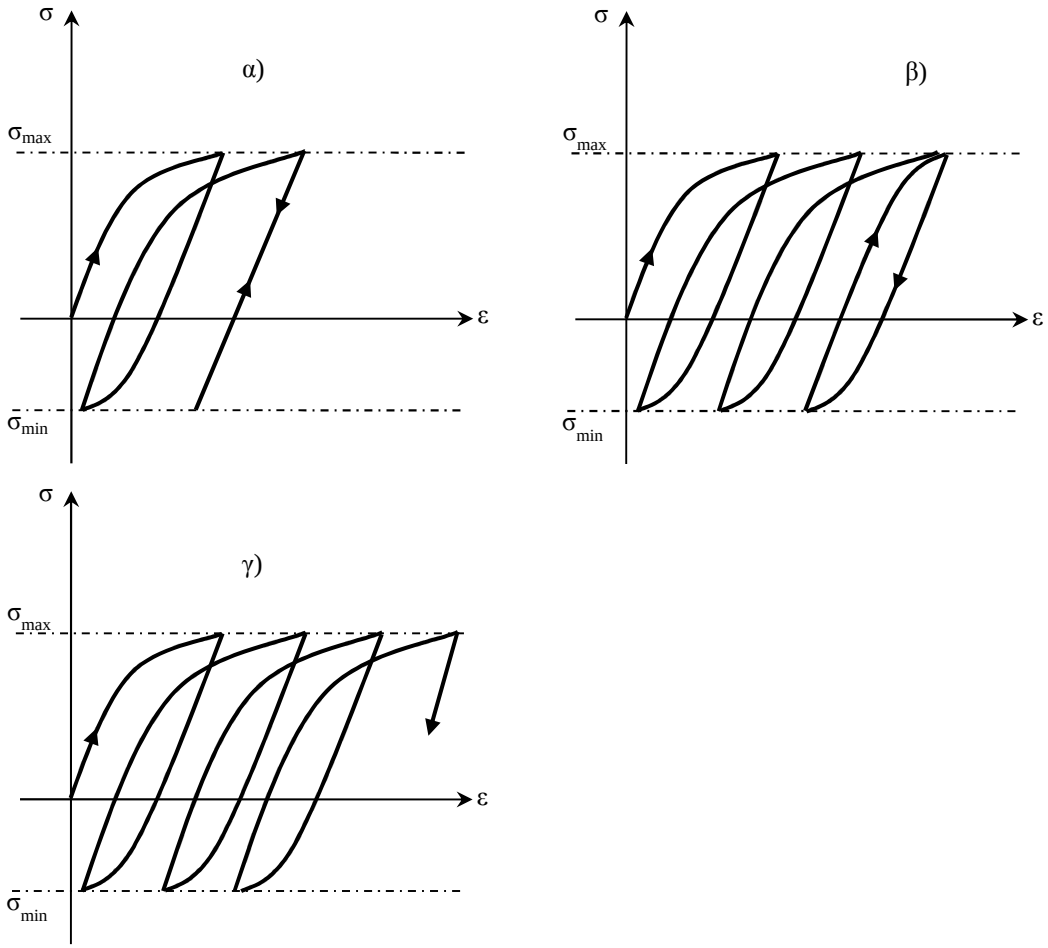

Σχήμα 2 Ελαστική προσαρμογή (elastic shakedown), β) εναλλασσόμενη πλαστικότητα (alternating plasticity), γ) επαυξητική κατάρρευση (ratcheting)

α) **Ελαστική προσαρμογή** (elastic shakedown or elastic adaptation), όπου ο ρυθμός μεταβολής των πλαστικών παραμορφώσεων μηδενίζεται σε όλα τα σημεία της κατασκευής ($\dot{\boldsymbol{\varepsilon}}^{pl} = 0$) (σχήμα 2α). Αυτό σημαίνει ότι μετά από μια αρχική παροδική φάση ανάπτυξης πλαστικών παραμορφώσεων, η κατασκευή θα συνεχίσει να συμπεριφέρεται πλέον ελαστικά και δε θα αναπτύξει πλαστικές παραμορφώσεις σε επόμενους κύκλους φόρτισης. Σε αυτή την κατάσταση δεν υφίστανται βρόχοι φόρτισης - αποφόρτισης. Όπως γίνεται κατανοητό πρόκειται για μία ασφαλή κατάσταση.

β) **Εναλλασσόμενη πλαστικοποίηση** (alternating plasticity), όπου ο ρυθμός μεταβολής των πλαστικών παραμορφώσεων ναι μεν είναι μη μηδενικός αλλά δεν αναπτύσσεται επαύξηση στις πλαστικές παραμορφώσεις στο τέλος του κύκλου,

δηλαδή $\Delta\boldsymbol{\varepsilon}^{pl} = 0$ (σχήμα 2β). Αυτή η κατάσταση είναι επικίνδυνη καθώς θα οδηγήσει την κατασκευή σε ολιγοκυκλική κόπωση (low cycle fatigue).

γ) **Συσσωρευμένη πλαστικοποίηση** (incremental collapse or ratcheting) όπου και ο ρυθμός μεταβολής των πλαστικών παραμορφώσεων είναι μη μηδενικός αλλά επίσης αναπτύσσεται και συνολική επαύξηση στις πλαστικές παραμορφώσεις στο τέλος του κύκλου σε κάποια σημεία στην κατασκευή, δηλαδή $\Delta\boldsymbol{\varepsilon}^{pl} \neq 0$ (σχήμα 2γ). Αυτό συμβαίνει για σχετικά μεγάλες στάθμες φορτίου και αποτελεί μία επικίνδυνη κατάσταση για την κατασκευή καθώς οι πλαστικές παραμορφώσεις συνεχίζουν να μεγαλώνουν σε κάθε επόμενο κύκλο φόρτισης οδηγώντας την κατασκευή σε μεγάλες μετατοπίσεις.

Ένα σημαντικό θεώρημα που αφορά τις συνθήκες για προσαρμογή είναι το θεώρημα του Melan, ή αλλιώς το στατικό θεώρημα, το οποίο μπορεί να διατυπωθεί με τους εξής δύο τρόπους:

α) Μία κατασκευή, υπό ανακυκλιζόμενη φόρτιση, θα προσαρμοστεί ελαστικά, δηλαδή η συμπεριφορά της μετά από κάποιους κύκλους θα γίνει ελαστική, εάν υπάρχει μία κατανομή παραμενουσών τάσεων $\overline{\boldsymbol{\rho}}$ ανεξάρτητη του χρόνου, τέτοια ώστε κάτω από οποιοδήποτε συνδυασμό φορτίων εντός κάποιων προκαθορισμένων ορίων, η υπέρθεση της με τις ελαστικές τάσεις $\boldsymbol{\sigma}^{el}$, δηλαδή $\boldsymbol{\sigma}^{el} + \overline{\boldsymbol{\rho}}$, οδηγεί σε ένα ασφαλές πεδίο τάσεων σε οποιοδήποτε σημείο της κατασκευής.

β) Δε θα συμβεί ποτέ ελαστική προσαρμογή σε μία κατασκευή εκτός και αν βρεθεί μία ανεξάρτητη του χρόνου κατανομή παραμενουσών τάσεων τέτοια ώστε κάτω από όλους τους πιθανούς συνδυασμούς φόρτισης το άθροισμα παραμενουσών και ελαστικών τάσεων συνιστά ένα ασφαλές πεδίο τάσεων.

Αυτές οι διατυπώσεις του θεωρήματος οδηγούν στην ύπαρξη του *οριακού κύκλου* (limiting cycle) για μία κατασκευή, υπό ανακυκλιζόμενη φόρτιση. Αυτός ο κύκλος είναι το όριο της ανάπτυξης ή μη περαιτέρω πλαστικών παραμορφώσεων. Αποδεικνύεται ότι η κατανομή των παραμενουσών τάσεων σε αυτόν τον κύκλο είναι μοναδική και ανεξάρτητη της προηγούμενης ιστορίας παραμόρφωσης.

3. Αριθμητικές μέθοδοι που αναπτύχθηκαν στη διδακτορική διατριβή

3.1. Περιγραφή της αριθμητικής μεθόδου RSDM

Κατά τη διάρκεια της διδακτορικής διατριβής, αρχικά, αναπτύχθηκε μία αριθμητική διαδικασία που ονομάζεται RSDM, η όποια προβλέπει σε τι είδους ελαστοπλαστική συμπεριφορά θα οδηγηθεί μία κατασκευή υπό ανακυκλιζόμενη φόρτιση, αν θα οδηγηθεί δηλαδή είτε σε ελαστική προσαρμογή, εναλλασσόμενη πλαστικοποίηση ή επαυξητική κατάρρευση [1,4]. Εφόσον ισχύει η διαπίστωση ότι οι συνολικές τάσεις μετά από κάποιους κύκλους φόρτισης θα γίνουν κυκλικές και εφόσον εξ' ορισμού οι ελαστικές τάσεις είναι κυκλικές τότε προκύπτει ότι και οι παραμένουσες τάσεις $\boldsymbol{\rho}(\tau)$ θα είναι κι αυτές με τη σειρά τους κυκλικές. Αυτή η κυκλική μορφή των παραμενουσών τάσεων μας δίνει τη δυνατότητα να τις αναλύσουμε σε σειρές Fourier σε σχέση με το χρόνο τ. Έτσι, έχουμε την ακόλουθη έκφραση:

$$\boldsymbol{\rho}(\tau) = \frac{\mathbf{a}_0}{2} + \sum_{k=1}^{\infty} \left(\cos 2k\pi\tau \cdot \mathbf{a}_k + \sin 2k\pi\tau \cdot \mathbf{b}_k \right) \tag{8}$$

Διαφορίζοντας την πιο πάνω εξίσωση ως προς το χρόνο και κάνοντας χρήση της ορθογονικότητας των τριγωνομετρικών συναρτήσεων καταλήγουμε στις ακόλουθες εκφράσεις για τους συντελεστές των σειρών Fourier:

$$\begin{aligned}
\mathbf{a}_k &= -\frac{1}{k\pi} \int_0^1 \dot{\boldsymbol{\rho}}(\tau) \cdot \sin(2k\pi\tau)\, d\tau \\
\mathbf{b}_k &= \frac{1}{k\pi} \int_0^1 \dot{\boldsymbol{\rho}}(\tau) \cdot \cos(2k\pi\tau)\, d\tau \\
\frac{1}{2}\mathbf{a}_{0,e} &= \left(\frac{1}{2}\mathbf{a}_{0,b} + \sum_{k=1}^{\infty} \mathbf{a}_{k,b} \right) - \sum_{k=1}^{\infty} \mathbf{a}_{k,e} + \int_0^1 \dot{\boldsymbol{\rho}}(\tau) d\tau
\end{aligned} \tag{9}$$

όπου τα e, b συμβολίζουν την αρχή και το τέλος του κύκλου αντίστοιχα.

Η βάση λοιπόν της μεθόδου είναι η ανάλυση των παραμενουσών τάσεων σε σειρές Fourier σε σχέση με το χρόνο. Οι συντελεστές των σειρών αυτών

υπολογίζονται επαναληπτικά ικανοποιώντας την ισορροπία και τη συμβιβαστότητα σε κάθε χρονικό σημείο εντός του κύκλου φόρτισης.

Μία σύντομη περιγραφή της μεθόδου και η εφαρμογή της σε συνδυασμό με τη μέθοδο των πεπερασμένων στοιχείων ακολουθεί:

Υποθέτουμε ότι η κατασκευή διακριτοποιείται με πεπερασμένα στοιχεία. Οι τάσεις και οι παραμορφώσεις υπολογίζονται σε κάθε σημείο Gauss των πεπερασμένων στοιχείων. Αρχικά υποθέτουμε πλήρως ελαστική συμπεριφορά και παίρνουμε το διάνυσμα των ελαστικών τάσεων $\boldsymbol{\sigma}^{el}(\tau)$ σε κάθε χρονικό σημείο τ του κύκλου φόρτισης.

Ακολουθούν οι εξής επαναλήψεις σε κάθε επανάληψη *μ*:

1) Γνωρίζοντας την τρέχουσα κατανομή των συντελεστών Fourier (στο τέλος δηλαδή του προηγούμενου βήματος *μ-1*), υπολογίζουμε μία πρώτη εκτίμηση των παραμενουσών τάσεων μέσω της σχέσης:

$$\boldsymbol{\rho}^{(\mu)}(\tau) = \frac{1}{2}\mathbf{a}_0^{(\mu)} + \sum_{k=1}^{\infty}\left\{\cos(2k\pi\tau)\cdot\mathbf{a}_k^{(\mu)} + \sin(2k\pi\tau)\cdot\mathbf{b}_k^{(\mu)}\right\} \tag{10}$$

2) Σε κάθε σημείο Gauss υπολογίζουμε τις συνολικές τάσεις

$$\boldsymbol{\sigma}^{(\mu)}(\tau) = \boldsymbol{\sigma}^{el}(\tau) + \boldsymbol{\rho}^{(\mu)}(\tau) \tag{11}$$

3) Ελέγχουμε εάν $\overline{\sigma}^{(\mu)}(\tau) > \sigma_Y$. Σε τέτοια περίπτωση υπολογίζουμε το υπερβαίνων διάνυσμα τάσεων $\boldsymbol{\sigma}_{pl}^{(\mu)}(\tau)$, υποθέτοντας von Mises κριτήριο διαρροής και υιοθετώντας έναν αλγόριθμο ακτινικής επιστροφής:

$$\xi = \frac{\overline{\sigma}^{(\mu)}(\tau) - \sigma_Y}{\overline{\sigma}^{(\mu)}(\tau)} \Rightarrow \boldsymbol{\sigma}_{pl}^{(\mu)}\left(\tau\right) = \xi\cdot\boldsymbol{\sigma}^{(\mu)}\left(\tau\right) \tag{12}$$

όπου $\overline{\sigma}^{(\mu)}(\tau)$ η ισοδύναμη τάση von Mises και σ_Y η τάση διαρροής.

4) Τα βήματα 1-3 επαναλαμβάνονται για όλα τα σημεία Gauss.
5) Υπολογίζουμε το νέο διάνυσμα των χρονικών παραγώγων των επικόμβιων δράσεων, λόγω εξωτερικής φόρτισης και λόγω $\boldsymbol{\sigma}_{pl}^{(\mu)}(\tau)$:

$$\dot{\mathbf{R}}'(\tau) = \dot{\mathbf{R}}\ (\tau) + \int_V \mathbf{B}^T \cdot \boldsymbol{\sigma}_{pl}^{(\mu)}(\tau) dV \tag{13}$$

6) Υπολογίζουμε το νέο διάνυσμα $\dot{\mathbf{r}}^{(\mu)}(\tau)$ από τη λύση του συστήματος

$$\mathbf{K}\dot{\mathbf{r}}^{(\mu)}(\tau) = \dot{\mathbf{R}}'(\tau) \tag{14}$$

7) Υπολογίζουμε σε κάθε σημείο Gauss τις χρονικές παραγώγους των παραμενουσών τάσεων από τη σχέση:

$$\dot{\boldsymbol{\rho}}^{(\mu)}(\tau) = \mathbf{DB}\dot{\mathbf{r}}^{(\mu)}(\tau) - \dot{\boldsymbol{\sigma}}^{el}(\tau) - \boldsymbol{\sigma}_{pl}^{(\mu)}(\tau) \tag{15}$$

8) Επαναλαμβάνουμε τα βήματα 1-7 για όλα τα προκαθορισμένα χρονικά σημεία

9) Υπολογίζουμε τους νέους συντελεστές Fourier, πραγματοποιώντας αριθμητική ολοκλήρωση σε όλο τον χρονικό κύκλο:

$$\begin{aligned}
\mathbf{a}_k^{(\mu+1)} &= -\frac{1}{k\pi}\int_0^1 \left\{\left[\dot{\boldsymbol{\rho}}^{(\mu)}\left(\tau\right)\right]\left(\sin 2k\pi\tau\right)\right\} d\tau \\
\mathbf{b}_k^{(\mu+1)} &= \ \ \frac{1}{k\pi}\int_0^1 \left\{\left[\dot{\boldsymbol{\rho}}^{(\mu)}\left(\tau\right)\right]\left(\cos 2k\pi\tau\right)\right\} d\tau \\
\frac{\mathbf{a}_0^{(\mu+1)}}{2} &= -\sum_{k=1}^{\infty}\mathbf{a}_k^{(\mu+1)} + \frac{\mathbf{a}_0^{(\mu)}}{2} + \sum_{k=1}^{\infty}\mathbf{a}_k^{(\mu)} + \int_0^1 \left[\dot{\boldsymbol{\rho}}^{(\mu)}\left(\tau\right)\right] d\tau
\end{aligned} \tag{16}$$

10) Υπολογίζουμε την νέα κατανομή των παραμενουσών τάσεων από τη σχέση (8)

11) Ελέγχουμε τη σύγκλιση μεταξύ δυο διαδοχικών λύσεων μέσω της σχέσης:

$$\frac{\left\|\boldsymbol{\rho}^{(\mu+1)}(1)\right\|_2 - \left\|\boldsymbol{\rho}^{(\mu)}(1)\right\|_2}{\left\|\boldsymbol{\rho}^{(\mu+1)}(1)\right\|_2} \leq tol \tag{17}$$

Εάν έχει επιτευχθεί η σύγκλιση τότε η διαδικασία σταματάει καθώς έχουμε φτάσει σε ένα σταθεροποιημένο κύκλο και θέτουμε $\boldsymbol{\rho}^{(\mu)} \approx \boldsymbol{\rho}^{(\mu+1)} = \boldsymbol{\rho}^{cs}$. Αλλιώς ξαναπηγαίνουμε στο βήμα 1.

Μετά τη σύγκλιση θέτουμε $\boldsymbol{\sigma}_{pl}^{cs} = \boldsymbol{\sigma}_{pl}^{(\mu+1)} \approx \boldsymbol{\sigma}_{pl}^{(\mu)}$ και υπολογίζουμε το ακόλουθο ολοκλήρωμα σε όλο τον κύκλο για κάθε σημείο Gauss:

$$\alpha_i = \int_0^1 \sigma_{pl,i}^{cs}(\tau) d\tau \tag{18}$$

όπου το i αναφέρεται σε κάθε στοιχείο του διανύσματος $\boldsymbol{\sigma}_{pl}^{cs}$.

Οι τρεις διαφορετικές ασυμπτωτικές καταστάσεις υπολογίζονται ως εξής:

α) αν $\alpha_i \neq 0$ τότε οδηγούμαστε σε *συσσωρευμένη πλαστικοποίηση*.

Αν $\alpha_i = 0$ ελέγχουμε εάν

β) $\sigma_{pl,i}^{cs}(\tau) \neq 0$ τότε το αντίστοιχο σημείο Gauss είναι σε κατάσταση *εναλλασσόμενης πλαστικοποίηση*.

γ) $\sigma_{pl,i}^{cs}(\tau) = 0$ τότε το αντίστοιχο σημείο Gauss είναι σε κατάσταση *ελαστικής προσαρμογής*.

Εάν όλα τα σημεία Gauss είναι σε κατάσταση *ελαστικής προσαρμογής* τότε η κατασκευή μας συνολικά θα προσαρμοστεί για τη δεδομένη εξωτερική φόρτιση. Στην περίπτωση αυτή, η αριθμητική διαδικασία θα έχει συγκλίνει στις πραγματικές, σταθερές με το χρόνο παραμένουσες τάσεις. Από την άλλη εάν ένας ικανός αριθμός σημείων Gauss ικανοποιεί τη συνθήκη $\alpha_i \neq 0$ τότε συνολικά η κατασκευή μας κινδυνεύει από επαυξητική κατάρρευση. Το διάγραμμα ροής της αριθμητικής διαδικασίας φαίνεται στο σχήμα 3 που ακολουθεί.

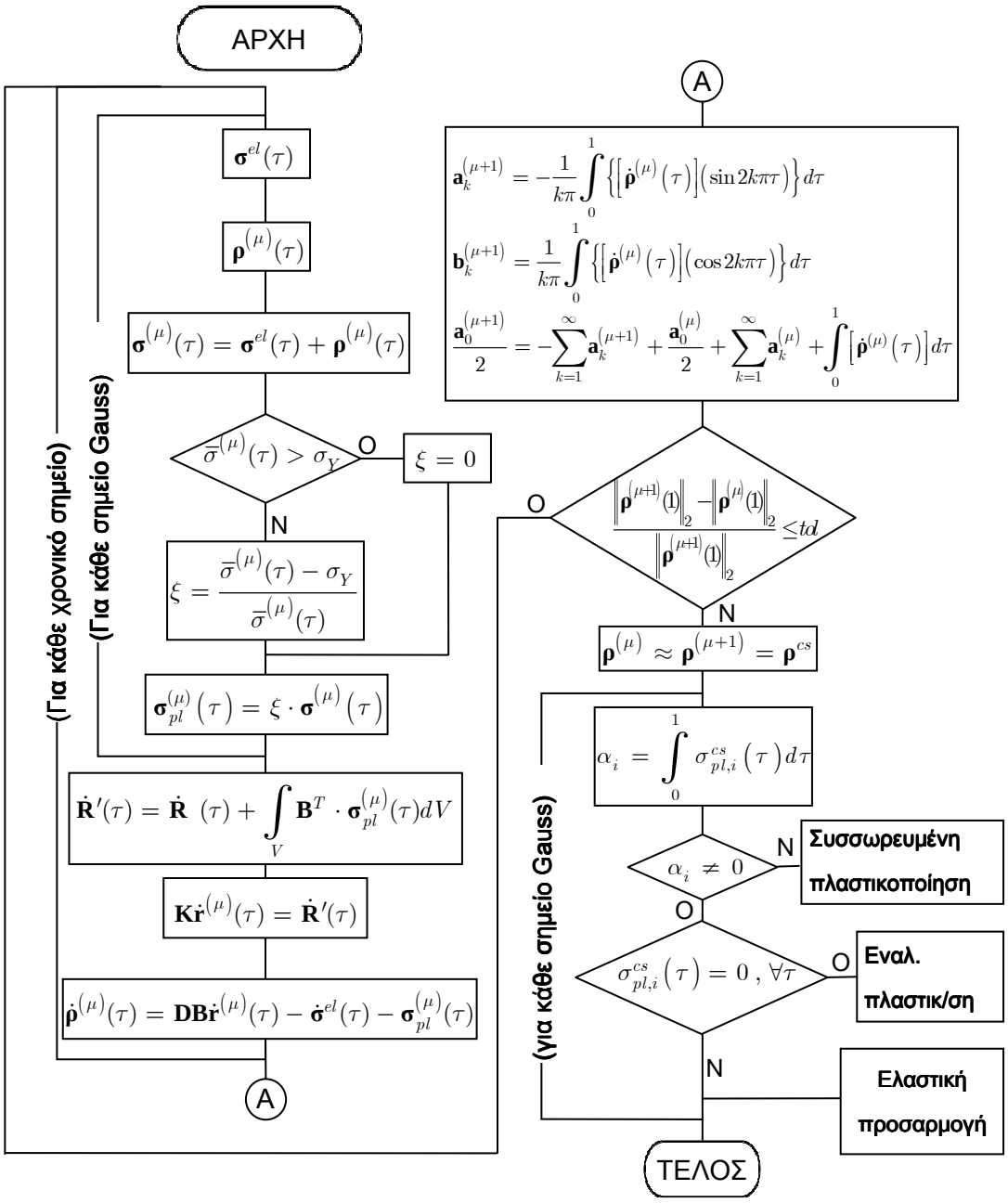

Σχήμα 3 Διάγραμμα ροής της RSDM

3.1.1. Παράδειγμα εφαρμογής της RSDM

Ας θεωρήσουμε την πλάκα του σχήματος 4 η οποία υπόκειται σε δύο κατανεμημένα φορτία στις πλευρές της. Για λόγους συμμετρίας εξετάζουμε το ένα τέταρτο της πλάκας. Τα γεωμετρικά χαρακτηριστικά της πλάκας είναι: $D / L = 0.2$, $d / L = 0.05$ και $L = 20cm$. Οι ιδιότητες του υλικού είναι: $E = 208Gpa$, $\nu = 0.3$ και $\sigma_Y = 360Mpa$. Θα επιλέξουμε τρεις διαφορετικές περιπτώσεις χρονικών κατανομών των φορτίων ώστε να οδηγούν σε τρεις διαφορετικές κυκλικές συμπεριφορές την κατασκευή. Τα αποτελέσματα θα αφορούν τα πλέον εντεινόμενα σημεία Gauss της κατασκευής 1 και 2 (σχήμα 4).

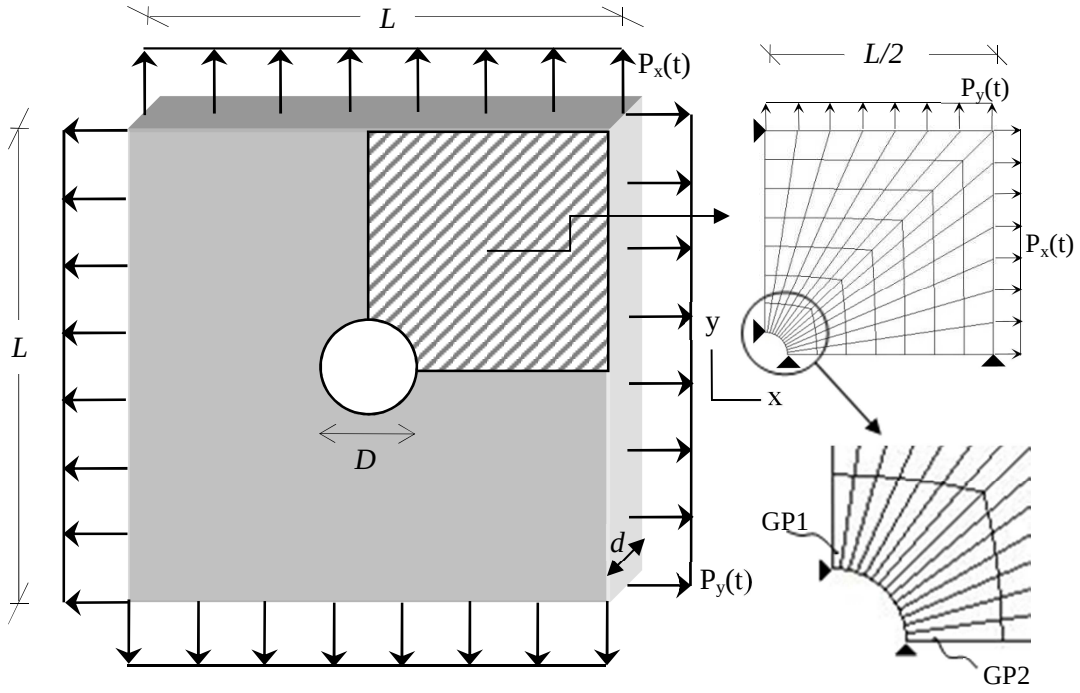

Σχήμα 4 Τετραγωνική πλάκα (γεωμετρία, φόρτιση, δίκτυο πεπερασμένων στοιχείων)

α) Η πρώτη περίπτωση φόρτισης έχει την ακόλουθη κατανομή με το χρόνο:

$$P_y(\tau) = 0.65\sigma_y \sin^2(\pi\tau), \quad P_x(\tau) = 0$$

όπου $\tau = \frac{t}{T}$. Στο σχήμα 5 φαίνεται η σταθεροποιημένη κατανομή παραμενουσών τάσεων για το σημείο Gauss 2. Όπως φαίνεται η κατανομή αυτή είναι ανεξάρτητη με το χρόνο και η RSDM προβλέπει ότι η κατασκευή θα οδηγηθεί σε ελαστική

προσαρμογή. Η σύγκριση των συνολικών τάσεων με το πρόγραμμα Abaqus φαίνεται στο σχήμα 6.

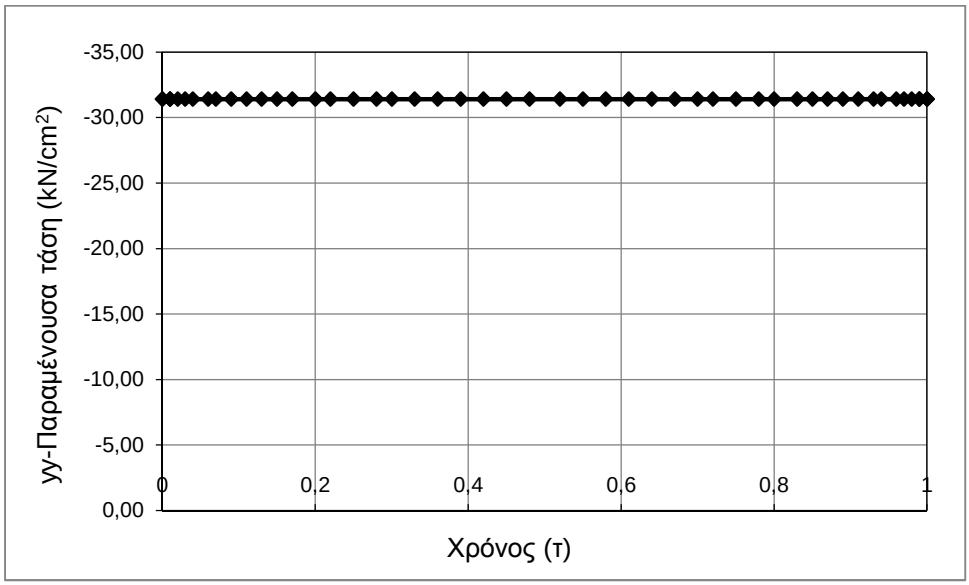

Σχήμα 5 Κατανομή σταθεροποιημένης παραμένουσας τάσης

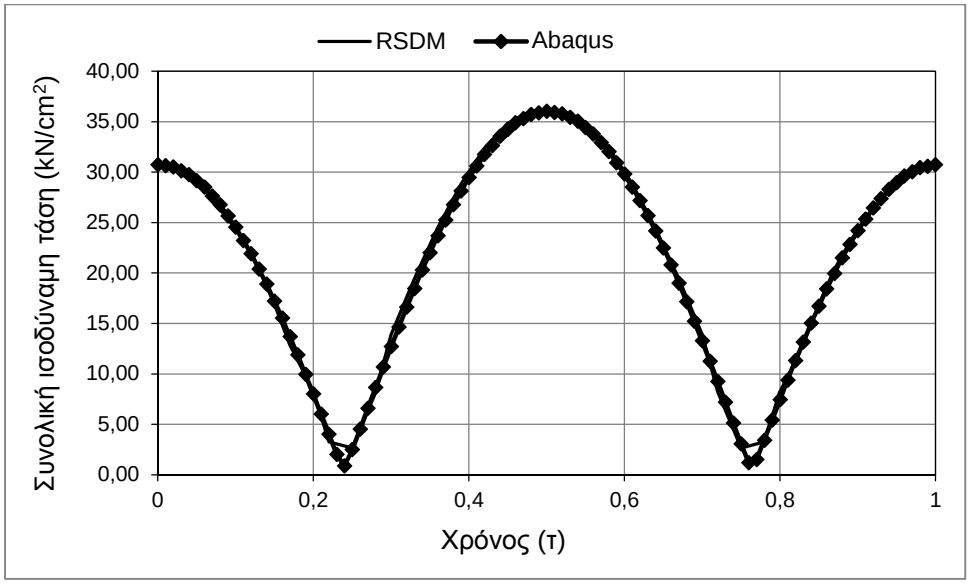

Σχήμα 6 Κατανομή σταθεροποιημένης συνολικής τάσης

β) Η δεύτερη περίπτωση φόρτισης έχει την ακόλουθη κατανομή με το χρόνο:

$$P_y(\tau) = 0.65\sigma_y \sin(2\pi\tau), \quad P_x(\tau) = 0$$

Η προτεινόμενη μεθοδολογία (RSDM) προβλέπει ότι αυτή η φόρτιση θα οδηγήσει κάποια σημεία Gauss σε τοπική εναλλασσόμενη πλαστικοποίηση. Ο τοπικός μηχανισμός εναλλασσόμενης πλαστικοποίηση που προβλέπει η RSDM φαίνεται στο σχήμα 8 και είναι σύμφωνος με τον αντίστοιχο μηχανισμό που προβλέπεται από το Abaqus (σχήμα 8).

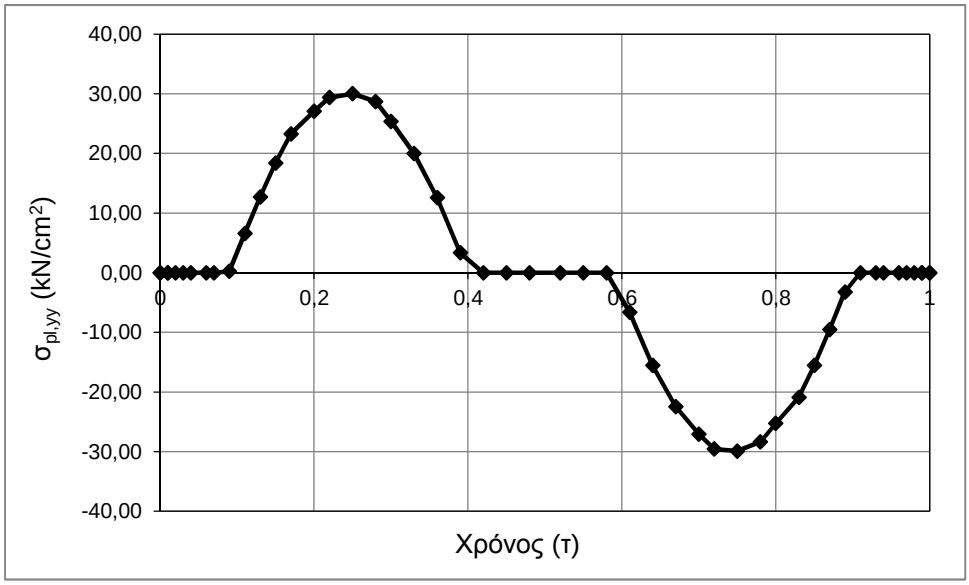

Σχήμα 7 Κατανομή του $\boldsymbol{\sigma}_{pl}$ στο σταθεροποιημένο κύκλο

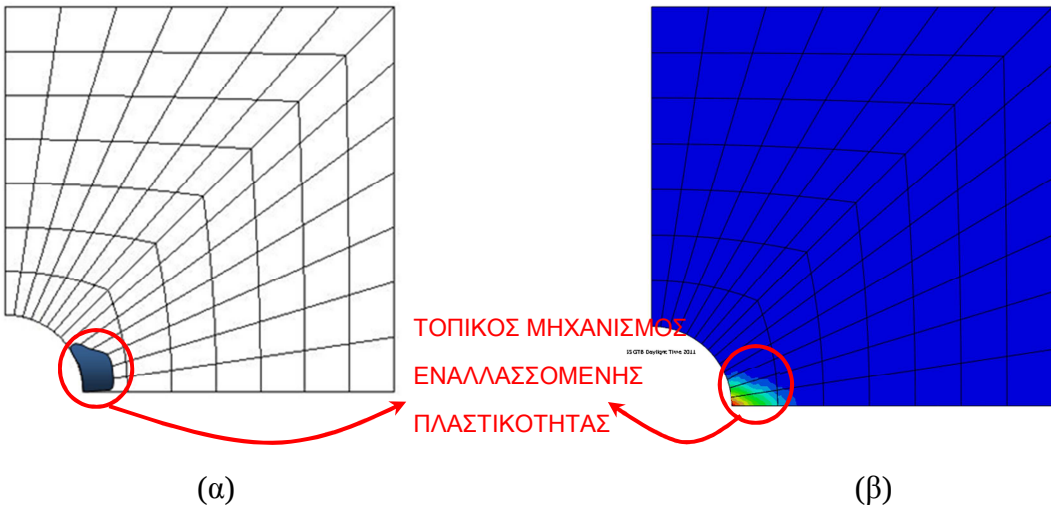

Σχήμα 8 Τοπικός μηχανισμός εναλλασσόμενης πλαστικοποίησης

Στο σχήμα 7 φαίνεται η κατανομή της yy-διεύθυνσης του διανύσματος $\boldsymbol{\sigma}_{pl}^{cs}$ στο σημείο Gauss 2. Μπορούμε λοιπόν να διακρίνουμε το εναλλασσόμενο πρόσημο αυτής της κατανομής εντός του κύκλου στα χρονικά διαστήματα $\left[0.06, 0.42\right]$ και $\left[0.58, 0.91\right]$.

γ) Η τελευταία περίπτωση φόρτισης έχει την ακόλουθη κατανομή με το χρόνο:

$P_x(\tau) = 0.85\sigma_y = const$

$P_y(\tau) = 0.5\sigma_y \sin^2(\pi\tau)$

Στο σχήμα 9 φαίνεται η κατανομή της χχ-διεύθυνσης του διανύσματος $\boldsymbol{\sigma}_{pl}^{cs}$ στο σημείο Gauss 1. Όπως παρατηρούμε η πλαστική παραμόρφωση είναι του ίδιου προσήμου στα χρονικά διαστήματα $\left[0, 0.22\right]$ και $\left[0.78, 1\right]$. Αυτή η συμπεριφορά ισχύει για πολλά σημεία στην κατασκευή, τα οποία συνιστούν ένα μηχανισμό επαυξητικής κατάρρευσης. Αυτός ο μηχανισμός επαληθεύεται και από το πρόγραμμα Abaqus (σχήμα 10).

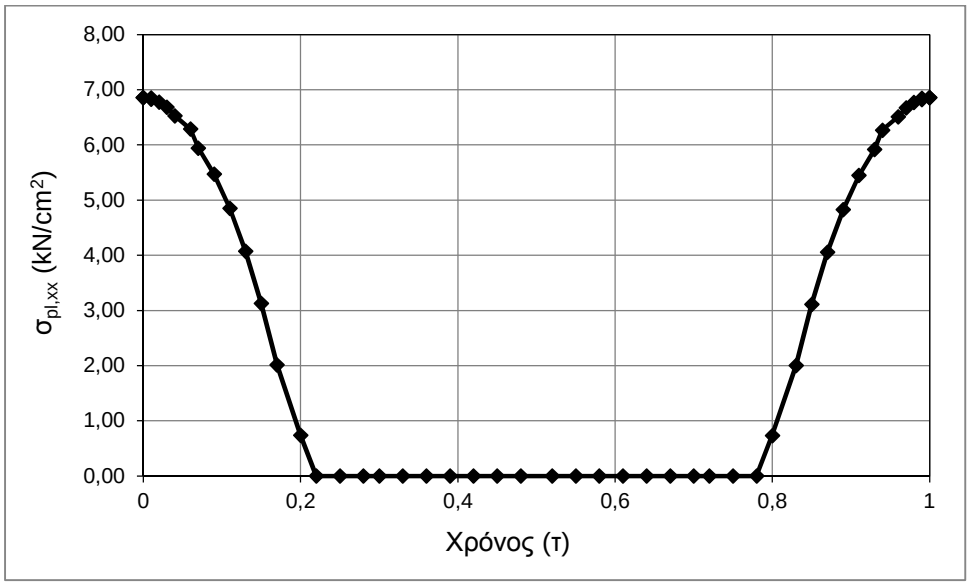

Σχήμα 9 Κατανομή του $\boldsymbol{\sigma}_{pl}$ στο σταθεροποιημένο κύκλο

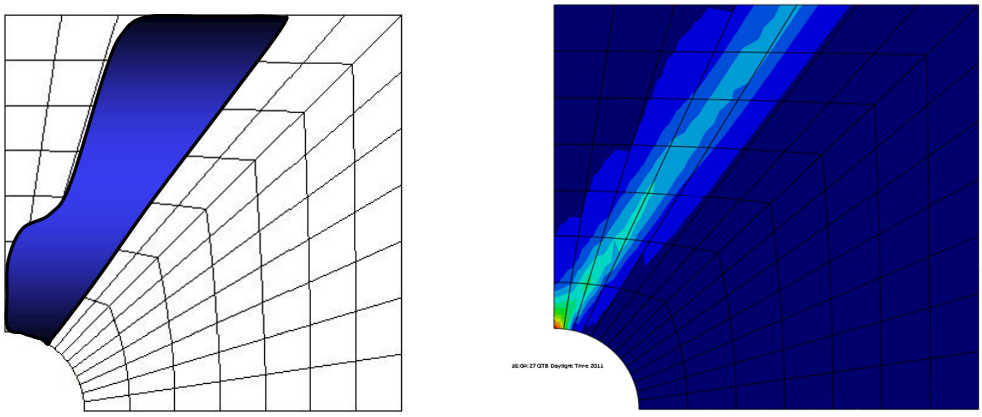

(α) (β)

Σχήμα 10 Μηχανισμός επαυξητικής κατάρρευσης

3.2. Προτεινόμενη διαδικασία για τον υπολογισμό του φορτίου ελαστικής προσαρμογής

3.2.1. Περιγραφή της μεθόδου RSDM-S

Ας θεωρήσουμε μία κατασκευή (σχήμα 11) η οποία υπόκειται σε κάποια μηχανικά φορτία. Παρόλο που η μεθοδολογία όπως θα δούμε παρακάτω μπορεί να εφαρμοστεί για παραπάνω από δύο φορτία, για λόγους απλοποίησης θα υποθέσουμε τώρα ότι ένας μέγιστος αριθμός δύο φορτίων ασκούνται στην κατασκευή. Η μεθοδολογία που ακολουθεί υιοθετεί την επιφάνεια διαρροής von Mises για το υλικό.

Υποθέτουμε λοιπόν ότι αυτά τα φορτία μεταβάλλονται ανεξάρτητα μεταξύ τους, με οποιοδήποτε τρόπο, στο χωρίο που ορίζουν τα όριά τους (σχήμα 11α). Οι μέγιστες τιμές των φορτίων συμβολίζονται με P_1^* και P_2^* αντίστοιχα. Για λόγους ευκολίας υποθέτουμε ότι η ελάχιστη τιμή των φορτιών είναι μηδέν.

Το πιο συνηθισμένο χωρίο φόρτισης στην ανάλυση προσαρμογής (shakedown analysis) είναι ένα κυρτό υπερ-πολύεδρο που ορίζεται από τα μέγιστα και ελάχιστα όρια των φορτίων, για παράδειγμα στην περίπτωση διπαραμετρικής φόρτισης μπορούμε να ορίσουμε το ορθογωνικό χωρίο Ω του σχήματος 11α.

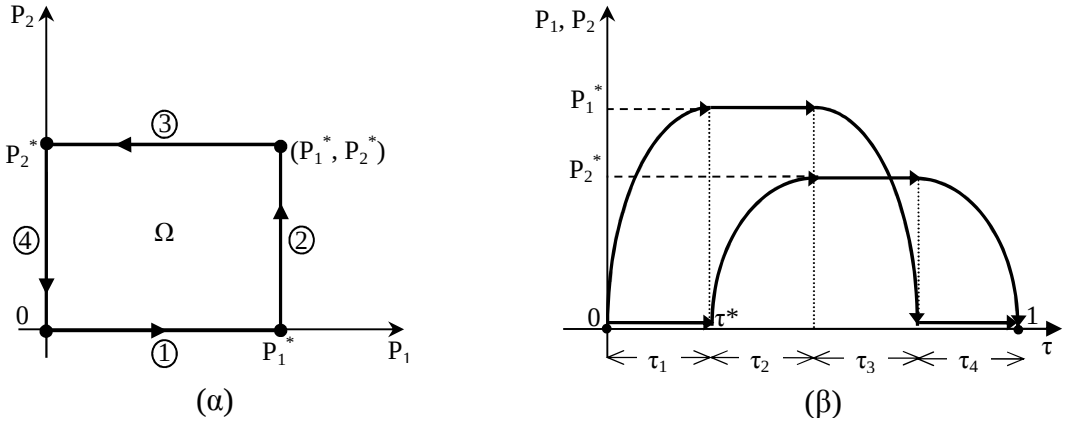

Σχήμα 11 Ανεξάρτητη κυκλική μεταβολή φορτίων α) στο χώρο των φορτίων, β) στο πεδίο του χρόνου

Η κυρτότητα της επιφάνειας διαρροής μας εξασφαλίζει ότι εάν η κατασκευή προσαρμόζεται ελαστικά για ένα κυκλικό πρόγραμμα φόρτισης που περνάει από τα όρια του χωρίου φόρτισης τότε θα προσαρμόζεται ελαστικά για οποιοδήποτε πρόγραμμα μεταβαλλόμενης φόρτισης περιέχεται εντός αυτού του χωρίου. Υποθέτοντας ότι το χωρίο είναι συνεχές και κυρτό.

Μπορούμε λοιπόν να σχεδιάσουμε μία οποιαδήποτε καμπύλη που να περνάει από αυτά τα όρια (σχήμα 11β). Έτσι θεωρούμε ένα κυκλικό πρόγραμμα φόρτισης που περνάει από τις τέσσερις κορυφές αυτού του ορθογωνικού χωρίου φόρτισης Ω, δηλαδή που ακολουθεί τη διαδρομή $\left(0 \to P_1^* \to (P_1^*, P_2^*) \to P_2^* \to 0\right)$ (σχήμα 11α). Σε σχέση με το χρόνο αυτό το κυκλικό πρόγραμμα φόρτισης μπορεί να εκφραστεί με τη βοήθεια των εξισώσεων:

$$\mathbf{P}(\tau) = \begin{Bmatrix} P_1(\tau) \\ P_2(\tau) \end{Bmatrix} = \begin{Bmatrix} P_1^* \cdot \alpha_1(\tau) \\ P_2^* \cdot \alpha_2(\tau) \end{Bmatrix} \tag{19}$$

Ενδεικτικές κατανομές αυτών των δύο φορτίων φαίνονται στο σχήμα 11β.

Το χωρίο της φόρτισης ή το ισοδύναμο κυκλικό πρόγραμμα φόρτισης στο πεδίο του χρόνου είναι δυνατόν να μεταβάλλεται ισοτροπικά εφόσον πολλαπλασιάζεται με έναν συντελεστή γ. Με τη μεθοδολογία (RSDM-S) που προτείνεται στη διατριβή αναζητείται ο μεγαλύτερος συντελεστής φόρτισης για τον οποίο τα ισοδύναμα προγράμματα φόρτισης οδηγούν την κατασκευή στην προσαρμογή [2,3,5]. Ο οριακός

αυτός συντελεστής ονομάζεται συντελεστής προσαρμογής (shakedown factor). Με άλλα λόγια ο συντελεστής αυτός θα μας προσδιορίσει τη μέγιστη δυνατή περιοχή φόρτισης η οποία περιέχει όλα τα δυνατά προγράμματα ανακυκλιζόμενης φόρτισης που μπορούν να ασκηθούν στην κατασκευή αυτή και να εξασφαλίζουν ότι οι πλαστικές παραμορφώσεις είναι φραγμένες. Ακολουθεί μια συνοπτική περιγραφή της αριθμητικής διαδικασίας.

Υπολογισμός ενός αρχικού συντελεστή φόρτισης για την εκκίνηση της διαδικασίας

Ο αρχικός συντελεστής φόρτισης υπολογίζεται έτσι ώστε να πλαστικοποιείται ολόκληρη η κατασκευή, και δίνεται από τη σχέση:

$$\gamma^{(1)} = \frac{\sigma_Y}{\min \overline{\sigma}^{el}} \tag{20}$$

όπου σ_Y είναι η ισοδύναμη τάση διαρροής von Mises και $\min \overline{\sigma}^{el}$ η ελάχιστη ισοδύναμη τάση von Mises όλων των σημείων Gauss της διακριτοποιημένης κατασκευής την χρονική στιγμή τ^* όπου ένα από τα δύο φορτία παίρνει τη μέγιστη του τιμή (π.χ. δες σχήμα 11β).

Υλοποίηση της επαναληπτικής διαδικασίας RSDM-S

Όπως έχει τονισθεί και προηγουμένως, για να οδηγηθεί μία κατασκευή στην ελαστική προσαρμογή, οι παραμένουσες τάσεις στον σταθεροποιημένο κύκλο εντατικής κατάστασης πρέπει να είναι σταθερές με το χρόνο. Άρα λοιπόν, εφόσον αυτές οι τάσεις αναλυθούν σε σειρές Fourier με τη βοήθεια της RSDM, η βάση της νέας μεθοδολογίας έγκειται στο να οδηγηθούν οι συντελεστές των τριγωνομετρικών όρων $\mathbf{a}_k$ και $\mathbf{b}_k$ στο μηδέν ώστε ο παραμένων όρος των σειρών Fourier να είναι ο σταθερός όρος. Το άθροισμα των νορμών των όρων του συνημιτόνου και του ημιτόνου χρησιμοποιείται για το σκοπό αυτό [2,3,5].

Ένα διάγραμμα ροής της αριθμητικής διαδικασίας φαίνεται στο σχήμα 12. Μετά από μία αρχική φάση αρχικοποίησης, μπαίνουμε σε μία επαναληπτική διαδικασία, η όποια αποτελείται από δύο βρόχους, έναν μέσα στον άλλον.

Ο εξωτερικός βρόχος καθορίζεται από τις επαναλήψεις *μ*, ξεκινώντας με *μ=1*. Εντός αυτού του εξωτερικού βρόχου ακολουθούνται τα επόμενα βήματα:

1. Εισερχόμαστε στον εσωτερικό βρόχο που αποτελείται από τα βήματα (1-11) της μεθόδου RSDM. Αφού υπολογίσουμε τις ελαστικές τάσεις και τις παραγώγους αυτών για την τρέχουσα τιμή του συντελεστή φόρτισης $\gamma^{(\mu)}$, οι επαναλήψεις ξεκινούν χρησιμοποιώντας, σαν αρχική εκτίμηση, τους συντελεστές των σειρών Fourier και τις παραμένουσες τάσεις της κυκλικής λύσης για τον προηγούμενο φορτιστικό συντελεστή $\gamma^{(\mu-1)}$.
2. Βγαίνοντας από τον εσωτερικό βρόχο, όλες οι απαραίτητες τιμές της κυκλικής λύσης που προέκυψαν από την RSDM για τον τρέχοντα φορτιστικό συντελεστή $\gamma^{(\mu)}$ είναι πλέον γνωστές.
3. Υπολογίζουμε την συνάρτηση φ που είναι το άθροισμα των νορμών των διανυσμάτων των συντελεστών των τριγωνομετρικών όρων των σειρών Fourier.
4. Παράγουμε μία φθίνουσα ακολουθία των συντελεστών φόρτισης μέσω της συνάρτησης φ. Μία παράμετρος ω για τη σύγκλιση μπορεί να είναι χρήσιμη. Αναλυτική περιγραφή για τη χρήση αυτής της παραμέτρου υπάρχει στη δημοσίευση [2]. Παρακολουθώντας την τιμή $\gamma^{(\mu)} \cdot P_1^*$ μπορούμε να ελέγχουμε τη συρρίκνωση της φόρτισης είτε στο πεδίο του χρόνου, είτε ισοδύναμα, στο χώρο των φορτίων.
5. Ελέγχουμε τον νέο συντελεστή φόρτισης έναντι του προηγούμενου. Εάν έχει επιτευχθεί σύγκλιση, τότε η διαδικασία σταματάει, καθώς μόνο ο σταθερός όρος των σειρών Fourier έχει παραμείνει. Αλλιώς συνεχίζουμε τη διαδικασία και επαναλαμβάνουμε τα βήματα 1-5.

Η προτεινόμενη διαδικασία RSDM-S καταλήγει με τις παραμέτρους του οριακού κύκλου (limiting cycle) για ελαστική προσαρμογή. Έτσι λοιπόν, ο συντελεστής γ_{sh} είναι ο συντελεστής προσαρμογής (shakedown factor), και ο μόνος παραμένων όρος των συντελεστών Fourier, συμπίπτει με τη σταθερή με το χρόνο κατανομή των παραμενουσών τάσεων η οποία είναι μοναδική για το πρόγραμμα φόρτισης που υιοθετήθηκε κατά τη διαδικασία.

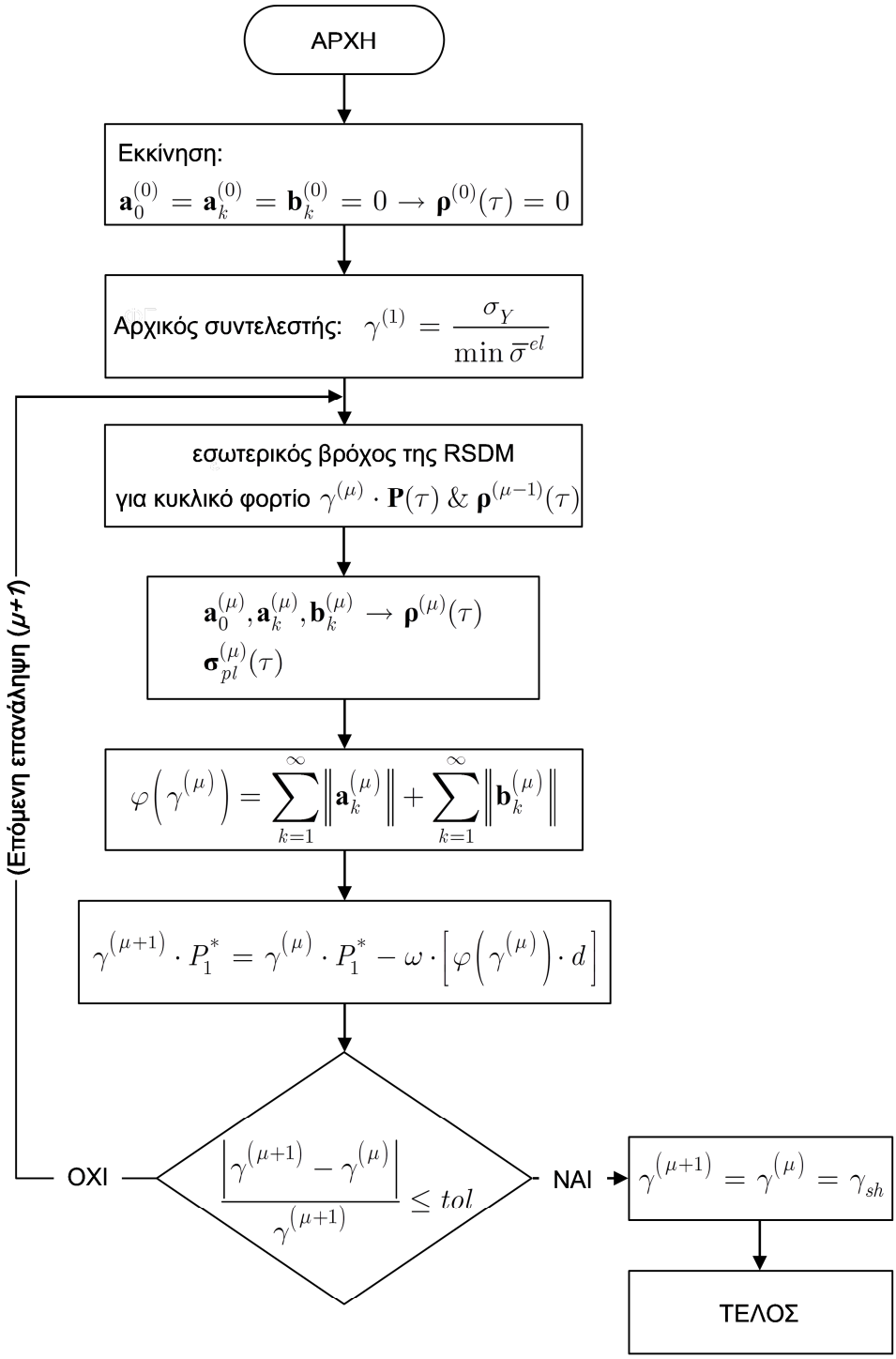

Σχήμα 12 Διάγραμμα ροής της RSDM-S

3.2.1.1. Παράδειγμα εφαρμογής της RSDM-S για μηχανικά φορτία

Ας θεωρήσουμε μία συμμετρική δοκό τριών ανοιγμάτων η οποία καταπονείται από δύο χρονικά μεταβαλλόμενα κατανεμημένα φορτία. Λόγω συμμετρίας επιλέγουμε να μελετήσουμε τη μισή δοκό (σχήμα 13). Οι ιδιότητες του υλικού της δοκού είναι: $E = 180Gpa$, $\nu = 0.3$ και $\sigma_Y = 100Mpa$.

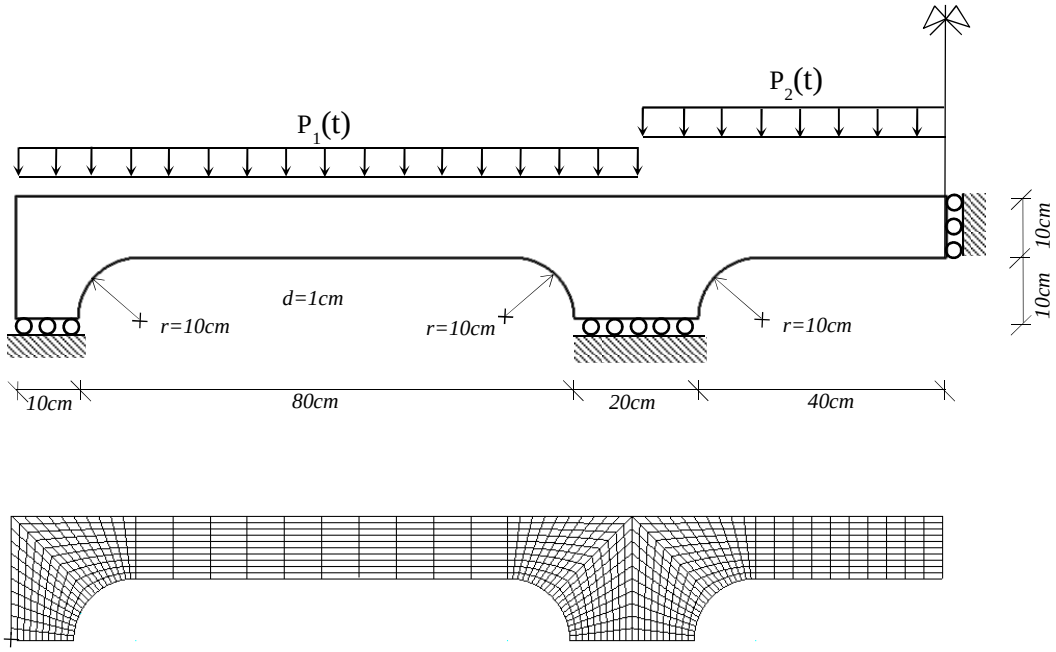

Σχήμα 13 Συμμετρική συνεχής δοκός (γεωμετρία, φόρτιση, δίκτυο πεπερασμένων στοιχείων)

Περιγραφή του χωρίου φόρτισης

Θεωρούμε το ορθογωνικό χωρίο φόρτισης του σχήματος 14β. Τα φορτία μεταβάλλονται μεταξύ των ορίων $P_1 \in \left[0, P_1^*\right]$ και $P_2 \in \left[0, P_2^*\right]$ όπου $P_1^* = 1$ και $P_2^* = 2$. Ένα ισοδύναμο κυκλικό πρόγραμμα φόρτισης στο πεδίο του χρόνου που περνάει από τις τέσσερις κορυφές του ορθογωνικού χωρίου προκύπτει με τη βοήθεια των εξισώσεων του σχήματος 14α.

Ο συντελεστής προσαρμογής (shakedown factor) που προκύπτει από την προτεινόμενη μεθοδολογία RSDM-S είναι ίσος με **0.191** [2]. Η σύγκλιση της μεθόδου φαίνεται στο σχήμα 15. Για λόγους καλύτερης παρουσίασης, στο εσωτερικό διάγραμμα φαίνεται η σύγκλιση μετά τις 12 πρώτες επαναλήψεις. Μόλις 96 επαναλήψεις χρειάστηκαν για να καταλήξουμε σε λύση σε αυτό το πρόβλημα της δοκού που θεωρείται ένα πρόβλημα σχετικά πολλών βαθμών ελευθερίας καθώς

αποτελείται από 800, 8-κομβικά, ισοπαραμετρικά πεπερασμένα στοιχεία με 3x3 σημεία αριθμητικής ολοκλήρωσης Gauss.

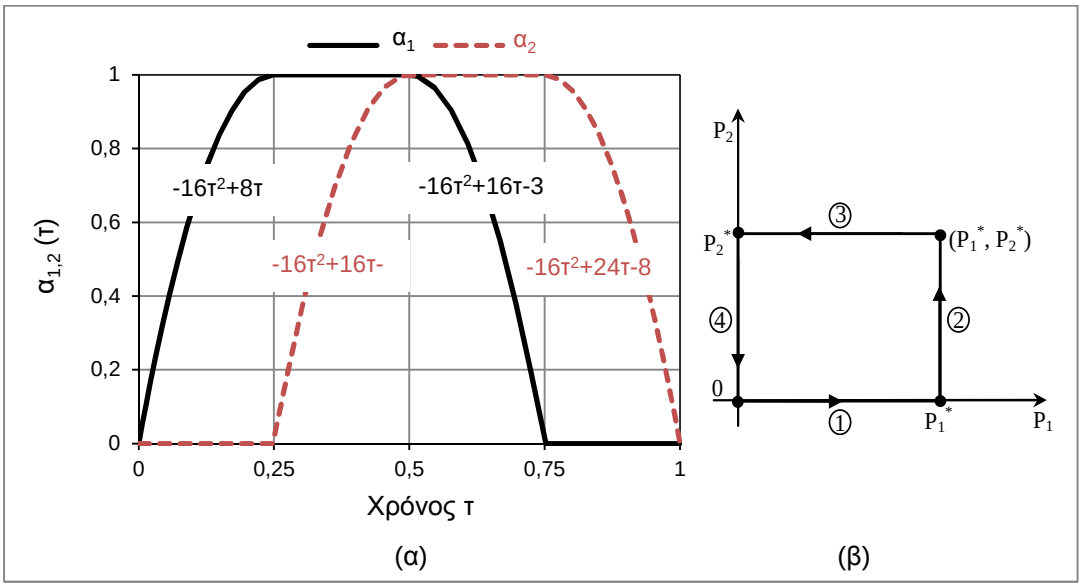

Σχήμα 14 Μεταβολή των συναρτήσεων χρόνου σε μία περίοδο

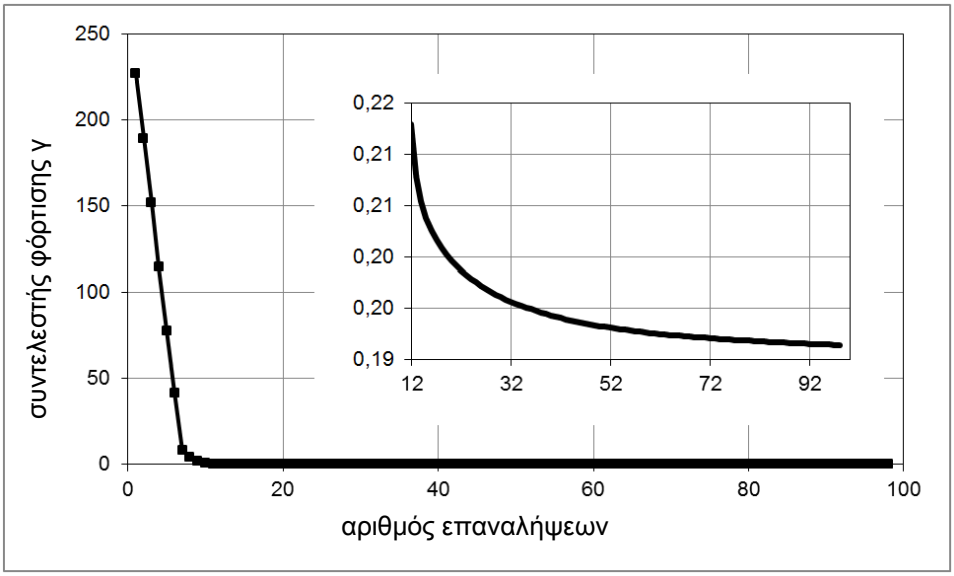

Σχήμα 15 Σύγκλιση της RSDM-S για την περίπτωση της δοκού

3.2.2. Επέκταση της RSDM-S σε θερμομηχανικές φορτίσεις

Η παραπάνω μεθοδολογία RSDM-S αφού εφαρμόστηκε σε κατασκευές υπό μηχανικά φορτία, επεκτάθηκε ώστε να μπορεί να υπολογίζει το φορτίο προσαρμογής

(shakedown load) για κατασκευές που συνδυάζουν μηχανικά αλλά και θερμικά φορτία [3].

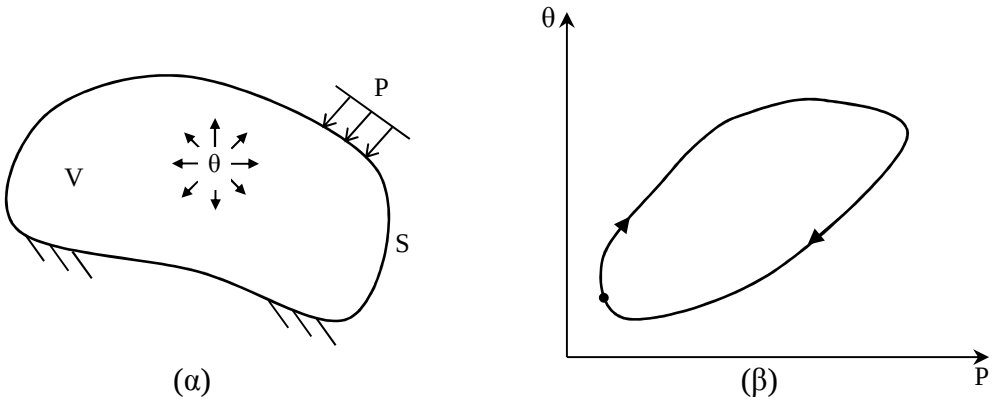

Σχήμα 16 α) Κατασκευή υπό επιβαλλόμενα φορτία, β) κυκλική φόρτιση

Για παράδειγμα ας θεωρήσουμε το σώμα του σχήματος 16α το οποίο υπόκειται σε ένα μηχανικό και ένα θερμικό φορτίο. Η μεθοδολογία, αν και όπως θα δούμε σε επόμενη παράγραφο μπορεί να εφαρμοστεί σε περισσότερα από δύο φορτία, αρχικά εφαρμόστηκε για συνδυασμό δύο φορτίων.

Κατά τον ίδιο τρόπο με την περίπτωση των μηχανικών φορτίων επιλέγουμε να μετατρέψουμε το χωρίο φόρτισης σε ένα ισοδύναμο φορτίο στο πεδίο του χρόνου (σχήμα 17). Αυτό γίνεται με τη βοήθεια των παρακάτω εξισώσεων:

$$\mathbf{P}(\tau) = \begin{Bmatrix} P(\tau) \\ \theta(\tau) \end{Bmatrix} = \begin{Bmatrix} P^* \cdot \alpha_1(\tau) \\ \theta^* \cdot \alpha_2(\tau) \end{Bmatrix} \tag{21}$$

Ενδεικτικές κατανομές για τα δύο φορτία φαίνονται στο σχήμα 17β.

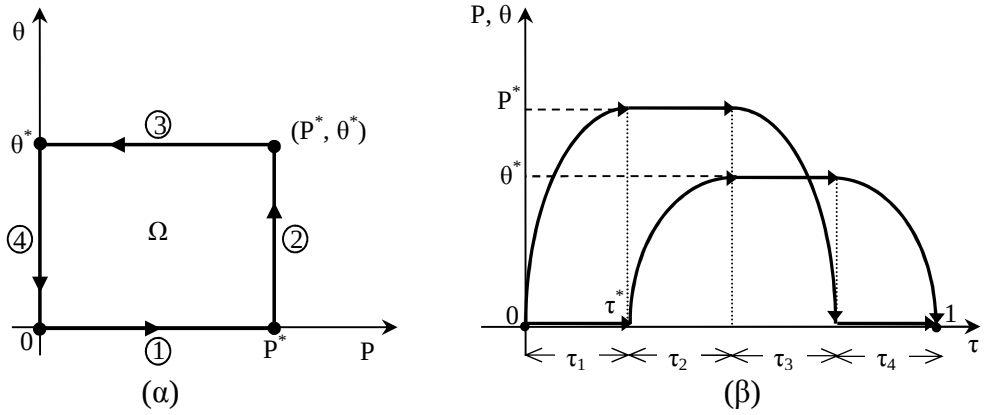

Σχήμα 17 Ανεξάρτητη κυκλική μεταβολή φορτίων α) στο χώρο των φορτίων, β) στο πεδίο του χρόνου

Ο αρχικός φορτιστικός συντελεστής της διαδικασίας υπολογίζεται κατά παρόμοιο τρόπο με πριν.

Το διάγραμμα ροής του σχήματος 12 παραμένει ουσιαστικά το ίδιο και είναι επαρκές για να περιγράψει τη γενική διαδικασία. Οι διαφορές σε σχέση με την περίπτωση της μηχανικής φόρτισης είναι κυρίως οι εξής:

α) Στον υπολογισμό των ελαστικών τάσεων. Οι ελαστικές τάσεις δίνονται πλέον από τη σχέση:

$$\boldsymbol{\sigma}^{el}(\tau) = \alpha_1(\tau)\boldsymbol{\sigma}^{el}_{P^*} + \alpha_2(\tau)\boldsymbol{\sigma}^{el}_{\theta^*} \tag{22}$$

όπου τα $\alpha_1(\tau), \alpha_2(\tau)$ είναι οι συναρτήσεις χρόνου του σχήματος 17β. Να σημειωθεί ότι $\boldsymbol{\sigma}^{el}_{P^*}$ και $\boldsymbol{\sigma}^{el}_{\theta^*}$ είναι οι ελαστικές τάσεις για P^* και θ^* αντίστοιχα.

β) Στον εσωτερικό βρόχο της RSDM το νέο διάνυσμα των παραγώγων των επικόμβιων δράσεων για τον τρέχων συντελεστή φόρτισης $\gamma^{(\mu)}$ της διαδικασίας θα δίνεται από τη σχέση:

$$\dot{\mathbf{R}}' = \gamma^{(\mu)}\left\{\dot{\alpha}_1(\tau)\mathbf{R}_{P^*} + \dot{\alpha}_2(\tau)\int_V \mathbf{B}^T\mathbf{D}\mathbf{e}^{\theta^*}dV\right\} + \int_V \mathbf{B}^T\boldsymbol{\sigma}^{(\kappa)}_{pl}dV \tag{23}$$

κατά αναλογία με τη σχέση (13).

γ) Οι χρονικές παράγωγοι των παραμενουσών τάσεων θα δίνονται από τη σχέση:

$$\dot{\boldsymbol{\rho}}^{(\kappa)}(\tau) = \mathbf{D}\mathbf{B}\dot{\mathbf{r}}^{(\kappa)}(\tau) - \gamma^{(\mu)}\dot{\boldsymbol{\sigma}}^{el}(\tau) - \mathbf{D}\dot{\mathbf{e}}^{\theta,(\mu)} - \boldsymbol{\sigma}^{(\kappa)}_{pl}(\tau) \tag{24}$$

κατά αναλογία με τη σχέση (15).

δ) Τέλος, ο νέος φορτιστικός συντελεστής που θα υπολογίζεται σε κάθε εξωτερικό βρόχο θα δίνεται από τη σχέση:

$$\gamma^{(\mu+1)} \cdot P^* = \gamma^{(\mu)} \cdot P^* - \omega \cdot [\varphi\left(\gamma^{(\mu)}\right) \cdot d] \tag{25}$$

3.2.2.1. Παράδειγμα εφαρμογής της RSDM-S για θερμομηχανικά φορτία

Στη συνέχεια θεωρούμε το κλασσικό πρόβλημα του Bree (σχήμα 18). Η κατασκευή μας υπόκειται σε μία σταθερή μονοαξονική τάση σ_P, σταθερή με το χρόνο, και σε μία γραμμική μεταβολή της θερμοκρασίας $\Delta\theta(t)$ μεταξύ της εσωτερικής και εξωτερικής

πλευράς η όποια μεταβάλλεται με το χρόνο. Οι ιδιότητες του υλικού είναι: $E = 208Gpa$, $\nu = 0.3$, $\sigma_Y = 360Mpa$ και ο συντελεστής θερμικής διαστολής $5 \times 10^{-5}\ °C^{-1}$.

Οι συναρτήσεις χρόνου που χρησιμοποιήθηκαν φαίνονται στο σχήμα 19. Η ασφαλής περιοχή της ελαστικής προσαρμογής (shakedown domain) που προκύπτει από την RSDM-S φαίνεται στο σχήμα 20, καθώς και η σύγκριση της με την αναλυτική λύση το Bree. Να σημειωθεί, ότι στο σχήμα 20 σ_t είναι η μέγιστη ελαστική τάση λόγω της θερμοκρασιακής μεταβολής.

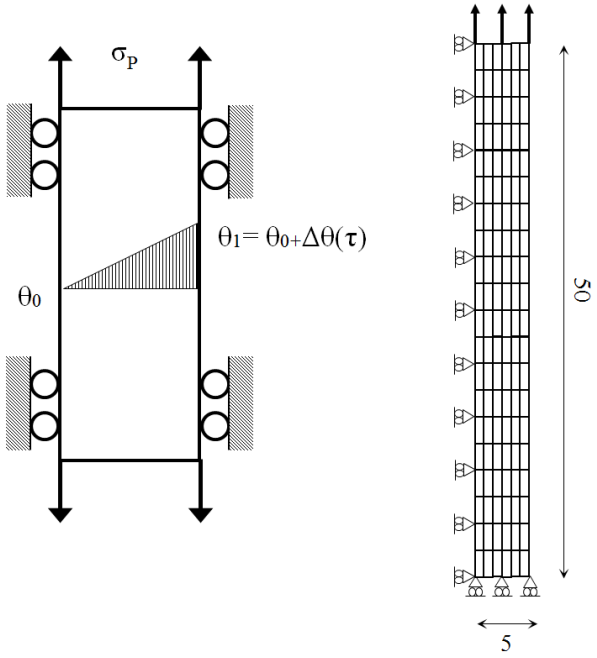

Σχήμα 18 Το πρόβλημα του Bree (γεωμετρία, φόρτιση, δίκτυο πεπερασμένων στοιχείων)

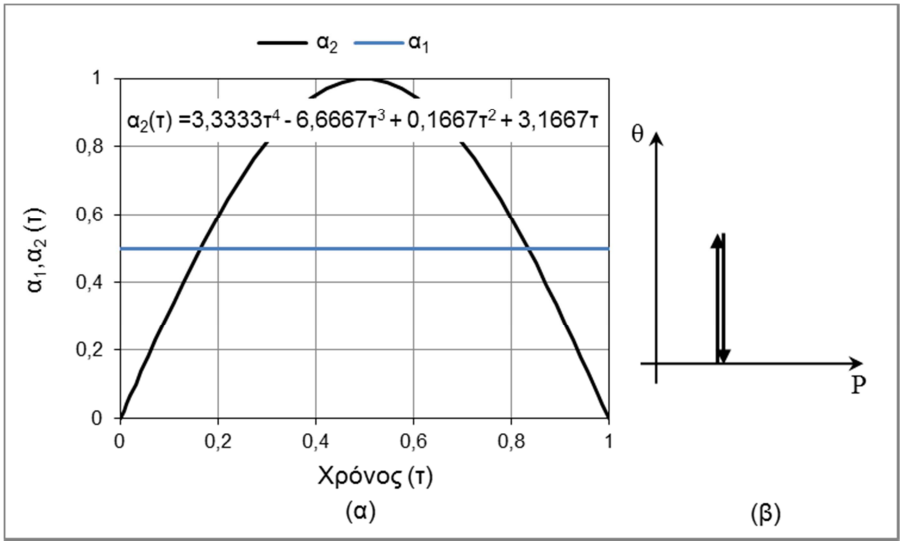

Σχήμα 19 Μεταβολή συναρτήσεων χρόνου σε μία περίοδο

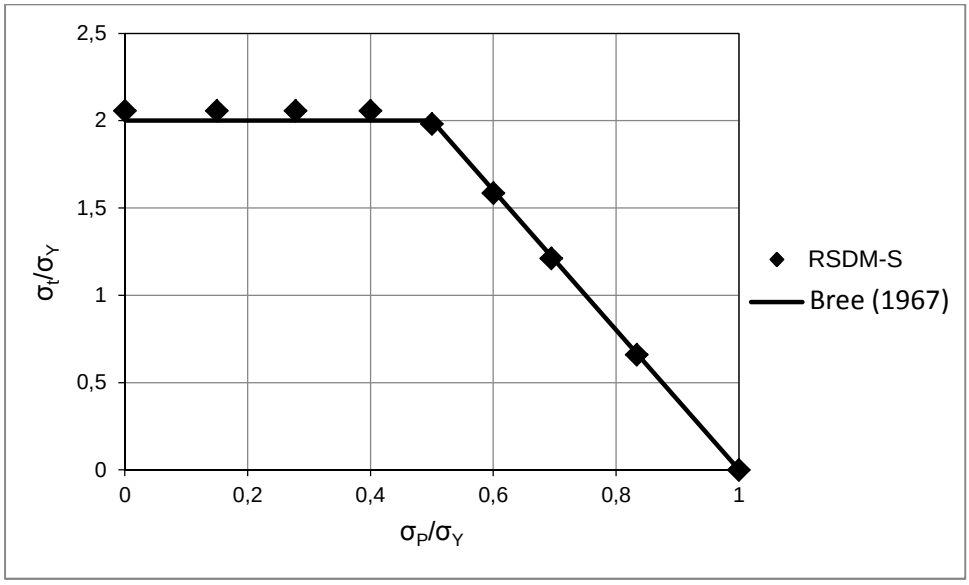

Σχήμα 20 Περιοχή ελαστικής προσαρμογής (shakedown domain)

3.2.3. Γενικευμένα χωρία φόρτισης

Η μεθοδολογία μπορεί να εφαρμοστεί κατά τον ίδιο τρόπο με προηγουμένως σε κατασκευές όπου το χωρίο φόρτισης αποτελείται από φορτία όπου έχουν την ελάχιστη τιμή τους διαφορετική από το μηδέν. Για παράδειγμα, αν θεωρήσουμε το χωρίο του σχήματος 21α τότε μπορούμε και πάλι να θεωρήσουμε ένα ισοδύναμο κυκλικό πρόγραμμα φόρτισης που περνάει από το εξωτερικό όριο του χωρίου (σχήμα 21β). Η RSDM-S εφαρμόζεται εν συνεχεία κατά τα γνωστά.

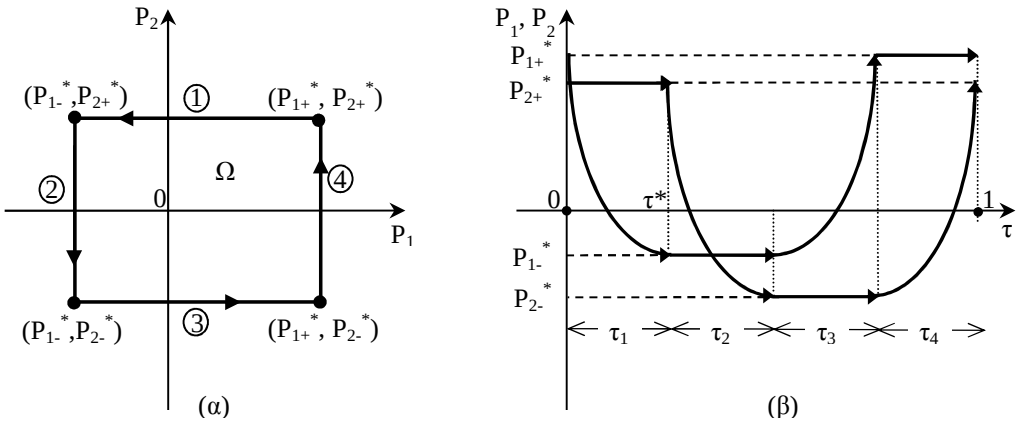

Σχήμα 21 Ανεξάρτητη κυκλική μεταβολή φορτίων α) στο χώρο των φορτίων, β) στο πεδίο του χρόνου

3.2.3.1. Παράδειγμα εφαρμογής της RSDM-S για γενικευμένα χωρία φόρτισης

Ας θεωρήσουμε τη συμμετρική δοκό της παραγράφου 3.2.1.1 ψάχνοντας όμως τον συντελεστή προσαρμογής για ένα γενικευμένο χωρίο φόρτισης.

Περιγραφή του χωρίου φόρτισης

Συγκεκριμένα, θεωρούμε το ορθογωνικό χωρίο φόρτισης του σχήματος 22. Τα φορτία μεταβάλλονται μεταξύ των ορίων $P_1 \in \left[1.2,2\right]$ και $P_2 \in \left[0,1\right]$. Ένα ισοδύναμο κυκλικό πρόγραμμα φόρτισης στο πεδίο του χρόνου που περνάει από τις τέσσερις κορυφές του ορθογωνικού χωρίου προκύπτει με τη βοήθεια των εξισώσεων του σχήματος 23.

Τα αποτελέσματα της RSDM-S και η σύγκρισή τους με αποτελέσματα της βιβλιογραφίας φαίνονται στον πίνακα 1.

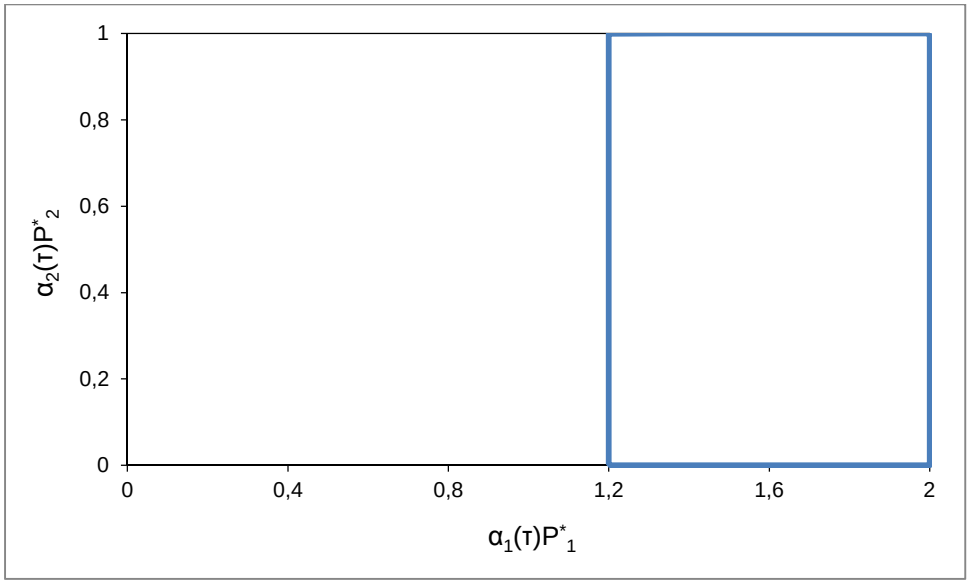

Σχήμα 22 Χωρίο φόρτισης

Συγγραφείς	Φορτίο ελαστικής προσαρμογής
Garcea *et al.* (2005)	3,244
Tran *et al.* (2010)	3,377
Pham (2011)	3,264
RSDM-S	**3,177**

Πίνακας 1. Σύγκριση των αποτελεσμάτων για τη δοκό

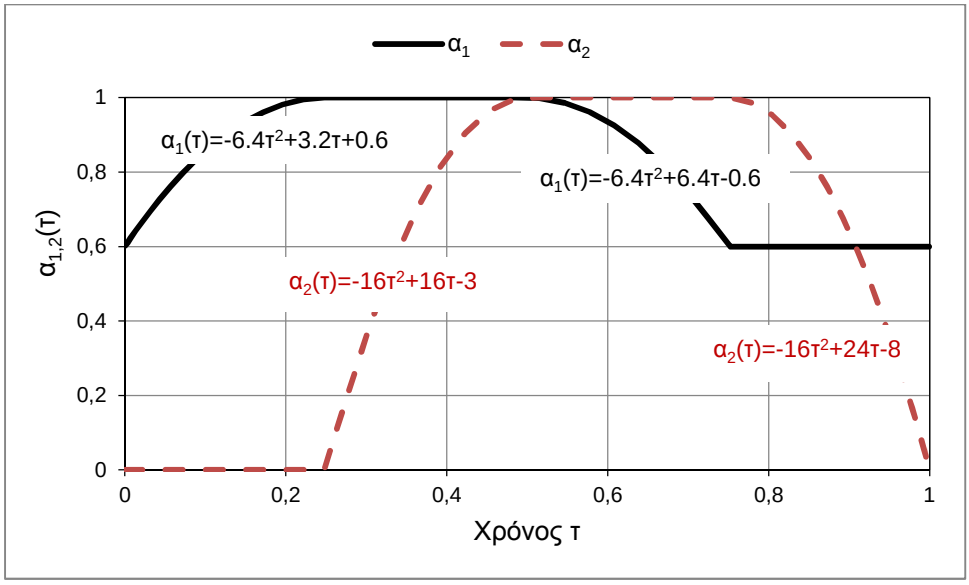

Σχήμα 23 Μεταβολή συναρτήσεων χρόνου σε μία περίοδο

3.2.4. Επέκταση της RSDM-S σε πολυδιάστατα χωρία φόρτισης.

Σε αυτή την παράγραφο θα περιγράψουμε συνοπτικά το πως υλοποιείται η επέκταση της RSDM-S για την περίπτωση θερμομηχανικής φόρτισης τριών μεταβλητών. Για το σκοπό αυτό θεωρούμε ένα σώμα που καταπονείται από δύο μηχανικά και ένα θερμικό φορτίο (σχήμα 24).

Ας θεωρήσουμε λοιπόν ότι ψάχνουμε τον συντελεστή προσαρμογής για το τρισδιάστατο χωρίο του σχήματος 25α. Η φιλοσοφία της διαδικασίας παραμένει η ίδια και ξεκινάμε μετατρέποντας το πρόβλημα σε ένα ισοδύναμο πρόβλημα θεωρώντας μία κυκλική φόρτιση στο πεδίο του χρόνου που περνάει από τις κορυφές του κύβου (σχήμα 25β). Για το σκοπό αυτό χρησιμοποιούμε τις εξισώσεις:

$$\mathbf{P}(\tau) = \begin{Bmatrix} P_1(\tau) \\ P_2(\tau) \\ \theta(\tau) \end{Bmatrix} = \begin{Bmatrix} P_1^* \cdot \alpha_1(\tau) \\ P_2^* \cdot \alpha_2(\tau) \\ \theta^* \cdot \alpha_3(\tau) \end{Bmatrix} \tag{26}$$

Στο σχήμα 25β μπορούμε να δούμε ενδεικτικές κατανομές για τα φορτία.

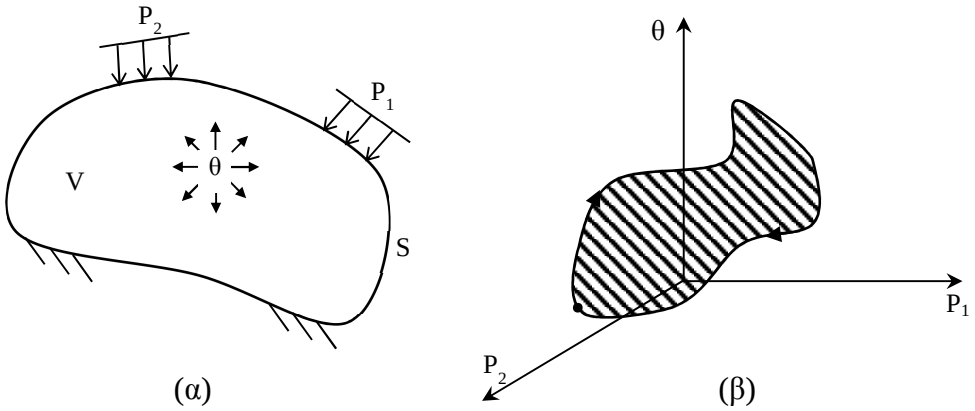

Σχήμα 24 α) Κατασκευή υπό επιβαλλόμενα φορτία, β) κυκλική φόρτιση

Η διαδικασία στη συνέχεια είναι παρόμοια με αυτή της προηγούμενης παραγράφου. Ενδεικτικά να αναφέρουμε ότι νέο διάνυσμα των παραγώγων των επικόμβιων δράσεων για τον τρέχων συντελεστή φόρτισης $\gamma^{(\mu)}$ της διαδικασίας θα δίνεται από τη σχέση:

$$\dot{\mathbf{R}} = \gamma^{(\mu)} \left\{ \dot{\alpha}_1(\tau)\mathbf{R}_{P_1^*} + \dot{\alpha}_2(\tau)\mathbf{R}_{P_2^*} + \dot{\alpha}_3(\tau) \int_V \mathbf{B}^T \mathbf{D} \mathbf{e}^{\theta^*} dV \right\} + \int_V \mathbf{B}^T \boldsymbol{\sigma}_{pl}^{(\kappa)} dV \qquad (27)$$

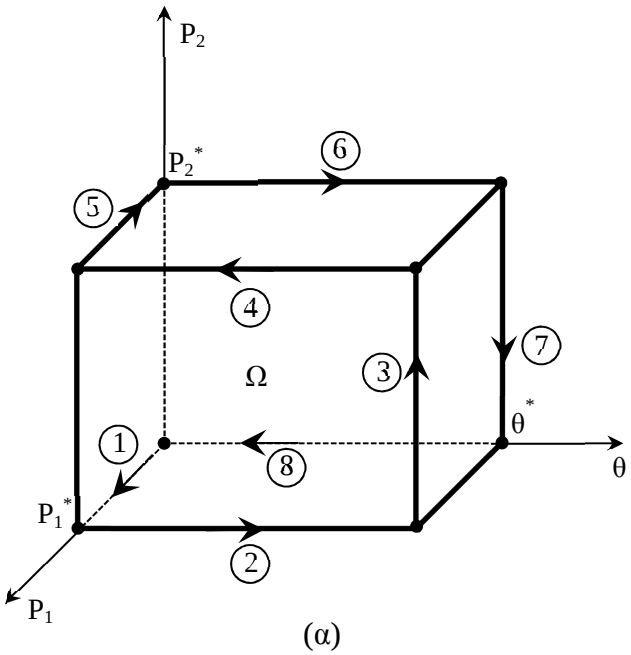

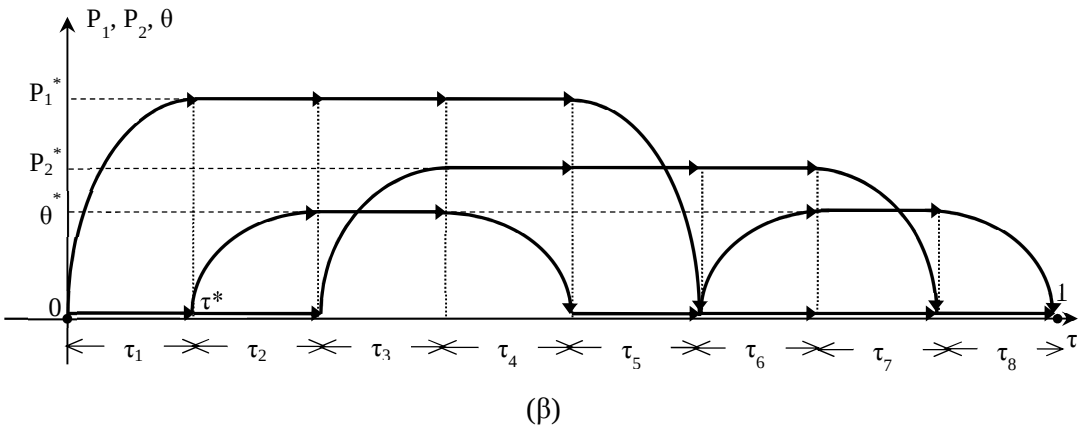

Σχήμα 25 Ανεξάρτητη κυκλική μεταβολή φορτίων α) στο χώρο των φορτίων, β) στο πεδίο του χρόνου

3.2.4.1. Παράδειγμα εφαρμογής της RSDM-S για τρισδιάστατο χωρίο φόρτισης

Ας θεωρήσουμε την πλάκα του σχήματος 26 η οποία καταπονείται από μία φόρτιση τριών μεταβλητών α) ένα οριζόντιο κατανεμημένο φορτίο, β) ένα κατακόρυφο κατανεμημένο φορτίο και γ) ένα θερμικό φορτίο δηλαδή μία θερμοκρασιακή διαφορά $\Delta\theta(t)$ μεταξύ της τρύπας και της άκρης της πλάκας.

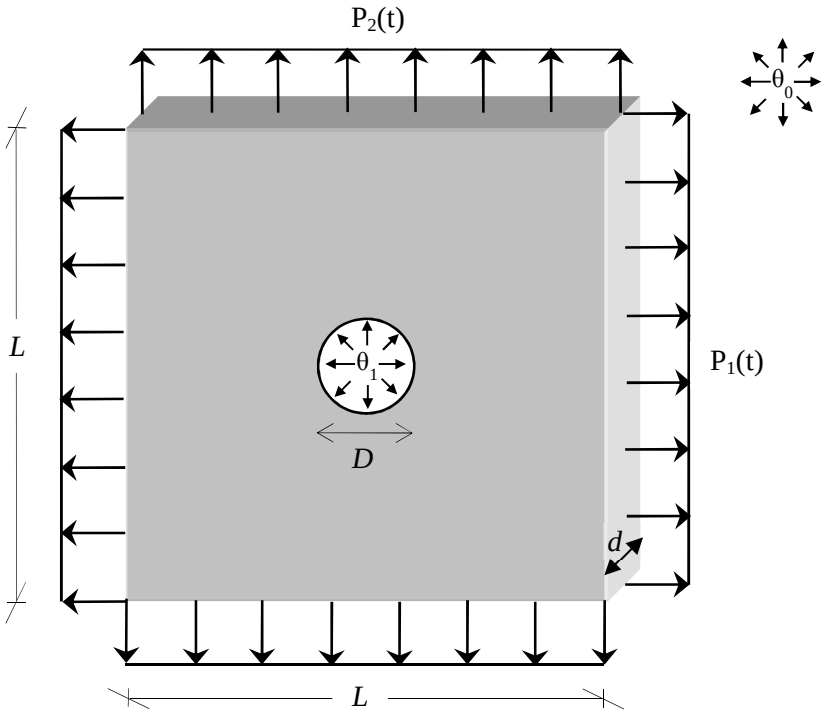

Σχήμα 26 Τετραγωνική πλάκα (γεωμετρία, φόρτιση, δίκτυο πεπερασμένων στοιχείων)

Η ακτινική μεταβολή της θερμοκρασίας στην πλάκα δίνεται προσεγγιστικά από τη σχέση:

$$\theta(r,\tau) = \theta_0 + \frac{\Delta\theta(\tau) * \ln\left(\frac{5\,D/2}{r}\right)}{\ln 5}$$

με θ_0 ίσο με μηδέν. Τα γεωμετρικά χαρακτηριστικά είναι: $D\ /\ L = 0.2$, $d\ /\ L = 0.05$ και $L = 20cm$. Οι ιδιότητες του υλικού είναι: $E = 208Gpa$, $\nu = 0.3$ και $\sigma_Y = 360Mpa$.

Περιγραφή του χωρίου φόρτισης

Θεωρούμε το τρισδιάστατο χωρίο φόρτισης του σχήματος 28. Τα φορτία μπορούν να μεταβάλλονται ανεξάρτητα μεταξύ τους σε αυτό το χωρίο που ορίζεται από τα όρια: $P_1 \in \left[0, P_1^*\right], P_2 \in \left[0, P_2^*\right], \Delta\theta \in \left[0, \Delta\theta^*\right]$ όπου οι μέγιστες τιμές είναι $P_1^* = P_2^* = \Delta\theta^* = 1$.

Μία ισοδύναμη φόρτιση στο πεδίο του χρόνου που περνάει από τις οχτώ κορυφές του χωρίου μπορεί να οριστεί με τη βοήθεια των εξισώσεων (σχήμα 28):

$P(\tau) = \begin{Bmatrix} P_1^*\alpha_1(\tau) \\ P_2^*\alpha_2(\tau) \\ \Delta\theta^*\alpha_3(\tau) \end{Bmatrix}$ όπου οι συναρτήσεις χρόνου $\alpha_1(\tau), \alpha_2(\tau), \alpha_3(\tau)$ είναι:

$$\alpha_1(\tau) = 0,\ \ \alpha_2(\tau) = -16\tau^2 + 16\tau - 3,\ \ \alpha_3(\tau) = 0,\ \ \tau \in [0, 1/8]$$
$$\alpha_1(\tau) = 0,\ \ \alpha_2(\tau) = 1,\ \ \alpha_3(\tau) = -64\tau^2 + 32\tau - 3,\ \ \tau \in (1/8, 2/8]$$
$$\alpha_1(\tau) = -64\tau^2 + 48\tau - 8,\ \ \alpha_2(\tau) = 1,\ \ \alpha_3(\tau) = 1,\ \ \tau \in (2/8, 3/8]$$
$$\alpha_1(\tau) = 1,\ \ \alpha_2(\tau) = 1,\ \ \alpha_3(\tau) = -64\tau^2 + 48\tau - 8,\ \ \tau \in (3/8, 4/8]$$
$$\alpha_1(\tau) = 1,\ \ \alpha_2(\tau) = -64\tau^2 + 64\tau - 15,\ \ \alpha_3(\tau) = 0,\ \ \tau \in (4/8, 5/8]$$
$$\alpha_1(\tau) = 1,\ \ \alpha_2(\tau) = 0,\ \ \alpha_3(\tau) = -64\tau^2 + 96\tau - 35,\ \ \tau \in (5/8, 6/8]$$
$$\alpha_1(\tau) = -64\tau^2 + 96\tau - 35,\ \ \alpha_2(\tau) = 0,\ \ \alpha_3(\tau) = 1,\ \ \tau \in (6/8, 7/8]$$
$$\alpha_1(\tau) = 0,\ \ \alpha_2(\tau) = 0,\ \ \alpha_3(\tau) = -64\tau^2 + 112\tau - 48,\ \ \tau \in (7/8, 1]$$

Τελικά, η συνολική 3Δ περιοχή ελαστικής προσαρμογής (shakedown domain) του προβλήματος φαίνεται στο σχήμα 29. Να σημειώσουμε ότι κάθε λύση για

καθορισμένους διαφορετικούς λόγους P_1^* / P_2^*, αναπαριστά μία καθορισμένη γωνία φ στο επίπεδο $P_1 - P_2$ (σχήμα 29).

Ο υπολογιστικός χρόνος CPU που χρειάστηκε η RSDM-S για να συγκλίνει σε αυτό το παράδειγμα ήταν της τάξης των 50 δευτερολέπτων, σε έναν σταθμό εργασίας με επεξεργαστή των εξής χαρακτηριστικών: Intel Core i7 στα 2.93 GHz με 4096 MB RAM.

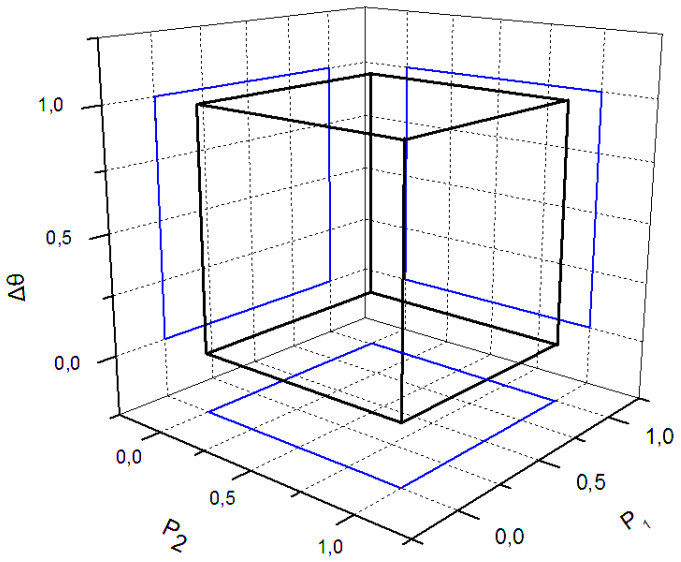

Σχήμα 27 Τρισδιάστατο χωρίο φόρτισης

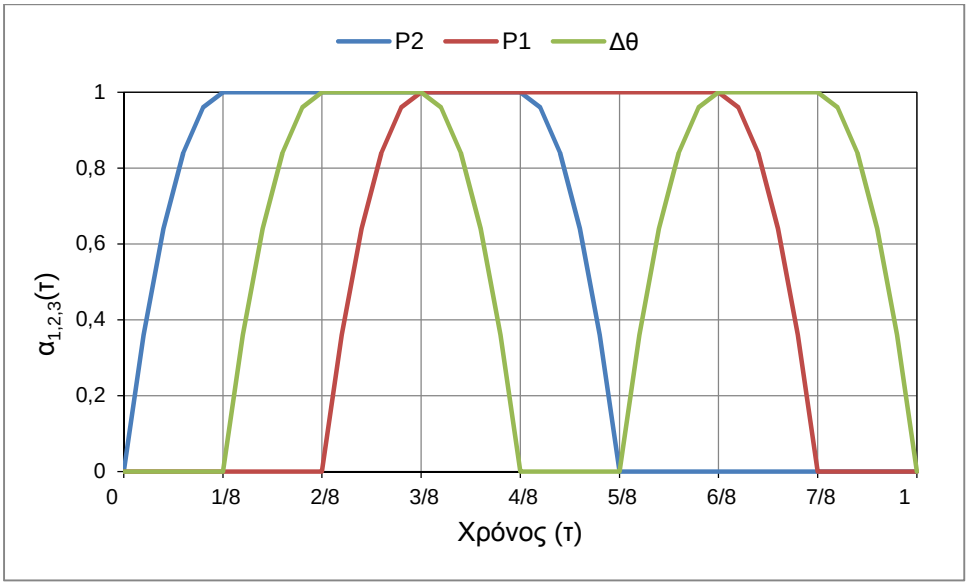

Σχήμα 28 Μεταβολή συναρτήσεων χρόνου σε μία περίοδο

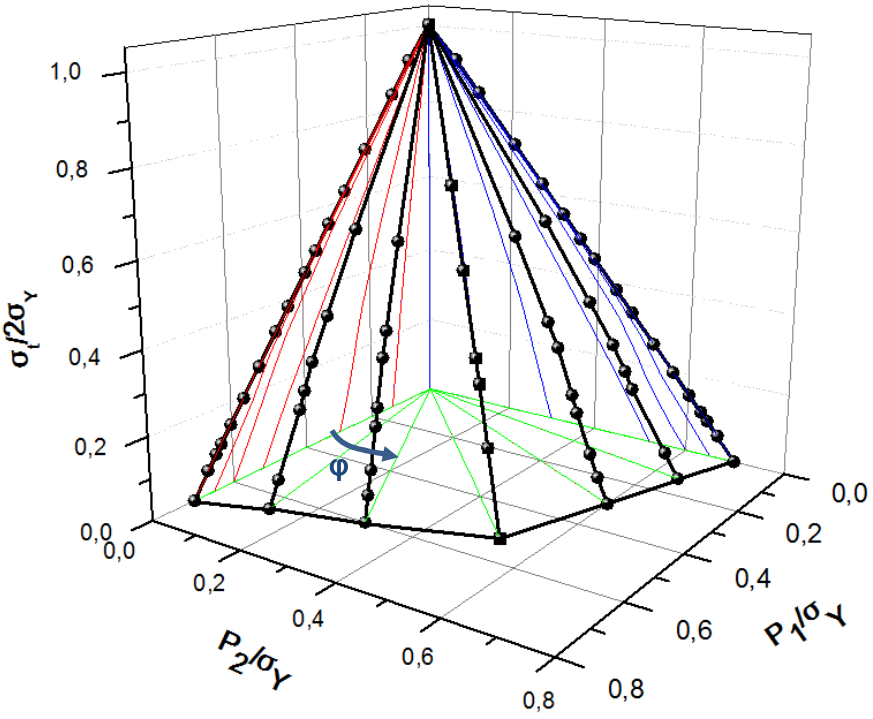

Σχήμα 29 3Δ περιοχή ελαστικής προσαρμογής (3D elastic shakedown domain)

4. Συμπεράσματα:

Συνοψίζοντας λοιπόν όλα τα παραπάνω, κατά τη διάρκεια της παρούσας διατριβής αναπτύχθηκαν δύο νέες αριθμητικές μεθοδολογίες που αφορούν τη συμπεριφορά κατασκευών υπό ανακυκλιζόμενη φόρτιση. Συγκεκριμένα:

α) αναπτύχθηκε η άμεση μέθοδος RSDM [1,4] η οποία προσδιορίζει το είδος της κυκλικής ελαστοπλαστικής συμπεριφοράς που θα οδηγηθεί μία κατασκευή υπό ανακυκλιζόμενα φορτία. Εάν δηλαδή μία ελαστοπλαστική κατασκευή υπό ανακυκλιζόμενη φόρτιση θα οδηγηθεί είτε σε ελαστική προσαρμογή (elastic shakedown), είτε σε εναλλασσόμενη πλαστικοποίηση (alternating plasticity) ή σε επαυξητική κατάρρευση (incremental collapse).

β) αναπτύχθηκε η νέα αριθμητική μέθοδος RSDM-S [2,5] για τον προσδιορισμό του φορτίου ελαστικής προσαρμογής (elastic shakedown load) κατασκευών υπό ανακυκλιζόμενη φόρτιση. Η μέθοδος αρχικά διατυπώθηκε για μηχανικά φορτία και στη συνέχεια επεκτάθηκε ώστε να λαμβάνει υπόψη και θερμικά φορτία [3]. Τέλος,

η αριθμητική διαδικασία αναπτύχθηκε και για την ανάλυση προσαρμογής κατασκευών υπό πολυδιάστατα χωρία φόρτισης.

Για καθεμία από τις παραπάνω περιπτώσεις αναπτύχθηκε κι ο αντίστοιχος αλγόριθμος σε περιβάλλον Fortran.

Κατά τη διάρκεια της διατριβής δημοσιεύτηκαν οι παρακάτω πρωτότυπες εργασίες σε:

Α) διεθνή επιστημονικά περιοδικά:

[1] Spiliopoulos K.V., Panagiotou K.D., A direct method to predict cyclic steady states of elastoplastic structures. Comput. Methods Appl. Mech. Engrg. **223**, 186-198 (2012).

[2] Spiliopoulos K.V., Panagiotou K.D., A Residual Stress Decomposition Based Method for the Shakedown analysis of structures. Comput. Methods Appl. Mech. Engrg., **276**, 410-430 (2014).

[3] Spiliopoulos K.V., K.D. Panagiotou K.D., A numerical procedure for the shakedown analysis of structures under thermomechanical loading. Arch. Appl. Mech., doi: 10.1007/s00419-014-0947-6 (2014).

[*] Panagiotou K.D., Spiliopoulos K.V., Shakedown analysis of civil engineering structural elements. Engineering and Computational Mechanics, Proc. of the Institution of Civil Engineers, (accepted for publication) (2015).

Β) κεφάλαια επιστημονικών βιβλίων

[4] Spiliopoulos K.V., Panagiotou K.D., The Residual Stress Decomposition Method (RSDM): A Novel Direct Method to Predict Cyclic Elastoplastic States. In: K. Spiliopoulos and D. Weichert (Eds.), Direct Methods for Limit States in Structures and Materials, Springer Science + Business Media, Dordrecht, 139-155 (2014).

[5] Spiliopoulos K.V., Panagiotou K.D., RSDM-S: A Method for the Evaluation of the Shakedown Load of Elastoplastic Structures. In: P. Fuschi, A. Pisano and D. Weichert (Eds.), Direct Methods for Limit and

Shakedown Analysis of Structures, Springer International Publishing, 159-175 (2015).

Γ) διεθνή επιστημονικά συνέδρια και συμπόσια

[6] Spiliopoulos K.V., Panagiotou K.D., “A Direct Method for the Cyclic Elastoplastic Analysis of Simple Structures”, Proc. 3rd Intern. Conf. Nonlinear Dynamics, Kharkov, September 2010.

[7] Spiliopoulos K.V., Panagiotou K.D., “A Direct Method for the Cyclic Plasticity of Structures”, 4th Serbian-Greek Symposium on Recent Advances in Mechanics, Vlasina Lake, Serbia, 9 -10 September 2011.

[8] Spiliopoulos K.V., Panagiotou K.D., “A Computational Procedure for the Cyclic Steady State Elastoplastic Analysis of Structures”, Proc. COMPLAS XI, Barcelona, September 2011.

[9] Spiliopoulos K.V., Panagiotou K.V., “The Residual Stress Decomposition Method (RSDM): A Novel Direct Method to Predict Cyclic Elastoplastic States”, 3rd International Workshop on Direct Methods, Athens, 20-21 February 2012.

[10] Spiliopoulos K.V., Panagiotou K.D., “A New Numerical Approach for the Evaluation of the Shakedown Load of Elastoplastic Structures”, 8th German-Greek-Polish Symposium on Recent Advances in Mechanics, Goslar, Germany, 9-13 September 2013.

[11] Spiliopoulos K.V., Panagiotou K.D., “A Computational Method for the Shakedown Analysis of Structures”, Euromech 548, Direct and Variational Methods for non smooth problems in Mechanics, Amboise, 2013.

[12] Spiliopoulos K.V., Panagiotou K.D., “Extension of the RSDM to the Shakedown Analysis of Structures”, 4th International Workshop on Direct Methods, Reggio di Calabria, Italy, 1-2 October 2013.

[13] Panagiotou K.D., Spiliopoulos K.V., “Shakedown analysis of structures under thermomechanical loading based on the RSDM”, WCCM-XI, Barcelona, 2014.

Contents

1. Introduction

1.1. Motivation

The high level of loadings, that most civil and mechanical engineering structures are subjected to, force them to develop irreversible strains, such as plastic strains. For civil engineering structures, like bridges, pavements, buildings, and offshore structures, such typical loadings are heavy traffic, earthquakes or waves. On the other hand, the coexistence of thermal and mechanical loadings on mechanical engineering structures, like, for example, nuclear reactors and aircraft propulsion engines, leads them also to stress regimes well beyond their elastic limit.

The complete response of a structure, which is subjected to a given thermo-mechanical loading and exhibits inelastic time-independent plastic strains, is quite complex. The reason of the complexity is the need to perform cumbersome time stepping calculations. A much better alternative, that requires much less computing time, is offered by the direct methods that may predict whether, under the given loading, the structure will become unserviceable due to collapse or excessive inelastic deformations. Moreover, it very often happens that the complete time history of loading is not known, but only its variation intervals. In these cases, direct methods are the only way to establish safety margins.

Based on the fact that for structures made of stable materials (Drucker, 1959) an asymptotic state exists, direct methods try to estimate this state right from the start of

the calculations. Typical examples of such methods are the limit analysis for monotonic loading and the shakedown analysis for loading varying cyclically. Most of the numerical approaches towards the solution of the shakedown problem are based on either the lower or the upper bound theorems and they are cast in the form of mathematical programming (MP). The disadvantage of these methods is that they usually lead to optimization problem that needs special algorithms for its solution. Thus, they are not easily implemented in finite element codes.

Therefore, the need for developing efficient numerical approaches that based on physical arguments and that are directly implementable in existing FE codes is of great importance.

1.2. Aim and objectives

Considering the above, the aim of this work is to develop numerical approaches that address the limit states of cyclically loaded elastoplastic structures, based on a different framework of the optimization algorithms. To that end, the main objectives were:

- To develop a numerical approach that predicts the characteristics of the cyclic steady state of an elastic-perfectly plastic structure under a given cyclic loading history.
- To develop a direct method for the shakedown analysis of structures in order to provide safety margins for cyclically loaded elastoplastic structures.

Both the two methodologies exploit the cyclic nature of the residual stresses distribution at the steady cycle.

1.3. Organization and outline

The current introductory chapter describes the motivation and the objectives of this thesis. A short outline of the current thesis is described in this section. Furthermore, an illustration of the outline may be seen in Fig.1.1.

In **Chapter 2** a literature review on the topic of limit states of cyclically loaded structures may be found. A historical sketch on the shakedown theory, as well as recent developments on this field are extensively described.

Chapter 3 presents some fundamentals in plasticity i.e. the von Mises yield function and its properties, the Drucker's postulate as well some basic principles.

In **Chapter 4** a description of the shakedown theory is presented. The chapter begins with a discussion on the limit states of cyclically loaded structures. A presentation of the concept of the shakedown domain and of the steady cycle is following. An analytical description of the shakedown theorems and the parameters of the limit cycle are presented next. Finally, a simple example is being considered in order to illustrate the limit states of shakedown, alternating plasticity and incremental collapse.

In **Chapter 5** the developed numerical approaches in this work are described. In the first part, a procedure for the cyclic limit states of elastoplastic structures, named RSDM, is proposed. Moreover, in the second part, a novel direct method for the shakedown analysis of structures is presented. The formulation of this method, which is in short called RSDM-S, for the evaluation of shakedown limits of structures under cyclic thermomechanical loadings is following.

Chapter 6 is dedicated to the validation of the developed procedures, described in the previous chapter, through some numerical examples. Initially, examples on the prediction of cyclic elastoplastic states, using the RSDM, are presented. The second part, contains several applications of the RSDM-S on the shakedown analysis of elastoplastic structures under thermal or/and mechanical cyclic loadings.

Finally, a summary of the work is given in **Chapter 7,** along with a discussion about recommendations for future work and extensions of the developed procedures.

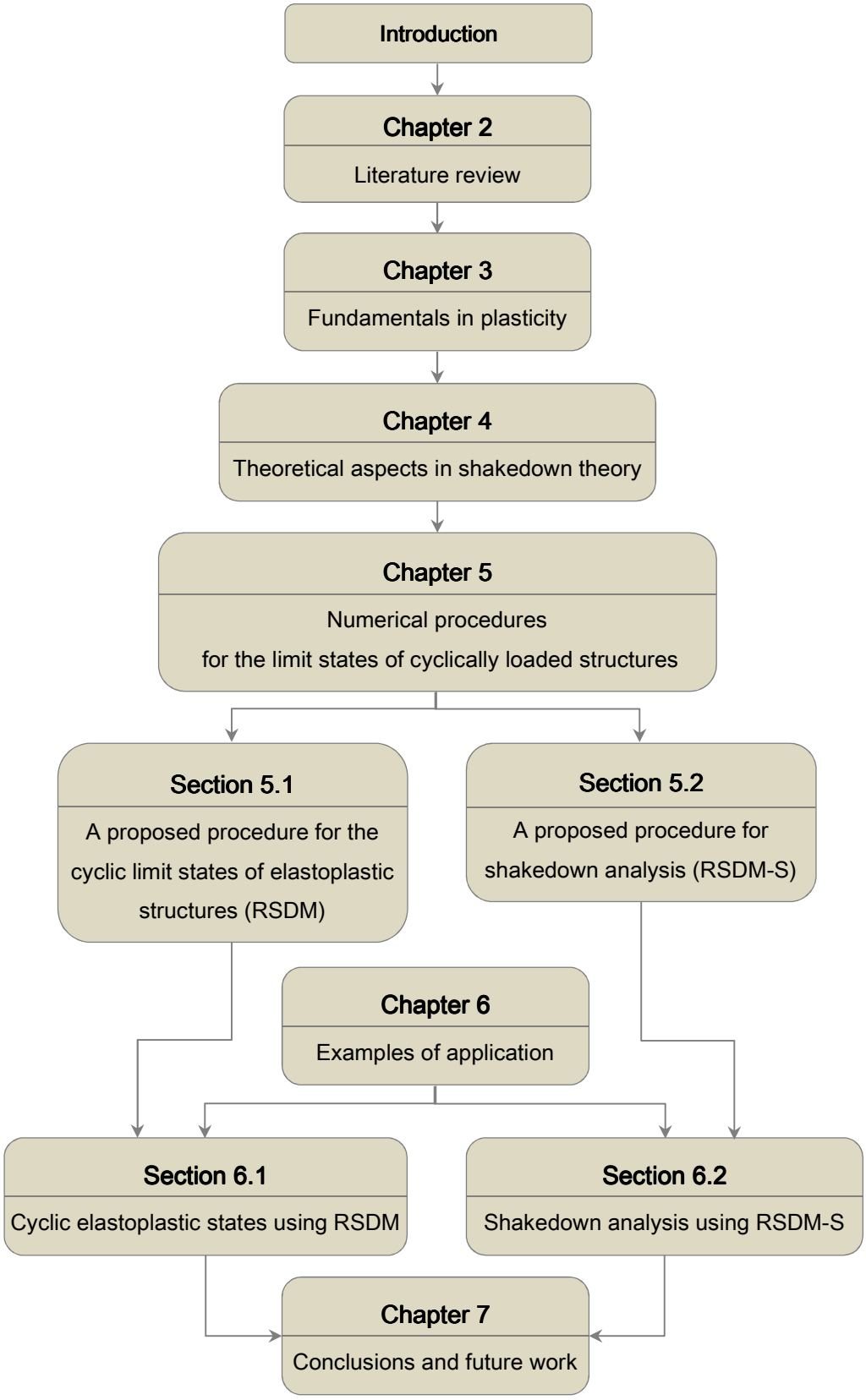

Figure 1.1 Outline of the thesis

2.

Literature review

2.1. A Historical sketch on the Shakedown theory – From the beginnings to the classical formulation of the shakedown theorems

Plastic design of structures came into the picture of structural engineering in the beginning of the 20th century, when steel was increasingly used in civil engineer constructions like steel bridges and steel skeleton buildings. Engineers found that the commonly used elastic design was very conservative, thus plastic design became a major issue for this type of structures in the 2nd decade. Therefore related studies were first focused on the load carrying capacity of beams and trusses under monotonically increasing, “dead” loading.

Afterwards, the extension of these studies to the problem of plastic design of structures under variable loads took place. In this section, a short historical view on shakedown theory will be presented, based on the survey work of Weichert and Ponter (2014).

In 1926 Martin Grüning was the first to discuss the beneficial effect of limited plastic deformation in hyperstatic truss elements under repeated loading: Plastic deformation occurring in the first cycles of loading may lead to a redistribution of stresses having as a consequence some members of the structure respond elastically for higher load levels than the elastic limit. He pointed out that the collapse

loads obtained by limit analysis may fail to provide a safety measure in the case of repeated loads. His works (Grüning, 1925, 1926) might be considered as the first appearance of the idea of shakedown.

The initial stage of development of the shakedown theory dates to the 30s and is connected with bar structures in civil engineering. Hans Bleich (1932) was inspired from Grüning's work and he proved the static shakedown theorem (or lower bound shakedown theorem) for a system of beams of ideal I –cross–sections. It was Bleich who gave a closer meaning to the today's notion of shakedown.

In 1936 Melan formulated a more general lower bound theorem for bar systems and later in 1938 extended it to the general case of a continuum in his key work "Der Spannungszustand eines Mises-Hencky'schen Kontinuums bei veränderlicher Belastung" (Melan, 1938a). It is worth mentioning that the shakedown theory was developed quite independently of the limit analysis theory. It is known that Gvozdev in 1936 arrived at his fundamental results of the limit analysis of elastic-plastic structures under a single load.

Although Melan's theorem was powerful enough, there was no scientific evolution to this direction for many years due to the second world war. It was Prager then who came back to the problem in his work "Problem types in theory of perfectly plastic materials" in 1948. It should be mentioned that Prager was the first who introduced the term "Shakedown".

Besides Prager, Symonds and Neal should be also mentioned, as they have a great contribution in the determination of limit loads for frame structures under variable loads with their works (Symonds and Prager 1950; Symonds 1951; Neal 1950; Symonds and Neal 1951a,b; Neal and Symonds 1951). Their paper (Symonds and Neal 1951a), "Recent progress in the plastic methods of structural analysis" is of great importance as it is a first idea of the upper bound theorem of shakedown. Moreover, Symonds (1950), formulated for a first time an upper bound approach in shakedown theory for frames as well as he simplified the proof of Melan's theorem (Symonds 1951) in a form adopted by Koiter in 1960.

It was Koiter in 1956 who formulated the upper bound theorem of shakedown in a general form in his paper “A new general theorem of shakedown of elastic-plastic structures”.

Prager (1956) and Rozenblum (1957) further extended the Melan’s theorem to account for thermal stresses while later Rozenblum (1965) and De Donato (1970) extended the upper bound theorem to allow for thermal loadings.

On the other hand, Gokhfeld (1966) and Sawczuk (1967) derived from Koiter’s theorem a criterion of incremental collapse.

Summarizing the above, we could say that, mainly, with Koiter’s formulation, the first major step in the development of shakedown theory has been accomplished.

During the second half of the twentieth century, the parallel development of the computers, material models, finite element method and the mathematical programming algorithms encouraged a large number of contributions to shakedown analysis.

2.2. Development of numerical methods on cyclic states

2.2.1. Motivations of Direct Methods

In many structural engineering problems the crucial issue is the estimation of the “safety factor” or the “life cycle assessment” of structures with respect to limit states. This task is practically impossible to be addressed by performing time consuming incremental analysis which additionally, requires the complete knowledge of the loading history. However, only variation intervals of the loads are known, unlike the usual description of a particular loading history. Methods that aim toward this end, avoiding step-by-step calculations, are called *Direct Methods* (Maier *et al*. 2003). In fact, the fundamental question about whether, or not, critical load or cycles do exist, independent of loading histories, can only be answered by the Direct Methods. Furthermore, if an incremental elastic-plastic analysis for a particular loading program converges to a safe state, there is still no guaranty that another loading history,

having the same amplitudes, would not produce alternating plasticity or incremental collapse.

Thus, such methods have an increasing role in structural analysis and design.

2.2.2. The computational optimization framework

Most of the developed direct methods towards the solution of the shakedown problem are based on either the lower or the upper bound theorems. They are cast in the form of mathematical programming (MP) aiming to maximize or minimize an objective function which normally represents the loading factor.

In the first period of the MP techniques for the shakedown analysis, the problem of shakedown was treated as a linear programming (LP) problem (Maier, 1969). The basis of these methods is the linearization of the yield surfaces involved and the classical Simplex algorithm (Vanderbei, 2001) was the mathematical programming method for their solution.

A typical LP problem has the following form:

$$\left.\begin{array}{ll} \text{minimize} & \mathbf{c}^T\mathbf{x} \\ s.t. & \mathbf{A}\mathbf{x}=\mathbf{b} \\ & \mathbf{x}\geq\mathbf{0} \end{array}\right\}\left(LP\right) \tag{2.1}$$

where $\mathbf{c},\mathbf{x}\in\mathbb{R}^{n\times 1}$, $\mathbf{A}$ is in $\mathbb{R}^{m\times n}$ and $\mathbf{b}\in\mathbb{R}^{m\times 1}$. The vector $\mathbf{x}$ represents the vector of variables to be determined.

Indeed, most of the early extensions of shakedown fundamentals have been obtained in the framework of LP theory (e.g. Maier, 1970; Cohn and Maier, 1977; König and Maier, 1981). The issue of linear programming, applied to shakedown may be found in the survey article by Maier *et al.*, 2000. Examples of more recent relevant achievements can be found in (Ngo and Tin-Loi, 2007; Ardito *et al.*, 2008).

However, even in the simplest case of a von Mises yield condition, due to the fact that the yield condition is nonlinear, the resulting MP problem is a nonlinear programming problem. A typical form of a NLP is:

$$\left.\begin{array}{ll} \text{minimize} & \mathbf{c}^T\mathbf{x} \\ s.t. & \mathbf{g}(\mathbf{x}) \leq \mathbf{0} \\ & \mathbf{A}\mathbf{x} = \mathbf{b} \end{array}\right\} \left(NLP\right) \tag{2.2}$$

where $\mathbf{A}$ is in $\mathbb{R}^{m\times n}$, $\mathbf{c},\mathbf{x} \in \mathbb{R}^{n\times 1}$, $\mathbf{b} \in \mathbb{R}^{m\times 1}$ and $\mathbf{g}(\mathbf{x}) : \mathbb{R}^n \rightarrow \mathbb{R}^p$ is a vector of convex and twice continuously differentiable functions representing the yield condition.

Summarizing the above, if the involved yield criteria are linear or piecewise linearized, the optimization problem becomes a linear programming (LP) problem.

Otherwise, if the yield surfaces are kept as nonlinear functions, due to the convexity of the discretized resulted MP from e.g. the statical approach of shakedown, it is a Convex Nonlinear Programming (CNLP) problem with a great number of variables and nonlinear constraints.

Discretization of the optimization problem with FEM

The resulting nonlinear optimization problem for i.e. the static shakedown theorem for an elastic-perfectly plastic structure is solved, with the use of the finite element method, in a discretized form, which is defined by

$$\left.\begin{array}{ll} \text{maximize} & a \\ s.t. & \sum_{i=1}^{NG} \mathbf{C}_i\overline{\boldsymbol{\rho}}_i = \mathbf{0} \\ & \forall j \in \left[1, NV\right], \quad \forall i \in \left[1, NG\right] \\ & F(a\boldsymbol{\sigma}_i^{E,j} + \overline{\boldsymbol{\rho}}_i) \leq \sigma_{Y,i}^2 \end{array}\right\} \tag{2.3}$$

where a is the loading factor need to be maximized; NG is the number of Gauss points of the structure; NV is the number of the load vertices of the load domain and $\mathbf{C}_i$ is the equilibrium matrix that takes into account the boundary conditions. It is obvious that the restrictions of the optimization problems are checked only in the Gauss points.

The discretization of the continuum by a large number of finite elements and the big number of constrains often lead to the solution of large size optimization

problems. To solve these problems various numerical techniques have been developed. A short description of these numerical techniques will be presented next.

For each numerical approach, some basic references are given.

2.2.3. Interior point algorithms for convex programming

Interior point methods (IPM) (also referred to as barrier methods) are a certain class of algorithms to solve linear and nonlinear convex optimization problems (Vanderbei, 2001). Their name reflects the fact that the points generated by the algorithms lie in the interior of the feasible region. This is in contrast to the Simplex method which is an active set method, moving along the boundary of the feasible region. An interior point algorithm is proven to be polynomial in a measure of the problem data but the number of required iterations does not increase proportionally to the size of the problem. Thus, it is a very useful tool to the shakedown analysis of large-scale engineering structures.

The key of the interior point methods is, after introducing some slack variables that replace the inequality constraints with equality constraints, to add some *barrier terms* in the objective function which are connected with those variables. These barrier terms penalize directions leading outside the feasible region. The simplest such barrier function is the logarithmic and the new objective function improves the ability to apply calculus to its study. Denoting with μ the barrier parameter and introducing the slack vector $\mathbf{z} \in \mathbb{R}^p$ we may write the following μ-parametrized NLP:

$$\begin{aligned} \text{minimize} \quad & \mathbf{c}^T\mathbf{x} - \mu\sum_{i=1}^{p}\ln(z_i) \\ s.t. \quad & \mathbf{g}(\mathbf{x}) + \mathbf{z} = \mathbf{0} \\ & \mathbf{A}\mathbf{x} = \mathbf{b} \end{aligned} \tag{2.4}$$

with $\mathbf{z} > \mathbf{0}$. The necessary and sufficient optimal conditions, or KKT System, for this problem are

$$\begin{aligned} \mathbf{g}(\mathbf{x}) + \mathbf{z} &= \mathbf{0} \\ \mathbf{c} - \mathbf{A}^T\mathbf{y} + \left(\frac{\partial \mathbf{g}}{\partial \mathbf{x}}\right)\mathbf{w} &= \mathbf{0} \\ \mathbf{A}\mathbf{x} - \mathbf{b} &= \mathbf{0} \\ \mathbf{Z}\mathbf{w} - \mu\mathbf{e} &= \mathbf{0} \end{aligned} \tag{2.5}$$

with $\mathbf{y} \in \mathbb{R}^m$, $\mathbf{w} \in \mathbb{R}^p$ vectors of multipliers and $\mathbf{w}, \mathbf{z} \geq \mathbf{0}$; $\partial \mathbf{g} / \partial \mathbf{x} = \left\{ \partial g_i(\mathbf{x}) / \partial x_j \right\}$ is the $p \times n$ Jacobian matrix of the nonlinear constraints.

After applying the Karush-Kuhn-Tucker (KKT) conditions a system of nonlinear equations is results, which is usually solved iteratively using the Newton method.

Based on the interior point method a variety of powerful algorithms or related techniques have been developed by many authors either for limit or shakedown analysis e.g. Pastor and Loute, 2005; Akoa *et al.*, 2007; Krabbenhøft *et al.*, 2007c; Hachemi *et* al., 2009; Tran *et al.*, 2010; Simon and Weichert, 2011; Garcea and Leonetti, 2011; Simon and Weichert, 2012; Simon *et al.*, 2013;).

Moreover, a number of alternative algorithms based on Newton iterations have been presented (e.g. Zouain *et al.*, 2002; Lyamin and Sloan, 2002, Vu *et al.*, 2004; Vu and Staat, 2007). The optimization problem was solved in (Hachemi and Weichert, 1998) based on an augmented Lagrangian method combined with the Broyden–Fletcher–Goldfarb–Shanno (BFGS) algorithm.

2.2.4. Second order cone programming

A key concept within the IPMs for CNLP is the Conic Programming (CP) problem i.e. the solution of a minimization problem with linear objective function and feasible region defined by some cone (Nesterov and Nemirovskii, 1994). A special case of CP is the Second Order Cone Programming (SOCP) that can be solved with great efficiency by interior point methods.

In a SOCP a linear function is minimized over the intersection of an affine set with the product of second-order (quadratic) cones. A typical form of a SOCP is the following:

$$\left.\begin{array}{ll} \text{minimize} & \mathbf{c}^T\mathbf{x} \\ s.t. & \left\|\mathbf{A}_i\mathbf{x}+\mathbf{b}_i\right\| \le \mathbf{g}_i{}^T\mathbf{x}+\mathbf{d}_i, \quad i=1,2,\ldots,m \end{array}\right\}(SOCP) \tag{2.6}$$

where the problem parameters are $\mathbf{c},\mathbf{x}\in\mathbb{R}^n$, $\mathbf{A}_i$ is in $\mathbb{R}^{n_i\times n}$, $\mathbf{b}_i\in\mathbb{R}^{n_i}$, $\mathbf{g}_i\in\mathbb{R}^n$, $\mathbf{d}_i\in\mathbb{R}$. Here, $\mathbf{x}\in\mathbb{R}^n$ is the optimization variable.

Concerning the connection between the SOCP problem and the shakedown problem, a discretized formulation of the shakedown theorems is usually worked out, leading to a SOCP problem, for which efficient algorithms exists (Makrodimopoulos and Bisbos, 2003). Following (Christiansen and Andersen, 1999) Second Order Cone Programming has been used by many authors in the field of direct methods e.g. Bisbos *et al.*, 2005; Makrodimopoulos, 2006; Krabbenhøft *et al.*, 2007a; Pastor *et al.*, 2008; Munoz *et* al., 2009; Bisbos and Ampatzis, 2008; Skordeli and Bisbos, 2010, Skordeli, 2010 among others. A widely used software package for SOCP is MOSEK (Andersen *et al.*, 2003, 2009).

2.2.5. The basis reduction technique

Another method for handling large-scale optimization problems is the basis reduction technique or subspace iteration that keeps only a small number of unknowns. The method for the perfectly plastic behavior and for solving a linear optimization problem was proposed in (Shen, 1986) and then extended to nonlinear optimization problem in (Zhang, 1991), (Gross-Weege, 1997), (Staat and Heitzer, 1997), (Heitzer, 1999) using the same constitutive setting. The extension to the more realistic bounded kinematic hardening material has been achieved in (Stein *et* al., 1993; Heitzer *et al.*, 2000). A short description of the method is presented next.

Instead of searching the whole vector space B for a solution to the optimization problem, a d-dimensional subspace B_d is searched. Iteratively, a different subspace B_d^k is chosen in the k-th step of the algorithm to improve the current load factor a^{k-1}. The dimension of the chosen subspace is rather small compared to the dimension of B, typically $\dim B_d^k = d \le 6$. The subspaces $B_d^k \subset B$ could be

generated by d linear independent base vectors $\boldsymbol{\rho}^{k,r}$, $r=1,...,d$, such that for all $\boldsymbol{\rho}^k \in B_d^k$ there exists $\mu_1,...,\mu_d \in \mathbb{R}$ with

$$\boldsymbol{\rho} = \mu_1 \boldsymbol{\rho}^{k,1} + \mu_2 \boldsymbol{\rho}^{k,2} + ... + \mu_d \boldsymbol{\rho}^{k,d} \tag{2.7}$$

Instead of the unknown residual stresses $\boldsymbol{\rho}^k \in B_d^k$ the unknown $\boldsymbol{\mu}^k = (\mu_1,...,\mu_d)^T \in \mathbb{R}^d$ are chosen. The base vectors $\boldsymbol{\rho}_i^k$, $i=1,...,d$ are assembled into the matrix $\mathbf{B}^{d,k}$:

$$\mathbf{B}^{d,k} = \left(\boldsymbol{\rho}_1^k,...,\boldsymbol{\rho}_d^k\right) \tag{2.8}$$

With the load factor a^{k-1} and the stresses $\boldsymbol{\sigma}^{k-1}$ resulting from the step $k-1$ of the algorithm, the new maximization problem in B_d^k is given, in a discretized form (Heitzer *et al.*, 2000), by

$$\begin{aligned} &\max && a^k \\ &s.t. && F\left[a^k \boldsymbol{\sigma}_i^E(j) + \boldsymbol{\sigma}_i^{k-1} + \mathbf{B}_i^{d,k}\boldsymbol{\mu}^k\right] \le \sigma_{Y,i}^2, \quad j=1,...,NV, \boldsymbol{\mu} \in \mathbb{R}^d \end{aligned} \tag{2.9}$$

where i denotes the Gauss points (see also eqn.(2.3). This convex problem has $d+1$ unknowns ($\boldsymbol{\mu}$ and a) and $NG \times NV$ restrictions, where NG is the number of Gauss Points of the structures and NV the number of load vertices of the load domain. For obtaining a solution a^k, any optimization algorithm may be used. This basis reduction technique is well known in the field of optimization. Instead of searching the whole feasible region for the optimum a subspace with a small dimension is chosen and one searches for the best value in this subspace.

2.2.6. Non-standard FEM

All the above procedures are illustrated with the aim of the standard finite element method. Although, there are also several techniques that improve the performance of the numerical procedures, described above, through a more accurate finite element discretization instead of the applied solution method of the optimization problem. For example, instead of the standard finite element method (FEM), in (Liu *et al.*, 2005) the symmetric Galerkin boundary element method (BEM) has been used. Non-standard FEM has been also applied e.g. in (Le CV *et al.*, 2010) for cell-based

smoothed elements (CS-FEM) and in (Tran *et al.*, 2010) for edge-based smoothed elements (ES-FEM).

Particularly, Tran *et al.* (2010) propose an ES-FEM for the discretization of the problem and an interior point algorithm is then following. Using some smooth functions, only one Gauss point is required for each smoothing domain, ensuring that the total number of variables in the resulting optimization problem is smaller compared with the standard FEM.

2.2.7. Elastic simulations to shakedown – The Linear Matching Method

Another group of computational methods is intended to solve the shakedown problem by taking full advantages of existing finite elements and codes used in linear structural analysis. These methods adopt a similar philosophy, matching a linear rate problem to the plasticity problem by performing linear solutions with spatially varying moduli. In this spirit Ponter and coworkers developed the “Linear Matching Method” (LMM) for both the limit and the shakedown analysis of structures while Polizzotto *et al.* (2000) presented a general theoretical background to perform shakedown analysis by elastic simulations.

The Linear Matching Method for the shakedown analysis

The LMM is originated in (Ponter and Carter, 1997a, 1997b) for limit and shakedown analysis and provides a development of the “elastic compensation method” (Mackenzie and Boyle, 1993; Mackenzie *et al.*, 1994; Mackenzie *et al.* 2000). It is an upper bound approach that generates a sequence of linear solutions, with spatially varying moduli, which converges either to the collapse load (Ponter *et al.*, 2000) or to the shakedown load (Ponter and Engelhardt, 2000; Chen and Ponter, 2001a; Ponter, 2002).

Due to the fact that the LMM uses more physical arguments, like the developed methods in this thesis, we present in the sequel an analytical sketch of the Ponter and Engelhardt simulation technique for the evaluation of the shakedown factor λ. For simplicity, the method is presented, assuming a von Mises yield criterion

$$f(\sigma_{ij}) = \overline{\sigma} - \sigma_Y = 0 \tag{2.10}$$

where $\overline{\sigma} = \sqrt{\frac{3}{2}\sigma'_{ij}\sigma'_{ij}}$ is the effective stress and σ'_{ij} denotes the deviatoric stress.

This method generates a sequence of linear problems where the fictitious elastic moduli are found by a matching process. For the von Mises model, each iteration consists of obtaining an incompressible linear elastic solution with a shear modulus $\mu(x,t)$, which varies both spatially and during the cycle. Corresponding to an initial estimate of the strain history $\dot{\varepsilon}^i_{ij}$, the shear modulus is chosen so that the rate of energy dissipation in the linear material is matched to that of the perfectly plastic material for the same strain rate history. Specifically, the following matching condition is satisfying:

$$\frac{3}{2}\mu\dot{\overline{\varepsilon}}^i = \sigma_Y \tag{2.11}$$

at each instant in the cycle.

The linear problem for a new kinematically admissible strain rate history, $\dot{\varepsilon}^f_{ij}$, and a time constant residual stress field $\overline{\rho}^f_{ij}$, may now be defined by

$$\dot{\varepsilon}^f_{ij} = \frac{1}{\mu}\left(\overline{\rho}^f_{ij} + \lambda\hat{\sigma}_{ij}\right) \tag{2.12}$$

where $\hat{\sigma}_{ij}$ is the linear solution associated with the load history. Integrating over the cycle $0 \le t \le \Delta t$

$$\Delta\varepsilon^f_{ij} = \frac{1}{\overline{\mu}}\left(\overline{\rho}^f_{ij} + \sigma^{in}_{ij}\right) \tag{2.13}$$

where we assume $\lambda = \lambda^i_{UB}$,

$$\frac{1}{\overline{\mu}} = \int_0^{\Delta t}\frac{1}{\mu(t)}dt, \quad \sigma^{in}_{ij} = \overline{\mu}\left\{\int_0^{\Delta t}\frac{1}{\mu(t)}\lambda^i_{UB}\hat{\sigma}_{ij}dt\right\} \tag{2.14}$$

In terms of kinematically admissible strain rate history $\dot{\boldsymbol{\varepsilon}}^c$ an upper bound on the shakedown limit is given by (Koiter, 1960; Gokhfeld and Cherniavsky, 1980; König, 1987)

$$\int_V \int_0^{\Delta t} \sigma_{ij}^c \dot{\varepsilon}_{ij}^c dt dV = \lambda_{UB}^c \int_V \int_0^{\Delta t} (\hat{\sigma}_{ij} \dot{\varepsilon}_{ij}^c) dt dV \tag{2.15}$$

where $\lambda_{UB}^c \geq \lambda_s$, the exact shakedown limit and σ_{ij}^c denotes the stress at yield associated $\dot{\varepsilon}_{ij}^c$.

Thus, by substituting $\dot{\varepsilon}_{ij}^f$ into (2.15), an upper bound estimation of the factor λ_{UB}^f is then calculated for the current iteration

$$\lambda_{UB}^f = \frac{\int_V \sigma_Y \bar{\dot{\varepsilon}}(\Delta \varepsilon_{ij}^f) dV}{\int_V \int_0^{\Delta t} (\hat{\sigma}_{ij} \dot{\varepsilon}_{ij}^f) dt dV} \tag{2.16}$$

where $\lambda_{UB}^f \leq \lambda_{UB}^i$. The equality occurs if and only if $\dot{\varepsilon}_{ij}^f = \dot{\varepsilon}_{ij}^i$. Hence, the repeated application of this algorithm produces a monotonically reducing sequence of upper bounds which converges to a minimum upper bound.

Furthermore, there are several applications of the LMM in different kind of problems like cracked structures (Habibullah and Ponter, 2004), pavements (Ponter *et al.*, 2006) and geotechnical problems (Boulbibane and Ponter, 2005a,b).

Extensions of the theory for the cyclic behavior of creeping structures have been given by Ponter, 2001; Ponter and Boulbibane, 2003; Boulbibane and Ponter, 2003; Chen *et al.*, 2003; Chen and Ponter, 2004, 2006.

Extension of the Linear Matching Method to the evaluation of ratchet limits

An extension of the method to the evaluation of the ratchet limit for certain types of loading problems has been given by Ponter and Chen 2001; Chen and Ponter, 2001. The basis of the method is provided by a minimum theorem that provides an extension of the upper bound theorem to load histories in excess of shakedown. The theorem is then applied to the evaluation of the ratchet limit in excess of a reverse plasticity limit. This involves a two-stage process of a sequential minimization of two functionals. The first one for a cyclic history of varying residual stress field in a cycle

and the second one for a load parameter which takes the load history to the ratchet limit. This second stage involves the evaluation of the magnitude of an additional constant load which takes the body to the ratchet limit and may be understood as a shakedown solution for this extra load.

A short description of the method is described next:

Consider the problem of a body subjected to external loads

$$P(x_i,t) = \lambda \overline{P}(x_i) + P(x_i,t) \tag{2.17}$$

where λ is a load parameter, $\overline{P}(x_i)$ a constant load distribution and $P(x_i,t)$ and $\theta(x_i,t)$ are cyclic loading histories associated with the mechanical load and temperature respectively. The associated linear elastic solution is defined by

$$\hat{\sigma}_{ij} = \lambda \hat{\sigma}_{ij}^{\overline{P}} + \hat{\sigma}_{ij}^{\Delta}(x,t) \tag{2.18}$$

where $\hat{\sigma}_{ij}^{\Delta} = \hat{\sigma}_{ij}^{P} + \hat{\sigma}_{ij}^{\theta}$, the varying elastic stress components due to $P(x_i,t)$ and $\theta(x_i,t)$. The choice of this form of loads allows us to separate the problem into two subproblems a) the evaluation of a changing residual stress field due to $\hat{\sigma}_{ij}^{\Delta}$ and b) the determination of the value of λ at the ratchet limit i.e. the magnitude of the additional load that takes the load history to a ratchet limit. For this class of loading a functional I may be written as:

$$I(\dot{\varepsilon}_{ij}^{c},\lambda) = \int_0^{\Delta t} \int_V \left\{ \sigma_{ij}^{c} - \left(\lambda \hat{\sigma}_{ij}^{\overline{P}} + \hat{\sigma}_{ij}^{\Delta} + \rho_{ij}^{c} \right) \right\} \dot{\varepsilon}_{ij}^{c} dt dV \tag{2.19}$$

Whereas the shakedown load is characterized by a cyclic state of stress involving a constant residual stress field, the ratchet limit, allows for the possibility that there are changes in the residual stress field in the absence of cyclic strain growth. Over regions of the body a finite cycle of strain will generate a changing residual stress field that retains the stress history within yield. Additionally at the ratchet limit there will be a ratchet mechanism that produces a negligible residual stress field. Thus, the strain rate history of a structure will be given by:

$$\dot{\varepsilon}_{ij}^{c} = \dot{\varepsilon}_{ij}^{rc} + \dot{\varepsilon}_{ij}^{sc} \tag{2.20}$$

where the reverse plasticity mechanism $\dot{\varepsilon}_{ij}^{rc}$ satisfies and produces a finite residual stress field $\dot{\rho}_{ij}^{rc}$. The method relies upon the subdivision of I into two components I_r and I_s given by the expressions:

$$\begin{aligned} I_r &= \int_0^{\Delta t} \int_V \left\{ \sigma_{ij}^{rc} - \left(\hat{\sigma}_{ij}^{\Delta} + \rho_{ij}^{rc} \right) \right\} \dot{\varepsilon}_{ij}^{rc} dt dV, \\ I_s &= \int_0^{\Delta t} \int_V \left\{ \sigma_{ij}^{sc} - \left(\lambda \hat{\sigma}_{ij}^{\bar{P}} + \hat{\sigma}_{ij}^{\Delta} + \rho_{ij}^{rc} \right) \right\} \dot{\varepsilon}_{ij}^{sc} dt dV \end{aligned} \tag{2.21}$$

The subdivision of the functional I into two components allows a two stage solution of the problem.

Stage 1 : I_r is minimized with respect to $\dot{\varepsilon}_{ij}^{rc}$. The solution to this problem will yield an optimal history of stress $\hat{\sigma}_{ij}^{\Delta} + \rho_{ij}^{rc}(t)$.

Stage 2 : I_s is minimized with respect to $\dot{\varepsilon}_{ij}^{sc}$. This problem is equivalent to the evaluation of the shakedown limit. The principal difference is the need to take into account the varying residual stress field $\rho_{ij}^{rc}(t)$ calculated from the Stage 1. Hence, an upper bound on the ratchet limit is given by:

$$\lambda_{UB} = \frac{\int_0^{\Delta t} \int_V \left\{ \sigma_{ij}^{sc} - \left(\hat{\sigma}_{ij}^{\Delta} + \rho_{ij}^{rc} \right) \right\} \dot{\varepsilon}_{ij}^{sc} dt dV}{\int_0^{\Delta t} \int_V \hat{\sigma}_{ij}^{\bar{P}} \dot{\varepsilon}_{ij}^{sc} dt dV} \tag{2.22}$$

Applications of the LMM to structures beyond the shakedown limit may be found in Habibullah and Ponter, 2005; Chen and Ponter, 2004, 2010; Ure *et al.*, 2013; Chen *et al.*, 2013, among others.

2.2.8. Zarka's Method

The simplified method proposed by Zarka *et al.* (1990) is based on some transformed internal variables and is applied to structures made of elastoplastic-hardening

materials. The steady state is estimated here by an appropriate selection of the modified back stresses which are defined as the difference between the residual stresses and the plastic strains multiplied by the kinematic hardening modulus. The modified back stresses, similarly to plastic strains, uniquely determine the residual stress field and must be such that the resulting stresses are both plastically and statically admissible. These two conditions are satisfied iteratively, wherever the stresses state is outside the yield surface, a local projection is proposed (Zarka and Casier, 1981, Zarka, 1980).

2.2.9. A bipotential approach

Another alternative approach for non-associated plasticity is proposed by (Bousshine *et al.*, 1998, 2003; Bodoville and de Saxcè, 2001; Bouby *et al.*, 2006). The crucial idea consists in introducing the so-called bipotential, depending on both the stress and plastic strain rate. A set of admissible statical and kinematical fields can be incorporated in a variational formulation of shakedown problems built by a bifunctional. Thus, the kinematical and statical shakedown theorems are reformulated in terms of the bifunctionals.

2.2.10. A strain-driven strategy

An alternative method for the evaluation of the shakedown safety factor for elastic-perfectly plastic structures is presented in (Garcea *et al.*, 2005). It is an incremental-iterative procedure that may be considered a direct adaptation to shakedown of the so-called strain driven algorithm for incremental elastic-plastic analysis, and corresponds to a direct extension of the arc-length path-following method. The discrete formulation of the problem that is required is obtained using a mixed simplex finite element in which both stress and displacement fields are interpolated. A piecewise linearization of the elastic domain is performed in order to obtain a return mapping algorithm suitable for general application. The method requires a discrete

model based on two different finite elements, one with good behavior in the elastic range and the other suitable for performing elastoplastic analysis.

The methodology is applied to both plane frames (Casciaro and Garcea, 2002) and two-dimensional structures under plane stress or plane strain conditions (Garcea *et al.*, 2005). A more recent development of the method that avoids any linearization of the yield function is proposed by Garcea and Leonetti, 2011.

2.2.11. An eigen-mode method

Another alternative method to evaluate the shakedown factor is proposed by Zhang and Raad, 2000. In this work, the kinematic shakedown theorem is formulated for some deformation processes as a kinematic extremum problem based on a polyhedral load domain and a deformation mode domain. Each deformation mode is constructed by using eigen value/vector analysis. Every kinematically admissible strain field within some time interval can be derived from the deformation domain and used in the proposed shakedown formulation to evaluate the shakedown factor.

2.2.12. Direct Cyclic Analysis

Although important to evaluate the shakedown limit, it is equally an important issue to be able to determine the long-term effects that a given cyclic loading will have on the structure. To this end, an alternative to the cumbersome incremental procedure, a method called Direct Cycle Analysis (DCA) has been suggested in (Maitournam *et al.*, 2002) and has been implemented in the commercial program Abaqus (2010). This method is based on assuming that the displacements at the steady cycle will become cyclic. One then proceeds to decompose them into Fourier series whose coefficients are evaluated in an iterative way by linking them with the coefficients of the Fourier series of the residual load vector. This vector is evaluated as in an incremental procedure, and static admissibility is enforced by leading it to zero. The procedure, although involved, appears to be suited for the cases of alternating plasticity but fails to converge for loadings that are close to ratcheting (Abaqus,

2010), since, due to the assumed cyclic displacement behavior, it has the inherent inability to predict such a case. Furthermore the DCA procedure is not capable to predict shakedown or ratchet limits directly.

2.3. Application of shakedown on civil engineering structures

As it has been already discussed, the issue of shakedown on civil engineering is of great importance. Thus, there exist several approaches and applications for the determination of shakedown loads of specific civil engineering structures. A short list of indicative practical problems is described in this section. Several authors addressed the shakedown problem of bar systems (Atkociunas *et. al.*, 2008), frames (Cocchetti and Maier, 2003; Long and Nguyen, 2008; Atkociunas and Venskus, 2011; Barrera *et al.*, 2011), plates (Tran, 2011), shells (Tran *et al.*, 2008; Tran *et al.*, 2009) likewise steel-reinforced concrete structures (Giambanco *et al.*, 1994; Malena and Casciaro, 2008) and composites (Weichert *et al.*, 1999; Chen M. *et al.*, 2009).

Furthermore, there are many applications on geotechnical problems i.e. on pavements (Collins and Boulbibane, 1998; Boulibaine *et al.*, 2005) and soil mechanics (Boulbibane and Weichert, 1997; Krabbenhøft *et al.*, 2007b).

2.4. Other extensions of shakedown theory

In this section, a brief discussion on extensions of the shakedown theory beyond its basic assumptions is presented. For each topic of extension, some historical remarks and basic references are given. Firstly, the use of advanced material models in the context of shakedown theory is discussed; then discussion on inelastic crack bodies, on the dynamic shakedown and on the effects of geometrical nonlinearities follows.

2.4.1. Material hardening

In his pioneering work Melan (1938b) has already addressed the unlimited linear kinematic hardening in the framework of continuum mechanics. Based on this work

further results have been obtained by Neal (1950), Ponter (1975a, 1975b) and Zarka and Casier (1981). For discretized structures and piecewise linear yield function, Maier (1972) investigated linear hardening and softening effects while König and Siemaszko (1988) studied the effects of strainhardening in the shakedown of beams and frames. With the help of the generalized standard material model (GSMM) introduced by Halphen and Nguyen (1975), Mandel (1976) gives a simple formulation of Melan's theorem for hardening materials. The first explicit formulation for limited kinematical hardening material has been proposed by Weichert and Gross-Weege (1988), who introduce a two-surface model. Later, Stein *et al.* (1993) proposed the so-called "overlay model".

In general, the effect of limited kinematical hardening has been addressed by several authors (e.g. Polizzotto, 1986; Stein *et al.*, 1992; Corigliano *et al.*, 1995; Pycko and Maier, 1995; Fuschi, 1999; Pham and Weichert, 2001; Pham 2007, 2008; Pham *et al.*, 2010; Polizzotto, 2010; Simon and Weichert, 2012; Simon, 2013).

2.4.2. Non-associated constitutive laws

Extensions for non-associative flow rules have been first discussed in the framework of shakedown theory by Maier (1969) using piecewise linear yield functions and plastic potentials, and later by Pycko and Maier (1995). In general, non-associative flow rules can be considered if the domain of safe states is defined by means of plastic potential and not, as in the case of associated flow rules, by the yield condition (Boulbibane and Weichert, 1997; de Saxcè and Bousshine, 1998). As it has been already discussed (see section 2.2.9) generalization of the constitutive equations derived from bipotentials are proposed by de Saxcè and coworkers to formulate principles with non-associative laws (Bousshine *et al.*, 2003).

2.4.3. Shakedown of damaged structures

Another important task on extended shakedown theories deals with the influence of material damage. This influence on the formulation of the static shakedown theorem

was first investigated by Hachemi and Weichert (1992), for a damaging material with linear hardening, with the use of the energy-based isotropic elastoplastic damage models by Ju (1989). According to this approach damage is generated by plastic strains (Hachemi and Weichert, 1997, 1998; Hachemi *et al.*, 2003) and the undamaged material is assumed to obey the generalized standard material model. Then, the damaged material behavior is taken into account by a scalar valued damage variable based on the concept of effective stresses following Lemaitre and Chaboche (1985). An important difference between the basic model of elastic-perfectly plastic material and the shakedown formulation to damaged materials is that the material damage cannot grow indefinitely and is limited by local rapture (Hachemi and Weichert, 1992).

An extension of Melan's shakedown theorem has been also proposed by Pollizzotto *et al.* (1996) for elastic-plastic-damage material models. A concept of material stability condition, the D-stability principle, is used. According to this work, for most common materials the proposed extension of Melan's theorem differs from the classical one in that a) the elastic stress state must be evaluated at some trial damage state of the structure, and b) the sum of the latter damaged elastic stresses with the trial time-independent self-stresses must be inside the damage surface and the yield surface.

2.4.4. Inelastic cracked bodies

According to the classical theory, the shakedown limit of cracked bodies should be zero since the stress at the crack tip is singular. However, experiments predict that cracked structures under variable loadings may reach a safe state where the crack propagation stops.

The major issue in shakedown analysis of cracked structures is to find a modified shakedown condition that addresses the complex phenomenon related to crack initiation and crack propagation. Very few, but remarkable works to this direction can be found in the literature. In this class belong the work of Huang and Stein (1996), who consider the crack tip represented by a notch, thus, replacing the stress

singularity by a stress concentration; the work of Belouchrami and Weichert, (1998) who proposed an extended two-step procedure of a local and global analysis and the work of Feng and Gross (1999).

2.4.5. Dynamic shakedown

In the classical formulation of shakedown theory, the loads are assumed to change slowly in time so that inertia and damping effects are negligible. Extensions including dynamic effects were proposed by Ceradini (1969,1980), Corradi and Maier (1973, 1974), Maier and Novati (1990), Comi and Corigliano (1991) and Polizzotto *et al.* (1993), among others.

Shakedown is essentially checked by the existence or not of some fictitious initial conditions associated with a linear elastic dynamic response to the actual load program that, when superposed to a constant residual stress field, satisfies the yield condition at all times.

2.4.6. Effects of geometrical nonlinearities

A major research topic in continuum mechanics for many years was the development of so-called “geometrically nonlinear theories”. The geometrically nonlinear problem in the context of shakedown theory was studied first by Maier (1973a, 1973b). He extended Melan’s and Koiter’s theorems by proposing a second order approximation of geometrical effects. Siemaszko and König (1985) discussed the influence of geometric effects on the stability of the deformation process for particular structures.

Weichert (1984) extended the Melan’s theorem in the framework of geometrically nonlinear continuum mechanics, practically applicable to problems where information about the expected deformation pattern is available. Shakedown conditions assuming milder restrictions on the geometrical nonlinearities have been considered by Weichert (1986), Weichert and Gross-Weege (1988), Gross-Weege (1990) and Pycko and König (1991) among others. Particularly, Gross-Weege (1990) gave a unified formulation of Melan’s theorem for structures subjected to a constant load,

responsible for large displacements, and to small additional variable loads that cause small additional displacements.

Shakedown of structures undergoing finite elastoplastic strains has been studied by Polizzotto and Borino (1996) and Stumpf and Schieck (2000).

3.

Fundamentals in plasticity

3.1. Introduction

In this section some fundamentals in plasticity are described. The discussion is limited only on the theoretical background that is required to describe the research work contained in this thesis.

The main object of the mathematical theory of plasticity is to formulate a description of the relationship between stresses and strains for a material which exhibits an elasto-plastic response. This plastic response occurs once a certain level of stress has been reached, and is characterized by irreversible straining which is time independent. Some basic assumptions and theoretical aspects are described in this chapter. To provide a theory for elasto-plastic material behavior the following three considerations have to been taken into account (Owen and Hinton, 1980):

a) An explicit relation between stresses and strains has to be formulated to describe the elastic material behavior i.e. before the appearance of plastic straining.
b) A yield criterion which indicates the stress level at which plastic flow occurs.
c) A relation between stresses and strains for post-yield behavior.

3.2. Inelastic behavior of material

After initial yielding the material behavior will be partly elastic and partly plastic. Thus, assuming a geometrically linear theory, the total strain field $\boldsymbol{\varepsilon}$ can be decomposed into an elastic or reversible part $\boldsymbol{\varepsilon}^{el}$ and an irreversible part $\boldsymbol{\varepsilon}^{pl}$ (see also Fig.3.1.). If some thermal effects are assumed, a thermal strain field $\boldsymbol{\varepsilon}^{th}$ should be added and one may write the following expression for the total strain:

$$\boldsymbol{\varepsilon} = \boldsymbol{\varepsilon}^{el} + \boldsymbol{\varepsilon}^{pl} + \boldsymbol{\varepsilon}^{th} \tag{3.1}$$

In Fig.3.1 the idealized diagram of the uniaxial tensile test of mild steels is shown. σ_Y and σ_u denote the yield stress and the ultimate strength respectively.

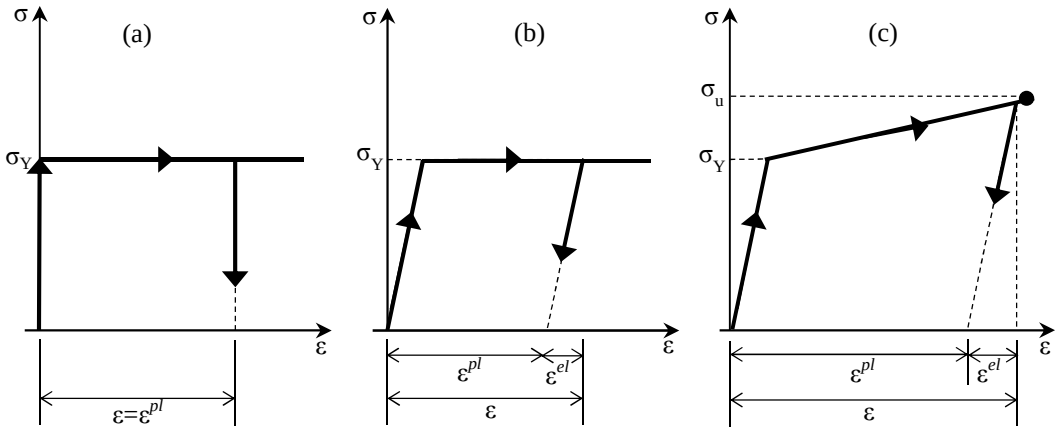

Figure 3.1 Idealized uniaxial stress-strain diagrams

The diagram indicates that there is an initial elastic range for the structural steel and there is no permanent deformation if unloading takes place. After exceeding the elastic limit the behavior of the material is described by the inelastic range. Considering a work hardening model, the inelastic range consists of a strain hardening range where the increase of stresses is connected with a significant increase in strains (see Fig.3.1(c)). If hardening is ignored, an elastic-perfectly plastic model is considered where strains increase without an increase in stresses (see Fig.3.1(b)). Sometimes the plastic strains are much larger than the elastic strains and the material behavior may be further simplified to be as rigid plastic (see Fig.3.1(a)).

With the exception of very fast deformation processes, the deformation of metals can be considered as rate-independent. In other words, two strain controlled tests in which the inertia forces are negligible, performed at different rates would result in the same stress.

If a strain hardening model is first deformed plastically, then unloaded, and again loaded but in the opposite direction, then the onset of yielding is earlier than for the virgin material. This phenomenon is called the *Bauschinger effect*.

The elastic part of the strains $\boldsymbol{\varepsilon}^{el}$ is related to the stresses through the generalized Hooke's law:

$$\boldsymbol{\varepsilon}^{el} = \mathbf{C}^{-1}\boldsymbol{\sigma} \tag{3.2}$$

where $\mathbf{C}$ is a fourth rank tensor of elastic constants.

For an isotropic material the expression for $\mathbf{C}^{-1}$ is given by:

$$\mathbf{C}^{-1} = \frac{1}{E}\begin{bmatrix} 1 & -\nu & -\nu & 0 & 0 & 0 \\ -\nu & 1 & -\nu & 0 & 0 & 0 \\ -\nu & -\nu & 1 & 0 & 0 & 0 \\ 0 & 0 & 0 & 2(1+\nu) & 0 & 0 \\ 0 & 0 & 0 & 0 & 2(1+\nu) & 0 \\ 0 & 0 & 0 & 0 & 0 & 2(1+\nu) \end{bmatrix} \tag{3.3}$$

where E is the *Young's modulus* and ν is the *Poisson's ratio*.

On the other hand the plastic strain field obeys an associated flow rule:

$$\boldsymbol{\varepsilon}^{pl} = \lambda \frac{\partial f}{\partial \boldsymbol{\sigma}} \tag{3.4}$$

where λ is a non-negative plastic multiplier and $f(\boldsymbol{\sigma})$ represents a time-independent yield function, which will be discussed in detail later.

3.3. Yield function - yield criterion

The *yield criterion* determines the stress level at which plastic deformation begins and may be written in the following general form

$$f(\boldsymbol{\sigma}) = k(\kappa) \tag{3.5}$$

where the yield function $f(\boldsymbol{\sigma})$ is a continuous scalar function and k is a material parameter which is determined experimentally. On physical grounds any yield criterion should be independent of the orientation of the coordinate system employed and therefore it is a function only of the stress invariants. According to experimental observations, by Bridgman (1923, 1952), the plastic deformation of metals is essentially independent on the hydrostatic pressure. Thus, the yield function can be only of the form

$$f(J_2, J_3) = k(\kappa) \tag{3.6}$$

where J_2, J_3 are the second and third invariant of the deviatoric stress tensor.

Experimental data confirm that ductile metals yield much more consistently at prescribed von Mises stress levels regardless of the loading state than at any other criteria.

3.3.1. Von Mises yield criterion

According to *von Mises criterion* (Mises, 1913) the yielding occurs when the second deviatoric stress invariant J_2 reaches a critical value. It is a yield criterion that applies best to ductile materials, such as metals (Lubliner, 1990).

In materials science and engineering the von Mises yield criterion can be also formulated in terms of the von Mises stress or equivalent stress $\overline{\sigma}$. Thus, a material begins yielding when its von Mises stress reaches a critical value known as the yield stress.

Mathematically the yield function of the von Mises condition is expressed by:

$$f(J_2) = \sqrt{J_2} - k \tag{3.7}$$

where the constant k is the yield stress of the material in pure shear. At the onset of yielding, the yield shear stress is $\sqrt{3}$ times lower than the yield stress in pure tension. Thus, we get:

$$k = \frac{\sigma_Y}{\sqrt{3}} \tag{3.8}$$

If we use the effective (or equivalent) stress $\overline{\sigma} = \sqrt{3J_2}$ the von Mises yield criterion may be written as:

$$\begin{aligned} f(J_2) = \sqrt{3J_2} - \sigma_Y = 0 \Rightarrow \overline{\sigma} - \sigma_Y = 0 \Rightarrow \\ \Rightarrow \overline{\sigma} = \sigma_Y \end{aligned} \tag{3.9}$$

Expressing J_2 in terms of the principal stresses, we may formulate the Mises yield criterion as:

$$(\sigma_1 - \sigma_2)^2 + (\sigma_2 - \sigma_3)^2 + (\sigma_1 - \sigma_3)^2 = 6k^2 = 2{\sigma_Y}^2 \tag{3.10}$$

or

$${\sigma_1}^2 + {\sigma_2}^2 + {\sigma_3}^2 - \sigma_1\sigma_2 - \sigma_2\sigma_3 - \sigma_3\sigma_1 = 3k^2 = {\sigma_Y}^2 \tag{3.11}$$

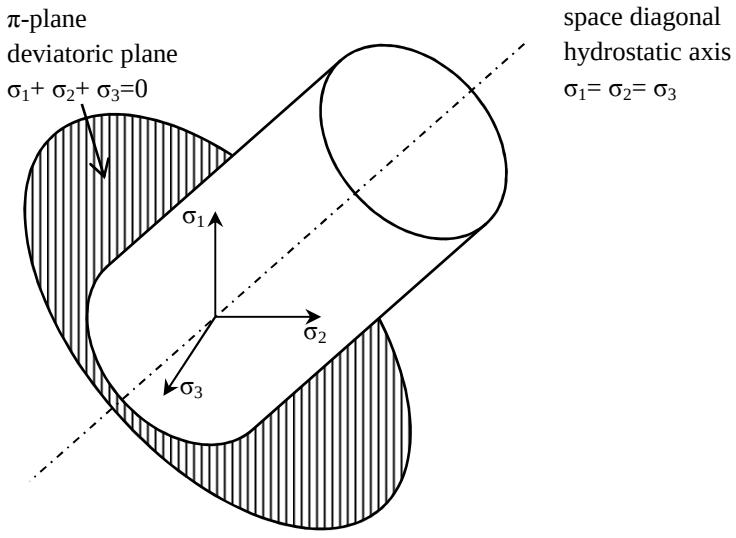

Figure 3.2 Geometrical representation of the von Mises yield surface in principal stress space

Fig.3.2 shows the geometrical interpretation of the von Mises yield surface to be a circular cylinder whose projection onto the deviatoric plane is a circle of radius $\sqrt{2}k$

or $\sqrt{\frac{2}{3}}\sigma_Y$. The axis of the cylinder coincides with the space diagonal, defined by points $\sigma_1 = \sigma_2 = \sigma_3$, and since each section of the cylinder is identical, a consequence of the assumption is that the hydrostatic stress has no influence on yielding. Thus, it is convenient to represent the yield surface geometrically by projecting it onto the so called *π*-plane, where $\sigma_1 + \sigma_2 + \sigma_3 = 0$, as it may be seen in Fig.3.3(b). The two dimensional plot of the von Mises yield criterion is an ellipse shown in Fig.3.3(a).

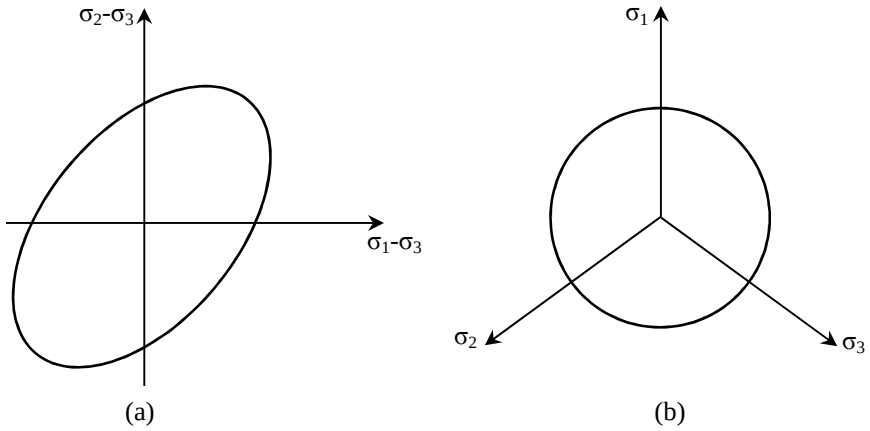

Figure 3.3 Two-dimensional representation of the von Mises yield criterion a) conventional engineering representation, b) *π*-plane representation

There are two physical interpretations of the von Mises yield criterion. Henky (1924) pointed out that yielding begins when the *elastic energy distortion* reaches a critical value. Thus, the von Mises criterion is also known as the maximum distortion strain energy criterion. This comes from the relation between the elastic energy of distortion W_D and J_2:

$$W_D = \frac{J_2}{2G} \tag{3.12}$$

where G is the elastic shear modulus.

Alternatively, the yielding begins when the *octahedral shear stress* τ_{oct} reaches a critical value. Thus, the von Mises criterion is also known as the maximum shear stress criterion. The value of τ_{oct} is related to J_2 by

$$\tau_{oct} = \sqrt{\frac{2}{3} J_2} \tag{3.13}$$

3.4. Drucker's postulate

The Drucker's postulate was introduced in the 1950s (Drucker, 1959) and it is a general framework for the constitutive relations in plasticity. The postulate is a generalization of the characteristics of the uniaxial stress-strain curves of work-hardening materials (Fig.3.4(a)) and can be formulated as follows.

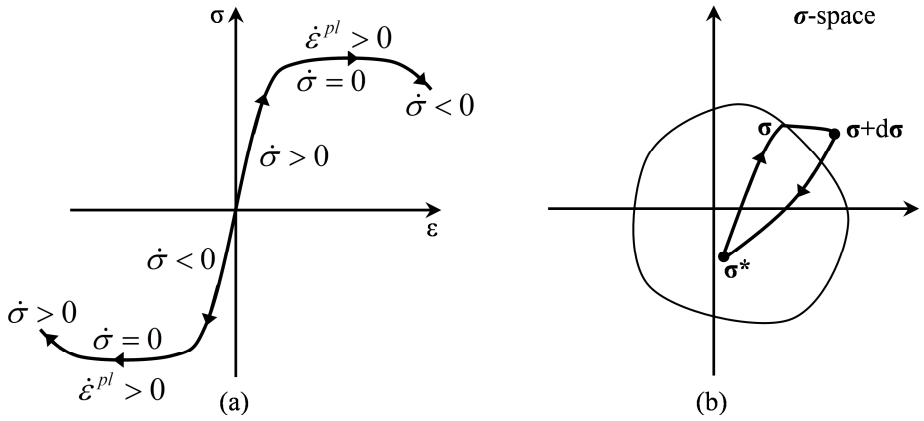

Figure 3.4 Drucker's postulate a) in the uniaxial stress-strain plane, b) in stress space

Let us consider an elastic-plastic unit volume in the structure under a certain initial stress state. Let us further assume that this volume is subjected to a slow incremental load resulting in a stress increment $d\boldsymbol{\sigma}$ (which causes the elastic $d\boldsymbol{\varepsilon}^{el}$ and plastic strain $d\boldsymbol{\varepsilon}^{pl}$ increments, respectively) and subsequently it is slowly removed. This process of application and removal of the additional stress is called *stress cycle*. By removing this additional stress, the stress point of the structure may

return to its original stress state, but the strain rate may be different, if plastic strain has been generated. The *Drucker's postulate* asserts:

a) that the work of additional stresses on a closed path of stress (loading-unloading cycle) is non-negative, or that no energy can be recovered from the initial stressed point. Thus, according to Drucker, we may write for a *stable* or *work hardening* material:

$$d\boldsymbol{\sigma} \cdot d\boldsymbol{\varepsilon}^{pl} \geq 0 \tag{3.14}$$

where $d\boldsymbol{\varepsilon}^{pl}$ is the plastic strain increment that is not recovered during the unloading. The equality holds only if $d\boldsymbol{\varepsilon}^{pl} = 0$.

Also according to Drucker the following condition holds true:

b) the work done during an incremental loading is positive i.e.

$$d\boldsymbol{\sigma} \cdot d\boldsymbol{\varepsilon} > 0 \tag{3.15}$$

For perfectly plastic materials Drucker's inequalities are $d\boldsymbol{\sigma} \cdot d\boldsymbol{\varepsilon} \geq 0$ and $d\boldsymbol{\sigma} \cdot d\boldsymbol{\varepsilon}^{pl} = 0$. It can be seen that the inequality

$$\dot{\boldsymbol{\sigma}} \cdot \dot{\boldsymbol{\varepsilon}}^{pl} \geq 0 \tag{3.16}$$

sometimes known simply as *Drucker's inequality*, is valid for both work-hardening and perfectly plastic materials.

Drucker's statement of his postulate is broader than described above, in that the additional stress produced by the external loading need not to be a small increment. Particularly, the initial stress, denoted by $\boldsymbol{\sigma}^*$, may be inside the elastic region, or at a point on the yield surface far away from $\boldsymbol{\sigma}$, and the process followed by the external agency may consist of elastic loading to a stress $\boldsymbol{\sigma}$ on the current yield surface, a small stress increment $d\boldsymbol{\sigma}$ producing an incremental plastic strain $d\boldsymbol{\varepsilon}^{pl}$, and finally unloading back to $\boldsymbol{\sigma}^*$; the path may be seen in Fig.3.4(b). With $d\boldsymbol{\sigma}$ neglected alongside $\boldsymbol{\sigma} - \boldsymbol{\sigma}^*$, the work per unit volume done by the external load is $(\boldsymbol{\sigma} - \boldsymbol{\sigma}^*) \cdot d\boldsymbol{\varepsilon}^{pl}$. Drucker's postulate, consequently, implies that:

$$(\boldsymbol{\sigma} - \boldsymbol{\sigma}^*) \cdot \dot{\boldsymbol{\varepsilon}}^{pl} \geq 0 \tag{3.17}$$

A strictly inequality holds if $\boldsymbol{\sigma}^*$ is inside the yield surface being a safe state ($f(\boldsymbol{\sigma}^{(s)}) < 0$). An illustration of Drucker's postulate may be seen in Fig.3.5.

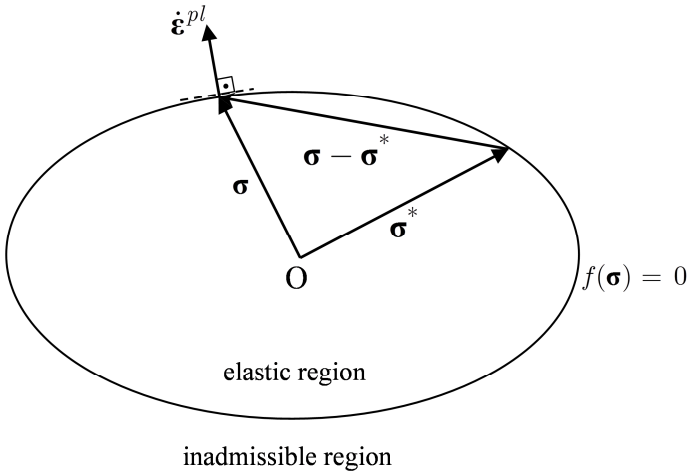

Figure 3.5 Corresponding pairs of stresses and plastic strain rates on convex yield surface

3.4.1. Consequences of Drucker's postulate

Drucker's inequality (3.17) has consequences of highly importance in plasticity theory. In discussing the consequences of Drucker's inequality, it is convenient to consider a two-dimensional representation. Thus, we plot the plastic strain rate $\dot{\boldsymbol{\varepsilon}}^{pl}$, caused by the stress program $\boldsymbol{\sigma}^{(0)} \rightarrow \boldsymbol{\sigma}$, in the stress space with its origin at the stress point $\boldsymbol{\sigma}^{(0)}$. $(\boldsymbol{\sigma} - \boldsymbol{\sigma}^{(0)})$ is a vector in stress space joining the stress points $\boldsymbol{\sigma}$ and $\boldsymbol{\sigma}^{(0)}$. This is shown diagrammatically in Fig.3.6. Inequality (3.17) may then be interpreted in turn as requiring that the scalar product of the vectors $(\boldsymbol{\sigma} - \boldsymbol{\sigma}^{(0)})$ and $\dot{\boldsymbol{\varepsilon}}^{pl}$ should be non-negative.

This consideration has two implications that play a very important role in plasticity (Lubliner, 1990). First, requires that $\dot{\boldsymbol{\varepsilon}}^{pl}$ must be directed along the outward normal to the yield surface at point $\boldsymbol{\sigma}$. This consequence is known as the **normality rule**. Secondly, requires that the ***yield surface is convex***, i.e. the straight line joining any two stress points lying inside or on the yield surface must itself lie completely within or on the yield surface.

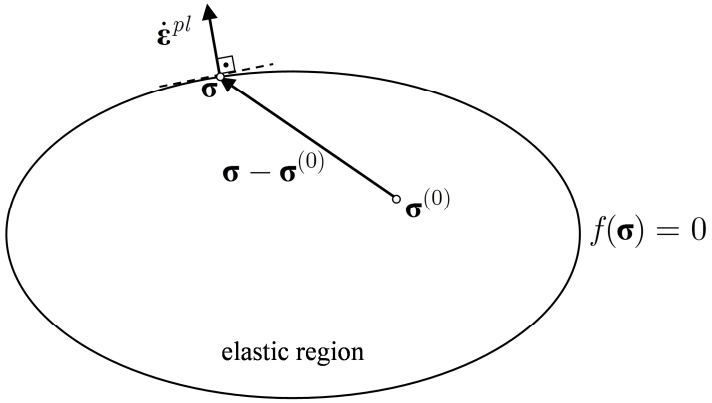

Figure 3.6 Properties of yield surface with associated flow rule – convexity and normality

Let us now demonstrate the convexity of the yield surface and the normality rule. To this end, we consider a smooth yield surface assuming that the above are not true. Geometrical arguments may be used to show that this assumption is unrealistic. We may choose any stress points $\boldsymbol{\sigma}$ and $\boldsymbol{\sigma}^{(0)}$ that satisfies $f(\boldsymbol{\sigma}) = 0$ and $f(\boldsymbol{\sigma}^{(0)}) \leq 0$. Firstly, we assume that the plastic strain rate $\dot{\boldsymbol{\varepsilon}}^{pl}$, that occurs as a result of a stress increment imposed on stress $\boldsymbol{\sigma}$, does not have the direction of the outward normal (see Fig.3.7). It is obvious that any choice of $\boldsymbol{\sigma}$ and $\boldsymbol{\sigma}^{(0)}$ will lead to a violation of ineq.(3.17).

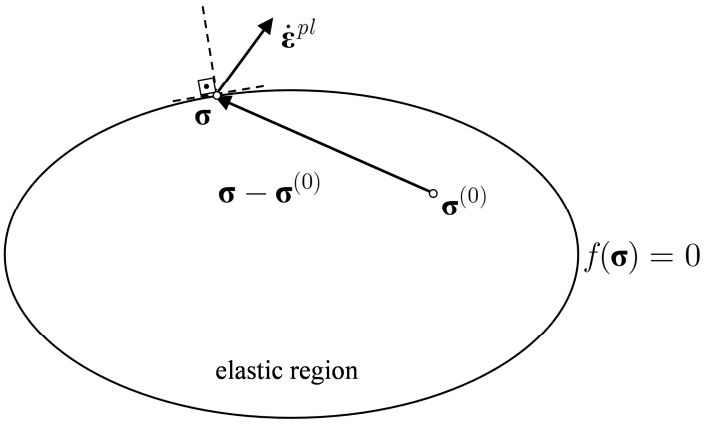

Figure 3.7 Yield surface without normality

Next, let us assume that the plastic strain rate satisfies the normality rule, but the yield surface is not convex. As it is shown in Fig.3.8, $\boldsymbol{\sigma}$ may be chosen to lie in a non-convex part of the surface. Again, a process of elimination leads to the conclusion that the surface must be convex if it is possible to choose any $\boldsymbol{\sigma}$ and $\boldsymbol{\sigma}^{(0)}$ such that ineq.(3.17) is always true.

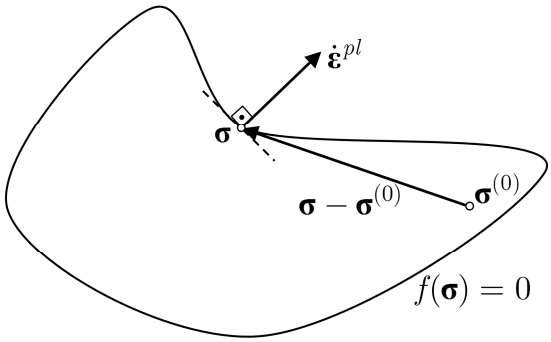

Figure 3.8 Normality without convexity

3.4.1.1. Normality rule - Associated flow rule

The normality rule is now discussed in more detail. At any point of the yield surface $f(\boldsymbol{\sigma}) = 0$ where the surface is smooth, the outward normal vector is proportional to the gradient of f (in stress space), and therefore, we may express the normality rule as:

$$\dot{\boldsymbol{\varepsilon}}^{pl} = \dot{\lambda} \frac{\partial f}{\partial \boldsymbol{\sigma}} \tag{3.18}$$

where $\dot{\lambda} \geq 0$ to ensure the direction is that of the outward normal. If the point turns out to be on the yield surface where the outward normal is discontinuous, the plastic strain rate must be bounded in direction by the outward normal vectors at all adjacent points on the yield surface. Those points are called *singular points* or *corners*.

The normality rule is thus associated with the yield function and the above equation (3.18) is well known in plasticity as *associated flow rule*. The following states are possible for an elasto-plastic structure:

$\dot{\lambda} = 0$ if $f(\boldsymbol{\sigma}) < 0$ (elastic state) or $f(\boldsymbol{\sigma}) = 0$ and $\dot{f} = \dfrac{\partial f}{\partial \boldsymbol{\sigma}} \dot{\boldsymbol{\sigma}} < 0$ (unloading from the plastic state), and

$\dot{\lambda} > 0$ if $f(\boldsymbol{\sigma}) = 0$ and $\dot{f} = 0$ (plastic loading).

3.5. Plastic dissipation function

During plastic deformation in a structure a dissipation of energy is found to take place in the form of heat. The dissipation energy rate per unit volume can be shown to be

$$D(\dot{\boldsymbol{\varepsilon}}^{pl}) = \boldsymbol{\sigma} \cdot \dot{\boldsymbol{\varepsilon}}^{pl} > 0, \quad (\dot{\boldsymbol{\varepsilon}}^{pl} \neq \mathbf{0}) \tag{3.19}$$

where $\boldsymbol{\sigma}$ is the yield surface stress state associated by the flow rule with the plastic strain rates $\dot{\boldsymbol{\varepsilon}}^{pl}$.

The plastic dissipation for the von Mises criterion and associated flow rule is given by (see Lubliner, 1990):

$$D(\dot{\boldsymbol{\varepsilon}}^{pl}) = \boldsymbol{\sigma} \cdot \dot{\boldsymbol{\varepsilon}}^{pl} = \sqrt{2J_2}\sqrt{\dot{\boldsymbol{\varepsilon}}^{pl} \cdot \dot{\boldsymbol{\varepsilon}}^{pl}} \tag{3.20}$$

3.6. Fundamental principles

Let us consider a body of volume V enclosed inside the surface S that is in the state of equilibrium (Fig.3.9). Any mechanical field such as displacement, strain, and stress depend on the position vector $\mathbf{x} \in V$. The surface S consists of S_U and S_T, where S_U is the surface on which prescribed displacements are imposed and S_T is the surface where the external surface tractions $\mathbf{t}$ are imposed. We also consider that the structure is subjected on body forces denoted by the vector field $\mathbf{b}$.

The stress field $\boldsymbol{\sigma}$ has to satisfy the following **equation of equilibrium**:

$$div\boldsymbol{\sigma} + \mathbf{b} = 0 \quad \text{in } V \tag{3.21}$$

with the following boundary conditions:

$$\begin{aligned} \boldsymbol{\sigma}\mathbf{n} &= \mathbf{t} \quad \text{on } S_T \\ \mathbf{u} &= \bar{\mathbf{u}} \quad \text{on } S_U \end{aligned} \tag{3.22}$$

where $\mathbf{n}$ is the normal unit outward normal vector to S.

Any stress field $\boldsymbol{\sigma}$ that satisfies eqns.(3.21) and (3.22) is called a *statically admissible* field. If this stress field also satisfies the yield condition $f(\boldsymbol{\sigma}) \leq 0$ is called *plastically admissible* field.

Under the assumption of small strains, the compatibility equations relating the strain and displacements fields are:

$$\boldsymbol{\varepsilon} = \frac{1}{2}\left(\nabla\mathbf{u} + \left(\nabla\mathbf{u}\right)^T\right) \quad \text{in } V \tag{3.23}$$

where the displacement field $\mathbf{u}$ are subjected to the following boundary kinematical conditions:

$$\mathbf{u} = \overline{\mathbf{u}} \quad \text{on } S_U \tag{3.24}$$

Similar relationships hold true for the displacement rates $\dot{\mathbf{u}}$ and the strain rates $\dot{\boldsymbol{\varepsilon}}$.

Any field of deformation rates (or increments) obeying the compatibility eqns.(3.23) and the kinematic boundary conditions (3.24) is termed *kinematically admissible* field.

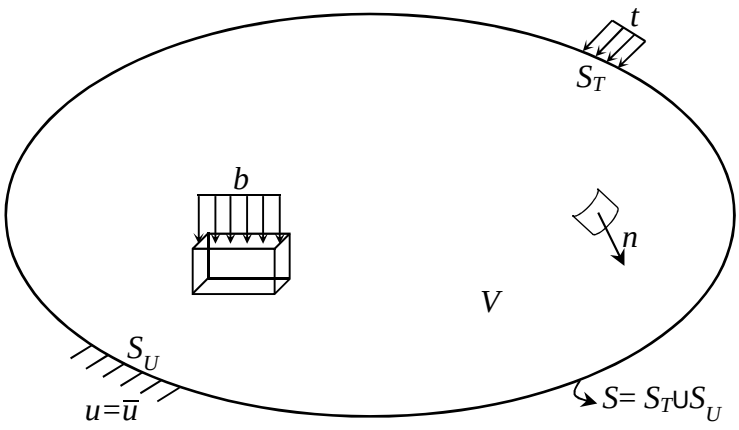

Figure 3.9 A body in the state of equilibrium

3.6.1. Principle of virtual work

Given a set of loads and a virtual displacement field $\delta\mathbf{u}$ (a *virtual displacement* field is defined as the difference between two neighboring kinematically displacement fields) we define the *external virtual work* as (Lubliner, 1990):

$$\delta W_{ext} = \int_V \mathbf{b} \cdot \delta\mathbf{u} dV + \int_{S_T} \mathbf{t} \cdot \delta\mathbf{u} dS \tag{3.25}$$

The *internal virtual work* is defined as:

$$\delta W_{\text{int}} = \int_V \boldsymbol{\sigma} \cdot \delta\boldsymbol{\varepsilon} dV \tag{3.26}$$

Thus the body is in equilibrium under the applied loads if and only if the **principle of virtual work**, namely,

$$\begin{gathered} \delta W_{ext} = \delta W_{\text{int}} \Rightarrow \\ \int_V \mathbf{b} \cdot \delta\mathbf{u} dV + \int_{S_T} \mathbf{t} \cdot \delta\mathbf{u} dS = \int_V \boldsymbol{\sigma} \cdot \delta\boldsymbol{\varepsilon} dV \end{gathered} \tag{3.27}$$

is obeyed.

Writen in this form the principle of virtual work is also known as principle of virtual displacements and is a generalization of the equilibrium conditions (3.21) and (3.22). It remains valid for an arbitrary system of external body forces $\mathbf{b}$ and surface tractions $\mathbf{t}$ supported by the stress field $\boldsymbol{\sigma}$ and for any arbitrary displacement field $\delta\mathbf{u}$ compatible with a kinematically admissible strain distribution $\delta\boldsymbol{\varepsilon}$.

Equation (3.27) holds good if the displacement field and the corresponding strain field are both replaced by the displacement rates $\dot{\mathbf{u}}$ and the strain rates $\dot{\boldsymbol{\varepsilon}}$ respectively.

Furthermore, eqn.(3.27) indicates that the work done by a self-equilibrating stress system on a kinematically admissible strain (or strain rate) field is nil.

In the above principle no assumption about the constitutive model of the material has been done. Thus eqn.(3.27) may be applied for any inelastic material behavior.

Approximate treatments of continuum mechanics are usually based on a

procedure known as discretization, and virtual work provides a consistent framework for the procedure.

3.7. Superposition of elastic and residual stress distributions

Consider an elastoplastic structure that is subjected to a general loading program $\mathbf{\Gamma}(t)$. A convenient tool by means of which the discussion of shakedown and steady states of the next chapter can be carried out, is that of expressing the stress field $\boldsymbol{\sigma}(t)$ as the sum of two parts. Let us suppose that the problem is solved on the assumption that the material is purely elastic and let us denote with $\boldsymbol{\sigma}^{el}(t)$ the resulting stress field. This stress field is both path and time independent and consequently depends only on the instantaneous values of the applied loads $\mathbf{\Gamma}(t)$.

Let the stresses in the elastic, perfectly plastic structure $\boldsymbol{\sigma}(t)$ be written as

$$\boldsymbol{\sigma}(t) = \boldsymbol{\sigma}^{el}(t) + \boldsymbol{\rho}(t) \tag{3.28}$$

Because the equilibrium equations are linear, and because $\boldsymbol{\sigma}(t)$ and $\boldsymbol{\sigma}^{el}(t)$ are each statically admissible and in equilibrium with the same external loading $\mathbf{\Gamma}(t)$, it follows that $\boldsymbol{\rho}(t)$ is statically admissible and in equilibrium with zero external loading. The field $\boldsymbol{\rho}$ will be termed a *residual stress field* and is a *self-equilibrating stress field*. It can also be thought of as the stress field which would appear in the structure if the loads $\mathbf{\Gamma}(t)$ were removed, provided that no further plastic deformation took place at the structure during the unloading. The residual stress field is of course a function of the loading history.

In any particular problem the initial stress field is given by

$$\boldsymbol{\sigma}(0) = \boldsymbol{\sigma}^{el}(0) + \boldsymbol{\rho}(0) \tag{3.29}$$

and since $\boldsymbol{\sigma}^{el}(0)$ is a function only of $\mathbf{\Gamma}(0)$, any effects of previous history of deformation are stored in the initial residual stress field.

On substituting (3.28) into (3.1) and using (3.2) one obtains the following decomposition of the actual strain field

$$\boldsymbol{\varepsilon} = \mathbf{C}^{-1}\boldsymbol{\sigma}^{el} + \boldsymbol{\varepsilon}^{th} + \boldsymbol{\varepsilon}^{pl} + \mathbf{C}^{-1}\boldsymbol{\rho} \tag{3.30}$$

It can be easily seen that the first two terms constitute the strain field in the fictitious perfectly elastic structure when exposed to the same loads and temperature. This field is compatible with the displacement field $\mathbf{u}^E$ appropriate for the perfectly elastic structure. As the total strain field $\boldsymbol{\varepsilon}$ is also compatible, the last two terms in (3.30) clearly result from a certain displacement called the residual displacement $\mathbf{u}^R$. The sum of these two terms gives the residual stain field $\boldsymbol{\varepsilon}^r$. Thus, we have

$$\begin{aligned} \boldsymbol{\varepsilon}^r &= \boldsymbol{\varepsilon}_r^{el} + \boldsymbol{\varepsilon}^{pl} \\ \boldsymbol{\varepsilon}_r^{el} &= \mathbf{C}^{-1}\boldsymbol{\rho} \end{aligned} \tag{3.31}$$

$$\begin{aligned} \boldsymbol{\varepsilon}^{th} + \mathbf{C}^{-1}\boldsymbol{\sigma}^{el} &= \frac{1}{2}\left(\nabla \mathbf{u}^E + \left(\nabla \mathbf{u}^E \right)^T \right) \\ \boldsymbol{\varepsilon}^{pl} + \mathbf{C}^{-1}\boldsymbol{\rho} &= \frac{1}{2}\left(\nabla \mathbf{u}^R + \left(\nabla \mathbf{u}^R \right)^T \right) \\ \mathbf{u} &= \mathbf{u}^E + \mathbf{u}^R \end{aligned} \tag{3.32}$$

where $\mathbf{u}$ denotes the actual displacement in the elastoplastic structure. It may be shown that, at every instant, the residual stress and displacement fields are uniquely defined by the instantaneous plastic strain field $\boldsymbol{\varepsilon}^{pl}$.

4.

Theoretical aspects in shakedown theory

If a given structure has been designed for a given load variation domain and considering that some initial plastic deformations have already occurred, then the structural safety requires that the stabilization of plastic deformations under service loads must be assured. However, step-by-step elastoplastic analyzes are unable to solve the problem not only due to the numerical difficulties but also due to the fact that the number of loading paths which should be accounted for, are infinite. Thus, only by an integral method of considering not particular load paths but the whole load domain of load variations the problem can be solved in a satisfactory manner. All the methods toward this direction are based on the fundamental shakedown theorems presented in this chapter. Furthermore, theoretical considerations on the cyclic elastoplastic behavior of structures will be discussed.

4.1. Limit states of cyclically loaded structures

In many problems of technological interest, structures or structural components are subjected to repeated programs of loading. For this reason it is of interest for a mechanical or civil engineer to consider in detail the response of elastic, perfectly plastic structures which are subjected to *cyclic loading*. A brief definition of a cyclic loading is presented below.

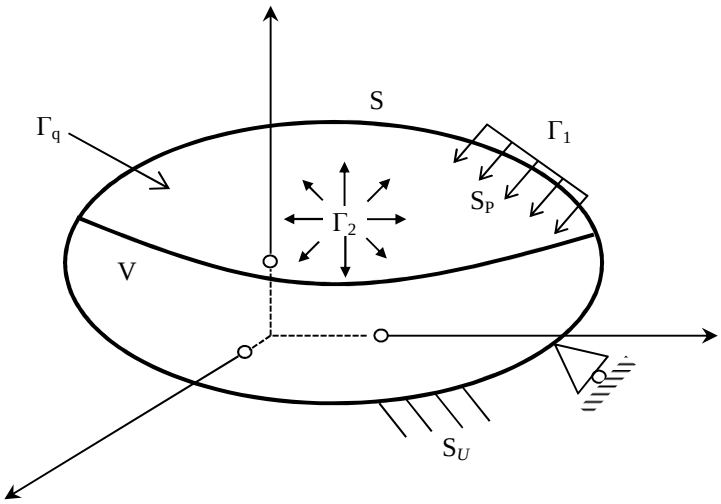

Figure 4.1 Structure with applied loads

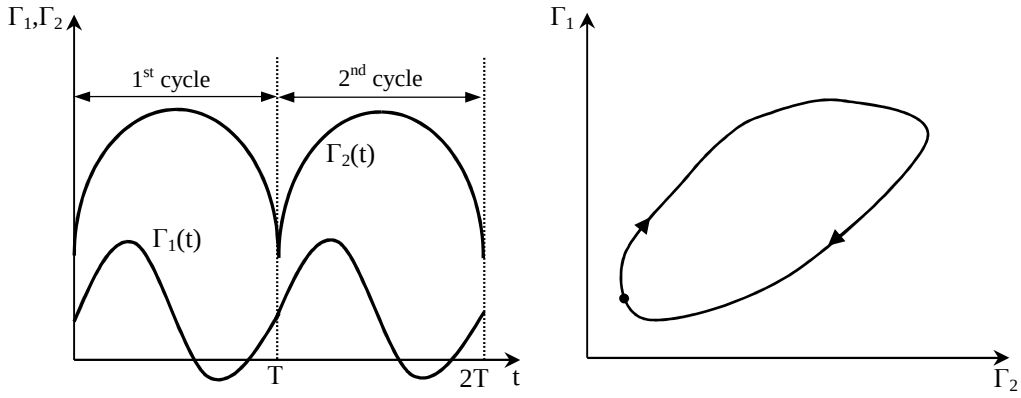

Figure 4.2 Cyclic loading state in a) time domain, b) load domain

Let us consider a body of volume V and a surface area S (see Fig.4.1). Let us assume that on a part of the surface S_U zero displacement conditions are applied. Body forces and surfaces loads on S_P may be applied on the structure. We shall carry out this discussion in terms of generalized loads $\mathbf{\Gamma}(t)$, where $\mathbf{\Gamma}(t) = \left\{\mathbf{\Gamma}_1(t), \mathbf{\Gamma}_2(t), ..., \mathbf{\Gamma}_q(t)\right\}$ is a general column vector that includes a total number of q loadings. They may represent e.g. volume forces, surface tractions, thermal loads or a combination of them. A cyclic loading program with period T must be such that

$$\mathbf{\Gamma}(t) = \mathbf{\Gamma}(t + nT) \tag{4.1}$$

for all t, where $n = 1,2,...$ denotes number of full cycles. A typical cyclic loading of two loads and its variation with time may be seen in Fig.4.2, where a loading trajectory of such a loading case in a two dimensional loading domain is shown in Fig.4.2(b). Considering t is a parameter which increases monotonically with real time, the above equation refers to an order in which the loading program is carried out, and the period T is not strictly related to real time.

Let us further consider that the structure of Fig.4.1 is made of an elastoplastic material and it is exposed to some cyclic loads of the form (4.1). Depending on the amplitude and the characteristics of the cyclic load, different asymptotic states may be realized, based on the evolution of the plastic strain rates. Thus, the structure may behave in one of the following ways (König, 1987):

a) For relative low load amplitudes, the plastic strain rates are identically zero after the structure attains a cyclic steady state 'cs' (Fig.4.3(a)). This may be asymptotically described by:

$$\dot{\boldsymbol{\varepsilon}}^{pl,cs} = \lim_{n\to\infty} \dot{\boldsymbol{\varepsilon}}^{pl} = 0 \tag{4.2}$$

where n denotes number of full cycles. The structure, after some plastic deformation in the initial load cycles, appears to be purely elastic. This type of behavior is characterized by stabilization of plastic deformations and is called *elastic shakedown* or *elastic adaptation*.

b) For certain patterns and levels of loadings, there might be points in the structure that undergo plastic strains of alternating sign over the cycle and tend to cancel each other (Fig.4.3(b)). Thus, the total deformation remains low. This asymptotically may be described as:

$$\begin{aligned} \dot{\boldsymbol{\varepsilon}}^{pl,cs} &= \lim_{\substack{n\to\infty \\ T}} \dot{\boldsymbol{\varepsilon}}^{pl} \neq 0 \\ \Delta\boldsymbol{\varepsilon}^{pl,cs} &= \int_0 \dot{\boldsymbol{\varepsilon}}^{pl,cs}(t)dt = 0 \end{aligned} \tag{4.3}$$

This type of cyclic state is called *alternating plasticity* or *reverse plasticity* or *plastic shakedown*. Consequently, cyclic loads on a structure which lead

eventually to alternating plasticity deformation may be expected to lead the structure to fail by localized fractures due to *low cycle fatigue*.

c) For certain patterns and high levels of loading (although below the statical load-carrying capacity of the structure), the plastic strain increments in each load cycle are of the same sign resulting to total strains and thus displacements to become large so that the structure becomes unserviceable (Fig.4.3(c)). The asymptotical behavior is described by:

$$\begin{aligned} \dot{\boldsymbol{\varepsilon}}^{pl,cs} &= \lim_{\substack{n\to\infty \\ T}} \dot{\boldsymbol{\varepsilon}}^{pl} \neq 0 \\ \Delta\boldsymbol{\varepsilon}^{pl,cs} &= \int_0 \dot{\boldsymbol{\varepsilon}}^{pl,cs}(t)dt \neq 0 \end{aligned} \tag{4.4}$$

This type of behavior is termed *incremental collapse* or *ratcheting*.

d) Finally, there might be cases where the load amplitude is higher than the ultimate strength capacity of the structure. Then the structures collapses instantaneously (plastic collapse) (see Fig.4.3(d)).

From the point of view of the designer, a cyclic loaded structure that does not shake down represents a situation in which failure is almost certain. The mechanism of failure may be that of reverse plasticity (low cycle fatigue), incremental collapse or a combination of these mechanisms. Thus, in the structural design process, the designer should ensure that, for any possible history of loading acting upon a given structure, its plastic deformation will stabilize, i.e. the structure will shake down.

It is worth mentioning that the phenomena of alternating plasticity and ratcheting may appear simultaneously in a structure, since one component of the plastic strain tensor increases with each subsequent load cycle whereas another one oscillates (König, 1987).

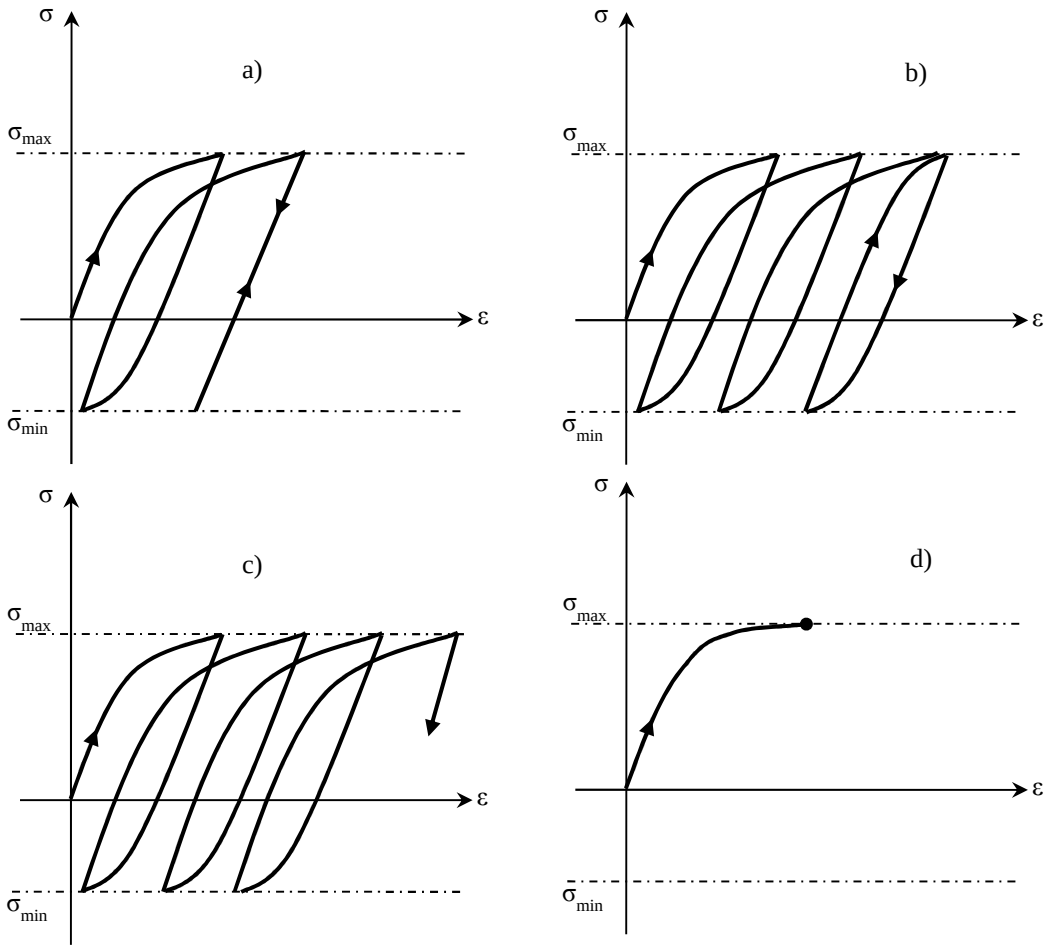

Figure 4.3 Structural response to cyclic loading a) shakedown, b) alternating plasticity, c) ratcheting collapse d) instantaneous plastic collapse

4.2. Definition of load domain and shakedown factor

For structures under cyclic loading, there are two major issues for a designer engineer. The first one, concerns the prediction of the possible cyclic behavior of an elastoplastic structure under a given cyclic loading program (i.e. loading program of Fig.4.2(a)) where the values of $\mathbf{\Gamma}(t)$ are known in some instants inside the cycle.

The second issue deals with the evaluation of safety margins through the shakedown analysis. The types of loads such as live load, wind load, water load, thermal load etc. are determined. The limits of variations of load intensities of particular types of loads are also known, given by the design codes or they follow

from some technological or service conditions. These applied loads may vary independently within some ranges. In the case of an independent variation of the loads, it is necessary to define a reference load domain Ω^0. This load domain Ω^0 represents a region in the space of variables and contains all possible load histories and any cyclic load program. This time history is not a-priori predictable. Any load path that belongs to Ω^0 represents a combination of external loadings, which may be applied out again and again. The bounds of this load domain are defined by some prescribed limits of each load that acts on the structure. Specifically, let us consider a set of loads $\mathbf{\Gamma}(t) = \left\{\mathbf{\Gamma}_1(t), \mathbf{\Gamma}_2(t), ..., \mathbf{\Gamma}_q(t)\right\}$ where any $\mathbf{\Gamma}_i(t)$ of them within a given range $\left[\mathbf{\Gamma}_i^-, \mathbf{\Gamma}_i^+\right]$ i.e.

$$\begin{aligned} \mathbf{\Gamma}_1^- &\le \mathbf{\Gamma}_1(t) \le \mathbf{\Gamma}_1^+ \\ \mathbf{\Gamma}_2^- &\le \mathbf{\Gamma}_2(t) \le \mathbf{\Gamma}_2^+ \\ &\vdots \\ \mathbf{\Gamma}_q^- &\le \mathbf{\Gamma}_q(t) \le \mathbf{\Gamma}_q^+ \end{aligned} \tag{4.5}$$

This set of loads span the convex polyhedral reference load domain Ω^0 of q dimensions having 2^q vertices in load space. Fig.4.4(a) and Fig.4.4(b) show the load domain of two and three load variables respectively.

Let all possible load combinations be multiplied by a load factor $\gamma > 0$ (negative values of γ have no physical meaning), namely let the reference domain Ω^0 either be expanded or be contracted or generally be varied (see Fig.4.4(a)). Hence, the actual set of loads acting on the structure is

$$\gamma * \mathbf{\Gamma}(t) \tag{4.6}$$

The main objective of the shakedown analysis is to evaluate the largest crucial value of the load factor γ which guarantees that the structure shakes down. This critical value is called *shakedown* factor and it is denoted by γ_{sh}. This means that for every variation of the load within the domain $\gamma_{sh} * \Omega^0$, during any time interval, the plastic deformation is stabilized and remains bounded. In other words, below γ_{sh} there exists a real constant $C > 0$ such that

$$\forall t \geq 0, \quad \int_0^t \int_V \sigma \cdot \varepsilon^p dV dt \leq C \tag{4.7}$$

This means that the total dissipation is *bounded in time*. A proof of this statement is described in section 4.11.

For a larger value $\gamma > \gamma_{sh}$ the structure may collapse due to either incremental collapse or alternating plasticity.

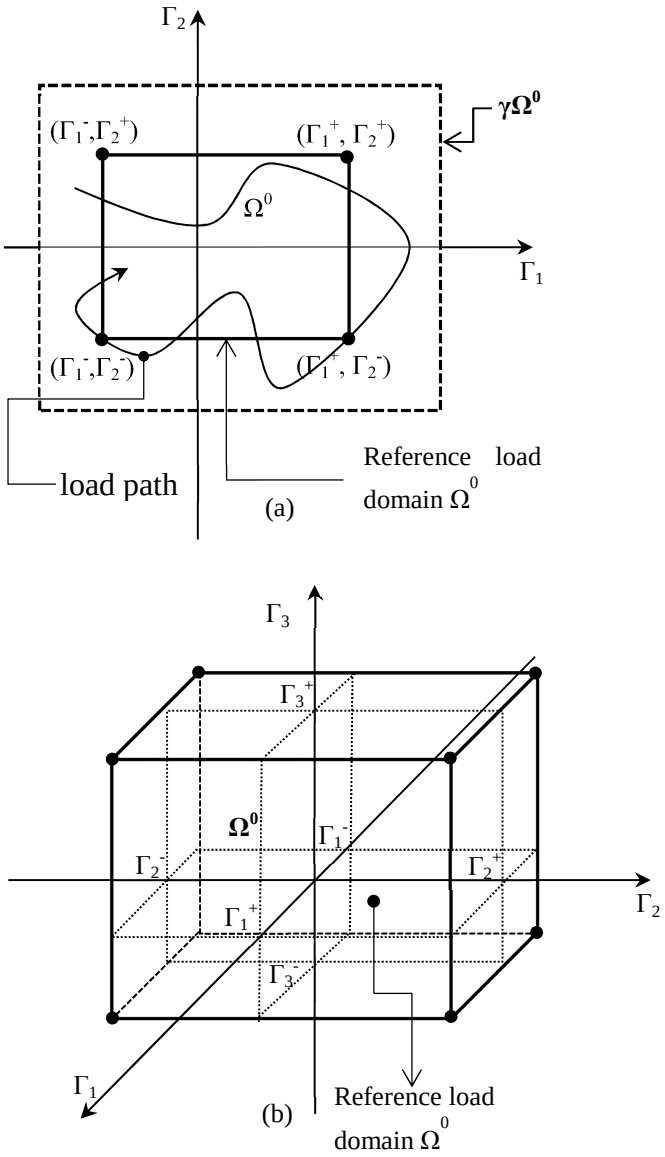

Figure 4.4 Load domain with a) two variable loads, b) three variable loads

4.3. Definition of shakedown domain

In order to define the shakedown domain, let us consider the problem of a set of two applied loads $\mathbf{\Gamma}(t) = \left\{\mathbf{\Gamma}_1(t), \mathbf{\Gamma}_2(t)\right\}$ that produces the reference load domain of Fig.4.5(a). Due to proportionality between loads and stresses, the load domain that produces shakedown is the largest rectangle in load space, defined by the shakedown factor γ_{sh}:

$$\mathbf{\Gamma}^{sh} = \gamma_{sh} * \mathbf{\Gamma}(t) \tag{4.8}$$

The residual stress field that is determined is common to all corners of the biggest rectangle due to the time independence of the residual stress field.

By repeating this process for different ratios of $\frac{\mathbf{\Gamma}_1}{\mathbf{\Gamma}_2}$, we may produce several loading points which are on the limit of the shakedown domain (Fig.4.5(b)). Then, the shakedown domain may be determined by the polygonal line joining the produced points (see Fig.4.5(b)).

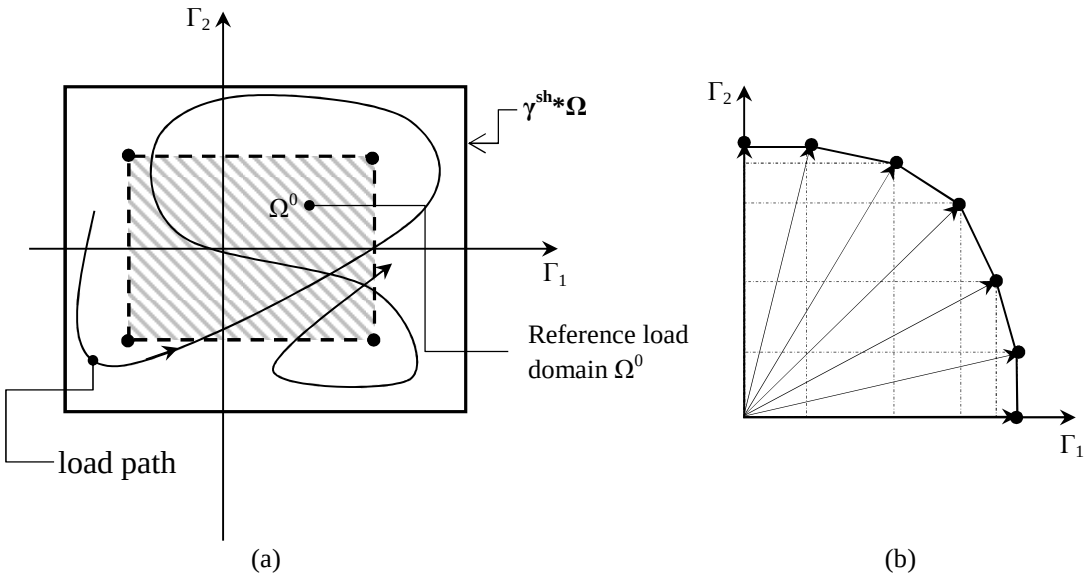

Figure 4.5 a) Load domain, b) shakedown domain

4.4. Existence and uniqueness of a steady stress cycle

Let us assume a body that is subjected to a cyclic mechanical loading program of the following form:

$$\mathbf{P}(t) = \mathbf{P}(t + nT) \tag{4.9}$$

where $\mathbf{P}(t) = \left\{P_1(t), P_2(t), ..., P_q(t)\right\}$ is a column vector, with q denoting the number of different loads.

Let us further consider that the body is also subjected to some temperature load of the form:

$$\theta(t) = \theta(t + nT), \qquad \theta(t) = \theta(x, y, z, t) \tag{4.10}$$

where t is the current time measured from the beginning of the cycle; T is the period of the cycle; $n = 1,2,...$ denotes the number of full cycles; and x, y, z are the spatial coordinates of a point inside the body.

Let us consider a stable material that obeys the Drucker's postulate (Drucker, 1959), (see also eqn.3.17), namely:

$$(\boldsymbol{\sigma} - \boldsymbol{\sigma}_*) \cdot \dot{\boldsymbol{\varepsilon}}^{pl} \geq 0, \quad (\boldsymbol{\sigma}_* - \boldsymbol{\sigma}) \cdot \dot{\boldsymbol{\varepsilon}}_*^{pl} \geq 0 \tag{4.11}$$

where $\boldsymbol{\sigma}$ and $\boldsymbol{\sigma}^*$ are two admissible stress states, and $\dot{\boldsymbol{\varepsilon}}^{pl}, \dot{\boldsymbol{\varepsilon}}_*^{pl}$ are the corresponding plastic strain rates associated with the yield surface. From (4.11) we get:

$$(\boldsymbol{\sigma} - \boldsymbol{\sigma}_*) \cdot (\dot{\boldsymbol{\varepsilon}}^{pl} - \dot{\boldsymbol{\varepsilon}}_*^{pl}) \geq 0 \tag{4.12}$$

The theorem on existence of steady cycles states as follows (Gokhfeld and Cherniavsky, 1980):

'At cyclic loading of a structure made of Drucker's material the stresses and the strain rates gradually stabilize to remain unaltered on passing to the next cycle'.

General proofs of the theorems on the existence of steady cycle stresses were given by Frederick and Armstrong (1966) and were based on Drucker's postulate. It should be mentioned that the steady state is reached in an asymptotic manner.

To prove the above statement, we consider the functional of the elastic energy potential I depending on the difference between the actual stresses at two instants of time differing by period T,

$$I = \int \frac{1}{2}\Big[\boldsymbol{\sigma}(t+T) - \boldsymbol{\sigma}(t)\Big] \cdot \Big[\boldsymbol{\varepsilon}^{el}(t+T) - \boldsymbol{\varepsilon}^{el}(t)\Big] dV \tag{4.13}$$

where $\boldsymbol{\varepsilon}^{el}$ are the stains corresponding to the stresses via Hooke's law in which, for simplicity, the tensor of elastic moduli is considered time-independent. The elastic strain energy potential I is positive when $\boldsymbol{\sigma}(t+T) \neq \boldsymbol{\sigma}(t)$ and vanishes only when at all points of the body the distribution of stress over two successive cycles is fully identical.

The rate of energy (4.13) is equal to:

$$\dot{I} = \int \Big[\boldsymbol{\sigma}(t+T) - \boldsymbol{\sigma}(t)\Big] \cdot \Big[\dot{\boldsymbol{\varepsilon}}^{el}(t+T) - \dot{\boldsymbol{\varepsilon}}^{el}(t)\Big] dV \tag{4.14}$$

Let us decompose the total strains into the elastic, plastic and thermal parts at a certain instant at which the actual stresses are $\boldsymbol{\sigma}(t)$:

$$\dot{\boldsymbol{\varepsilon}} = \dot{\boldsymbol{\varepsilon}}^{el} + \dot{\boldsymbol{\varepsilon}}^{pl} + \dot{\boldsymbol{\varepsilon}}^{th} \tag{4.15}$$

By substituting (4.15) to (4.14) we get:

$$\begin{aligned} \dot{I} = \int [\boldsymbol{\sigma}(t+T) - \boldsymbol{\sigma}(t)] \cdot [\dot{\boldsymbol{\varepsilon}}(t+T) - \dot{\boldsymbol{\varepsilon}}(t) - \dot{\boldsymbol{\varepsilon}}^{th}(t+T) + \\ + \dot{\boldsymbol{\varepsilon}}^{th}(t) - \dot{\boldsymbol{\varepsilon}}^{pl}(t+T) + \dot{\boldsymbol{\varepsilon}}^{pl}(t)] dV \end{aligned} \tag{4.16}$$

The stress field $\Big\{\boldsymbol{\sigma}(t+T) - \boldsymbol{\sigma}(t)\Big\}$ is clearly self-equilibrating or in equilibrium with zero external load since the body is loaded in exactly the same way both at the two time instants t and $t+T$ (see eqn.(4.9)). The total strain rates $\dot{\boldsymbol{\varepsilon}}(t+T)$ and $\dot{\boldsymbol{\varepsilon}}(t)$ are kinematically admissible. Thus, according to the Principle of Virtual Work (PVW) we may write:

$$\int [\boldsymbol{\sigma}(t+T) - \boldsymbol{\sigma}(t)] \cdot [\dot{\boldsymbol{\varepsilon}}(t+T) - \dot{\boldsymbol{\varepsilon}}(t)] dV = 0 \tag{4.17}$$

Since the thermal strain rates at the instant t and $t+T$ are identical (see eqn.(4.10)) we get:

$$\dot{\boldsymbol{\varepsilon}}^{th}(t+T) = \dot{\boldsymbol{\varepsilon}}^{th}(t) \tag{4.18}$$

Combining eqns.(4.18), (4.17) and (4.16) we get the following expression for the energy rate:

$$\dot{I} = -\int [\boldsymbol{\sigma}(t+T) - \boldsymbol{\sigma}(t)] \cdot [\dot{\boldsymbol{\varepsilon}}^{pl}(t+T) - \dot{\boldsymbol{\varepsilon}}^{pl}(t)] dV \tag{4.19}$$

Recalling (4.12), we conclude that $\dot{I}$ is non-positive.

Therefore eqns. (4.13) and (4.19) implies that $\dot{I} \leq 0$ and $I \geq 0$. Thus, the non-negative functional (4.13) is getting smaller as the time elapses and approaches zero as the difference between the stresses $\boldsymbol{\sigma}(t+T)$ and $\boldsymbol{\sigma}(t)$ decreases.

The theorem on uniqueness of stresses in the steady cycle can be written as follows (Gokhfeld and Cherniavsky, 1980):

'The stress distribution in the steady cycle does not depend upon the initial (prior to the first cycle) state of a structure and is unique in those regions in which the short-term plastic strains rates are non-vanishing in the steady cycle.'

The proof is similar to the above one of the existence theorem. Let us assume that at a certain instant inside the steady cycle two different instantaneous stress distributions $\boldsymbol{\sigma}$ and $\boldsymbol{\sigma}_0$ equilibrate the same magnitudes of external loading. It may be demonstrated that the non-negative functional (equivalently with eqn.(4.13))

$$I = \frac{1}{2}\int \left[\boldsymbol{\sigma} - \boldsymbol{\sigma}_0\right] \cdot \left[\boldsymbol{\varepsilon}^{el} - \boldsymbol{\varepsilon}_0^{el}\right] dV \tag{4.20}$$

has the following time derivative:

$$\dot{I} = -\int \left[\boldsymbol{\sigma} - \boldsymbol{\sigma}_0\right] \cdot \left[\dot{\boldsymbol{\varepsilon}}^{pl} - \dot{\boldsymbol{\varepsilon}}_0^{pl}\right] dV \tag{4.21}$$

which due to (4.12), is non-positive and hence it can only be decreasing. This decrease will not stop before the rates $\dot{\boldsymbol{\varepsilon}}^{pl}$ and $\boldsymbol{\varepsilon}_0^{pl}$ become equal to each other at those points of the body where they are non-vanishing over the cycle.

4.5. Classical formulations of the shakedown theorems

4.5.1. Statical shakedown theorem

The statical approach to the shakedown analysis of structures under repeated loading is based on the first or the statical shakedown theorem that was introduced by Melan (1938b). Thus the theorem is also known as *Melan's theorem*.

The theorem can be stated as follows (Gokhfeld and Cherniavsky, 1980):
'A structure under variable repeated loading will shake down, i.e. its behavior after a number of initial loading cycles will become purely elastic, if a time-independent distribution of residual stresses $\overline{\boldsymbol{\rho}}$ can be found, such that its superposition with elastic stresses $\boldsymbol{\sigma}^{el}$ results in a safe stress $\boldsymbol{\sigma}^{s}$ at any point in the structure:

$$\boldsymbol{\sigma}^{s} = \boldsymbol{\sigma}^{el} + \overline{\boldsymbol{\rho}} \tag{4.22}$$

or

$$\Phi\left(\boldsymbol{\sigma}^{el} + \overline{\boldsymbol{\rho}}\right) < 0 \tag{4.23}$$

under any combination of loads inside prescribed limits'. In (4.23) Φ denotes the yield function. The shakedown will be caused by plastic deformations during the first cycles which are followed by a certain steady, independent of a further loading program, residual stress distribution.

An alternative statement of the theorem can consequently be given as follows:
'Shakedown never takes place unless a time-independent residual stress distribution can be found such that under all possible load combinations the sum of the elastic stresses and the residual stresses leads to an admissible stress state.'

The second statement is obviously true whereas the first requires a formal proof. The following proof is a classical one on the whole theory of shakedown.

Let us assume that $\boldsymbol{\rho}$ is the current actual residual stress distribution, $\boldsymbol{\sigma}^{el}$ is the corresponding elastic stress and $\boldsymbol{\sigma}$ the current total stress in a considered cycle reaching the yield surface at an instant at which plastic strain rates at appropriate points of the body cease to be equal to zero.

$$\boldsymbol{\rho} = \boldsymbol{\sigma} - \boldsymbol{\sigma}^{el} \tag{4.24}$$

Let us consider the positive, elastic energy U corresponding to the self-equilibrating stress state $\left(\boldsymbol{\rho}-\overline{\boldsymbol{\rho}}\right)$:

$$U=\frac{1}{2}\int_{V}\left[\boldsymbol{\rho}-\overline{\boldsymbol{\rho}}\right]\cdot C\cdot\left[\boldsymbol{\rho}-\overline{\boldsymbol{\rho}}\right]dV \tag{4.25}$$

Taking into account that $\dot{\boldsymbol{\varepsilon}}_r^{el}=\mathbf{C}^{-1}\dot{\boldsymbol{\rho}}$ are the elastic strain rates corresponding to the residual stress rates that result from plastic deformation and that the residual stress field $\overline{\boldsymbol{\rho}}$ is time-independent we may write the following expression for the time derivative of energy U:

$$\dot{U}=\int_{V}\left[\boldsymbol{\rho}-\overline{\boldsymbol{\rho}}\right]\cdot\dot{\boldsymbol{\varepsilon}}_r^{el}dV \tag{4.26}$$

The distribution of the total residual strain rates may be decomposed into elastic an $\dot{\boldsymbol{\varepsilon}}_r^{el}$ and plastic part $\dot{\boldsymbol{\varepsilon}}^{pl}$:

$$\dot{\boldsymbol{\varepsilon}}_r=\dot{\boldsymbol{\varepsilon}}_r^{el}+\dot{\boldsymbol{\varepsilon}}^{pl} \tag{4.27}$$

Since the residual strain rate field is kinematically admissible we may use the Principle of Virtual Work (PVW) in the form:

$$\int_{V}\left[\boldsymbol{\rho}-\overline{\boldsymbol{\rho}}\right]\cdot\dot{\boldsymbol{\varepsilon}}_r dV=\int_{V}\left[\boldsymbol{\rho}-\overline{\boldsymbol{\rho}}\right]\cdot\left[\dot{\boldsymbol{\varepsilon}}_r^{el}+\dot{\boldsymbol{\varepsilon}}^{pl}\right]dV=0 \tag{4.28}$$

Combining eqns. (4.26) and (4.28) we get:

$$\dot{U}=-\int_{V}\left[\boldsymbol{\rho}-\overline{\boldsymbol{\rho}}\right]\cdot\dot{\boldsymbol{\varepsilon}}^{pl}dV \tag{4.29}$$

Using (4.22) and (4.24) we get the final expression for the time derivative of energy:

$$\dot{U}=-\int_{V}\left[\boldsymbol{\sigma}-\boldsymbol{\sigma}^{s}\right]\cdot\dot{\boldsymbol{\varepsilon}}^{pl}dV \tag{4.30}$$

According to Drucker's postulate (4.11) the derivative $\dot{U}$ is negative at those instants of time at which, non-vanishing plastic strain rates appear. Since the elastic energy U is non-negative it cannot decrease infinitely; eventually after a sufficiently large number n of cycles

$$\dot{U}(t) = 0 \tag{4.31}$$

and $U(t)$ becomes constant or zero. Eqn.(4.31) can be satisfied when

$$\boldsymbol{\sigma} = \boldsymbol{\sigma}^s, \quad \boldsymbol{\rho} = \overline{\boldsymbol{\rho}} \ \text{, or} \tag{4.32}$$

$$\dot{\boldsymbol{\varepsilon}}^{pl} = 0 \quad \text{for} \quad t > nT \tag{4.33}$$

at each point in the body. If eqn.(4.32) is satisfied at any point in the body $\Phi(\boldsymbol{\sigma}) < 0$ and hence no plastic strain can take place. Hence both (4.32) and(4.33) imply that the structure is behaving elastically and shakedown has occurred.

The above formulated statical shakedown theorem can be used to determine the parameters of the *limit cycle* for a structure subjected to a prescribed cyclic loading program. This cycle is the borderline state that separates shakedown from unrestrained cyclic plastic deformation. A detailed discussion of the characteristics of the limit cycle is given section 4.10.

It is worth mentioning that the kind of the elastic stresses was totally irrelevant as the kinematically admissible distribution of total residual strains and their rates was employed in the proof. Thus, these stresses could be developed either by mechanical loading or by thermal loading or by a combination of them. Thus the generalization of the theorem to cover thermal cyclic loading, requires no separate proof (Gokhfeld and Cherniavsky, 1980).

4.5.2. Kinematical shakedown theorem

The second shakedown theorem was established in 1956 by Koiter, who used the analogy between the theorems of limit analysis and those of shakedown. This theorem, generally referred to as *Koiter's theorem*, is formulated in terms of an admissible cycle of plastic strain rate cycle $\dot{\boldsymbol{\varepsilon}}_*^{pl}(t)$. The admissible cycle of plastic strain rate is thus characterized by plastic strain rates defined over one cycle of loading; it is further limited by the requirement that the plastic strain increment,

$$\Delta\boldsymbol{\varepsilon}_*^{pl} = \int_0^T \dot{\boldsymbol{\varepsilon}}_*^{pl} dt \tag{4.34}$$

should constitute a pertinent kinematically admissible strain distribution over a certain time interval. This is derived from

$$\Delta\boldsymbol{\varepsilon}_*^{pl} = \frac{1}{2}\left(\nabla\Delta\mathbf{u}^* + \left(\nabla\Delta\mathbf{u}^*\right)^T\right) \quad \text{in } V \tag{4.35}$$

i.e. by means of the equations of the type 3.23, and from the increments of residual displacements

$$\Delta\mathbf{u}^* = \int_0^T \dot{\mathbf{u}}^* dt \tag{4.36}$$

that satisfy the kinematic boundary conditions.

Since the plastic deformation increments per cycle of period T are kinematically admissible, they generate no changes in the elastic strains and stresses. Here is a short proof:

Since

$$\dot{\boldsymbol{\varepsilon}}_*^r = \dot{\boldsymbol{\varepsilon}}_*^{r,el} + \dot{\boldsymbol{\varepsilon}}_*^{pl} \tag{4.37}$$

and by integrating this equation over a cycle we may get:

$$\Delta\boldsymbol{\varepsilon}_*^r = \int_0^T \dot{\boldsymbol{\varepsilon}}_*^r dt = \int_0^T \dot{\boldsymbol{\varepsilon}}_*^{r,el} dt + \int_0^T \dot{\boldsymbol{\varepsilon}}_*^{pl} dt = \Delta\boldsymbol{\varepsilon}_*^{r,el} + \Delta\boldsymbol{\varepsilon}_*^{pl} \tag{4.38}$$

Since $\Delta\boldsymbol{\varepsilon}_*^r$ and $\Delta\boldsymbol{\varepsilon}_*^{pl}$ are kinematically admissible then the field $\Delta\boldsymbol{\varepsilon}_*^{r,el}$ is also kinematically admissible. Then, by the principle of virtual work

$$\int \Delta\boldsymbol{\varepsilon}_*^{r,el} \cdot \Delta\boldsymbol{\rho} dV = 0 \Rightarrow \int \Delta\boldsymbol{\varepsilon}_*^{r,el} \cdot \left(C\Delta\boldsymbol{\varepsilon}_*^{r,el}\right) dV = 0 \tag{4.39}$$

Thus, the elastic strain increments per cycle are equal to

$$\Delta\boldsymbol{\varepsilon}_{r*}^{el} = \int_0^T \dot{\boldsymbol{\varepsilon}}_r^{el} dt = 0 \tag{4.40}$$

Using an analogy with respective theorems of limit analysis, Koiter formulated the kinematical shakedown theorem in purely kinematical terms. His formulation is based

on the relationship between the work done by body forces and the plastic energy dissipation per cycle.

The energy dissipated in plastic work $W^*_{\text{int},pl}$ associated with this admissible cycle of plastic strain rate is

$$W^*_{\text{int},pl} = \int_0^T dt \int_V \boldsymbol{\sigma}^* \cdot \dot{\boldsymbol{\varepsilon}}^{pl}_* dV = \int_0^T dt \int_V D(\dot{\boldsymbol{\varepsilon}}^{pl}_*) dV \tag{4.41}$$

where $D(\dot{\boldsymbol{\varepsilon}}^{pl}_*)$ is the plastic energy dissipation and $\boldsymbol{\sigma}^*$ is the stress field associated with $\dot{\boldsymbol{\varepsilon}}^{pl}_*$ (see section 3.5).

The displacement rates $\dot{\mathbf{u}}^*$ can be used to define an expression that gives the external work W^*_{ext} done over a cycle by the external loads:

$$W^*_{ext} = \int_0^T dt \left\{ \int_V \mathbf{X}^T \dot{\mathbf{u}}^* dV + \int_S \mathbf{p}^T \dot{\mathbf{u}}^* dS \right\} \tag{4.42}$$

The virtual work equation (integrated over the cycle interval T) gives:

$$\int_0^T dt \left\{ \int_V \mathbf{X}^T \dot{\mathbf{u}}^* dV + \int_S \mathbf{p}^T \dot{\mathbf{u}}^* dS \right\} = \int_0^T dt \int_V \boldsymbol{\sigma} \cdot \dot{\boldsymbol{\varepsilon}}^r_* dV \tag{4.43}$$

The statement of Koiter's theorem involves the expressions defined in eqns.(4.41) and (4.42);

'If shakedown occurs in a given structure under given cyclic loading which vary within prescribed limits, then

$$W^*_{ext} \leq W^*_{\text{int},pl} \tag{4.44}$$

for all admissible cycles of plastic strain rates $\dot{\boldsymbol{\varepsilon}}^{pl}_*$'.

A proof of the above theorem is presented herein. It should be noted that the proof of Koiter's theorem is based on Melan's theorem.

If shakedown occurs in a structure, then according to Melan's theorem there exists a time independent residual stresses distribution $\overline{\boldsymbol{\rho}}$ such that stresses

$$\boldsymbol{\sigma} = \boldsymbol{\sigma}^{el} + \overline{\boldsymbol{\rho}} \tag{4.45}$$

satisfy the condition

$$\Phi\left(\boldsymbol{\sigma}\right) < 0 \tag{4.46}$$

i.e. the stress state $\boldsymbol{\sigma}$ is a safe stress field.

Let us choose *any* admissible cycle of strain rate $\dot{\boldsymbol{\varepsilon}}_*^{pl}$. Due to the fact that $\boldsymbol{\sigma}$ is a safe stress field, the Drucker's postulate gives

$$\left(\boldsymbol{\sigma}^* - \boldsymbol{\sigma}\right) \cdot \dot{\boldsymbol{\varepsilon}}_*^{pl} \geq 0 \tag{4.47}$$

at every point in the structure during the cycle. The stresses $\boldsymbol{\sigma}^*$ are associated with $\dot{\boldsymbol{\varepsilon}}_*^{pl}$ through the plastic flow rule.

Integration of ineq.(4.47) over the structure and over the cycle gives

$$\int_0^T dt \int_V \boldsymbol{\sigma} \cdot \dot{\boldsymbol{\varepsilon}}_*^{pl} dV \leq \int_0^T dt \int_V \boldsymbol{\sigma}^* \cdot \dot{\boldsymbol{\varepsilon}}_*^{pl} dV = W_{\mathrm{int},pl}^* \tag{4.48}$$

Making use of (4.43), (4.42) and since $\dot{\boldsymbol{\varepsilon}}_*^{r} = \dot{\boldsymbol{\varepsilon}}_*^{r,el} + \dot{\boldsymbol{\varepsilon}}_*^{pl}$ we may write

$$\begin{aligned} W_{ext}^* &= \int_0^T dt \left\{ \int_V \mathbf{X}^T \dot{\mathbf{u}}^* dV + \int_S \mathbf{p}^T \dot{\mathbf{u}}^* dS \right\} = \int_0^T dt \int_V \boldsymbol{\sigma} \cdot \dot{\boldsymbol{\varepsilon}}_*^{r} dV \\ &= \int_0^T dt \int_V \boldsymbol{\sigma} \cdot \dot{\boldsymbol{\varepsilon}}_*^{r,el} dV + \int_0^T dt \int_V \boldsymbol{\sigma} \cdot \dot{\boldsymbol{\varepsilon}}_*^{pl} dV \end{aligned} \tag{4.49}$$

The first term of the right hand of the above equation can be shown equal to zero:

$$\begin{aligned} &\int_0^T dt \int_V \boldsymbol{\sigma} \cdot \dot{\boldsymbol{\varepsilon}}_*^{r,el} dV = \int_0^T dt \int_V (\boldsymbol{\sigma}^{el} + \overline{\boldsymbol{\rho}}) \cdot \dot{\boldsymbol{\varepsilon}}_*^{r,el} dV = \\ &= \int_0^T dt \int_V \boldsymbol{\sigma}^{el} \cdot \dot{\boldsymbol{\varepsilon}}_*^{r,el} dV + \int_0^T dt \int_V \overline{\boldsymbol{\rho}} \cdot \dot{\boldsymbol{\varepsilon}}_*^{r,el} dV = \\ &= \int_0^T dt \int_V \boldsymbol{\sigma}^{el} \cdot \mathbf{C}^{-1} \dot{\boldsymbol{\rho}}_* dV + \int_0^T dt \int_V \overline{\boldsymbol{\rho}} \cdot \left(\mathbf{C}^{-1} \dot{\boldsymbol{\rho}}_*\right) dV = \\ &= \int_0^T dt \int_V \dot{\boldsymbol{\varepsilon}}^{el} \cdot \dot{\boldsymbol{\rho}}_* dV + \int_V \mathbf{C}^{-1} \overline{\boldsymbol{\rho}} \left(\int_0^T \dot{\boldsymbol{\rho}}_* dt \right) dV = 0 \end{aligned} \tag{4.50}$$

The first term is zero because $\dot{\boldsymbol{\rho}}$ is a self-equilibrating stress field since $\dot{\boldsymbol{\varepsilon}}^{el}$ is the strain field obtained from the elastic solution to the problem and it is kinematically admissible. The second term is equal to zero since the change in residual stresses over a cycle is zero.

Hence eqn.(4.49) becomes,

$$W_{ext}^{*} = \int_{0}^{T} dt \int_{V} \boldsymbol{\sigma} \cdot \dot{\boldsymbol{\varepsilon}}_{*}^{pl} dV \tag{4.51}$$

Consequently, substituting eqn.(4.51) into ineq.(4.48)

$$W_{ext}^{*} \leq W_{\mathrm{int},pl}^{*} \tag{4.52}$$

for all admissible plastic strain rate cycles if the structure shakes down. Koiter's theorem is thus established.

An alternative form of Koiter's theorem can be stated as follows:

'Shakedown never takes place, if any admissible plastic strain rate cycle $\dot{\boldsymbol{\varepsilon}}_{*}^{pl}$ can be found such that

$$W_{ext}^{*} > W_{\mathrm{int},pl}^{*} \tag{4.53}$$

Let us now make a useful observation. Combining the eqns.(4.51) and (4.45) we get

$$\begin{aligned} W_{ext}^{*} &= \int_{0}^{T} dt \int_{V} \boldsymbol{\sigma} \cdot \dot{\boldsymbol{\varepsilon}}_{*}^{pl} dV = \int_{0}^{T} dt \int_{V} \left(\boldsymbol{\sigma}^{el} + \overline{\boldsymbol{\rho}} \right) \cdot \dot{\boldsymbol{\varepsilon}}_{*}^{pl} dV = \\ &= \int_{0}^{T} dt \int_{V} \boldsymbol{\sigma}^{el} \cdot \dot{\boldsymbol{\varepsilon}}_{*}^{pl} dV + \int_{V} \overline{\boldsymbol{\rho}} \left(\int_{0}^{T} \dot{\boldsymbol{\varepsilon}}_{*}^{pl} dt \right) dV \end{aligned} \tag{4.54}$$

Since $\overline{\boldsymbol{\rho}}$ is self-equilibrating and $\Delta\boldsymbol{\varepsilon}_{*}^{pl} = \int_{0}^{T} \dot{\boldsymbol{\varepsilon}}_{*}^{pl} dt$ is kinematically admissible, the last term of the right hand is obviously equal to zero. Thus, eqn.(4.54) becomes

$$W_{ext}^{*} = \int_{0}^{T} dt \int_{V} \boldsymbol{\sigma}^{el} \cdot \dot{\boldsymbol{\varepsilon}}_{*}^{pl} dV \tag{4.55}$$

Thus, the kinematical theorems may be restated using this last equation.

4.6. Alternative statements of the shakedown theorems in terms of load factors

Let us suppose that our structure is subjected to a loading cycle $\gamma * \mathbf{\Gamma}(t)$, $0 \leq t \leq T$ (see eqn.(4.6)). As we already have mentioned, our objective is to evaluate the shakedown factor γ_{sh}. This limit load multiplier may be approached either from above (kinematic approach) or below (statical approach). Thus we can restate Melan's and Koiter's theorem in such a way that bounds on γ_{sh} are obtained.

Therefore Melan's theorem may be written in the form:

'The shakedown factor γ_{sh} is the largest load factor or multiplier γ for which a time independent residual stress field $\overline{\boldsymbol{\rho}}$ can be found such that

$$\Phi\left(\gamma \cdot \boldsymbol{\sigma}^{el} + \overline{\boldsymbol{\rho}}\right) < 0 \tag{4.56}$$

at all points in the body during the cycle of loading.' The stress field $\boldsymbol{\sigma}^{el}$ is the elastic solution for loads $\mathbf{\Gamma}(t)$.

The Koiter's theorem can be rewritten as follows:

'The shakedown factor γ_{sh} is the lowest multiplier γ obtained from the expression

$$\gamma = \frac{\int_0^T dt \int_V D(\dot{\boldsymbol{\varepsilon}}_*^{pl}) dV}{\int_0^T dt \int_V \boldsymbol{\sigma}^{el} \dot{\boldsymbol{\varepsilon}}_*^{pl} dV} \tag{4.57}$$

for any choice of admissible plastic strain rate cycle $\dot{\boldsymbol{\varepsilon}}_*^{pl}$.

Any value of γ obtained from equating W_{ext}^* and $W_{\mathrm{int},pl}^*$ in Koiter's theorem is thus an *upper bound* on γ_{sh}. The result implies that shakedown will not occur for any $\gamma > \gamma_{sh}$.

4.7. Shakedown theorem as a mathematical programming problem

The restatements of the theorems of the previous section may turn the problem of evaluating the shakedown factor into a mathematical programming problem.

4.7.1. Static shakedown theorem

Based on the static shakedown theorem of section 4.6, a permanent statically admissible residual stress field can be found in order to obtain a maximum load domain i.e. a maximum load factor γ_{sh} that satisfies (4.56). Thus the shakedown problem can be treated as the following maximization problem of nonlinear programming:

$$\begin{aligned} &\bar{\gamma_{sh}} = \max \gamma \\ &s.t.: \\ &\left| \begin{array}{ll} \Phi\left(\gamma \boldsymbol{\sigma}^{el}(\mathbf{x},t) + \bar{\boldsymbol{\rho}}(\mathbf{x})\right) \leq 0 & \forall \mathbf{x} \in V,\ \forall t \\ div\bar{\boldsymbol{\rho}}(\mathbf{x}) = \mathbf{0} & \forall \mathbf{x} \in V \\ \bar{\boldsymbol{\rho}}(\mathbf{x})\mathbf{n} = \mathbf{0} & \forall \mathbf{x} \in S_P \end{array} \right. \end{aligned} \tag{4.58}$$

The obtained shakedown load factor is generally a lower bound.

4.7.2. Kinematic shakedown theorem

Based on the kinematic theorem of section 4.6, an upper bound of the shakedown limit load factor can be evaluated. The shakedown problem using the kinematical approach can be seen as the following mathematical minimization problem of nonlinear programming:

$$\gamma_{sh}^{+} = \min \frac{\int_0^T dt \int_V D(\dot{\boldsymbol{\varepsilon}}_*^{pl}) dV}{\int_0^T dt \int_V \boldsymbol{\sigma}^{el}(\mathbf{x},t) \cdot \dot{\boldsymbol{\varepsilon}}_*^{pl} dV}$$

$$s.t.: \quad \left| \begin{array}{l} \Delta\boldsymbol{\varepsilon}^{pl} = \int_0^T \dot{\boldsymbol{\varepsilon}}_*^{pl} dt \\ \Delta\boldsymbol{\varepsilon}^{pl} = \frac{1}{2}\left(\nabla(\Delta\mathbf{u}) + (\nabla(\Delta\mathbf{u}))^T \right) \quad \text{in } V \\ \Delta\mathbf{u} = \mathbf{0} \quad \text{on } S_u \end{array} \right. \tag{4.59}$$

In Fig.4.6 one may see the comparison between a lower bound and an upper bound solution.

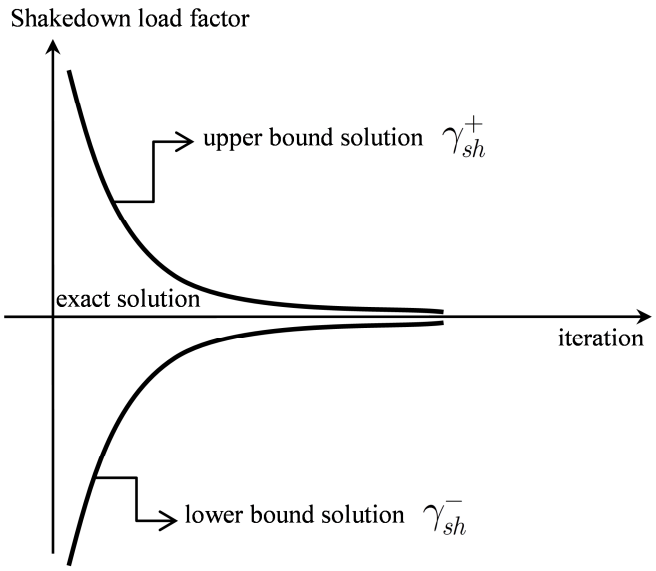

Figure 4.6 Exact and approximate solutions

4.8. Shakedown analysis via the analysis of some cyclic load process

Until now it has not been clear what the relationship is between the behavior of a given structure over a cyclic load path and over a general, arbitrary path contained

within some limits. However, these two cases are equivalent (König, 1987). A proof of this is described in this section.

According to König (1987) there are some important conclusions following directly from the static shakedown theorem that provide useful information on shakedown analysis. These conclusions are used to describe some different formulations of the shakedown theorems (Morelle, 1984). All the theorems below are based on the convexity of the yield surface and the load domain.

Convex envelope theorem. "Shakedown will occur for the load domain Ω if and only if it occurs for its convex envelope $\mathfrak{W}$".

Cyclic shakedown theorem. " Let us consider a cyclic loading

$$\beta_k(t) = \beta_k(t + nT), \quad k = 1,2,...,n \tag{4.60}$$

If shakedown occurs for this cyclic loading $\beta_k(t)$, then it will occur for every loading (even non-cyclic) contained inside this cycle".

Convex-cycle theorem. We can now combine the above two theorems into a new one: "If shakedown occurs for a cyclic loading containing all m points of the convex envelope $\mathfrak{W}$, then shakedown will occur for every load program in Ω (König and Kleiber, 1978).

This last conclusion provides a practical check on whether a given structure will shake down over any load path within Ω. Thus, one has to investigate the behavior of the structure over a cyclic load path which contains all the corners of the polyhedral load domain.

This theorem suggests that we should define a 'unitary loading cycle':

$$\mathbf{P}_0(\mathbf{x},t), \quad t \in \left[t_i, t_i + \Delta t\right] \tag{4.61}$$

such that

$$\mathbf{P}_0(\mathbf{x},t_i) = \mathbf{P}_0(\mathbf{x},t_i + \Delta t) \tag{4.62}$$

and contains all the vertices of the load domain Ω. This unitary load cycle for a two-dimensional case is shown in Fig.4.7.

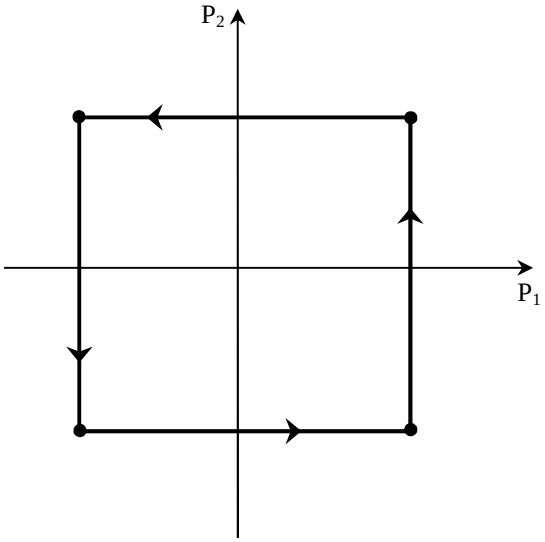

Figure 4.7 Unitary loading cycle – bidimensional case

The elastic solution corresponding to this cycle is:

$$(\boldsymbol{\sigma}^{*0}, \boldsymbol{\varepsilon}^{*0}) \tag{4.63}$$

If we increase the load domain proportionally to the load factor γ, we can define the 'γ-loading cycle':

$$\mathbf{P}_{\gamma}(\mathbf{x}, t) = \gamma \mathbf{P}_{0}(\mathbf{x}, t) \tag{4.64}$$

and the corresponding elastic solution, such that:

$$\begin{aligned} (\boldsymbol{\sigma}^{*})_{\gamma} &= \gamma \boldsymbol{\sigma}^{*0} \\ (\boldsymbol{\varepsilon}^{*})_{\gamma} &= \gamma \boldsymbol{\varepsilon}^{*0} \end{aligned} \tag{4.65}$$

The previous theorems allow us to say that the limit load factor corresponding to the 'γ^{sh}-loading cycle' will be the γ^{sh} corresponding to Ω.

We can now proceed to restate the lower bound theorem.

Restatement of the static or lower bound theorem and its proof

The limit load factor γ_{sh} is the largest of the statically admissible load factors γ^{sa} which are such that:

$$\boldsymbol{\sigma}^{sa}(\mathbf{x}, t) = \gamma^{sa} \boldsymbol{\sigma}^{*0}(\mathbf{x}, t) + \tilde{\boldsymbol{\rho}}^{sa}(\mathbf{x}) \tag{4.66}$$

is statically admissible with the 'γ^{sa}-loading cycle $\mathbf{P}_{\gamma^{sa}}$' and

$$\Phi\Big(\boldsymbol{\sigma}^{sa}(\mathbf{x},t)\Big) \leq 0 \quad \forall t \in \big[t_i, t_i + \Delta t_i\big] \tag{4.67}$$

where $\tilde{\boldsymbol{\rho}}^{sa}(\mathbf{x})$ is a time-independent residual stress field:

$$\dot{\tilde{\boldsymbol{\rho}}}^{sa}(\mathbf{x}) = 0 \tag{4.68}$$

Let us consider:

a) the real limit (shakedown) stress state, corresponding to the limit 'γ^{sh}-cycle':

$$\boldsymbol{\sigma}(\mathbf{x},t) = \gamma^{sh}\boldsymbol{\sigma}^{*0}(\mathbf{x},t) + \overline{\boldsymbol{\rho}}(\mathbf{x}) \tag{4.69}$$

such that $\dot{\overline{\boldsymbol{\rho}}}(\mathbf{x}) = \mathbf{0}$.

(b) the statically admissible stress field of the theorem of eqn.(4.66)

If $\dot{\boldsymbol{\varepsilon}}^{r}$ is the real residual strain-rate field corresponding to $\boldsymbol{\sigma}$ in the structure, we can define the following functional:

$$I = \int_V \Big[\boldsymbol{\sigma} - \boldsymbol{\sigma}^{sa}\Big] \cdot \dot{\boldsymbol{\varepsilon}}^{r} dV \tag{4.70}$$

Using eqns.(4.66) and (4.69) we get:

$$I = (\gamma^{sh} - \gamma^{sa}) \int_V \boldsymbol{\sigma}^{*0} \cdot \dot{\boldsymbol{\varepsilon}}^{r} dV + \cancel{\int_V \Big[\overline{\boldsymbol{\rho}} - \tilde{\boldsymbol{\rho}}^{sa}\Big] \cdot \dot{\boldsymbol{\varepsilon}}^{r} dV} \tag{4.71}$$

Since the field $\Big[\overline{\boldsymbol{\rho}} - \tilde{\boldsymbol{\rho}}^{sa}\Big]$ is a self-equilibrating distribution of time-independent stresses and $\dot{\boldsymbol{\varepsilon}}^{r}$ is zero kinematically admissible, from the principle of virtual work we get that the second part of eqn.(4.71) is equal to zero.

We also have

$$\dot{\boldsymbol{\varepsilon}}^{r}(\mathbf{x},t) = \mathbf{C}^{-1}\dot{\overline{\boldsymbol{\rho}}}(\mathbf{x}) + \dot{\boldsymbol{\varepsilon}}^{pl}(\mathbf{x},t) = \dot{\boldsymbol{\varepsilon}}^{pl}(\mathbf{x},t) \tag{4.72}$$

Combining (4.70) and (4.72) we obtain:

$$I = \int_V \Big[\boldsymbol{\sigma} - \boldsymbol{\sigma}^{sa}\Big] \cdot \dot{\boldsymbol{\varepsilon}}^{pl} dV \geq 0 \tag{4.73}$$

by Drucker's postulate, because of the eqn.(4.67).

On the other hand, using (4.69), we may write:

$$\int_V \boldsymbol{\sigma}^{*0} \cdot \dot{\boldsymbol{\varepsilon}}^r dV = \frac{1}{\gamma^{sh}} \int_V \left[\boldsymbol{\sigma}(\mathbf{x},t) - \overline{\boldsymbol{\rho}}(\mathbf{x}) \right] \cdot \dot{\boldsymbol{\varepsilon}}^r dV \geq 0 \tag{4.74}$$

where the integrand is also greater than or equal to zero according to Drucker's postulate, because we have $\Phi\left(\overline{\boldsymbol{\rho}}(\mathbf{x})\right) \leq 0$ with $\overline{\boldsymbol{\rho}}(\mathbf{x})$ being the real residual stress field in the body.

From (4.71), (4.73) and (4.74) we get that $(\gamma^{sh} - \gamma^{sa}) \geq 0$. Thus,

$$\gamma^{sa} \leq \gamma^{sh} \tag{4.75}$$

and the theorem is proved.

4.9. Statements of criteria for incremental collapse and alternating plasticity

In this section a short discussion about the conditions of safety against incremental collapse and alternating plasticity, based on a kinematical approach, is presented.

Firstly, it should be noticed that any plastic strain history $\dot{\boldsymbol{\varepsilon}}^{pl}(\mathbf{x},t)$ within any time interval $t \in (0,T)$, resulting in a kinematically admissible plastic strain increments can always be decomposed into two terms (König, 1987):

$$\dot{\boldsymbol{\varepsilon}}^{pl}(\mathbf{x},t) = \overline{\dot{\boldsymbol{\varepsilon}}}^{pl}(\mathbf{x},t) + \hat{\dot{\boldsymbol{\varepsilon}}}^{pl}(\mathbf{x},t) \tag{4.76}$$

where $\overline{\dot{\boldsymbol{\varepsilon}}}^{pl}(\mathbf{x},t)$ involves a perfect incremental collapse process, while $\hat{\dot{\boldsymbol{\varepsilon}}}^{pl}(\mathbf{x},t)$ involves an alternating plasticity process. As mentioned in section 4.1, both forms of inadaptation, incremental collapse and alternating plasticity, may happen to combine.

Therefore, two possible modes may be determined precisely in the following way (König, 1987):

1) A prefect incremental collapse process, over a certain time interval $(0,T)$, is a process of plastic deformation $\overline{\boldsymbol{\varepsilon}}^{pl}(\mathbf{x},t)$ in which a kinematically admissible plastic strain increment $\Delta\overline{\boldsymbol{\varepsilon}}^{pl}(\mathbf{x}) = \overline{\boldsymbol{\varepsilon}}^{pl}(\mathbf{x},T) - \overline{\boldsymbol{\varepsilon}}^{pl}(\mathbf{x},0)$ is attained in a proportional and monotonic way, for each $\mathbf{x} \in V$. Thus

$$
\begin{aligned}
&\Delta\overline{\boldsymbol{\varepsilon}}^{pl} = \frac{1}{2}\Big(\nabla\big(\Delta\mathbf{u}\big) + \big(\nabla\big(\Delta\mathbf{u}\big)\big)^{T}\Big) \quad \text{in } V \\
&\Delta\mathbf{u} = \mathbf{0} \quad \text{on } S_U \\
&\dot{\overline{\boldsymbol{\varepsilon}}}^{pl}(\mathbf{x},T) = \dot{\Lambda}(\mathbf{x},T)\cdot\Delta\overline{\boldsymbol{\varepsilon}}^{pl}(\mathbf{x}) \\
&\dot{\Lambda}(\mathbf{x},t) \geq 0 \\
&\Lambda(\mathbf{x},0) = 0 \\
&\Lambda(\mathbf{x},T) = 1
\end{aligned}
\tag{4.77}
$$

2) An alternating plasticity process is any process of plastic deformation $\hat{\dot{\boldsymbol{\varepsilon}}}^{pl}(\mathbf{x},t)$ within a certain time interval $(0,T)$, such that the total increment of plastic strains $\Delta\hat{\boldsymbol{\varepsilon}}^{pl}(\mathbf{x})$ over this period is equal to zero

$$
\Delta\hat{\boldsymbol{\varepsilon}}^{pl}(\mathbf{x}) = \int_0^T \hat{\dot{\boldsymbol{\varepsilon}}}^{pl}(\mathbf{x},t)dt = 0 \tag{4.78}
$$

for each $\mathbf{x} \in V$.

Based on the kinematical approach, the criteria of safety with respect to perfect incremental collapse may be obtained by considering the kinematic shakedown safety condition (4.44) and assuming the plastic strain history of eqn. (4.77). By substituting we obtain the following theorem:

'Incremental collapse will not happen in a structure if

$$
\int_0^T \int_V \sigma^{el}(\mathbf{x},t)\dot{\Lambda}(\mathbf{x},t)\Delta\overline{\boldsymbol{\varepsilon}}^{pl}(\mathbf{x})dVdt \leq \int_0^T \int_V D(\dot{\Lambda}\Delta\overline{\boldsymbol{\varepsilon}}^{pl})dVdt \tag{4.79}
$$

whereas incremental collapse will happen if

$$
\int_0^T \int_V \sigma^{el}(\mathbf{x},t)\dot{\Lambda}(\mathbf{x},t)\Delta\overline{\boldsymbol{\varepsilon}}^{pl}(\mathbf{x})dVdt > \int_0^T \int_V D(\dot{\Lambda}\Delta\overline{\boldsymbol{\varepsilon}}^{pl})dVdt \tag{4.80}
$$

with

$$\Delta\overline{\boldsymbol{\varepsilon}}^{pl}(\mathbf{x}) = \int_0^T \dot{\overline{\boldsymbol{\varepsilon}}}^{pl}(\mathbf{x},t)dt \neq 0$$
$$\Delta\overline{\boldsymbol{\varepsilon}}^{pl} = \frac{1}{2}\Big(\nabla\big(\Delta\mathbf{u}\big) + \big(\nabla\big(\Delta\mathbf{u}\big)\big)^T\Big) \quad \text{in } V \tag{4.81}$$
$$\Delta\mathbf{u} = \mathbf{0} \quad \text{on } S_U$$

The criteria of safety against alternating plasticity (or low cycle fatigue) may be obtained using the plastic strain history (4.78) and the kinematic safety condition (4.44). Thus, we get that

‘ Alternating plasticity will not happen if

$$\int_0^T \int_V \sigma^{el}(\mathbf{x},t)\cdot\hat{\dot{\boldsymbol{\varepsilon}}}^{pl}(\mathbf{x},t)dVdt \leq \int_0^T \int_V D\Big(\hat{\dot{\boldsymbol{\varepsilon}}}^{pl}\Big)dVdt \tag{4.82}$$

Alternating plasticity will happen if

$$\int_0^T \int_V \sigma^{el}(\mathbf{x},t)\cdot\hat{\dot{\boldsymbol{\varepsilon}}}^{pl}(\mathbf{x},t)dVdt > \int_0^T \int_V D\Big(\hat{\dot{\boldsymbol{\varepsilon}}}^{pl}\Big)dVdt \tag{4.83}$$

with

$$\Delta\hat{\boldsymbol{\varepsilon}}^{pl}(\mathbf{x}) = \int_0^T \hat{\dot{\boldsymbol{\varepsilon}}}^{pl}(\mathbf{x},t)dt = 0 \tag{4.84}$$

4.10. On the uniqueness of stress state at the limiting cycle

The statical and kinematical theorems allow someone, in the general case, to assess both from above and from below the limiting values of loading parameters at which shakedown occurs. Herein, a description of the uniqueness of the stresses at the limiting cycle is presented.

Considering a fixed program of cyclic loading, a demonstration that the residual stress distribution is unique, in those regions of the body where the plastic strains during the limiting cycle are non-vanishing, and independent of the preceding deformation history, will be described. Consequently the instantaneous distribution of

actual total stresses, i.e. elastic plus residual, is also unique. A proof constructed by reduction to absurdity will be presented (Gokhfeld and Cherniavsky, 1980).

Let us denote with $\boldsymbol{\sigma}(\tau)$ the actual total stresses in the limiting cycle, i.e. in the state preceding existence of cyclic plastic deformation under the prescribed loading. Let us consider that $\dot{\boldsymbol{\varepsilon}}^{pl}(\tau)$ is the corresponding, consistent with the associated flow rule, admissible cycle of plastic strain rates. Let us suppose that there exists an admissible stress field, denoted by $\boldsymbol{\sigma}'(\tau)$, different to $\boldsymbol{\sigma}(\tau)$, that is in equilibrium with the same program of cyclic loading but preceded by different history.

Based on Melan theorem, in the shakedown situation, we may write

$$\boldsymbol{\sigma} = \boldsymbol{\sigma}^{el} + \overline{\boldsymbol{\rho}}, \qquad \boldsymbol{\sigma}' = \boldsymbol{\sigma}^{el} + \overline{\boldsymbol{\rho}}' \tag{4.85}$$

where $\boldsymbol{\sigma}^{el}$ are the elastic stresses, common in both distributions under the given loading program, whilst $\overline{\boldsymbol{\rho}}$ and $\overline{\boldsymbol{\rho}}'$ are time-independent residual stresses, differing each other.

Thus, using the Principle of Virtual Work (PVW) we get:

$$\begin{aligned} &\int_0^T dt \int \left(\boldsymbol{\sigma} - \boldsymbol{\sigma}'\right) \cdot \dot{\boldsymbol{\varepsilon}}^{pl} dV = \int_0^T dt \int \left(\overline{\boldsymbol{\rho}} - \overline{\boldsymbol{\rho}}'\right) \cdot \dot{\boldsymbol{\varepsilon}}^{pl} dV = \\ &= \int \left(\overline{\boldsymbol{\rho}} - \overline{\boldsymbol{\rho}}'\right) \left(\int_0^T \dot{\boldsymbol{\varepsilon}}^{pl} dt \right) dV = \int \left(\overline{\boldsymbol{\rho}} - \overline{\boldsymbol{\rho}}'\right) \cdot \Delta\boldsymbol{\varepsilon}^{pl} dV = 0 \end{aligned} \tag{4.86}$$

since $\left(\overline{\boldsymbol{\rho}} - \overline{\boldsymbol{\rho}}'\right)$ is a self-equilibrating distribution of time-independent stresses and $\Delta\boldsymbol{\varepsilon}^{pl}$ is kinematical admissible.

Now, according to the Drucker's postulate we have

$$\left(\boldsymbol{\sigma} - \boldsymbol{\sigma}'\right) \cdot \dot{\boldsymbol{\varepsilon}}^{pl} \geq 0 \tag{4.87}$$

where the strict inequality applied at the points of the body where the stresses $\boldsymbol{\sigma}$ reach the yield surface during the cycle and $\boldsymbol{\sigma} \neq \boldsymbol{\sigma}'$ at the corresponding time instants. Thus, the conditions (4.86) and (4.87) are contradict, unless the stress field is unique in those regions of the body in which stresses over the cycle reach the yield surface.

According to (Gokhfeld and Cherniavsky, 1980) although the above proof is valid for a prescribed loading program, the argument concerning the uniqueness of self-equilibrating stresses over the limiting cycle can be extended to a general loading program varying between prescribed limits.

Finally, it should be mentioned that it was just the limiting cycle considered herein. If a structure shakes down at a cycle whose parameters are below the limiting ones, there is no evidence that the stabilized stress state is unique.

4.11. On the boundedness of inelastic deformation preceding shakedown

This issue was first addressed by Koiter (1960), who adopted the plastic work done in the shakedown process as the estimate of an average level of strain accumulation.

Let us assume that a time-independent distribution of residual stresses $\overline{\boldsymbol{\rho}}$ can be found, such that its superposition with elastic stresses $\boldsymbol{\sigma}^{el}$ results in a safe stress $\boldsymbol{\sigma}^{s}$ at any point in the structure:

$$\boldsymbol{\sigma}^{s} = \boldsymbol{\sigma}^{el} + \overline{\boldsymbol{\rho}} \tag{4.88}$$

or

$$\Phi\left(\boldsymbol{\sigma}^{el} + \overline{\boldsymbol{\rho}}\right) < 0$$

Let $\boldsymbol{\rho}$ be the current actual residual stress distribution, $\boldsymbol{\sigma}^{el}$ be the corresponding elastic stress and $\boldsymbol{\sigma}$ the current total stress in a considered cycle reaching the yield surface at an instant.

Let us consider the non-negative residual elastic energy of the stress difference $(\boldsymbol{\rho} - \overline{\boldsymbol{\rho}})$

$$U = \frac{1}{2}\int_{V} (\boldsymbol{\rho} - \overline{\boldsymbol{\rho}}) \cdot \mathbf{C} \cdot (\boldsymbol{\rho} - \overline{\boldsymbol{\rho}}) dV \geq 0 \tag{4.89}$$

Then using eqns. (4.25)-(4.30) we get the following expression for the residual elastic energy:

$$\dot{U} = -\int_V \left[\boldsymbol{\sigma} - \boldsymbol{\sigma}^s\right] \cdot \dot{\boldsymbol{\varepsilon}}^{pl} dV \leq 0 \tag{4.90}$$

Since $\boldsymbol{\sigma}^s$ is a safe stress, there exists a scalar $m > 1$ such that $m\boldsymbol{\sigma}^s$ is plastically admissible. Hence, according to Drucker's postulate we have:

$$(\boldsymbol{\sigma} - m\boldsymbol{\sigma}^s) \cdot \dot{\boldsymbol{\varepsilon}}^{pl} \geq 0 \tag{4.91}$$

which, after some rearrangements, gives

$$(m-1)\boldsymbol{\sigma} \cdot \dot{\boldsymbol{\varepsilon}}^{pl} \leq m(\boldsymbol{\sigma} - \boldsymbol{\sigma}^s) \cdot \dot{\boldsymbol{\varepsilon}}^{pl} \tag{4.92}$$

Integration over the body volume leads to

$$\int_V \boldsymbol{\sigma} \cdot \dot{\boldsymbol{\varepsilon}}^{pl} dV \leq -\frac{m}{m-1}\dot{U} \tag{4.93}$$

After integrating with respect to time we obtain:

$$W_{pl} = \int_0^t \int_V \boldsymbol{\sigma} \cdot \dot{\boldsymbol{\varepsilon}}^{pl} dV dt \leq -\frac{m}{m-1} \int_o^t \dot{U} dt = \frac{m}{m-1}\big(U(0) - U(t)\big) \tag{4.94}$$

where W_{pl} is the energy dissipated in plastic work.

Because of its definition, is $U(t)$ non negative and one has

$$U(0) \geq U(t) \tag{4.95}$$

and

$$\dot{U}(t) \to 0, \quad U(t) \to const \quad \text{for} \quad t \to \infty \tag{4.96}$$

that leads to:

$$\forall t \geq 0, \qquad W_{pl} = \int_0^t \int_V \boldsymbol{\sigma} \cdot \dot{\boldsymbol{\varepsilon}}^{pl} dV dt \leq \frac{m}{m-1} U(0) \tag{4.97}$$

The boundedness of the plastic work is thus established.

4.12. Limit states in a truss

In this section, an example of a cyclically loaded of truss will be considered in order to illustrate the limit states of shakedown, alternating plasticity and incremental

collapse. We consider a simple truss (Fig.4.8) composed of pin jointed bars which is indeterminate of degree one and is subjected to a horizontal and a vertical load (Martin, 1975). The bars are uniform along their length and have the same cross-sectional properties. The bars are made of an elastic-perfectly plastic material with yield values of the axial forces N_i equal to N_Y and $-N_Y$.

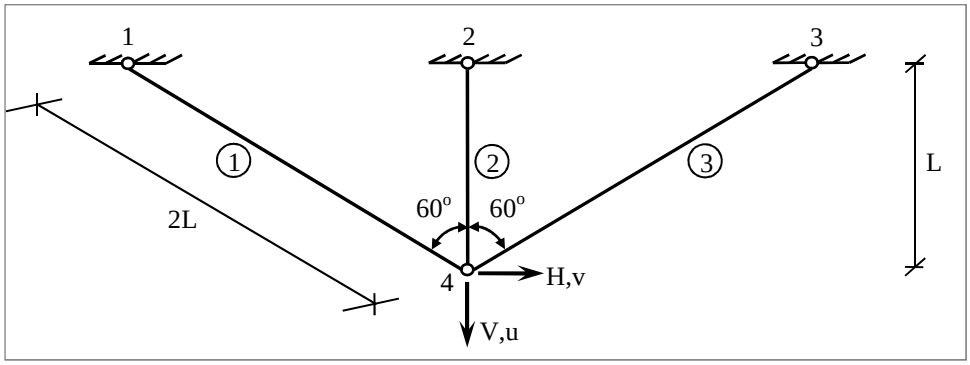

Figure 4.8 Truss example

Let us denote the tensile forces in the bars 1-4,2-4,3-4 by N_1, N_2, N_3 respectively. The equilibrium equation at node 4 gives:

$$\begin{aligned} N_1 + 2N_2 + N_3 &= 2V \\ N_1 - N_3 &= \frac{2H}{\sqrt{3}} \end{aligned} \tag{4.98}$$

The strain displacement relations give the expression of the strains in the bars, denoted by $\varepsilon_1, \varepsilon_2, \varepsilon_3$, related to the displacements v, u:

$$\begin{aligned} \varepsilon_1 &= \frac{1}{2L}\left(\frac{u}{2} + \frac{\sqrt{3}}{2}v\right) \\ \varepsilon_2 &= \frac{u}{L} \\ \varepsilon_3 &= \frac{1}{2L}\left(\frac{u}{2} - \frac{\sqrt{3}}{2}v\right) \end{aligned} \tag{4.99}$$

Elimination of v, u from the above equations leads to the compatibility equation:

$$\varepsilon_1 + \varepsilon_3 = \frac{1}{2}\varepsilon_2 \tag{4.100}$$

By substituting the elastic stress-strain relations:

$$\varepsilon_1 = \frac{N_1}{EA}, \quad \varepsilon_2 = \frac{N_2}{EA}, \quad \varepsilon_3 = \frac{N_3}{EA} \tag{4.101}$$

into eqn.(4.100) and solving the system of eqns.(4.98) and (4.100) we get the following elastic solutions:

$$N_1^{el} = \frac{V}{5} + \frac{H}{\sqrt{3}}, \quad N_2^{el} = \frac{4V}{5}, \quad N_3^{el} = \frac{V}{5} - \frac{H}{\sqrt{3}} \tag{4.102}$$

If plastic deformation takes place, the bar forces will change; however they can always be written as the sum of an elastic solution and a residual stress (force) field. Thus:

$$N_1 = N_1^{el} + N_1^r, \quad N_2 = N_2^{el} + N_2^r, \quad N_3 = N_3^{el} + N_3^r \tag{4.103}$$

This particular structure indeterminate to degree one; thus there is only one set of residual forces N_1^r, N_2^r, N_3^r that are in equilibrium with zero external forces. Thus we may write:

$$N_1^r = -\rho, \quad N_2^r = +\rho, \quad N_3^r = -\rho \tag{4.104}$$

Combining eqns.(4.102), (4.103) and (4.104) we get the final expressions for the total axial forces of the bars:

$$\begin{aligned} N_1 &= \frac{V}{5} + \frac{H}{\sqrt{3}} - \rho \\ N_2 &= \frac{4V}{5} + \rho \\ N_3 &= \frac{V}{5} - \frac{H}{\sqrt{3}} - \rho \end{aligned} \tag{4.105}$$

As the residual force distribution are related to the plastic strains in the bars, let us assume that the plastic strains in the bars are $\varepsilon_1^{pl}, \varepsilon_2^{pl}, \varepsilon_3^{pl}$. The total strains may be decomposed as:

$$\varepsilon_i = \varepsilon_i^{el} + \varepsilon_i^{el,r} + \varepsilon_i^{pl}, \quad i = 1,2,3 \tag{4.106}$$

where $\varepsilon_1^{el,r}, \varepsilon_2^{el,r}, \varepsilon_3^{el,r}$ are the elastic strains associated with the residual force distribution $\left\{\frac{-\rho}{EA}, \frac{\rho}{EA}, \frac{-\rho}{EA}\right\}$. The total strains must satisfy the compatibility equation

(4.100). Since the elastic strains associated with the elastic solution (4.102) already satisfy this condition by definition, the sum of the strains $\left(\varepsilon_i^{el,r} + \varepsilon_i^{pl}\right)$ should also satisfy the compatibility equations. Thus, we get that

$$\rho = \frac{2EA}{5}(\varepsilon_1^{pl} - \frac{1}{2}\varepsilon_2^{pl} - \varepsilon_3^{pl}) \tag{4.107}$$

The rate form of eqn.(4.107) gives:

$$\dot{\rho} = \frac{2EA}{5}(\dot{\varepsilon}_1^{pl} - \frac{1}{2}\dot{\varepsilon}_2^{pl} - \dot{\varepsilon}_3^{pl}) \tag{4.108}$$

It is obvious that $\rho = 0$ or ρ remains constant when the plastic strains are constant. Equivalently, ρ may change only when the plastic strains change i.e. only when one or more of the bars yields, with $N = \pm N_Y$.

Let us now consider the way in which ρ changes without evaluating the exact plastic strain distribution. First, we consider that the truss is subjected to a vertical load only i.e. $H = 0$. Therefore we may plot a plane diagram (Fig.4.9) where a state point for the structure is represented by a point with some coordinates $(V \,/\, N_Y, \rho \,/\, N_Y)$. The domain of admissible state points is limited by the yield condition $-N_Y \leq N \leq N_Y$. This boundary is defined by the inner envelope of the six lines:

$$N_1 = \pm N_Y, \quad N_2 = \pm N_Y, \quad N_3 = \pm N_Y \tag{4.109}$$

Using eqn.(4.105), we may plot these six lines in Fig.4.9. Due to the symmetry of the loading and the geometry, the lines $N_1 = N_3 = +N_Y$ and $N_1 = N_3 = -N_Y$ coincide.

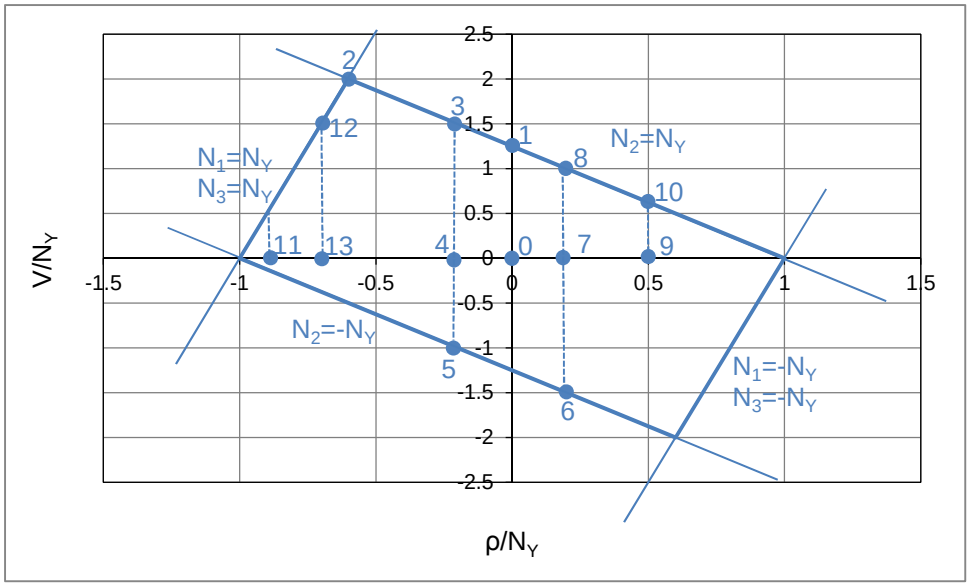

Figure 4.9 State diagram for H=0

Before we consider a cyclic loading program, let us assume a monotonic increase of the vertical load V. We assume that the structure is in its virgin state (point 0 of diagram 4.9). The load V is now increasing monotonically; the behavior remains initially elastic, so that ρ remains equal to zero and then the state point moves up the V axis. When the state point reaches at point 1, bar 2 yields in tension. The first yield in the truss occurs for $V = 1,25N_Y$. Since the state point cannot move outside the admissible domain, it will move up to the line $N_2 = N_Y$, if the load V is further increased. The parameter ρ changes during this process and it may be determined by using the horizontal axis of the diagram 4.9. The state point will continue to move up to line $N_2 = N_Y$ until it reaches point 2, with $V = 2N_Y$, $\rho = -0,6N_Y$. This point represents a limit state and the vertical load cannot be further increased. The forces that are developed in the bars are $N_1 = N_2 = N_3 = N_Y$, and flow takes place in the truss. It should be noticed that any loading program can be dealt with in this way. The diagram 4.9 provides which bars are yielding, the value of ρ, but it does not provide the exact value of $\varepsilon_1^{pl}, \varepsilon_2^{pl}, \varepsilon_3^{pl}$.

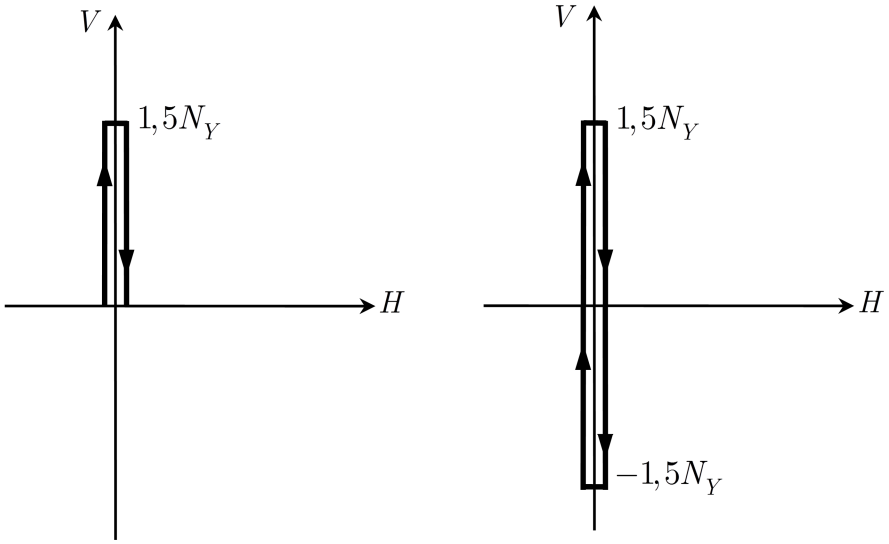

Figure 4.10 Loading program a) shakedown case, b) alternating plasticity case

Let us now consider three different types of cyclic loading program (Fig.4.10 and Fig.4.11).

Firstly, we consider a cyclic program of loading and unloading of the load $V = 1,5N_Y$ (see Fig.4.10(a)). The state point will follow the path 0-1-3-4 during the first cycle and some plastic strain will occur in the middle bar. Thereafter, for subsequent cycles, the state point will follow the path 4-3-4. Then, the parameter ρ will remain constant and no further plastic deformations will take place in the structure. The structure is said to be in the *shakedown* state and it will behave elastically at the next cycles. Suppose that the initial state point in the structure is 11, due to a previous plastic deformation, the first cycle of loading will lead the state point along the path 11-12-13, while for subsequent cycles of loading it will follow the path 13-12-13. Generally, there will be a dependence of the shakedown residual stress field on the initial residual stress field. Additionally, if shakedown occurs for one initial residual stress field it will occur place for all initial stress fields.

Now let us consider another cyclic loading, where its typical cycle consists of the application of the vertical load $V = 1,5N_Y$, the unloading to $V = 0$, the opposite application of the load $V = -1,5N_Y$ and finally, a second unloading to $V = 0$ (Fig.4.10(b)). This process is repeated continuously. The application of the first half

of cycle will lead the state point to the path 0-1-3, causing a plastic strain on the middle bar 2 and then to the path 3-4 where elastic unloading occurs. The second half of cycle loading and the decrease of the vertical load to the value $V = -1,5N_Y$ will cause the state point to move along the path 4-5-6, causing compressive plastic strain in bar 2. The removal of the load and the completion of the loading cycle, will again take place elastically, with the state point following the path 6-7. The response of the truss to this first cycle of loading is not cyclic, since the residual stress (see value of ρ in the diagram 4.9) are different at the beginning and end of the cycle.

However, if the load cycle is repeated the state point will follow the path 7-8-3-4-5-6-7 for every subsequent cycle. Thus, the response of the structure will become *cyclic* after the first cycle. In each cycle, after the first one, the bar 2 will develop plastic strain in tension at the first half (path 8-3) and plastic strain in compression at the second half (path 5-6). As it may be seen in Fig.4.9, the magnitude of the plastic strains in tension and compression will be equal (since ρ returns to the same value and bar 2 is the only bar that undergoes plastic straining). Thus, the structure is in an *alternating plasticity* state, and early fatigue failure may be expected.

Here is a short demonstration of the independence of the cyclic solution on the initial conditions in the structure. Let us assume that the initial state is point 9, due to an early plastic deformation. The application of the first load cycle will cause the state point to follow the path 9-10-3-4-5-6-7. Any subsequent cycle of loads will produce the same cyclic response as in the case of virgin initial state.

It is obvious that the structure under consideration will not exhibit incremental collapse when $H = 0$. In order to illustrate this different type of mechanism under a one parameter loading system we consider the cyclic loading of Fig.4.11. A vertical load of $V = N_Y$ is applied first and the loads V, H are then applied in such a way that the load point always lies on the line in load space $(V - \bar{H})$ defined by:

$$V = N_Y + \frac{H}{\sqrt{3}} \tag{4.110}$$

or

$$V = N_Y + \bar{H} \text{ where } \bar{H} = \frac{H}{\sqrt{3}} \tag{4.111}$$

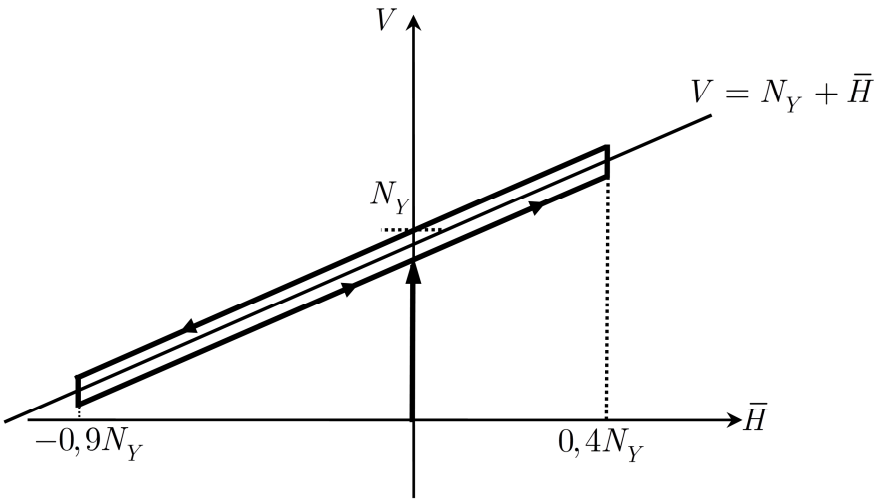

Figure 4.11 Loading program – ratcheting case

Then, as it is shown in Fig.4.11, the loads are increased until $\bar{H} = 0,4N_Y$. The loads are then decreased proportionally (the load point is still on the line $V = N_Y + \bar{H}$) until $\bar{H} = -0,9N_Y$. Finally, the loads are increased again until $\bar{H} = 0$, completing the cycle. As in the previous example, we introduce a state point with coordinates $(\bar{H} \,/\, N_Y, \rho \,/\, N_Y)$. Both $V, \bar{H}$ may be specified by one parameter $\bar{H}$. The admissible region is defined by the envelope of the six lines:

$$N_1 = \pm N_Y, \quad N_2 = \pm N_Y, \quad N_3 = \pm N_Y \tag{4.112}$$

where N_1, N_2, N_3 are obtained by substituting eqn.(4.111) into the set of eqns.(4.105). The admissible region is plotted in Fig.4.12; there is no contribution of the lines $N_2 = -N_y$ and $N_3 = -N_y$. It may also be seen from the previous case that the load $V = N_Y$ does not produce any plastic deformation. Thus, the stress point at the beginning of the cycle will be at the origin of the diagram 4.12 (point 0). As $\bar{H}$ is increased, at the point 1 the middle bar yields in tension, and the state point follows the line $N_2 = N_Y$. When $\bar{H} = 0,4N_y$, the state point will be at 2. $\bar{H}$ is then decreased until $\bar{H} = -0,9N_y$; the state point will be at 5 following the path 2-3-4-5. $\bar{H}$ is then again increased, ρ remains constant, and the first cycle is completed when the state point is at 6. The second load cycle is described by the path 6-7-2-3-4-5-6; the subsequent cycles will be identical and the response of the structure is thus cyclic.

Consequently, after the first cycle, the loading produces a plastic tension in bar 2 and a plastic tension in bar 3. These plastic strains $\Delta\varepsilon_2^{pl}, \Delta\varepsilon_3^{pl}$ will occur for each subsequent cycle of loading, producing some displacement increments $\Delta u, \Delta v$ over a cycle. The plastic strains must be kinematically admissible (i.e. must satisfy eqn.(4.100)) since they do not produce any change in the residual stress field over a cycle. Thus,

$$\Delta\varepsilon_3^{pl} = \frac{1}{2}\Delta\varepsilon_2^{pl} \tag{4.113}$$

The displacements increments will be equal to

$$\Delta u = L\varepsilon_2^{pl}, \quad \Delta v = \frac{-L}{\sqrt{3}}\varepsilon_2^{pl} \tag{4.114}$$

As the number of cycles increases the displacements will also increase. Thus, the structure undergoes *incremental collapse*.

Let us now consider an initial point away from the origin as a result of a previous plastic deformation. Suppose that this initial state is point 8. The response to the first cycle is then described by the path 8-9-10-11-5-6. Thereafter, the state point will follow the path 6-7-2-3-4-5-6. The same path is found when the initial state point is at the origin.

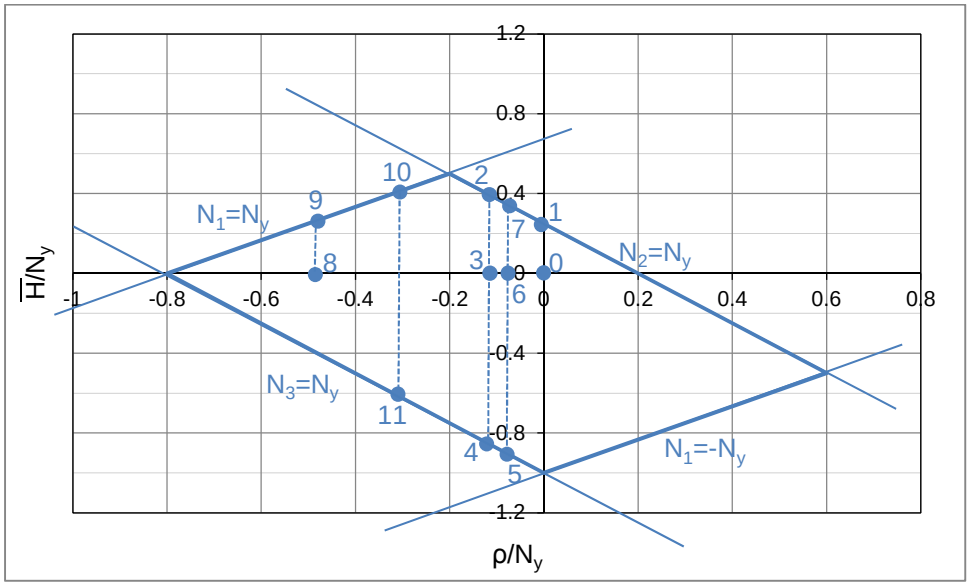

Figure 4.12 State diagram showing incremental collapse

5.

Numerical procedures for the limit states of cyclically loaded structures

5.1. A proposed procedure for the cyclic limit states of elastoplastic structures

Instead of approaching the steady state behavior of an elastic-perfectly plastic structure under cyclic loading, through incremental time-stepping calculations, one may alternatively use *Direct Methods.* In this section a novel numerical procedure that may predict any cyclic stress state for a cyclically loaded elastoplastic structure will be presented. This approach that belongs to the class of direct methods is in short called RSDM and has a more physical basis in comparison with the direct methods in the literature. The method is based on the cyclic nature of the expected residual stresses at the steady cycle (Spiliopoulos and Panagiotou, 2012, 2014c). The main ingredient of the method is the decomposition of the residual stresses into Fourier series with respect to time. The coefficients of these series are then calculated iteratively by satisfying equilibrium and compatibility. The process converges uniformly to the actual residual stress for a loading below shakedown limit or to an unsafe cyclic total stress. The method then continues to determine whether the applied loading would lead the structure to ratcheting or to regions that alternate plastically. A detailed description of the method is presented next. The procedure is

formulated within the finite element method and a von Mises yield surface is typically used.

5.1.1. Some theoretical considerations

Let us consider a structure having volume V and surface S subjected to cyclic surface tractions on one part and on the other part of S to zero displacements (Fig.5.1(a)).

If the set of loads $\mathbf{P}(t)$ that act on S is a cyclic loading we may write:

$$\mathbf{P}(t) = \mathbf{P}(t + nT) \tag{5.1}$$

where bold letters are used to denote vectors and matrices.

In eqn.(5.1) $\mathbf{P}(t) = \left\{P_1(t), P_2(t), ..., P_q(t)\right\}$ is a column vector, with q denoting the number of different loads (for example in Fig.5.1 $q = 2$). Also, t is a time point inside the cycle, T is the period of the cycle and $n = 1, 2, ...,$ denotes the number of full cycles. A loading trajectory of such a state in a two-dimensional loading domain may be seen in Fig.5.1(b).

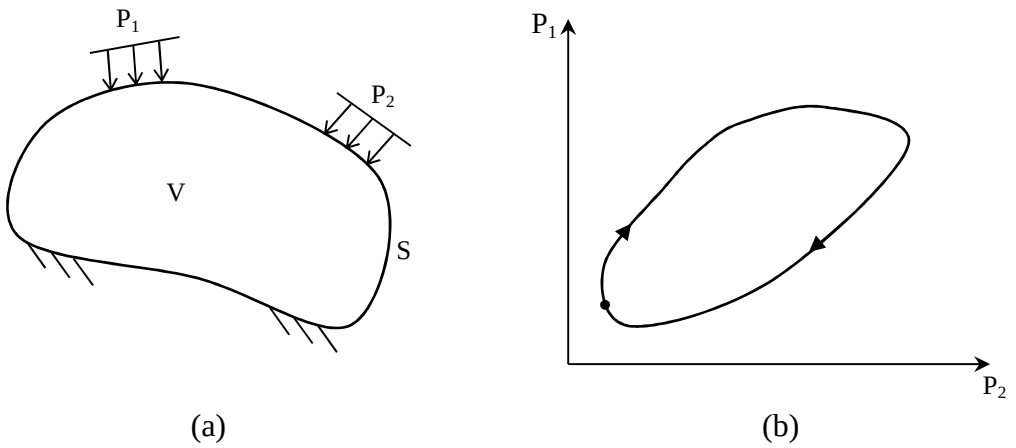

Figure 5.1 (a) Structure with applied loads, (b) cyclic loading state

Let us suppose that the structure is made of an elastic-perfectly plastic material. Let us further suppose that our structure has been discretized to finite elements and the stresses and strains refer to the Gauss points (GP).

The structure will develop, at a time point $\tau = \frac{t}{T}$ inside the cycle, a stress field $\boldsymbol{\sigma}(\tau)$ which may be decomposed into an elastic part $\boldsymbol{\sigma}^{el}(\tau)$, that equilibrates the external loading $\mathbf{P}(\tau)$, assuming a completely elastic behavior, and a self-equilibrating residual stress part $\boldsymbol{\rho}(\tau)$ that is due to inelasticity. Therefore:

$$\boldsymbol{\sigma}(\tau) = \boldsymbol{\sigma}^{el}(\tau) + \boldsymbol{\rho}(\tau) \tag{5.2}$$

The strain rates can also be decomposed analogously:

$$\dot{\boldsymbol{\varepsilon}}(\tau) = \dot{\mathbf{e}}^{el}(\tau) + \dot{\boldsymbol{\varepsilon}}_r(\tau) \tag{5.3}$$

The residual strain rate $\dot{\boldsymbol{\varepsilon}}_r(\tau)$ consists not only of the plastic strain rates $\dot{\boldsymbol{\varepsilon}}^{pl}(\tau)$ but also of an elastic strain rate part $\dot{\boldsymbol{\varepsilon}}_r^{el}(\tau)$ which is necessary so that the total strain compatibility is maintained. Thus eqn.(5.3) may be written as:

$$\dot{\boldsymbol{\varepsilon}}(\tau) = \dot{\mathbf{e}}^{el}(\tau) + \dot{\boldsymbol{\varepsilon}}_r^{el}(\tau) + \dot{\boldsymbol{\varepsilon}}^{pl}(\tau) \tag{5.4}$$

The elastic strain rates are related to the stress rates through the elasticity matrix $\mathbf{D}$, whereas the plastic strain rate vector $\dot{\boldsymbol{\varepsilon}}^{pl}(\tau)$ through the associated flow rule:

$$\begin{aligned} \dot{\boldsymbol{\sigma}}^{el}(\tau) &= \mathbf{D} \cdot \dot{\mathbf{e}}^{el} \\ \dot{\boldsymbol{\rho}}(\tau) &= \mathbf{D} \cdot \dot{\boldsymbol{\varepsilon}}_r^{el} \\ \dot{\boldsymbol{\varepsilon}}^{pl} &= \lambda \cdot \frac{\partial f}{\partial \boldsymbol{\sigma}} \end{aligned} \tag{5.5}$$

where f is the yield surface.

5.1.2. Residual stress Fourier series decomposition

As it has already been discussed in section 4.4, the total stress field of cyclic loaded elastoplastic structures will asymptotically become cyclic. The elastic stress field which is in equilibrium with the external cyclic loading is obviously cyclic. Consequently, the residual stress field will also become cyclic. Exploiting this cyclic nature of the residual stresses one may decompose them in Fourier series (see, for

example Tolstov, 1962). This decomposition has been originally proposed for creep cyclic states by Spiliopoulos, 2002. Therefore we may write:

$$\boldsymbol{\rho}(\tau) = \frac{\mathbf{a}_0}{2} + \sum_{k=1}^{\infty} \left(\cos 2k\pi\tau \cdot \mathbf{a}_k + \sin 2k\pi\tau \cdot \mathbf{b}_k \right) \tag{5.6}$$

Therefore in order to determine the residual stress distribution only the Fourier coefficients of (5.6) need to be evaluated.

By differentiating the above equation we get:

$$\dot{\boldsymbol{\rho}}(\tau) = 2\pi \sum_{k=1}^{\infty} \left\{ -k \sin(2k\pi\tau) \cdot \mathbf{a}_k + k \cos(2k\pi\tau) \cdot \mathbf{b}_k \right\} \tag{5.7}$$

If we multiply (5.7) by $\sin(2k\pi\tau)$ and then integrate over a cycle, using the orthogonality properties of the trigonometric functions, we obtain that the typical coefficient of the *cosine* series is given by:

$$\mathbf{a}_k = -\frac{1}{k\pi} \int_0^1 \dot{\boldsymbol{\rho}}(\tau) \cdot \sin(2k\pi\tau)\, d\tau \tag{5.8}$$

On the other hand, if we multiply (5.7) by $\cos(2k\pi\tau)$ and carry over the same procedure, the following expression for the coefficient of the *sine* series is obtained:

$$\mathbf{b}_k = \frac{1}{k\pi} \int_0^1 \dot{\boldsymbol{\rho}}(\tau) \cdot \cos(2k\pi\tau)\, d\tau \tag{5.9}$$

Finally, the integration of the equation (5.7) over a cycle, gives:

$$\int_0^1 \dot{\boldsymbol{\rho}}(\tau)\, d\tau = \boldsymbol{\rho}(1) - \boldsymbol{\rho}(0) = \left(\frac{\mathbf{a}_0}{2}(1) + \sum_{k=1}^{\infty} \mathbf{a}_k(1) \right) - \left(\frac{\mathbf{a}_0}{2}(0) + \sum_{k=1}^{\infty} \mathbf{a}_k(0) \right) \tag{5.10}$$

where use of the expression (5.6) was made at the beginning and at the end of the cycle. With all the coefficients known at the beginning of the cycle and the

coefficients of the *cosine* series also known at the end of the cycle, the constant term of the Fourier series may be calculated by the following equation:

$$\frac{1}{2}\mathbf{a}_{0,e} = \left(\frac{1}{2}\mathbf{a}_{0,b} + \sum_{k=1}^{\infty}\mathbf{a}_{k,b}\right) - \sum_{k=1}^{\infty}\mathbf{a}_{k,e} + \int_{0}^{1}\dot{\boldsymbol{\rho}}(\tau)d\tau \tag{5.11}$$

where the subscripts b and e denote the beginning and the end of the cycle respectively.

The Fourier coefficients appear explicitly on the left hand and implicitly (through $\dot{\boldsymbol{\rho}}$) on the right hand side of equations (5.8),(5.9) and (5.11). Consequently there is a nonlinear system of equations to be solved:

$$\mathbf{x} = \mathbf{g(x)} \tag{5.12}$$

where $\mathbf{x}$ is the vector of the unknown Fourier coefficients.

This system may be solved iteratively (see, for example Isaakson and Keller, 1966), by using the iterative procedure that is described in detail below. In each iteration the derivative of the residual stresses, at some preselected time points inside the cycle, may be evaluated. This can be accomplished by satisfying equilibrium and compatibility at these time points. The way to evaluate the time derivatives of the residual stresses may be done, for any structure, using the finite element method.

5.1.3. Evaluation of the derivative of the residual stresses

Let us suppose that our structure is discretized, in the standard way, into a finite number of elements which are assumed to be interconnected at a discrete number of nodal points situated on their boundaries.

Letting bold letters be used for vectors and matrices, we denote by $\dot{\mathbf{r}}$ the vector of the rates of the displacements of the nodal points of the discretized structure at some cycle time τ. We may then express the strain rates at the Gauss integration points (GPs), using the equation:

$$\dot{\boldsymbol{\varepsilon}} = \mathbf{B} \cdot \dot{\mathbf{r}} \tag{5.13}$$

Using the discretized form of eqns.((5.2)-(5.5)) we get the expression of the residual stress rates, also at the Gauss points:

$$\dot{\boldsymbol{\rho}} = \mathbf{D} \cdot \left(\dot{\boldsymbol{\varepsilon}} - \dot{\mathbf{e}}^{el} - \dot{\boldsymbol{\varepsilon}}^{pl} \right) \tag{5.14}$$

Where $\mathbf{D}$ is the elasticity matrix, $\dot{\mathbf{e}}^{el}$ is the vector of the elastic strain rates assuming a purely elastic behavior, and $\dot{\boldsymbol{\varepsilon}}^{pl}$ is the vector of plastic strain rates.

Since the strain rates are kinematically admissible, the residual stress rates are self-equilibrated, and fixed supports have been assumed, we may write, for a virtual strain field $\delta\dot{\boldsymbol{\varepsilon}}$, using the Principle of Virtual Work (PVW):

$$\int_V \delta\dot{\boldsymbol{\varepsilon}}^T \cdot \dot{\boldsymbol{\rho}} dV = 0 \tag{5.15}$$

where the superscript $(^T)$ denotes the transpose of a vector or a matrix.

By substituting (5.13) for the corresponding virtual displacement rates field, and (5.14) in (5.15), we get:

$$\delta\dot{\mathbf{r}}^T \cdot \left(\int_V \mathbf{B}^T \cdot \mathbf{D} \cdot \left(\mathbf{B} \cdot \dot{\mathbf{r}} - \dot{\mathbf{e}}^{el} - \dot{\boldsymbol{\varepsilon}}^{pl} \right) dV \right) = 0 \tag{5.16}$$

and since this equation must hold for any $\delta\dot{\mathbf{r}}$ (Cook *et al.*, 2002) we may write:

$$\left(\int_V \mathbf{B}^T \cdot \mathbf{D} \cdot \mathbf{B} dV \right) \cdot \dot{\mathbf{r}} = \int_V \mathbf{B}^T \cdot \dot{\boldsymbol{\sigma}}^{el} dV + \int_V \mathbf{B}^T \cdot \mathbf{D} \cdot \dot{\boldsymbol{\varepsilon}}^{pl} dV \tag{5.17}$$

or equivalently

$$\mathbf{K} \cdot \dot{\mathbf{r}} = \dot{\mathbf{R}} + \int_V \mathbf{B}^T \cdot \mathbf{D} \cdot \dot{\boldsymbol{\varepsilon}}^{pl} dV \tag{5.18}$$

Where $\mathbf{K}$ is the stiffness matrix and $\dot{\mathbf{R}}$ is the rate vector of the external forces acting on the structure at a specific time τ.

Plastic strain rates $\dot{\boldsymbol{\varepsilon}}^{pl}$ will develop only at the GPs at which the total stress exceeds the yield surface. A return mapping algorithm may be used to this end, to estimate, numerically, these rates. This procedure is generally quite involved (de Souza et al., 2008) and is based on the closest point projection (Simo and Hughes, 1998).

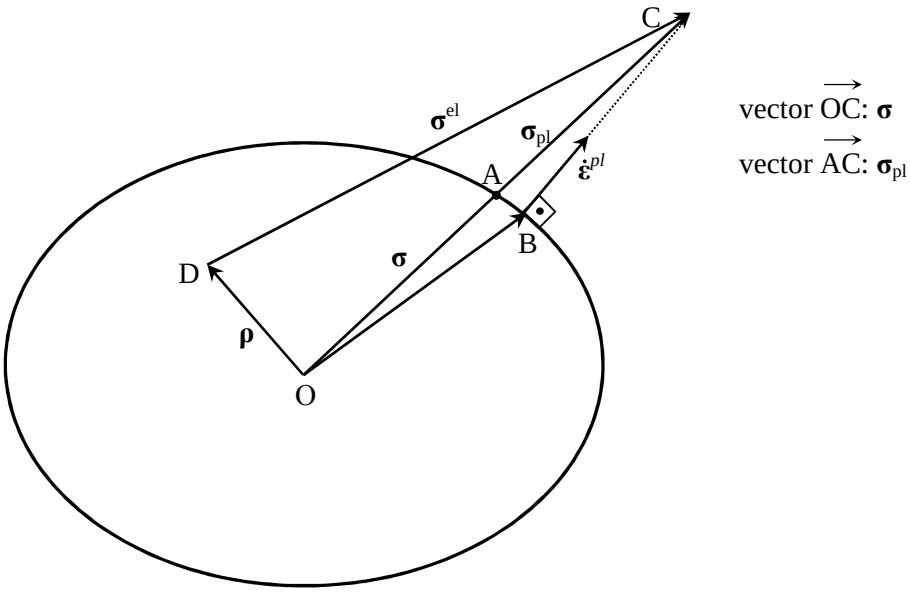

Figure 5.2 von Mises yield surface and radial return type of mapping

A procedure that is easy to implement for a von Mises yield surface is presented herein. Analogous procedures could be applied for other yield surfaces. In Fig.5.2 the vector $\overrightarrow{OC}$ is the total stress vector, which is the sum of elastic stress vector $\overrightarrow{DC}$ and the residual stress vector $\overrightarrow{OD}$. Let us consider that the total stress exceeds the yield surface. According to the closest point projection (Simo and Hughes, 1998), the returning on the yield surface stress vector $\mathbf{D}\cdot\dot{\boldsymbol{\varepsilon}}^{pl}$ is $\overrightarrow{CB}$ with the plastic strain rate $\dot{\boldsymbol{\varepsilon}}^{pl}$ being directed along $\overrightarrow{BC}$. Instead of $\overrightarrow{BC}$, $\overrightarrow{CA}$, i.e. $-\boldsymbol{\sigma}_{pl}$, is used as the returning vector, which is easy to find by performing a 'radial return' type of mapping along the known line $\overrightarrow{OC}$. The vector $\boldsymbol{\sigma}_{pl}$ is interlinked to $\dot{\boldsymbol{\varepsilon}}^{pl}$, in the sense that they

are both either equal to zero or different to zero. Thus, it constitutes an equivalent "measure" for it.

5.1.4. Description of the numerical procedure RSDM

Based on the theoretical and computational aspects discussed on the previous sections, a numerical procedure, which is in short called the Residual Stress Decomposition Method (RSDM), has been developed (Spiliopoulos and Panagiotou, 2012, 2014c). An analytical description of the steps of the RSDM is described below. A visualization of the method is shown in the flowchart of the Fig.5.3.

Firstly, we solve for the external loading and its cycle rate assuming elastic behavior. For each cycle point τ, we obtain the elastic stress $\boldsymbol{\sigma}^{el}(\tau)$ and the elastic stress rate $\dot{\boldsymbol{\sigma}}^{el}(\tau)$ at each Gauss point (GP) of a continuum finite element.

Let us suppose that after the completion of the iteration $(\mu-1)$ an estimate of the distribution of the Fourier coefficients $\mathbf{a}_0{}^{(\mu)}, \mathbf{a}_k{}^{(\mu)}, \mathbf{b}_k{}^{(\mu)}$ has been made (initial distribution may be taken equal to zero). The following steps are then followed inside an iteration μ:

1. For a specific cycle point τ compute $\boldsymbol{\rho}^{(\mu)}(\tau)$, at each GP, using (5.6):

$$\boldsymbol{\rho}^{(\mu)}(\tau) = \frac{1}{2}\mathbf{a}_0^{(\mu)} + \sum_{k=1}^{\infty}\left\{\cos(2k\pi\tau)\cdot\mathbf{a}_k^{(\mu)} + \sin(2k\pi\tau)\cdot\mathbf{b}_k^{(\mu)}\right\} \tag{5.19}$$

2. Evaluate, at each GP, the total stress $\boldsymbol{\sigma}^{(\mu)}(\tau)$, using (5.2)

$$\boldsymbol{\sigma}^{(\mu)}(\tau) = \boldsymbol{\sigma}^{el}(\tau) + \boldsymbol{\rho}^{(\mu)}(\tau) \tag{5.20}$$

3. Check whether, at each GP, $\bar{\sigma}^{(\mu)}(\tau) > \sigma_Y$. In such a case calculate the excess amount $\boldsymbol{\sigma}_{pl}^{(\mu)}(\tau)$:

$$\xi = \frac{\bar{\sigma}^{(\mu)}(\tau) - \sigma_Y}{\bar{\sigma}^{(\mu)}(\tau)} \Rightarrow \boldsymbol{\sigma}_{pl}^{(\mu)}(\tau) = \xi\cdot\boldsymbol{\sigma}^{(\mu)}(\tau) \tag{5.21}$$

where $\bar{\sigma}^{(\mu)}(\tau)$ is the effective stress at each GP.

4. Assemble for the whole structure the updated rate vector of the nodal forces $\dot{\mathbf{R}}'(\tau)$, which is the r.h.s. of eqns. (5.17), (5.18):

$$\dot{\mathbf{R}}'(\tau) = \dot{\mathbf{R}}\ (\tau) + \int_V \mathbf{B}^T \cdot \boldsymbol{\sigma}_{pl}^{(\mu)}(\tau) dV \tag{5.22}$$

5. Solve the following iterative form of the equilibrium equation (5.18) and obtain $\dot{\mathbf{r}}^{(\mu)}(\tau)$:

$$\mathbf{K}\dot{\mathbf{r}}^{(\mu)}(\tau) = \dot{\mathbf{R}}'(\tau) \tag{5.23}$$

6. Evaluate at each GP the residual derivative rate, using (5.14):

$$\dot{\boldsymbol{\rho}}^{(\mu)}(\tau) = \mathbf{DB}\dot{\mathbf{r}}^{(\mu)}(\tau) - \dot{\boldsymbol{\sigma}}^{el}(\tau) - \boldsymbol{\sigma}_{pl}^{(\mu)}(\tau) \tag{5.24}$$

7. Repeat the steps 1-6 for all the predefined cycle points.
8. Perform a numerical integration over the cycle points and update the Fourier coefficients, making use of the eqns. (5.8),(5.9) and (5.11):

$$\begin{aligned}
\mathbf{a}_k^{(\mu+1)} &= -\frac{1}{k\pi}\int_0^1 \left\{\left[\dot{\boldsymbol{\rho}}^{(\mu)}\left(\tau\right)\right]\left(\sin 2k\pi\tau\right)\right\} d\tau \\
\mathbf{b}_k^{(\mu+1)} &= \frac{1}{k\pi}\int_0^1 \left\{\left[\dot{\boldsymbol{\rho}}^{(\mu)}\left(\tau\right)\right]\left(\cos 2k\pi\tau\right)\right\} d\tau \\
\frac{\mathbf{a}_0^{(\mu+1)}}{2} &= -\sum_{k=1}^{\infty}\mathbf{a}_k^{(\mu+1)} + \frac{\mathbf{a}_0^{(\mu)}}{2} + \sum_{k=1}^{\infty}\mathbf{a}_k^{(\mu)} + \int_0^1 \left[\dot{\boldsymbol{\rho}}^{(\mu)}\left(\tau\right)\right] d\tau
\end{aligned} \tag{5.25}$$

9. Evaluate an update of the residual stress vector $\boldsymbol{\rho}^{(\mu+1)}(\tau)$ using (5.6).
10. Check the convergence between two successive iterations against a predefined tolerance using the Euclidian norm of the residual stress vector at the end of the cycle:

$$\frac{\left\|\boldsymbol{\rho}^{(\mu+1)}(1)\right\|_2 - \left\|\boldsymbol{\rho}^{(\mu)}(1)\right\|_2}{\left\|\boldsymbol{\rho}^{(\mu+1)}(1)\right\|_2} \leq tol \tag{5.26}$$

If inequality (5.26) holds, the procedure stops as we have reached a cyclic stress state (*cs*), and $\boldsymbol{\rho}^{(\mu)} \approx \boldsymbol{\rho}^{(\mu+1)} = \boldsymbol{\rho}^{cs}$;
otherwise we go back to step 1 and repeat the process until (5.26) is satisfied.

Prediction of the cyclic elastoplastic state

Once a cyclic stress state has been attained, we look at $\boldsymbol{\sigma}_{pl}^{cs} = \boldsymbol{\sigma}_{pl}^{(\mu+1)} \approx \boldsymbol{\sigma}_{pl}^{(\mu)}$, which was evaluated during the last iteration. We may determine the nature of the obtained cyclic solution, for each GP, by evaluating the following integral over the cycle:

$$\alpha_i = \int_0^1 \sigma_{pl,i}^{cs}(\tau) d\tau \tag{5.27}$$

with i spanning all the components of the stress vector $\boldsymbol{\sigma}_{pl}^{cs}$.

Three different asymptotic states may be predicted depending on the values of α_i and $\sigma_{pl,i}^{cs}(\tau)$:

(a) If $\alpha_i \neq 0$, a state of ***ratcheting*** exists at this GP.

If $\alpha_i = 0$, we check the value of $\sigma_{pl,i}^{cs}(\tau)$ for every cycle point τ:

(b) If $\sigma_{pl,i}^{cs}(\tau) \neq 0$, the Gauss point is in a state of ***reverse plasticity***, since this must hold for pairs of cycle points of equal value but of alternating sign.

(c) If $\sigma_{pl,i}^{cs}(\tau) = 0$, the point has remained either elastic or has developed an ***elastic shakedown*** state.

If all the Gauss points are either elastic or in a state of elastic shakedown, then our structure under the given external loading will also shake down. In this case the procedure will have converged to constant in time residual stresses. On the other hand, if a sufficient number of GPs are in a state of ratcheting, at the steady state, our structure will undergo incremental collapse. Numerically, this may be easily proved here, through the singularity of the stiffness matrix, which can be evaluated just at the end of the converged steady cycle, by zeroing the elasticity matrix $\mathbf{D}$ at the ratcheting GPs.

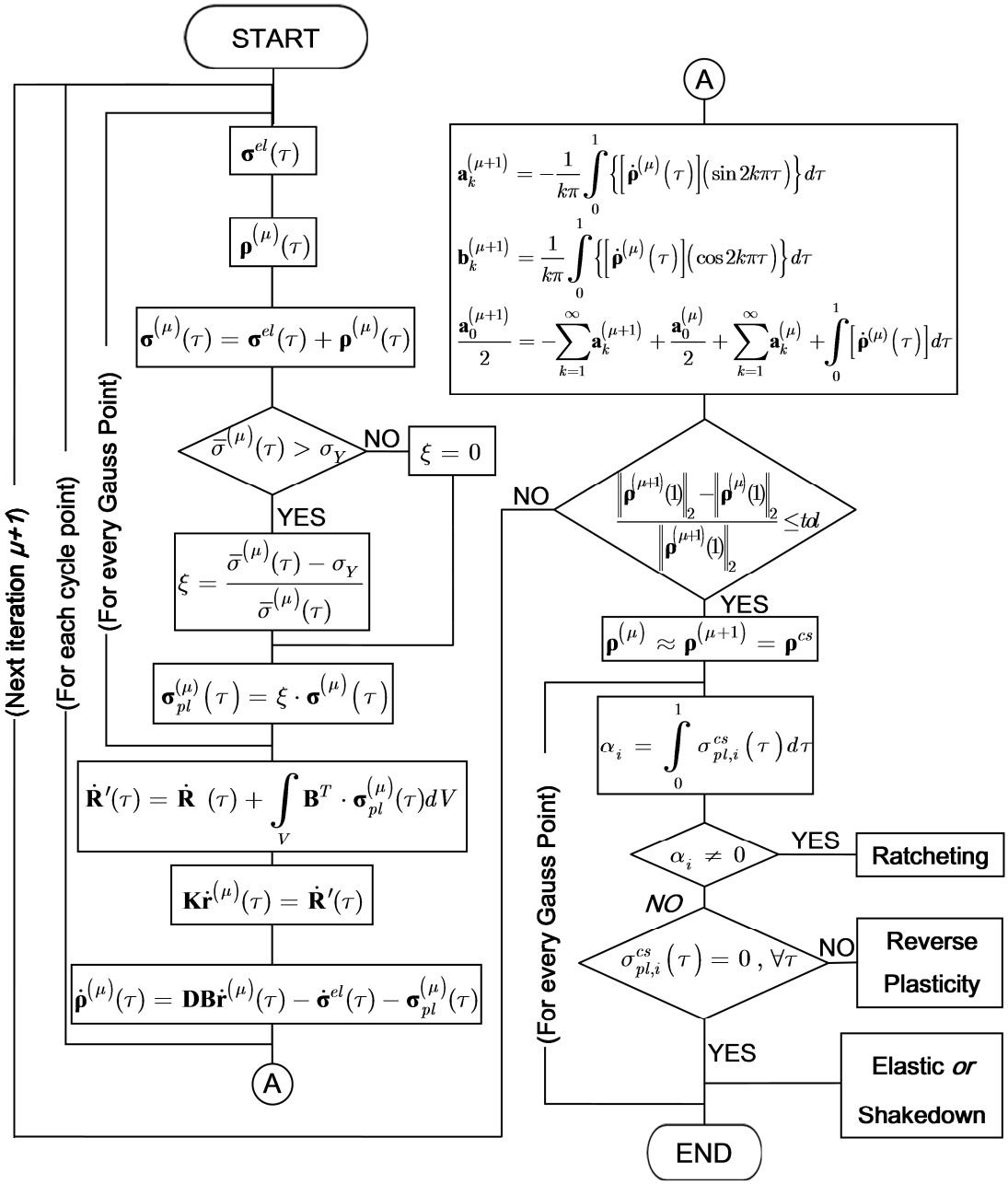

Figure 5.3 Flowchart of the RSDM

5.2. A proposed procedure for shakedown analysis

To estimate the life of a structure, or a component, which are subjected to a cyclic loading history, the civil or mechanical engineer must be able to provide safety margins against excessive inelastic deformations. *Direct methods* and particularly shakedown analysis constitutes a convenient tool towards this direction. Most of the existing numerical procedures addressing a shakedown analysis are based on the two theorems of shakedown and are formulated within the framework of mathematical programming (MP). A novel direct numerical procedure, which is called RSDM-S, is presented next (Spiliopoulos and Panagiotou, 2014a, 2014b, 2015, Panagiotou and Spiliopoulos, 2015). The method seeks to solve the main problem of shakedown in a different way. It is an iterative procedure and starts by converting the problem of loading margins to an equivalent loading of a prescribed time history. The approach makes use of the Residual Stress Decomposition Method (RSDM) of the previous section, which assumes the decomposition of the residual stress field into Fourier series. Starting from a high loading factor, the shakedown limit is estimated through an iterative procedure that updates the Fourier coefficients, reducing, at the same time, this loading factor until the only remaining term of the Fourier series is the constant term. An elastic-perfectly plastic material with a von Mises yield surface is currently assumed. The method may be implemented in any existing FE code and may be applied to structures under thermal and mechanical cyclic loading.

5.2.1. Case of mechanical loading

5.2.1.1. Description of the load variation

Let us consider a structure having thickness d and a volume V subjected to mechanical loadings (Fig.5.4) Although the procedure may be applied to more than two cyclic loadings (see the description for multidimensional loading space in section 5.2.4), for simplicity reasons, a maximum of two mechanical loads has firstly been considered.

These loads have a cyclic variation between a specified minimum and a maximum value. Without loss of generality, it is assumed in this section that the minimum values of the two loads are zero.

A key remark is that we may use any curve that passes through these limits to express a cyclic loading variation. In the search for shakedown the loads may vary either:

- proportionally (see Fig.5.5) or
- individually (see Figs.5.6,5.7)

The maximum values of the two loads are marked as P_1^* and P_2^* respectively.

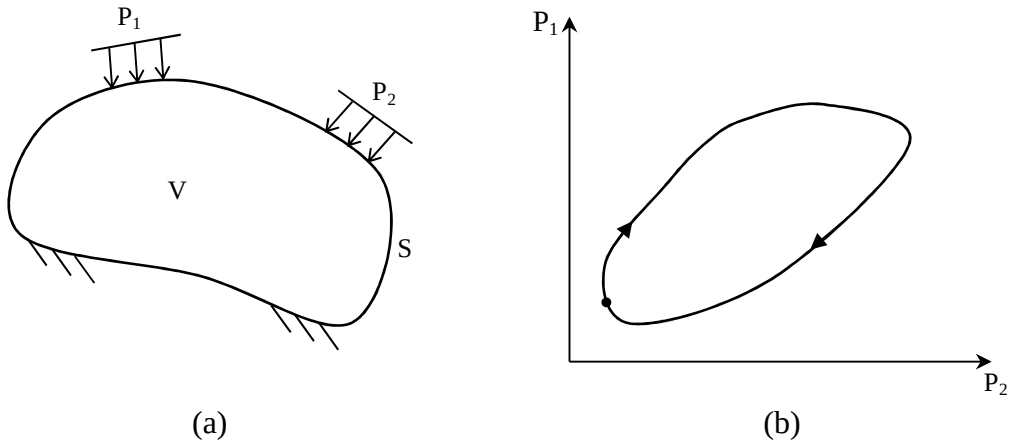

Figure 5.4 (a) Structure with applied loads, (b) cyclic loading state

5.2.1.1.1. Proportional loading variation

In Fig.5.5(a) a proportional variation of the cyclic loading $(0 \rightarrow (P_1^*, P_2^*) \rightarrow 0)$ in the load domain may be seen. Equivalently, one may establish a cyclic loading in the time domain (Fig.5.5(b)), which may be given by the following expression:

$$\mathbf{P}(\tau) = \begin{Bmatrix} P_1(\tau) \\ P_2(\tau) \end{Bmatrix} = \begin{Bmatrix} P_1^* \cdot \alpha(\tau) \\ P_2^* \cdot \alpha(\tau) \end{Bmatrix} \tag{5.28}$$

where $\alpha(\tau)$ is a time function that is used to describe a variation with respect to the cycle time, common for both loads.

5.2.1.1.2. Individual loading variation

A different type of load case may consist of an independent variation of the two loads. Such a case is the cyclic program $(0 \rightarrow (P_1^*, 0) \rightarrow (0, P_2^*) \rightarrow 0)$ of Fig.5.6(a) In time domain this cyclic loading may be expressed as:

$$\mathbf{P}(\tau) = \begin{Bmatrix} P_1(\tau) \\ P_2(\tau) \end{Bmatrix} = \begin{Bmatrix} P_1^* \cdot \alpha_1(\tau) \\ P_2^* \cdot \alpha_2(\tau) \end{Bmatrix} \tag{5.29}$$

Indicative variations of the two loads may be seen in Fig.5.6(b).

The most common load domain used in shakedown analysis is the convex hyper-polyhedron defined by the vertices of the minimum and maximum values of the applied loads, i.e. the rectangular domain Ω shown in Fig.5.7(a).

It has been proved (König and Kleiber, 1978) that due to the convexity of the yield surface, if a structure shakes down over the path that encloses the domain Ω, it certainly shakes down over any loading path contained inside this domain (see also section 4.8). This enclosing path i.e. $\left(0 \rightarrow P_1^* \rightarrow (P_1^*, P_2^*) \rightarrow P_2^* \rightarrow 0\right)$ may be described as well by the equation (5.29) in time domain with indicative variations $P_1(\tau)$ and $P_2(\tau)$ shown in Fig.5.7(b).

The load domains or the equivalent converted prescribed cyclic loadings in time domain may be isotropically varied by multiplying them with a factor γ (see section 4.2). Thus the numerical procedure is built so that starting from a load factor high above, this load factor is sequentially lowered by shrinking the load domain in a continuous way up to the point that the load factor that makes the structure shakedown, is reached.

5.2.1.2. Evaluation of an initial load factor γ

From the way the loading time history is being constructed, there always exists a cycle point τ^* that both the two loads (for proportional loading, Fig.5.5(b)) attain their maximum values at the same time, or one of the two loads become maximum with the other being zero (for independent loading, Figs.5.6,5.7).

For either case, one may find the elastic equivalent von Mises stress $\bar{\sigma}^{el}$ at all the GPs of the structure at time τ^*. Denoting by $\min \bar{\sigma}^{el}$ the non-zero minimum of these stresses one may use an initial load factor equal to:

$$\gamma^{(1)} = \frac{\sigma_Y}{\min \bar{\sigma}^{el}} \tag{5.30}$$

where σ_Y is the yield stress of the material.

It is obvious, that this load factor constitutes a starting loading factor which when multiplying the corresponding loads at τ^* will produce a load which, at least for this cycle time, is far above the shakedown or even the limit load, since all the elements of the structure will be plastic.

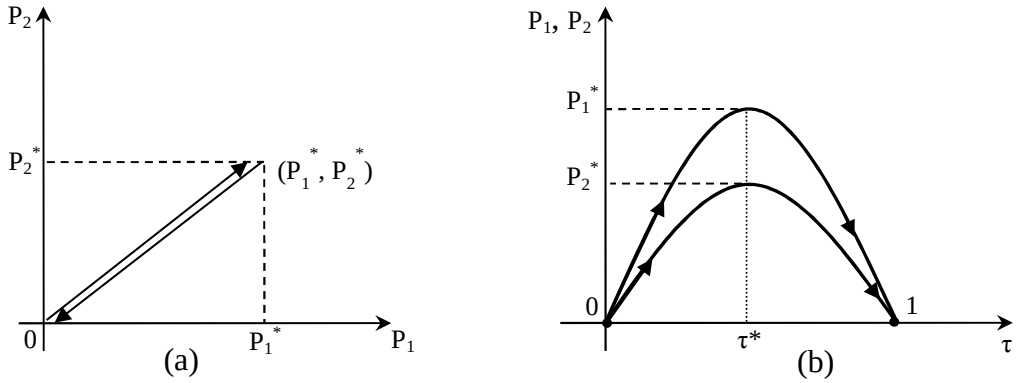

Figure 5.5 Proportional cyclic loading variation over one time period (a) in load space, (b) in time domain

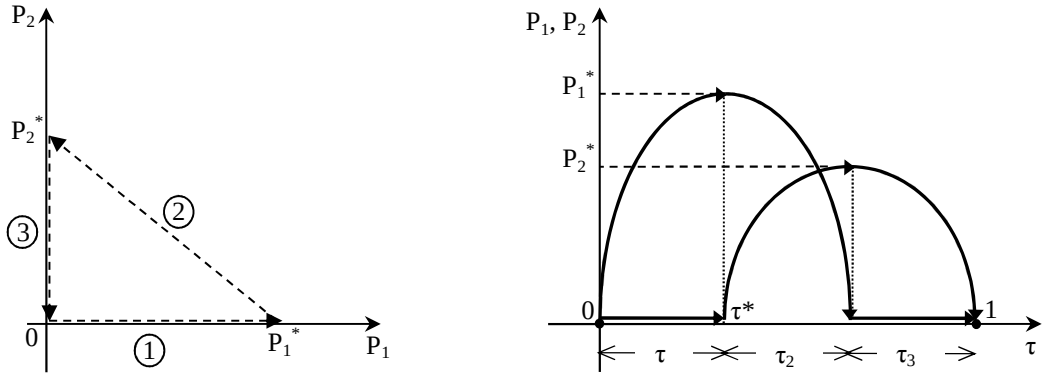

Figure 5.6 Individual cyclic loading variation over one time period (a) in load space, (b) in time domain

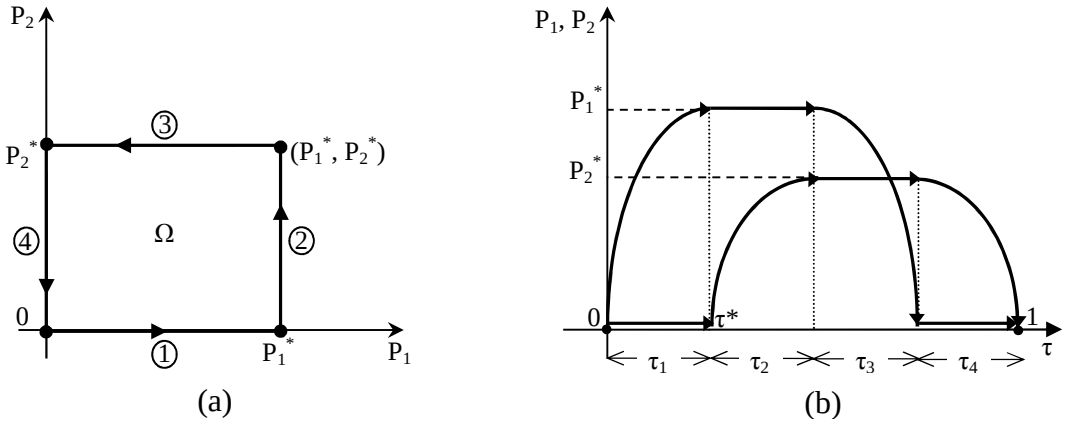

Figure 5.7 Individual cyclic loading variation over one time period (a) in load space, (b) in time domain

5.2.1.3. Development of the procedure RSDM-S (case of mechanical loading)

As already pointed out (see chapter 4) for a structure to shakedown the steady-state residual stresses must be constant in time. Thus, if the residual stresses are decomposed in Fourier series (eqn. (5.6) of the RSDM) the basis of the numerical approach is to lead the coefficients of the trigonometric part of the series $\mathbf{a}_k$ and $\mathbf{b}_k$ to zero, so that the only remaining term of the Fourier series is the constant term (Spiliopoulos and Panagiotou, 2014a, 2014b, 2015). The sum of the norms of the *cosine* and *sine* terms is used to succeed in this.

A flowchart of the RSDM-S procedure may be seen in Fig.5.8. After having the initial value of load factor $\gamma^{(1)} = \dfrac{\sigma_Y}{\min \overline{\sigma}^{el}}$ and an initialisation phase:

$$\mathbf{a}_0^{(0)} = \mathbf{a}_k^{(0)} = \mathbf{b}_k^{(0)} = 0 \rightarrow \boldsymbol{\rho}^{(0)}(\tau) = 0 \tag{5.31}$$

we enter an iterative phase, which virtually consists of two iterations loops, one inside the other. The outer loop is controlled by iterations μ, starting with $\mu = 1$. Inside the outer loop the following steps are followed:

1. Using the current load factor of the outer loop $\gamma^{(\mu)}$ and the residual stress $\boldsymbol{\rho}^{(\mu-1)}(\tau)$, an inner loop of iterations controlled by κ starts with $\kappa = 1$. The

steps of this inner loop (a to h) are virtually the same steps of the RSDM (see steps 1-10 of the section 5.1.4):

a) The following expression for total stress is computed for each cycle point τ and for each GP:

$$\boldsymbol{\sigma}^{(\kappa)}(\tau) = \gamma^{(\mu)}\boldsymbol{\sigma}^{el}(\tau) + \boldsymbol{\rho}^{(\kappa)}_{(\mu-1)}(\tau) \tag{5.32}$$

where

$$\boldsymbol{\sigma}^{el}(\tau) = \alpha_1(\tau)\boldsymbol{\sigma}^{el}_{P_1^*} + \alpha_2(\tau)\boldsymbol{\sigma}^{el}_{P_2^*} \tag{5.33}$$

with $\alpha_1(\tau), \alpha_2(\tau)$ being the time functions for independent loading (eqn.(5.29)), whereas $\alpha_1(\tau) = \alpha_2(\tau) = \alpha(\tau)$ is the time function for the proportional loading case (eqn.(5.28)).

b) Check whether the total effective stress $\overline{\sigma}^{(\kappa)}(\tau) > \sigma_Y$; if this does not hold we set $\xi = 0$, otherwise:

$$\xi = \frac{\overline{\sigma}^{(\kappa)}(\tau) - \sigma_Y}{\overline{\sigma}^{(\kappa)}(\tau)} \Rightarrow \boldsymbol{\sigma}^{(\kappa)}_{pl}\left(\tau\right) = \xi \cdot \boldsymbol{\sigma}^{(\kappa)}\left(\tau\right) \tag{5.34}$$

Steps b) and a) are repeated for every GP.

c) Assemble for the whole structure the new rate vector of the nodal forces $\dot{\mathbf{R}}'(\tau)$:

$$\dot{\mathbf{R}}'(\tau) = \gamma^{(\mu)}\dot{\mathbf{R}}(\tau) + \int_V \mathbf{B}^T \cdot \boldsymbol{\sigma}^{(\kappa)}_{pl}(\tau) dV \tag{5.35}$$

with $\dot{\mathbf{R}}(\tau)$ being derivative of the equivalent nodal forces for the loading $\dot{\mathbf{P}}(\tau)$ which may be evaluated by differentiating the eqns. (5.28) or (5.29), depending on the case of loading. $\mathbf{B}$ is the compatibility strain-displacement matrix for the given FE mesh.

d) Find an update for the vector of the rates of the displacements $\dot{\mathbf{r}}^{(\kappa)}(\tau)$ using the relation:

$$\mathbf{K}\dot{\mathbf{r}}^{(\kappa)}(\tau) = \dot{\mathbf{R}}'(\tau) \tag{5.36}$$

e) A value for $\dot{\boldsymbol{\rho}}^{(\kappa)}(\tau)$ is evaluated at each G.P.

$$\dot{\boldsymbol{\rho}}^{(\kappa)}(\tau) = \mathbf{DB}\dot{\mathbf{r}}^{(\kappa)}(\tau) - \gamma^{(\mu)}\dot{\boldsymbol{\sigma}}^{el}(\tau) - \boldsymbol{\sigma}_{pl}^{(\kappa)}(\tau) \tag{5.37}$$

where $\dot{\boldsymbol{\sigma}}^{el}(\tau) = \dot{\alpha}_1(\tau)\boldsymbol{\sigma}^{el}_{P_1^*} + \dot{\alpha}_2(\tau)\boldsymbol{\sigma}^{el}_{P_2^*}$

The steps a)-e) are repeated for all the cycle time points.

f) By performing a numerical time integration over the whole cycle an update of the Fourier coefficients may be obtained:

$$\begin{aligned}
\mathbf{a}_k^{(\kappa+1)} &= -\frac{1}{k\pi}\int_0^1 \left\{\left[\dot{\boldsymbol{\rho}}^{(\kappa)}(\tau)\right]\left(\sin 2k\pi\tau\right)\right\} d\tau \\
\mathbf{b}_k^{(\kappa+1)} &= \frac{1}{k\pi}\int_0^1 \left\{\left[\dot{\boldsymbol{\rho}}^{(\kappa)}(\tau)\right]\left(\cos 2k\pi\tau\right)\right\} d\tau \\
\frac{\mathbf{a}_0^{(\kappa+1)}}{2} &= -\sum_{k=1}^{\infty}\mathbf{a}_k^{(\kappa+1)} + \frac{\mathbf{a}_0^{(\kappa)}}{2} + \sum_{k=1}^{\infty}\mathbf{a}_k^{(\kappa)} + \int_0^1 \left[\dot{\boldsymbol{\rho}}^{(\kappa)}(\tau)\right] d\tau
\end{aligned} \tag{5.38}$$

g) From the expressions (5.38) one may get an update for $\boldsymbol{\rho}^{(\kappa+1)}(\tau)$ using the iterative form of (5.6):

$$\boldsymbol{\rho}^{(\kappa+1)}(\tau) = \frac{1}{2}\mathbf{a}_0^{(\kappa+1)} + \sum_{k=1}^{\infty}\left\{\cos(2k\pi\tau)\cdot\mathbf{a}_k^{(\kappa+1)} + \sin(2k\pi\tau)\cdot\mathbf{b}_k^{(\kappa+1)}\right\} \tag{5.39}$$

h) Check whether the values of the residual stresses at the current and at the previous iteration, differ within some tolerance at some cycle point, for example at the end of the cycle, i.e.:

$$\frac{\left\|\boldsymbol{\rho}^{(\kappa+1)}(1)\right\|_2 - \left\|\boldsymbol{\rho}^{(\kappa)}(1)\right\|_2}{\left\|\boldsymbol{\rho}^{(\kappa+1)}(1)\right\|_2} \leq tolr \tag{5.40}$$

In case this does not hold we set $\boldsymbol{\rho}_{(\mu-1)}^{(\kappa+1)}(\tau) = \boldsymbol{\rho}^{(\kappa+1)}(\tau)$ and go back to step a) and start a new iteration of the inner RSDM loop; otherwise we set $\boldsymbol{\rho}^{(\mu)}(\tau) = \boldsymbol{\rho}^{(\kappa+1)}(\tau)$ and we exit the inner loop.

2. On the exit of the inner loop, the cyclic solution values of $\mathbf{a}_0^{(\mu)}, \mathbf{a}_k^{(\mu)}, \mathbf{b}_k^{(\mu)}, \boldsymbol{\rho}^{(\mu)}(\tau)$, as well as the plastic stress vector $\boldsymbol{\sigma}_{pl}^{(\mu)}(\tau)$ for the current loading factor $\gamma^{(\mu)}$, have been obtained.
3. The function φ which is the sum of the norms of the vectors of the coefficients of the trigonometric part of the Fourier series is evaluated:

$$\varphi\left(\gamma^{(\mu)}\right) = \sum_{k=1}^{\infty}\left\|\mathbf{a}_k^{(\mu)}\right\| + \sum_{k=1}^{\infty}\left\|\mathbf{b}_k^{(\mu)}\right\| \tag{5.41}$$

4. A decreased update of the loading factor $\gamma^{(\mu+1)}$ is obtained through this sum of norms:

$$\gamma^{(\mu+1)} \cdot P_1^* = \gamma^{(\mu)} \cdot P_1^* - \omega \cdot [\varphi\left(\gamma^{(\mu)}\right) \cdot d] \tag{5.42}$$

It should be noted that ω is a convergence parameter that will be discussed below (see section 5.2.5). It is also recalled that d is the thickness of the structure, so that only loading terms are entered in (5.42). By monitoring the value of $\gamma^{(\mu)} \cdot P_1^*$ one may keep track of the shrinking of the loading in the time domain and also, equivalently, in the load domain.

5. The new loading factor is compared against the previous one by the inequality:

$$\frac{\left|\gamma^{(\mu+1)} - \gamma^{(\mu)}\right|}{\gamma^{(\mu+1)}} \leq tol \tag{5.43}$$

If the inequality holds, the procedure stops and $\gamma^{(\mu)} \approx \gamma^{(\mu+1)} = \gamma_{sh}$, as only constant terms in the Fourier series of the residual stresses. Otherwise steps 1-5 are repeated.

Because of eqn.(5.42) the proposed procedure produces a descending sequence of cyclic solutions that ends up with the parameters of the limiting cycle for elastic shakedown (see section 4.10). Thus, γ_{sh} is the elastic shakedown factor, and the constant term, the only remaining term from the Fourier series, coincides with the constant in time distribution of the residual stresses which is unique for the adopted prescribed loading domain (Gokhfeld and Cherniavsky, 1980).

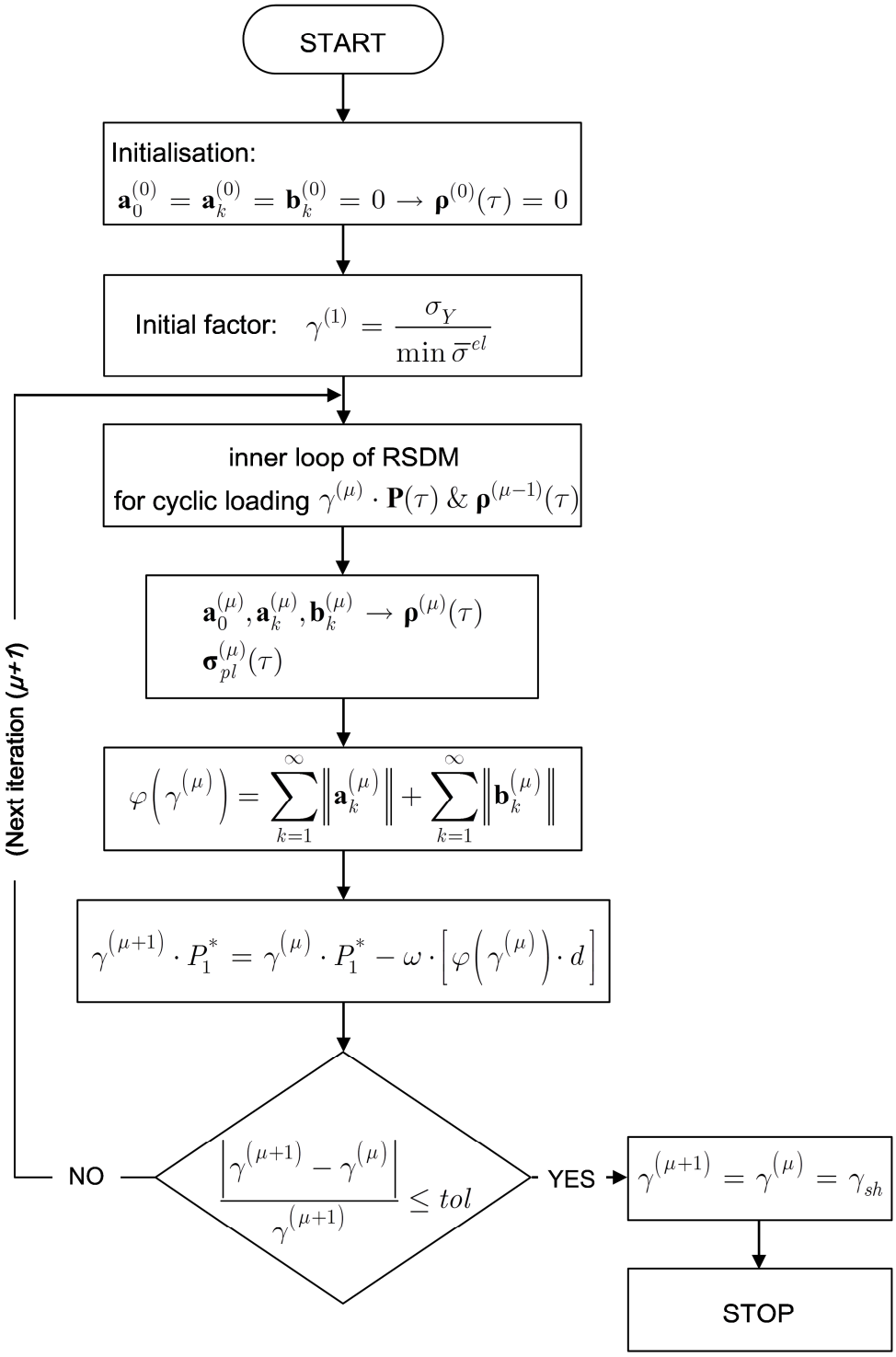

Figure 5.8 Flowchart of the proposed procedure RSDM-S

5.2.2. An extension of the RSDM-S for the shakedown analysis of structures under thermomechanical loading

In the present section a numerical approach for the evaluation of the shakedown load of elastoplastic structures under cyclic thermo-mechanical loading is proposed. The RSDM-S procedure that was previously described is herein extended in order to take into account thermal effects to the shakedown analysis of structures (Spiliopoulos and Panagiotou, 2014b).

5.2.2.1. Some theoretical and computational aspects

Let us consider a body of volume V and surface S that is subjected to a mechanical load on a part of S and another part of S has zero displacements. Let us further consider that the body (Fig.5.9(a)) is also subjected to some temperature load. The loads are assumed to be cyclic, having the following form:

$$P(t) = P(t + nT) \tag{5.44}$$

$$\theta(t) = \theta(t + nT), \qquad \theta(t) = \theta(x, y, z, t) \tag{5.45}$$

where x, y, z are the spatial coordinates of a point inside the body.

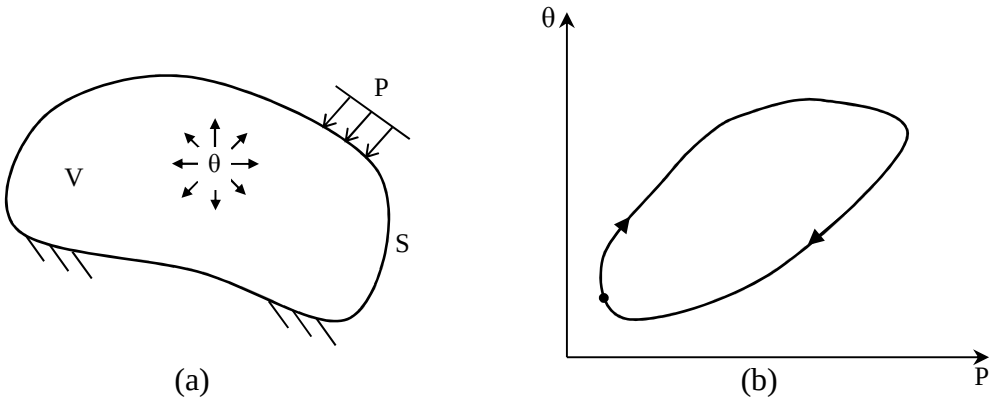

Figure 5.9 (a) Structure with applied thermomechanical loads, (b) cyclic loading state

Such a loading constitutes a cyclic loading state having a period T, with t denoting a time point inside a cycle and n being the number of full cycles. A loading trajectory in a two-dimensional loading domain may be seen in Fig.5.9(b).

For a material exhibiting elasto-plastic behavior we may assume that at any cycle point $\tau = t \,/\, T$ the stress field in the structure may be decomposed into two parts:

$$\boldsymbol{\sigma}(\tau) = \boldsymbol{\sigma}^{el}(\tau) + \boldsymbol{\rho}(\tau) \tag{5.46}$$

Considering the linear elastic behavior, we may split the loading into the mechanical and the thermal one. Let us briefly discuss the thermal loading; $\mathbf{r}(\tau)$ denotes the vector of the nodal displacements at some cycle time τ, due to this load. The strains at the Gauss integration points (GPs) may be expressed by (5.47):

$$\mathbf{e}(\tau) = \mathbf{B}\mathbf{r}(\tau) \tag{5.47}$$

Assuming some distribution of thermal strains $\mathbf{e}^{\theta}(\tau)$ an elastic strain field is needed in order to satisfy the compatibility:

$$\mathbf{e}(\tau) = \mathbf{e}^{el}(\tau) + \mathbf{e}^{\theta}(\tau) = \mathbf{D}^{-1}\boldsymbol{\sigma}_{\theta}^{el}(\tau) + \mathbf{e}^{\theta}(\tau) \tag{5.48}$$

where $\mathbf{D}$ is the material matrix. Thus, it may be written:

$$\boldsymbol{\sigma}_{\theta}^{el}(\tau) = \mathbf{D}\mathbf{e}(\tau) - \mathbf{D}\mathbf{e}^{\theta}(\tau) \tag{5.49}$$

With the use of virtual work we get:

$$\int_{V} \delta\mathbf{e}(\tau)^{T}\boldsymbol{\sigma}_{\theta}^{el}(\tau)dV = 0 \tag{5.50}$$

since there is no external loading, due to thermal loading develop. Combining (5.47), (5.49) and (5.50) the following expression may be written:

$$\left(\int_{V} \mathbf{B}^{T}\mathbf{D}\mathbf{B}dV\right)\mathbf{r}(\tau) = \int_{V} \mathbf{B}^{T}\mathbf{D}\mathbf{e}^{\theta}(\tau)dV \tag{5.51}$$

or equivalently:

$$\mathbf{Kr}(\tau) = \int_V \mathbf{B}^T \mathbf{D}\mathbf{e}^{\theta}(\tau) dV \tag{5.52}$$

where $\mathbf{K}$ is the stiffness matrix of the structure. Thus after the solution of (5.52) for $\mathbf{r}(\tau)$ we may get the values for $\boldsymbol{\sigma}_{\theta}^{el}(\tau)$ using eqns. (5.47) and (5.49). The corresponding values of the stresses $\boldsymbol{\sigma}_{P}^{el}(\tau)$ due to the mechanical loading may be easily obtained, in an analogous way, after the conversion of the loading to the equivalent nodal forces vector $\mathbf{R}(\tau)$, using this vector as the r.h.s of equation (5.52) and omitting the second part of eqn. (5.49).

5.2.2.2. Evaluation of the derivative of the residual stresses

As it has been already mentioned, inelasticity may be taken into account through the residual stress field of (5.46). An analogous decomposition to this equation holds for the strain rates, similarly to eqn.(5.3):

$$\dot{\boldsymbol{\varepsilon}}(\tau) = \dot{\mathbf{e}}(\tau) + \dot{\boldsymbol{\varepsilon}}_r(\tau) \tag{5.53}$$

where $\dot{\mathbf{e}}(\tau)$ may be evaluated from (5.48); $\mathbf{e}^{el}(\tau)$ will now concern elastic strains due to both thermal and mechanical loading. The residual strain rate $\dot{\boldsymbol{\varepsilon}}_r(\tau)$ may be itself decomposed into elastic and plastic parts. Thus, (5.53) becomes:

$$\dot{\boldsymbol{\varepsilon}}(\tau) = \dot{\mathbf{e}}^{el}(\tau) + \dot{\mathbf{e}}^{\theta}(\tau) + \dot{\boldsymbol{\varepsilon}}_r^{el}(\tau) + \dot{\boldsymbol{\varepsilon}}^{pl}(\tau) \tag{5.54}$$

The stress rates and elastic strain rates are given by the expressions:

$$\begin{aligned} \dot{\boldsymbol{\sigma}}^{el}(\tau) &= \mathbf{D}\dot{\mathbf{e}}^{el} \\ \dot{\boldsymbol{\rho}}(\tau) &= \mathbf{D}\dot{\boldsymbol{\varepsilon}}_r^{el} \end{aligned} \tag{5.55}$$

Combining (5.54) and (5.55), we get the below expression of the rates of the residual stresses. Thus eqn.(5.14) is converted to:

$$\dot{\boldsymbol{\rho}}(\tau) = \mathbf{D}\dot{\boldsymbol{\varepsilon}}(\tau) - \dot{\boldsymbol{\sigma}}^{el}(\tau) - \mathbf{D}\dot{\mathbf{e}}^{\theta}(\tau) - \mathbf{D}\dot{\boldsymbol{\varepsilon}}^{pl}(\tau) \tag{5.56}$$

We may now solve the rate problem with the aid of the FEM. Compatibility is written with respect to the rate of the nodal displacements, i.e.:

$$\dot{\boldsymbol{\varepsilon}}(\tau) = \mathbf{B}\dot{\mathbf{r}}(\tau) \tag{5.57}$$

Since the residual stresses are self-equilibrated we may have from the PVW:

$$\int_V \delta\dot{\boldsymbol{\varepsilon}}(\tau)^T \dot{\boldsymbol{\rho}}(\tau) dV = 0 \tag{5.58}$$

Thus, we end up by solving the following direct stiffness equation with its r.h.s. being known:

$$\mathbf{K}\dot{\mathbf{r}}(\tau) = \int \mathbf{B}^T \dot{\boldsymbol{\sigma}}^{el}(\tau) dV + \int \mathbf{B}^T \mathbf{D}\dot{\mathbf{e}}^{\theta}(\tau) dV + \int \mathbf{B}^T \mathbf{D}\dot{\boldsymbol{\varepsilon}}^{pl}(\tau) dV \tag{5.59}$$

With $\dot{\mathbf{r}}(\tau)$ known, we may estimate the values of $\dot{\boldsymbol{\rho}}(\tau)$, using (5.57) and (5.56).

5.2.2.3. Description of the extension of the RSDM-S for thermomechanical loadings

Let us assume that a structure is subjected to a mechanical and a thermal load (see Fig.5.10(a)) that vary independent to each other. These loads may have a cyclic variation between a specified maximum and a minimum value just like the cyclic program of Fig.5.10(b), which is typically described by the load path $\left(0 \rightarrow P^* \rightarrow (P^*,\theta^*) \rightarrow \theta^* \rightarrow 0\right)$. Once again, as in section 5.2.1, without loss of generality, we assume that the minimum values of the two loads are zero with the starred quantities corresponding to the maximum values of the loads. Although the procedure may be applied for more than two loads, for simplicity reasons, a maximum of one mechanical and one thermal load is considered herein.

In an analogous way to the description of RSDM-S of section 5.2.1 that addresses the problem of shakedown of structures under mechanical loadings, one may establish a load variation with time by drawing a curve that passes through the limits of the load domain. In the time domain this cyclic loading may be expressed as:

$$\mathbf{P}(\tau) = \begin{Bmatrix} P\ (\tau) \\ \theta(\tau) \end{Bmatrix} = \begin{Bmatrix} P^* \cdot \alpha_1(\tau) \\ \theta^* \cdot \alpha_2(\tau) \end{Bmatrix} \tag{5.60}$$

Indicative variations of the two loads may be seen in Fig.5.10(b).

Eqn. (5.60) converts the problem of a prescribed loading domain to an equivalent prescribed cyclic loading in the time domain. As previously, the loading domain may be isotropically varied by multiplying the variation of the loads with a factor γ. The proposed iterative procedure seeks to find the factor γ_{sh} for which the adopted cyclic loading leads the structure to shakedown. Thus we need to start from a value which is definitely above the shakedown load.

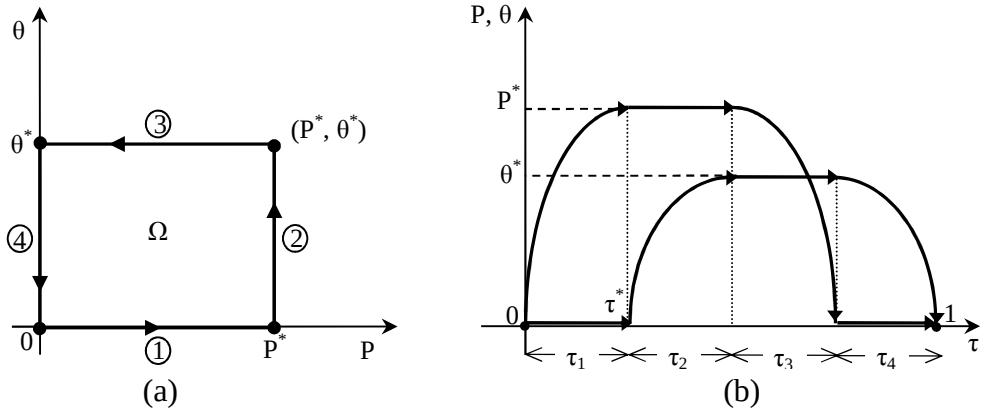

Figure 5.10 Individual cyclic loading variation over one time period (a) in load space, (b) in time domain

5.2.2.4. Evaluation of an initial load factor γ

One may find the elastic equivalent von Mises stress $\overline{\sigma}^{el}$ at all the GPs of the structure at time τ^*. This is the cycle time point that one of the loads, for example P, attains its maximum value P^* and the other load θ is zero. Denoting by $\min \overline{\sigma}^{el}$ the non-zero minimum of these stresses one may use an initial load factor equal to:

$$\gamma^{(1)} = \frac{\sigma_Y}{\min \overline{\sigma}^{el}} \tag{5.61}$$

It may be observed that the initial load factor is calculated in the same way as in the case of mechanical loads (see section 5.2.1.2).

5.2.2.5. Layout of the numerical procedure for thermomechanical loading

The numerical procedure consists, in general, of the steps described in section 5.2.1.3. Although, in order to take into account the thermal effects, the RSDM-S as it has been described in section 5.2.1.3, should be modified in the next points:

1. Eqn. (5.33) that describes the total elastic stresses converts to:

$$\boldsymbol{\sigma}^{el}(\tau) = \alpha_1(\tau)\boldsymbol{\sigma}^{el}_{P^*} + \alpha_2(\tau)\boldsymbol{\sigma}^{el}_{\theta^*} \tag{5.62}$$

   with $\alpha_1(\tau), \alpha_2(\tau)$ the time functions of the loading (eqn. (5.60)). Note that $\boldsymbol{\sigma}^{el}_{P^*}$ and $\boldsymbol{\sigma}^{el}_{\theta^*}$ are the elastic stresses for P^* and θ^* respectively.

2. The updated rate vector of the nodal forces $\dot{\mathbf{R}}'(\tau)$ of eqn. (5.35) is now described by the relation:

$$\dot{\mathbf{R}}' = \gamma^{(\mu)}\left\{\dot{\alpha}_1(\tau)\mathbf{R}_{P^*} + \dot{\alpha}_2(\tau)\int_V \mathbf{B}^T\mathbf{D}\boldsymbol{\varepsilon}^{\theta^*}dV\right\} + \int_V \mathbf{B}^T\boldsymbol{\sigma}^{(\kappa)}_{pl}dV \tag{5.63}$$

   This expression is obtained if we substitute first $\dot{\boldsymbol{\varepsilon}}^{\theta^*} = \dot{\alpha}_2(\tau)\boldsymbol{\varepsilon}^{\theta^*}$, and then eqn. (5.62), in the expression (5.59), with $\mathbf{R}_{P^*}$ being the equivalent nodal forces of the elastic FE solution for P^*.

3. Instead of eqn.(5.37) a value for $\dot{\boldsymbol{\rho}}^{(\kappa)}(\tau)$ is now given by:

$$\dot{\boldsymbol{\rho}}^{(\kappa)}(\tau) = \mathbf{DB}\dot{\mathbf{r}}^{(\kappa)}(\tau) - \gamma^{(\mu)}\dot{\boldsymbol{\sigma}}^{el}(\tau) - \mathbf{D}\dot{\boldsymbol{\varepsilon}}^{\theta,(\mu)} - \boldsymbol{\sigma}^{(\kappa)}_{pl}(\tau) \tag{5.64}$$

   where $\dot{\boldsymbol{\sigma}}^{el}(\tau) = \dot{\alpha}_1(\tau)\boldsymbol{\sigma}^{el}_{P^*} + \dot{\alpha}_2(\tau)\boldsymbol{\sigma}^{el}_{\theta^*}$ for all the GPs.

4. The last modification, concerns the decreased update of the loading factor which is now obtained by the relation:

$$\gamma^{(\mu+1)} \cdot P^* = \gamma^{(\mu)} \cdot P^* - \omega \cdot [\varphi\left(\gamma^{(\mu)}\right) \cdot d] \tag{5.65}$$

5.2.3. General loading domains

In the previous sections the RSDM-S has been described assuming that a structure is subjected to loads that have a cyclic variation between a specified minimum equal to zero and a maximum value. An application of the RSDM-S for a general loading domain, where the applied loads have both their minimum and maximum values different to zero (Figs.5.11(a),5.12(a)), is described herein.

A basic remark is that we may use any curve, either polynomial or linear, that passes through these limits to express a cyclic loading variation (Figs.5.11(b),5.12(b)).

The maximum values of the two loads are marked as P_{1+}^* and P_{2+}^* respectively, and the minimum values denoted by P_{1-}^* and P_{2-}^*.

A general type of loading case may consists of the convex hyper-polyhedron defined by the vertices of the minimum and maximum values of the applied loads, i.e. the rectangular domain Ω shown in Fig.5.11(a). An arbitrary established cyclic loading path may be the following:

$\left((P_{1+}^*, P_{2+}^*) \rightarrow (P_{1-}^*, P_{2+}^*) \rightarrow (P_{1-}^*, P_{2-}^*) \rightarrow (P_{1+}^*, P_{2-}^*) \rightarrow (P_{1+}^*, P_{2+}^*)\right)$

In time domain this cyclic loading may be expressed as:

$$\mathbf{P}(\tau) = \begin{Bmatrix} P_1(\tau) \\ P_2(\tau) \end{Bmatrix} = \begin{Bmatrix} P_1^* \cdot \alpha_1(\tau) \\ P_2^* \cdot \alpha_2(\tau) \end{Bmatrix} \tag{5.66}$$

Indicative variations of the two loads are shown in Fig.5.11(b).

Thereby, an equivalent load of prescribed time history is obtained. Thereinafter, the RSDM-S may be applied in the way it is described in sections 5.2.1, 5.2.2.

In an analogous way, different types of load domains, like the domain of Fig.5.12, may be treated.

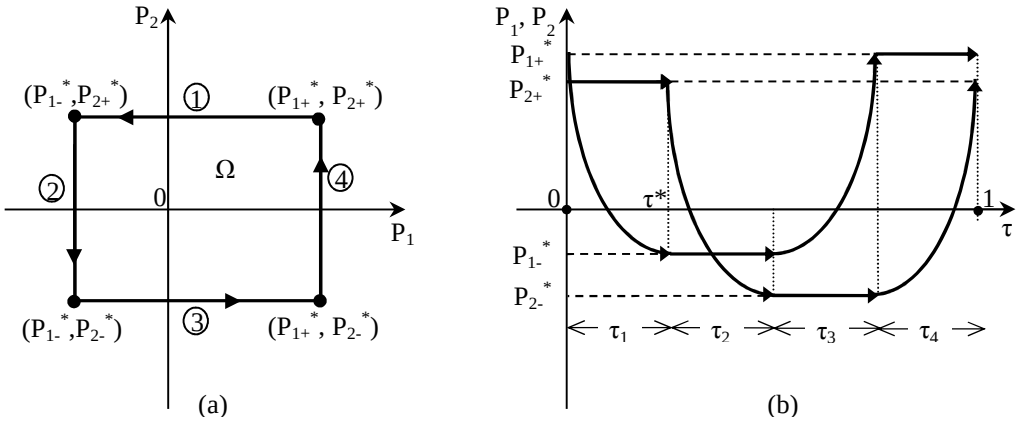

Figure 5.11 Individual cyclic loading variation over one time period (a) in load space, (b) in time domain

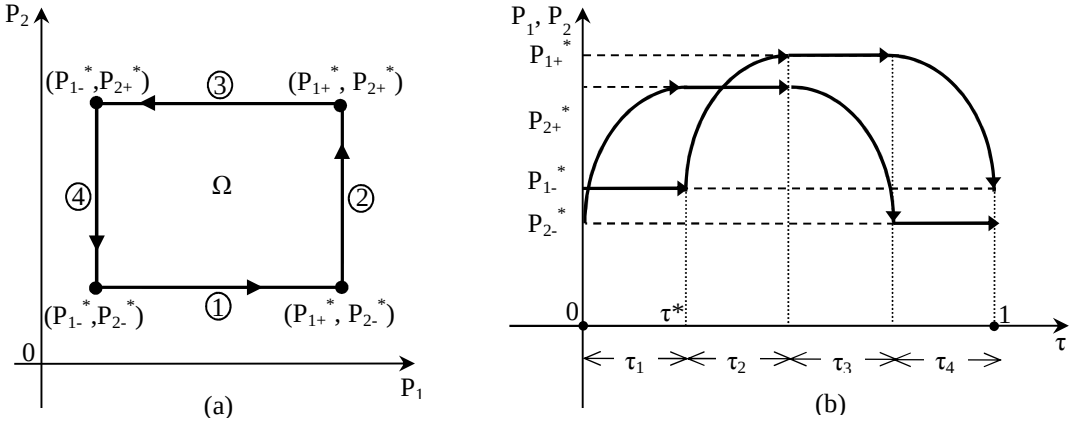

Figure 5.12 Individual cyclic loading variation over one time period (a) in load space, (b) in time domain

5.2.4. Shakedown analysis with multidimensional loading spaces

The numerical procedure (RSDM-S) described in sections 5.2.1 and 5.2.2, has been extended in order to provide shakedown limits of structures subjected to varying thermal and mechanical loadings for the case of multidimensional loading space.

5.2.4.1. Description of the loading domain

Let us consider a structure having thickness d and a volume V subjected to mechanical loadings and thermal loadings (Fig.5.13(a)). Although the procedure may be applied for more than three loadings (mechanical, or thermal), for simplicity reasons, a case of a maximum of three loads will be described herein. An arbitrary loading trajectory in a three-dimensional loading domain may be seen in Fig.5.13(b).

These loads have a cyclic variation between a specified minimum and a maximum value. For illustration, it is assumed in this section that the minimum values of the three loads are zero.

The key remark that remains unaltered is that we may use any curve that passes through these limits to express a cyclic loading variation.

Let us consider a common loading case in shakedown analysis of an independent variation of the loads. The pertinent three-dimensional loading space is described by the rectangular parallelepiped of Fig.5.14(a). We may establish a cyclic loading in time domain that passes through the eight corners of the parallelepiped. To this end, the cyclic program in time domain may be expressed as:

$$\mathbf{P}(\tau) = \begin{Bmatrix} P_1(\tau) \\ P_2(\tau) \\ \theta(\tau) \end{Bmatrix} = \begin{Bmatrix} P_1^* \cdot \alpha_1(\tau) \\ P_2^* \cdot \alpha_2(\tau) \\ \theta^* \cdot \alpha_3(\tau) \end{Bmatrix} \tag{5.67}$$

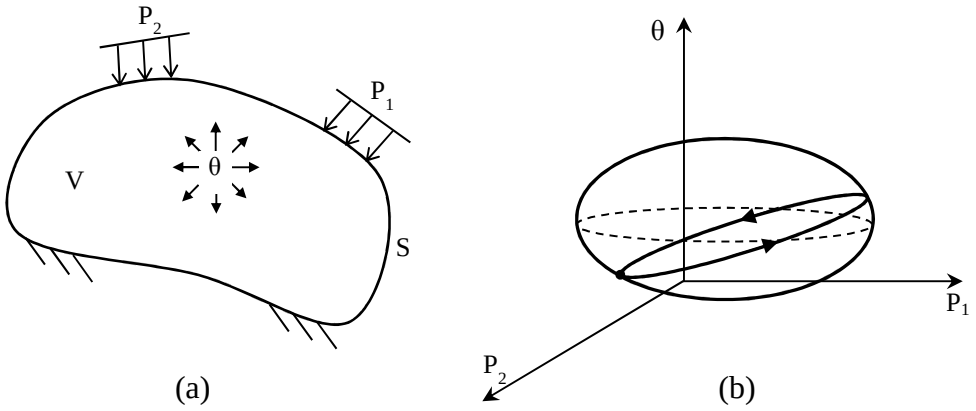

Figure 5.13 (a) Structure with applied thermomechanical loads, (b) 3-D cyclic loading state

where $\alpha_i(\tau)$ is a time function that is used to describe a variation with respect to the cycle time, different for the three loads.

Indicative variations of the two loads may be seen in Fig.5.14(b).

It should be noticed that any continuous loading path that passes through the edges of loading space could be used, regardless the sequence of the corners.

It is useful to be reminded that due to the convexity of the yield surface, if a structure shakes down over the path that encloses the domain Ω, it certainly shakes down over any loading path contained inside this domain (König and Kleiber, 1978).

5.2.4.2. Evaluation of an initial load factor γ

One may find the elastic equivalent von Mises stress $\bar{\sigma}^{el}$ at all the GPs of the structure at time τ^*. This is the cycle time point that one of the loads, for example P_1, attains its maximum value P_1^* and the other loads are zero. Denoting by $\min \bar{\sigma}^{el}$ the non-zero minimum of these stresses one may use an initial load factor equal to:

$$\gamma^{(1)} = \frac{\sigma_Y}{\min \bar{\sigma}^{el}} \tag{5.68}$$

It may be observed that the initial load factor is calculated in the same way as in the previous cases (see sections 5.2.1.2, 5.2.2.4).

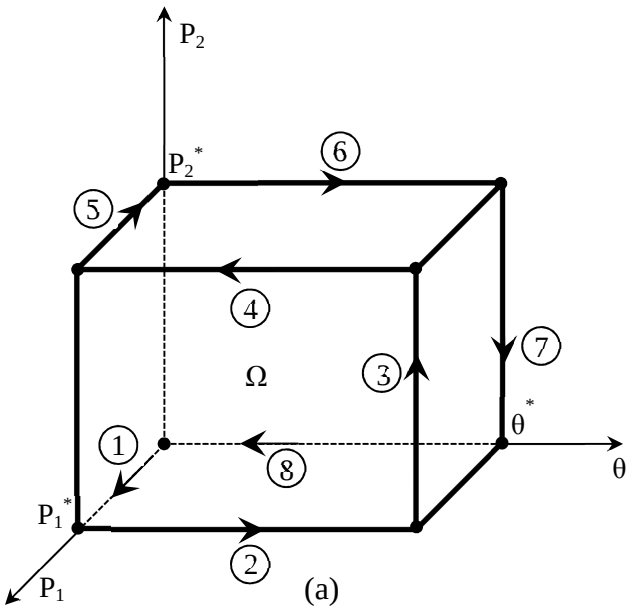

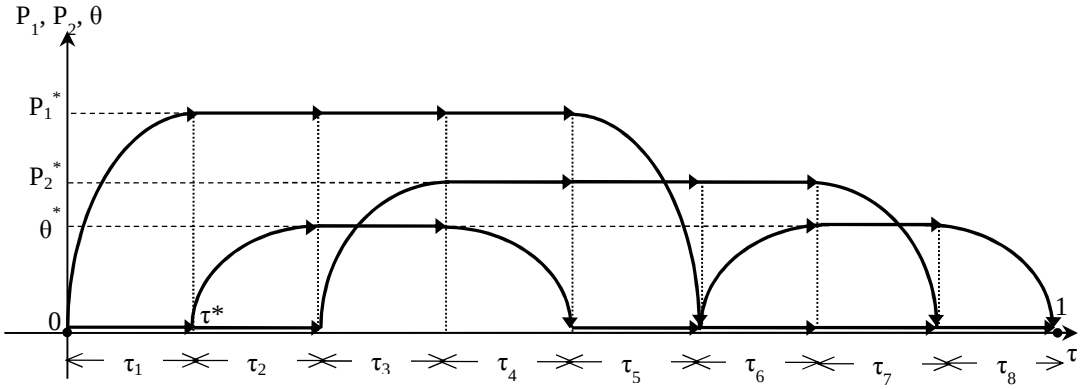

Figure 5.14 Individual three dimensional cyclic loading variation over one time period (a) in load space, (b) in time domain

5.2.4.3. Layout of the numerical procedure

The numerical procedure follows the basic steps of RSDM-S (see 5.2.1.3). Although, the updated formulation for three-dimensional loading domain differs to the following points:

1. The total stress (see eqn.(5.33) or eqn.(5.62)) is given by:

$$\boldsymbol{\sigma}^{el}(\tau) = \alpha_1(\tau)\boldsymbol{\sigma}^{el}_{P_1^*} + \alpha_2(\tau)\boldsymbol{\sigma}^{el}_{P_2^*} + \alpha_3(\tau)\boldsymbol{\sigma}^{el}_{\theta^*} \tag{5.69}$$

   with $\alpha_1(\tau), \alpha_2(\tau), \alpha_3(\tau)$ denoting the time functions of the loading (see eqn. (5.67)). Note that $\boldsymbol{\sigma}^{el}_{P_1^*}$, $\boldsymbol{\sigma}^{el}_{P_2^*}$ and $\boldsymbol{\sigma}^{el}_{\theta^*}$ are the elastic stresses for P_1^*, P_2^* and θ^* respectively.

2. The updated rate vector of the nodal forces $\dot{\mathbf{R}}'(\tau)$ of eqn. (5.35),(5.63) is now described by the relation:

$$\dot{\mathbf{R}} = \gamma^{(\mu)}\left\{\dot{\alpha}_1(\tau)\mathbf{R}_{P_1^*} + \dot{\alpha}_2(\tau)\mathbf{R}_{P_2^*} + \dot{\alpha}_3(\tau)\int_V \mathbf{B}^T\mathbf{D}\boldsymbol{\varepsilon}^{\theta^*}dV\right\} + \int_V \mathbf{B}^T\boldsymbol{\sigma}^{(\kappa)}_{pl}dV \tag{5.70}$$

3. Instead of eqn.(5.37), a value for $\dot{\boldsymbol{\rho}}^{(\kappa)}(\tau)$ is now given by:

$$\dot{\boldsymbol{\rho}}^{(\kappa)}(\tau) = \mathbf{D}\mathbf{B}\dot{\mathbf{r}}^{(\kappa)}(\tau) - \gamma^{(\mu)}\dot{\boldsymbol{\sigma}}^{el}(\tau) - \mathbf{D}\dot{\mathbf{e}}^{\theta,(\mu)} - \boldsymbol{\sigma}_{pl}^{(\kappa)}(\tau) \tag{5.71}$$

where $\dot{\boldsymbol{\sigma}}^{el}(\tau) = \dot{\alpha}_1(\tau)\boldsymbol{\sigma}^{el}_{P_1^*} + \dot{\alpha}_2(\tau)\boldsymbol{\sigma}^{el}_{P_2^*} + \dot{\alpha}_3(\tau)\boldsymbol{\sigma}^{el}_{\theta^*}$ for all the GPs.

4. The decreased update of the loading factor is obtained by the relation:

$$\gamma^{(\mu+1)} \cdot P_1^* = \gamma^{(\mu)} \cdot P_1^* - \omega \cdot [\varphi\left(\gamma^{(\mu)}\right) \cdot d] \tag{5.72}$$

An analytical flowchart of the RSDM-S procedure for the shakedown analysis of structures subjected to three-dimensional loading domain of mechanical and thermal loadings is shown in Fig.5.16. In this flowchart the new convergence criterion of section 5.2.6 has been considered.

5.2.5. Convergence considerations of RSDM-S

The numerical strategy adopted is to start the procedure with the convergence parameter $\omega = 1$. For most of the considered examples described in section 6.2, this normally leads to a monotonic convergence, from above, to the shakedown load. The algorithm is guaranteed to converge monotonically to the solution, as the continuous shrinking of the loading domain produces a strictly descending continuous function (Luenberger and Ye, 2008). In RSDM-S such a function is the function φ which is used to control and stop the iterative procedure, when the specified tolerance tol is reached for the first time. For accurate results, a value of tol of 10^{-4} proved sufficient. This is equivalent to a tolerance for φ of 10^{-3}.

There might be cases, though, especially when we start from a high initial value that an overshooting of the shakedown factor may occur, which means that the procedure bypasses the predefined tolerance tol for φ. To deal with the overshooting, a numerical convergence scheme for this current iteration of bypassing, denoted here with $\mu + 1$, is then followed (see Fig.5.15) . For the loading factor evaluated at the current iteration $\gamma^{(\mu+1)}$, we would have $\varphi(\gamma^{(\mu+1)}) < tol$; this loading factor is then not accepted and the convergence factor is halved sequentially

(see eqns.(5.42),(5.65),(5.72)) till we get a loading factor that corresponds to a value of $\varphi(\gamma^{(\mu+1)}) > tol$. Similarly, if the overshooting concerns a negative value of $\gamma^{(\mu+1)}$, such an overshooting occurrence encountered in a couple of our examples, the convergence factor is halved till we get a positive value of $\gamma^{(\mu+1)}$ which produces a value of $\varphi(\gamma^{(\mu+1)}) > tol$.

Another continuous descending function is the maximum Euclidian norm, over all the cycle points, of the plastic stress vector $\boldsymbol{\sigma}_{pl}^{(\mu)}(\tau)$. When the load factor reaches shakedown this norm should approach zero numerically, reaching some tolerance $tolpl$; from the considered examples of application the value of $tolpl$ turns out to be roughly of the order of 1%.

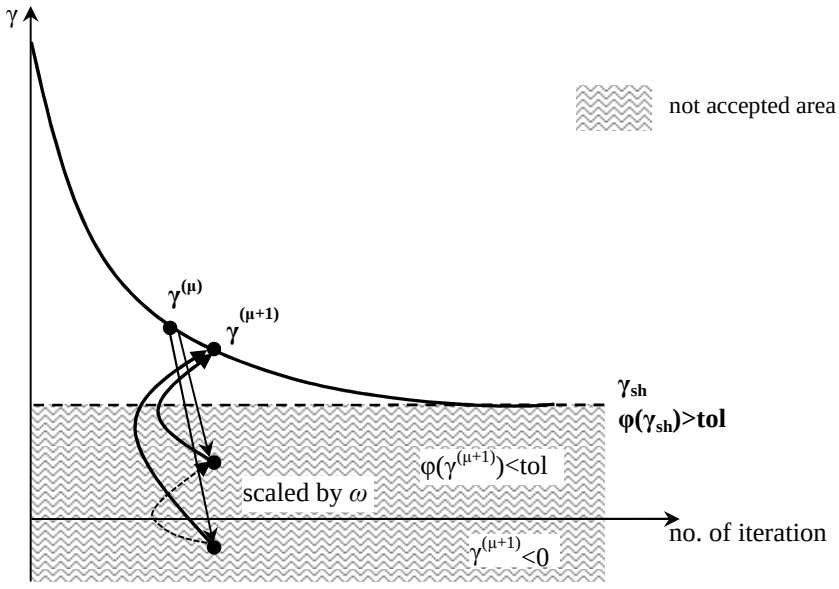

Figure 5.15 Convergence scheme of RSDM-S

5.2.6. A new convergence criterion

In order to succeed an acceleration of the numerical procedure an alternative convergence criterion was adopted. It was noted, in a couple of our tested examples, that although the RSDM-S required a small number of iterations to reach the final shakedown load factor, there might be cases that the inner loop of RSDM needed a

lot of iterations to converge to a final cyclic state. This observation implies that the previous convergence criterion of the RSDM (eqn.(5.26)) was quite strict and there might be a different criterion that while keeping the appropriate accuracy of the procedure it converges faster. Therefore, an improved convergence criterion of RSDM was devised.

Consequently, the convergence between two successive iterations, of the inner loop, is checked against a tolerance using the sum of the norms of the coefficients of the trigonometric part $\mathbf{a}_k$ and $\mathbf{b}_k$:

$$\left|\varphi^{(\kappa+1)} - \varphi^{(\kappa)}\right| < tol \tag{5.73}$$

where $\varphi^{(\kappa)} = \sum_{k=1}^{\infty}\left\|\mathbf{a}_k^{(\kappa)}\right\| + \sum_{k=1}^{\infty}\left\|\mathbf{b}_k^{(\kappa)}\right\|$ is calculated inside an iteration κ of the RSDM.

Thus, the convergence criterion of eqn.(5.40), has been replaced by the updated one of eqn.(5.73).

Therefore, step (h) of the iterative procedure RSDM-S (see section 5.2.1.3) is herein reformulated and states as:

“Next we check whether the value of the sum of the norm of the coefficients $\mathbf{a}_k$ and $\mathbf{b}_k$ at the current and at the previous iteration differ within some tolerance, see inequality (5.73). In case the inequality (5.73) does not hold, we set $\boldsymbol{\rho}_{(\mu-1)}^{(\kappa+1)}(\tau) = \boldsymbol{\rho}^{(\kappa+1)}(\tau)$ and go back to step a) and start a new iteration of the inner RSDM loop; otherwise we set $\boldsymbol{\rho}^{(\mu)}(\tau) = \boldsymbol{\rho}^{(\kappa+1)}(\tau)$ and we exit the inner loop.”

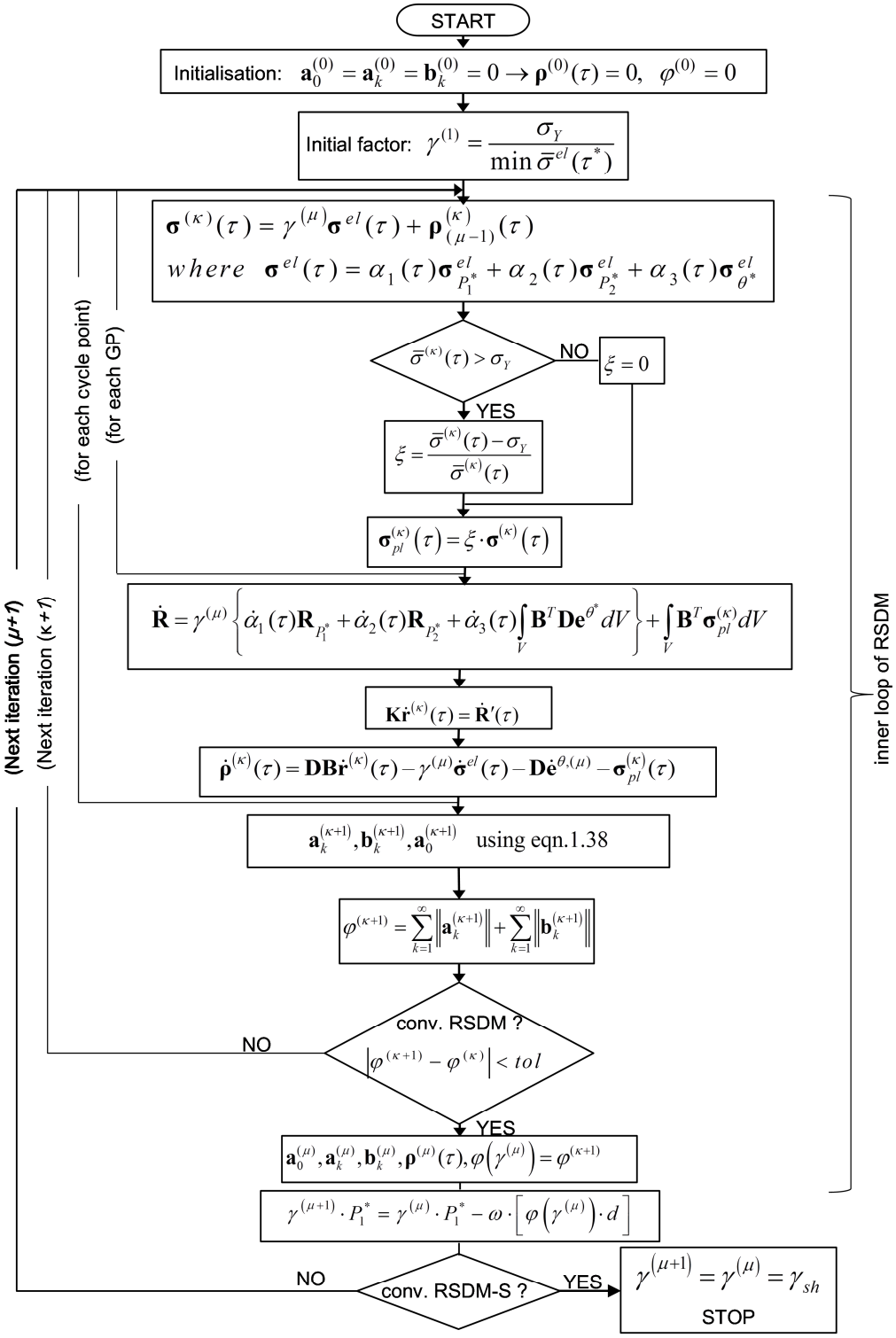

Figure 5.16 Flowchart of the RSDM-S for three thermomechanical dimensional loading case

6.

Examples of application

In this chapter several numerical examples are chosen to investigate and validate the capabilities of the proposed methodologies RSDM and RSDM-S, presented in Chapter 5. The chapter is divided into two sections: the first section deals with the results obtained using the RSDM to predict the steady state behavior of cyclically loaded structures, while the second one presents the results of shakedown analysis of structures using the RSDM-S.

The numerical approaches developed in this thesis were coded in Fortran.

6.1. Cyclic elastoplastic states using RSDM

6.1.1. Three bar truss

The first example of application is the truss structure of Fig.6.1, which was analytically studied in (Martin, 1965). A detailed description of the analytical solution of this example may be also seen in section 4.12. This example paves the way of the physical understanding of the procedure.

It is assumed that all the bars of the truss have an equal cross sectional area of $A = 5cm^2$ and are made of steel having the material data of Table 1. The length L is taken equal to $300cm$.

Three two noded plane truss elements were used to analyze the structure. It should be mentioned that the numerical procedure presented in section 5.1 for a continuum, was slightly altered to suit the needs of this one-dimensional stress problem. The geometry of this symmetric structure and the self-equilibrating nature of the residual stress field render the residual stresses for the inclined bars 1,3 equal to the ones of bar 2, but of opposite sign.

The truss was subjected to two concentrated cyclic loads $V(t), H(t)$ which were applied at node 4. Three cases of loading have been considered which lead the structure to three different cyclic states (Spiliopoulos and Panagiotou, 2012).

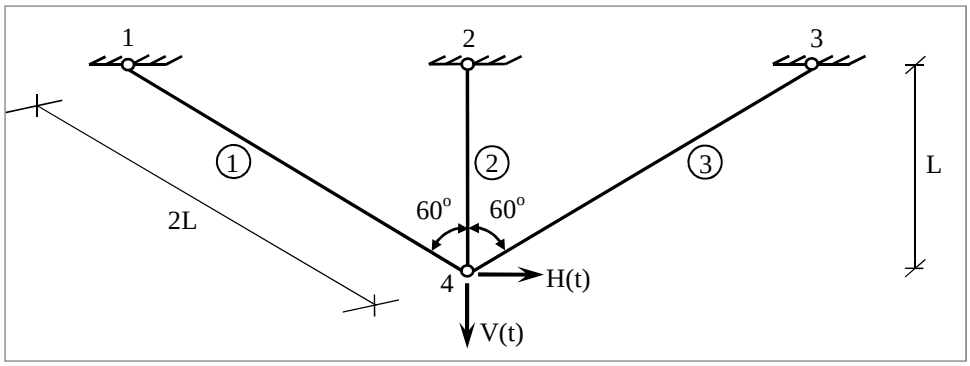

Figure 6.1 Three bar truss example

Young's modulus	E=208GPa
Poisson's ratio	v= 0,3
Yield stress	σ_Y=400MPa

Table 1. Material properties of the truss

a) The first loading case under consideration assumes the following variation with time (Fig.6.2)

$$V(t) = 300\sin^2(\pi t / T), \quad H(t) = 0$$

The RSDM predicts that the structure will shakedown. The computed, by the procedure, constant in time steady state residual stress of the middle bar is seen (Fig.6.3). In Fig.6.4 it may be seen that the total stress inside the cycle nowhere exceeds the yield stress. Additionally, this total stress distribution coincides with the

one that was calculated by a time-stepping commercial program (Abaqus, 2010), confirming that the computed residual stress (Fig.6.4) is the actual one.

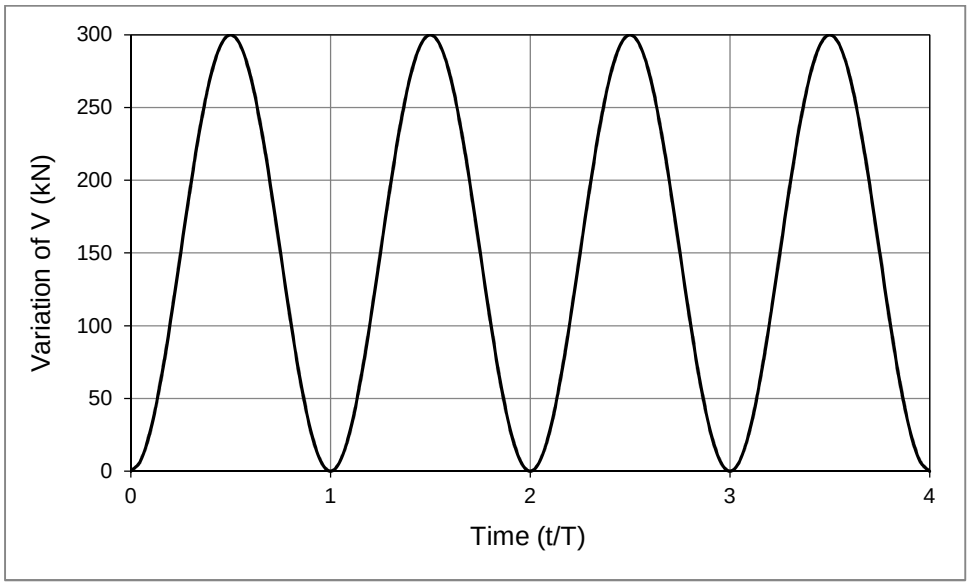

Figure 6.2 Load variation with time over four periods (load case a)

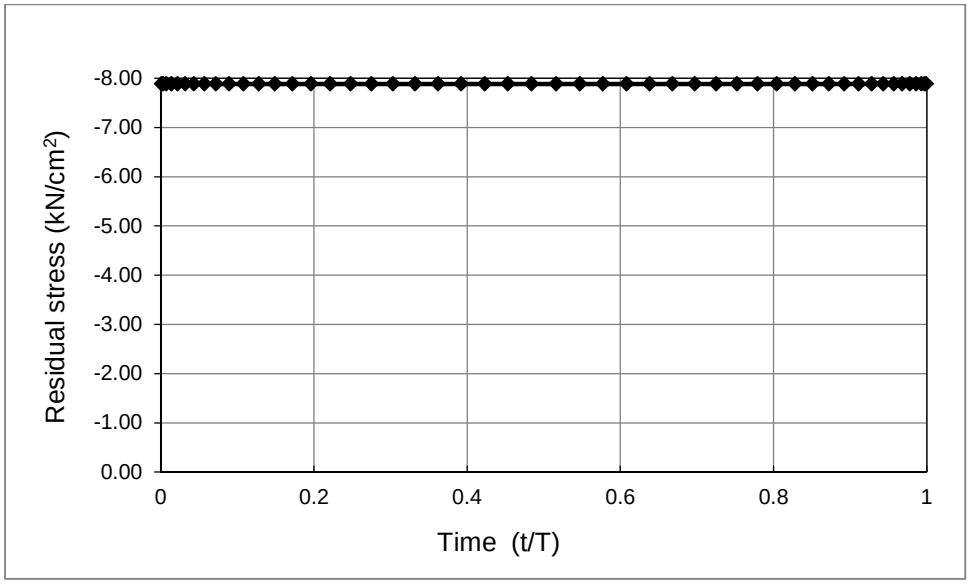

Figure 6.3 Residual steady stress distribution inside a cycle for bar 2 (load case a - shakedown)

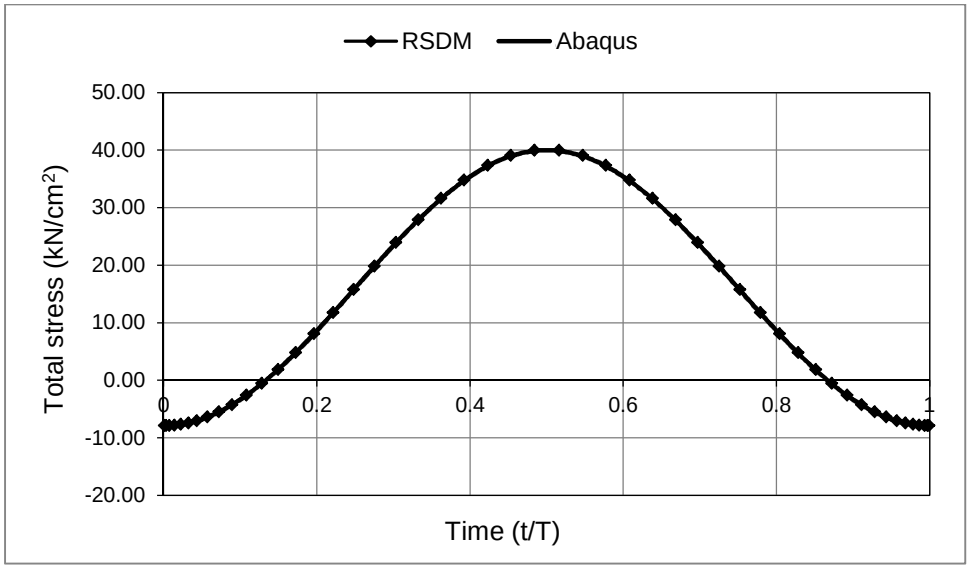

Figure 6.4 Total steady stress distribution inside a cycle for bar 2 (load case a – shakedown)

b) The second cyclic loading case has the following variation with time (Fig.6.5)

$$V(t) = 300\sin(2\pi t \,/\, T), \quad H(t) = 0$$

For this case the RSDM predicts an alternating plasticity state. In Fig.6.6, the distribution of the cyclic residual stress predicted for the middle bar inside the cycle it is shown. While the outer bars, in the steady state, are strained only elastically, the middle bar develops plastic strain rates, of alternating nature. These strains spread within the time intervals $\left[0.149, 0.362\right]$ and $\left[0.638, 0.851\right]$ inside the cycle. The total plastic strain over the cycle (see the parameter a_2 - expression (5.27) in section 5.1.4), which is equal to the total area under the curve (Fig.6.7), is equal to zero.

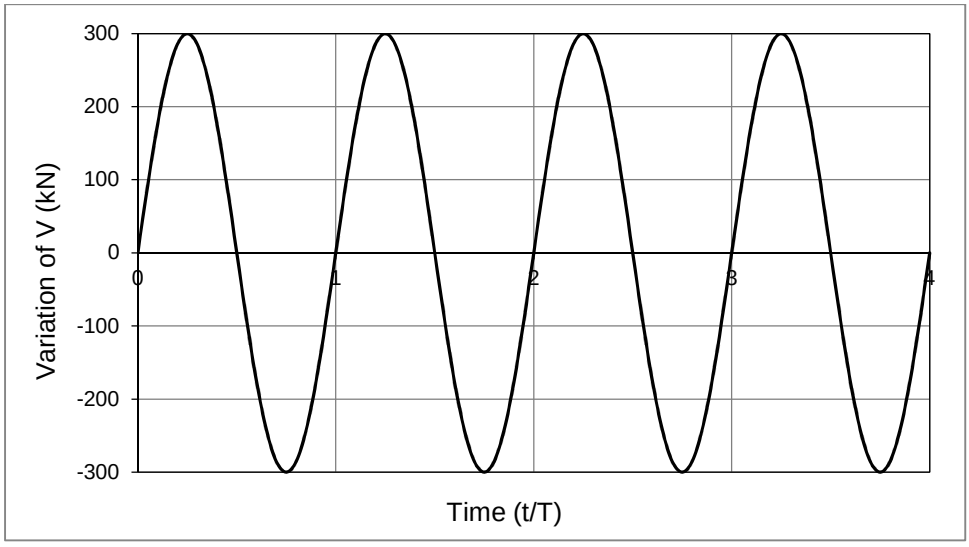

Figure 6.5 Load variation with time over four periods (load case b)

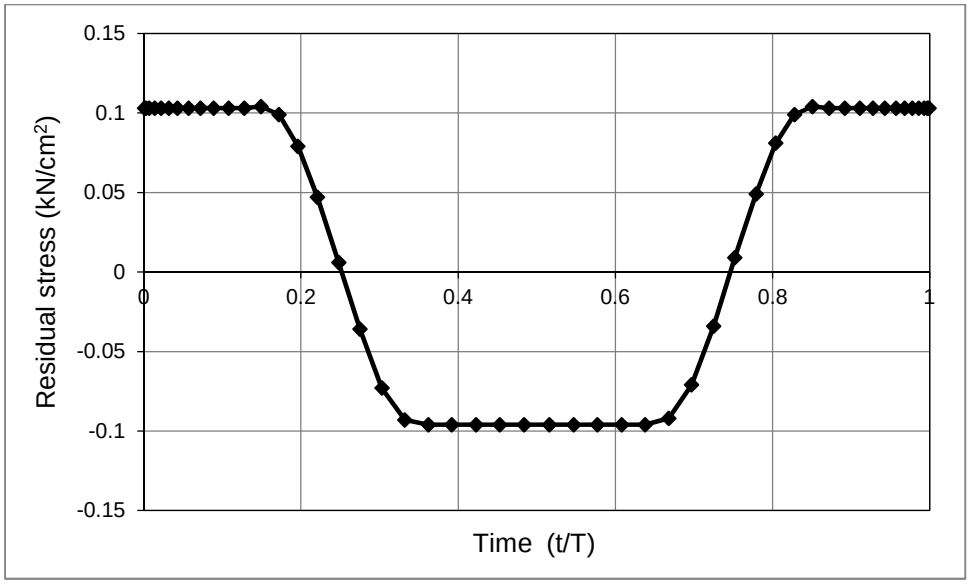

Figure 6.6 Predicted steady state residual stress distribution for bar 2 inside a cycle (load case b – alternating plasticity)

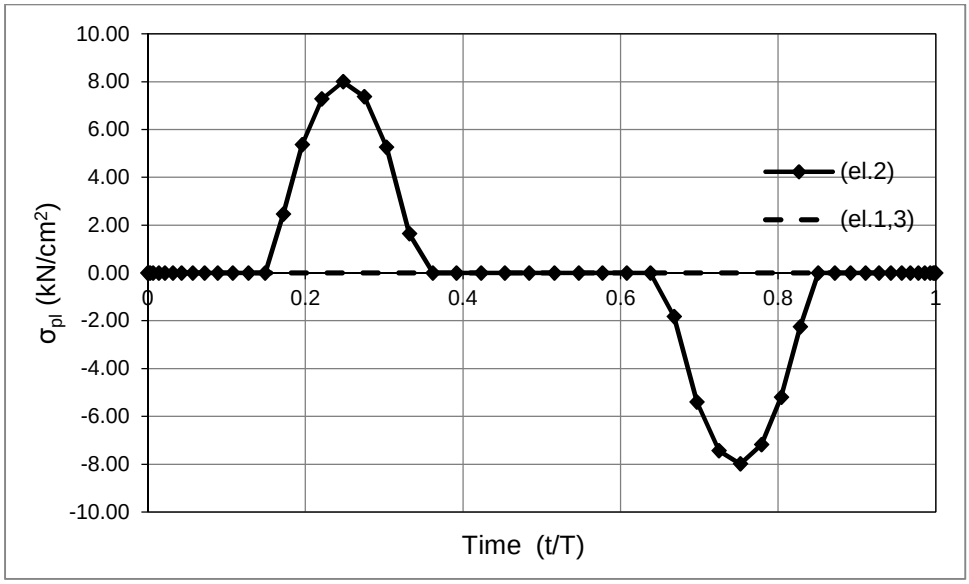

Figure 6.7 Predicted distributions $\sigma_{pl}^{cs}(t)$ at steady state inside a cycle for all three elements (load case b – alternating plasticity)

c) The last cyclic loading case assumes that both horizontal and vertical cyclic loads are applied, having the variation (Fig.6.8):

$$V(t) = 400\sin^2(\pi t \,/\, T), \quad H(t) = 220\sin(2\pi t \,/\, T)$$

The distribution of the predicted, by the RSDM, steady state residual stress inside a cycle for the middle bar may be seen in Fig.6.9.

The values of the parameters $a_i, i = 1,2,3$, for all the three bars, turn out to be different to zero. It's pointed out that this loading case leads the structure to ratcheting, since the non-simultaneous plasticization of all the bars inside the cycle (Fig.6.10) constitutes an incremental collapse mechanism.

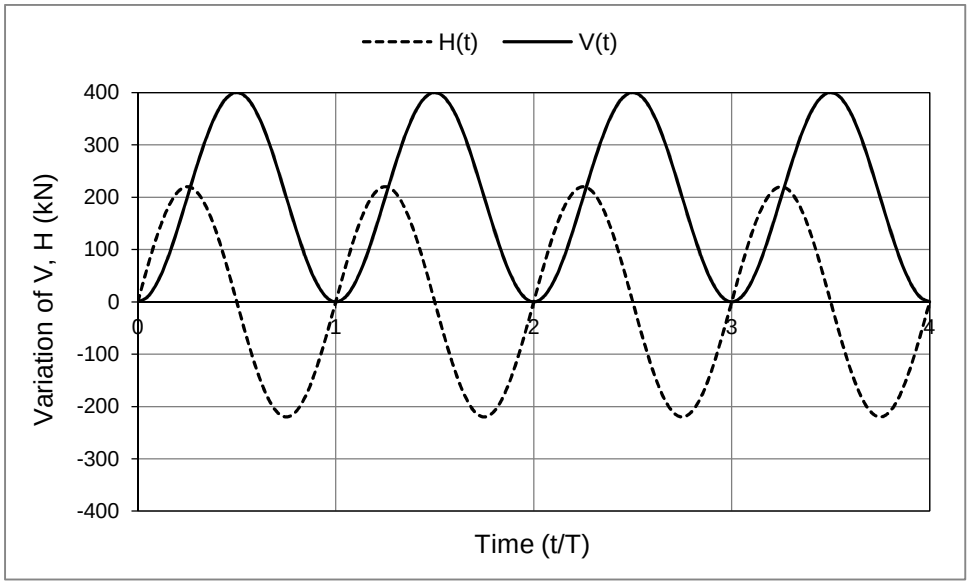

Figure 6.8 Load variation with time over four periods (load case c)

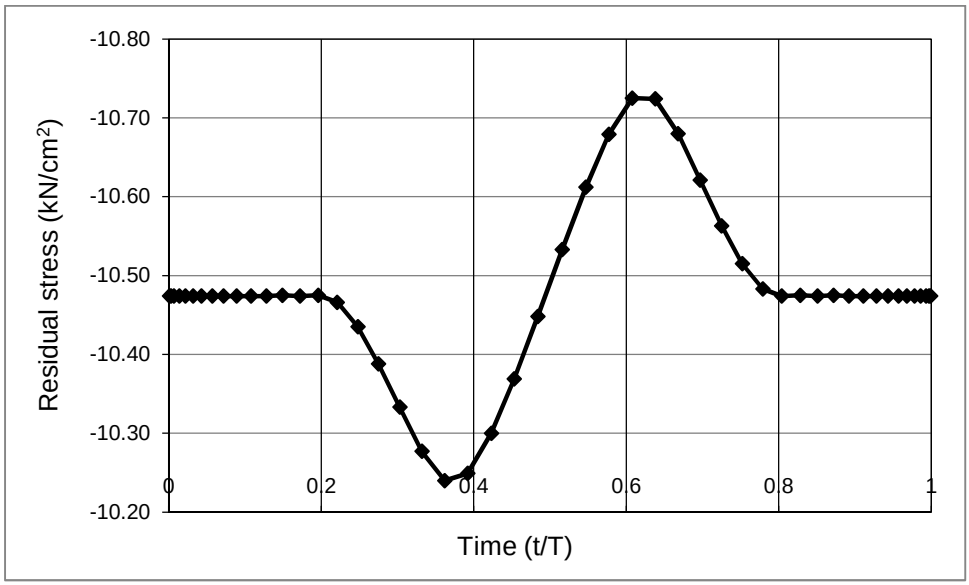

Figure 6.9 Predicted steady state residual stress distribution for bar 2 inside a cycle (load case c – ratcheting)

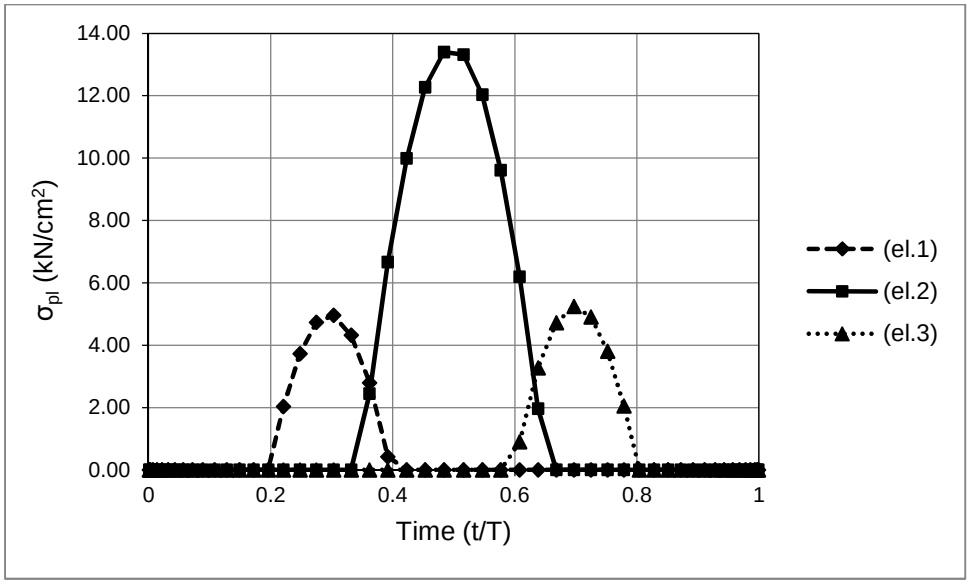

Figure 6.10 Predicted distributions $\sigma_{pl}^{cs}(t)$ at steady state inside a cycle for all three elements (load case c – ratcheting)

6.1.2. Square plate with a circular hole

The second example of application is a benchmark problem of a square plate having a circular hole in its center. The plate is subjected to two biaxial uniform loads $P_x(t)$, $P_y(t)$ applied in equal pairs along the edges of the plate (Fig.6.11). Due to the symmetry of the structure and the loading, only a quarter of the plate is considered (Spiliopoulos and Panagiotou, 2012).

The boundary conditions as well as its finite element mesh discretization are shown in Fig.6.11. The ratio between the diameter D of the hole and the length L of the plate is equal to 0.2. Also the ratio of the depth d of the plate to the length L is equal to 0.05. A case of $L = 20cm$ has been chosen herein. The finite element mesh used consists of ninety-eight, eight-noded, iso-parametric elements with 3x3 Gauss integration points. The plate has the material data of the Table 2.

Different loading cases were taken into account so as to examine different regions below and above the shakedown and ratcheting boundaries, as these have been estimated in (Chen and Ponter, 2001b). Results are plotted for the generally most highly stressed points, which depending on the load case, are either GP1 or GP2, the Gauss points closest to the cusp of the hole (Fig.6.11).

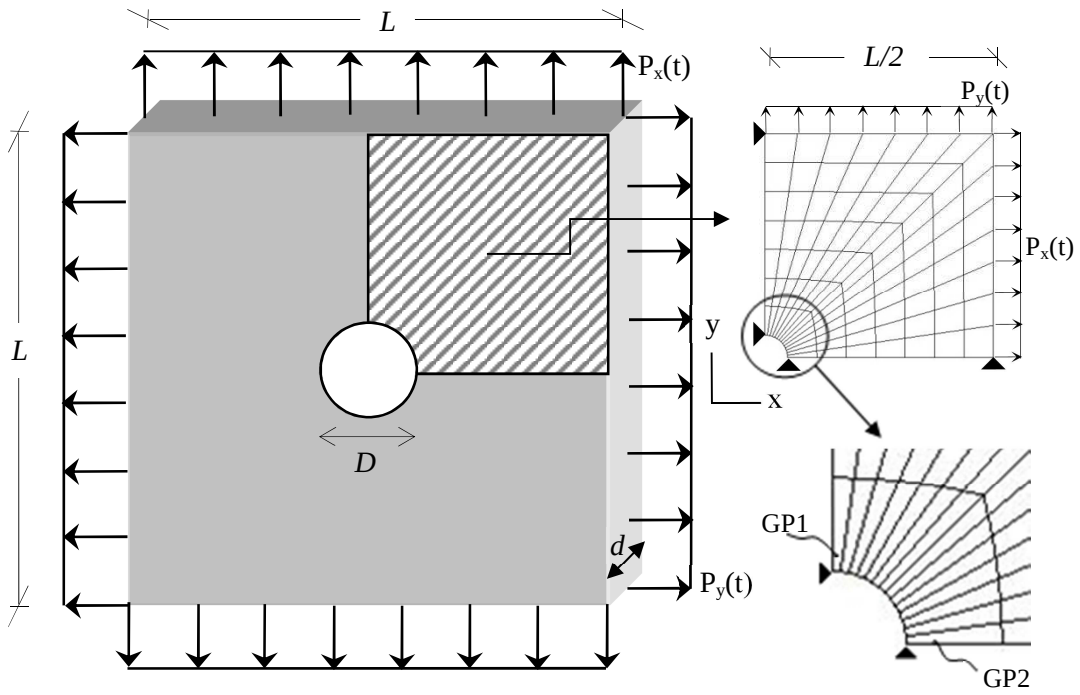

Figure 6.11 The geometry, loading and the finite element mesh of a quarter of a plate

Young's modulus	E=208GPa
Poisson's ratio	v= 0,3
Yield stress	σ_Y=360MPa

Table 2. Material properties of the square plate

(a) The first cyclic loading case has the following variation with time (Fig.6.12):

$$P_y(\tau) = 0.65\sigma_Y \sin^2(\pi\tau), \quad P_x(\tau) = 0$$

where $\tau = \frac{t}{T}$. In Fig.6.13 the computed by the RSDM steady-state residual stress distribution is plotted for the GP2.

The procedure predicts that the structure will shake down, and this complies with the fact that this loading is below the shakedown limit estimated in (Chen and Ponter, 2001b). The total stress distribution is the actual one as this may be confirmed in Fig.6.14, where the results of the time stepping program (Abaqus) coincide with the results of the RSDM.

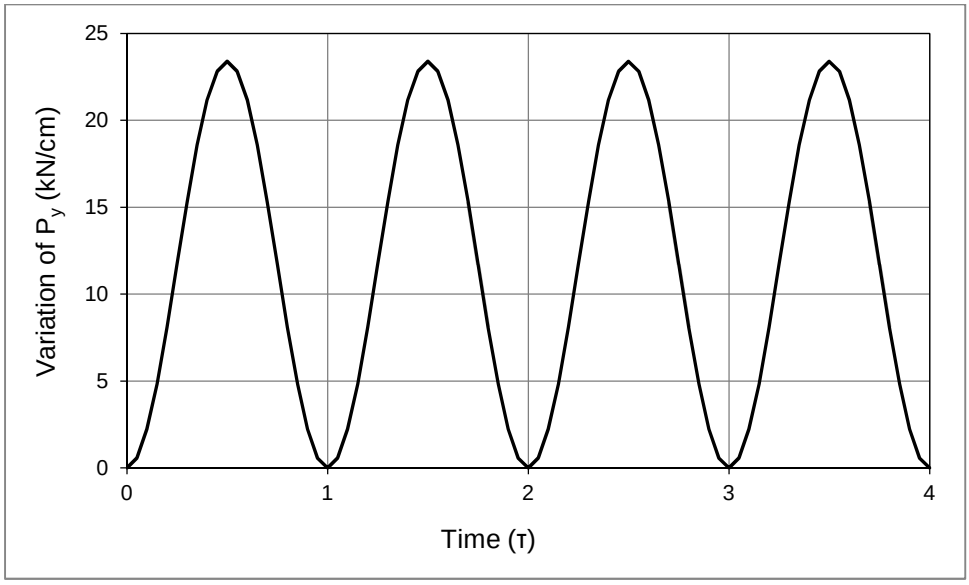

Figure 6.12 Load variation with time over four periods (load case b)

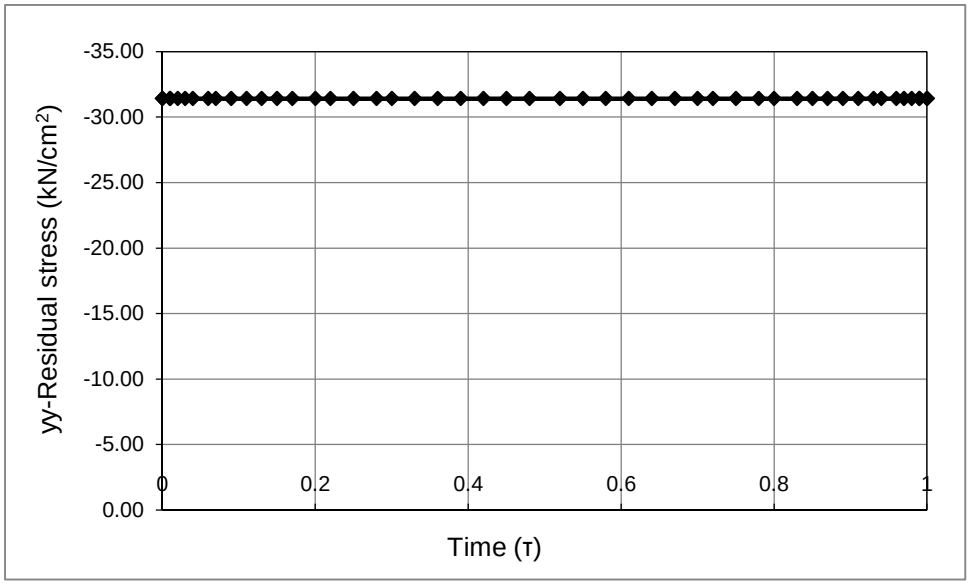

Figure 6.13 Residual stress distribution at GP2 inside a cycle at steady state (load case a – shakedown)

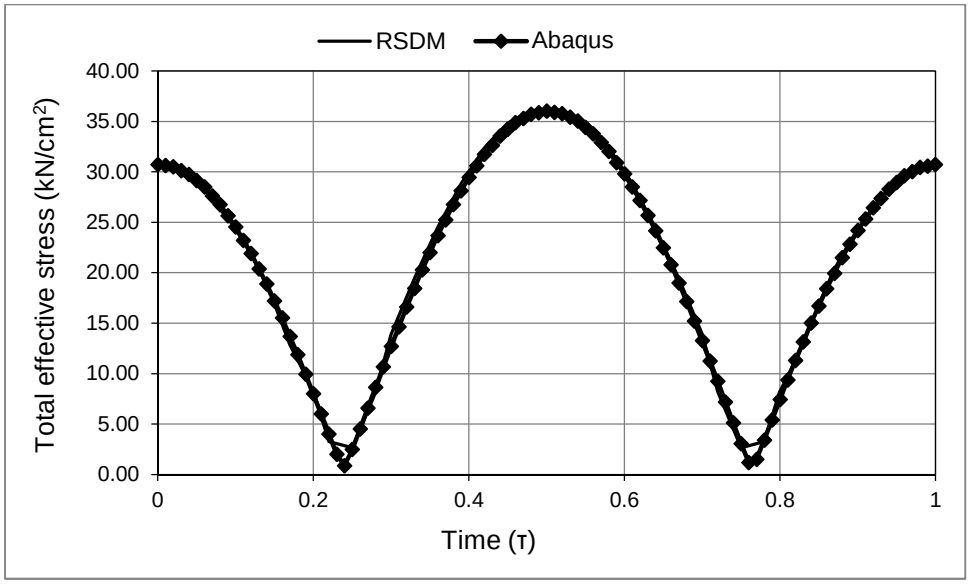

Figure 6.14 Effective total stress distribution at GP2 inside a cycle at steady state (load case a – shakedown)

(b) The second cyclic loading case has the following variation with time (Fig.6.15):

$$P_y(\tau) = 0.65\sigma_Y \sin(2\pi\tau), \quad P_x(\tau) = 0$$

According to (Chen and Ponter, 2001b) the maximum value of this loading, at many cycle points, proves to be well in excess of the shakedown-reverse plasticity boundary. The present numerical procedure (RSDM) also shows that this loading will lead some GPs to local reverse plasticity. The local reverse plasticity mechanism predicted by the RSDM is shown in Fig.6.16(a), which agrees with the time-stepping program (Abaqus) that also predicts such a mechanism (Fig.6.16(b)).

If we compare the values of the components of the excess vector $\boldsymbol{\sigma}_{pl}^{cs}$ at GP2, which is the most highly strained Gauss point of the structure, we conclude that the most plastically strained direction is yy. By plotting the variation of this component inside the cycle (Fig.6.17), one may see that plastic straining occurs, alternately, inside the time intervals $[0.06, 0.42]$ and $[0.58, 0.91]$ at the steady cycle. At the same time, the fluctuation around zero of the plastic strain along the yy direction for the first 50 cycles at this GP of the time stepping program (Abaqus), may be seen in Fig.6.18.

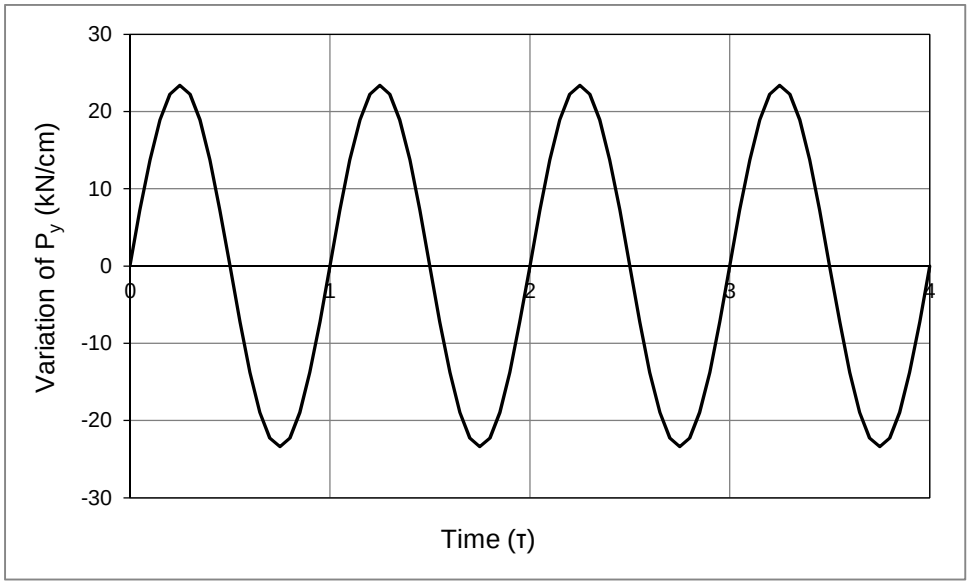

Figure 6.15 Load variation with time over four periods (load case b)

(a)

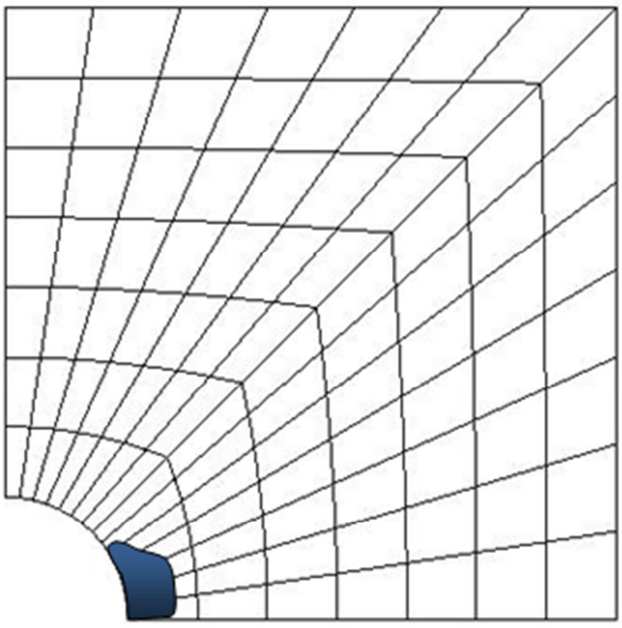

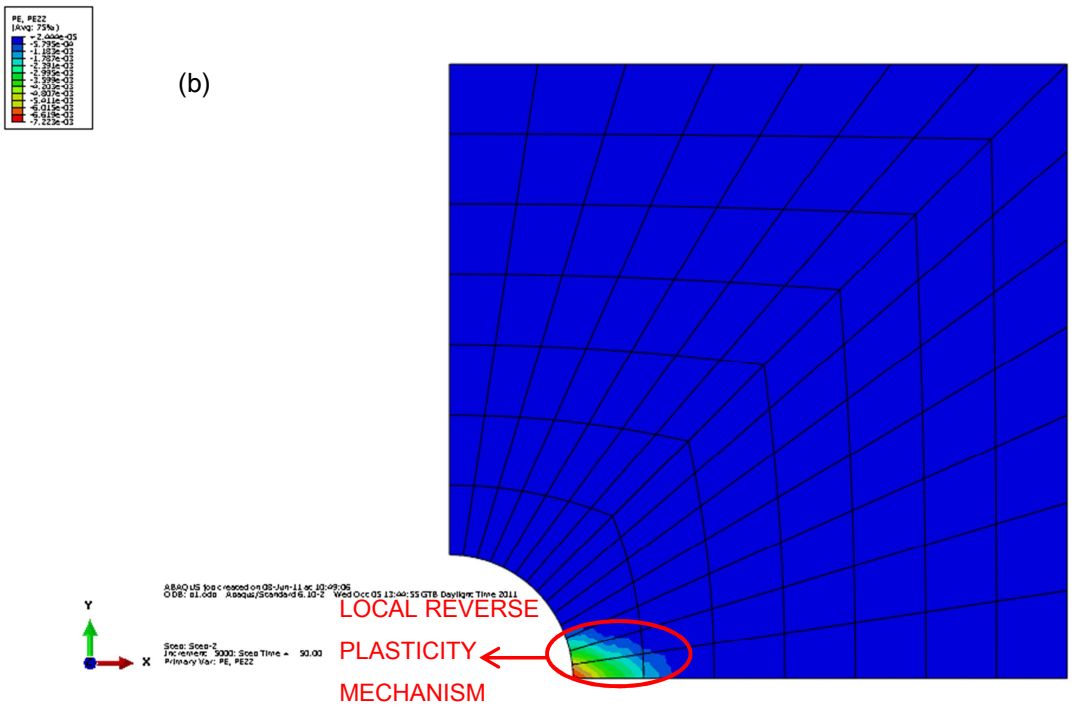

Figure 6.16 Local alternating plasticity mechanism for load case b. (a) RSDM and (b) Abaqus

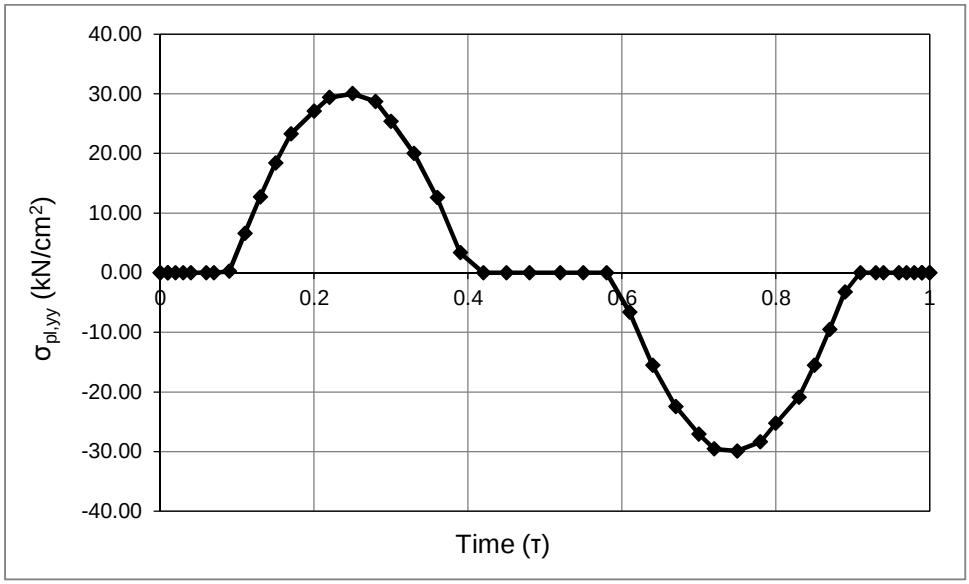

Figure 6.17 Predicted cyclic steady state distribution of the yy component of the stress vector $\boldsymbol{\sigma}_{pl}^{cs}(t)$ at GP2 (load case b – alternating plasticity)

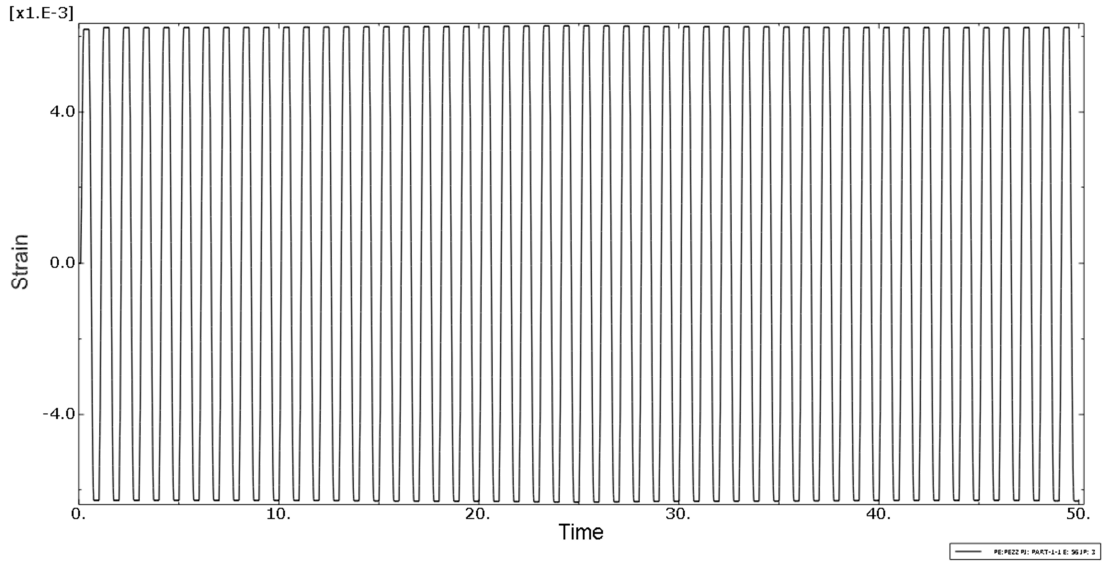

Figure 6.18 Abaqus yy-plastic strain variation over the first 50 cycles at the GP2 (load case b – alternating plasticity)

(c) The third cyclic loading case involves two loads, one constant in time and one varying with time (Fig.6.19):

$$P_x(\tau) = 0.6\sigma_Y = const$$

$$P_y(\tau) = 0.8\sigma_Y \sin^2(\pi\tau)$$

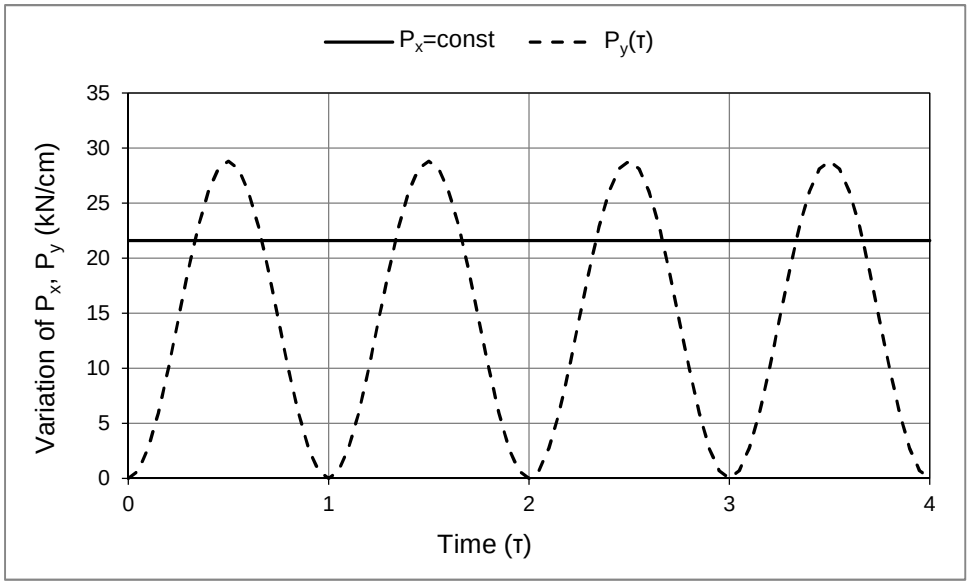

Figure 6.19 Load variation with time over four periods (load case c)

This load combination leads some GPs near the edge of the hole in a reverse plasticity state (Fig.6.20(a)), which is in agreement with (Chen and Ponter, 2001b). A very good match of this mechanism is observed with the one found by Abaqus (see also Fig.6.20(b)). As previously, the most strained GP is GP2, along the direction yy. In Fig.6.21 the variation of this component of $\boldsymbol{\sigma}_{pl}^{cs}$ is plotted. It may be observed that plastic straining of alternating nature occurs inside the time ranges $\left[0, 0.09\right]$, $\left[0.39, 0.61\right]$ and $\left[0.91, 1\right]$ at the steady cycle. One may now compare the results of a time-stepping program (Abaqus) (Fig.6.22). Looking at the plotting of the plastic strains over the first 100 cycles, one may see that for this loading we have alternating plastic strains around a non-zero value. The pattern of this straining does not seem to change as we approach 1000 cycles, although the mean value drops, thus making it difficult to decide whether the cumbersome time-stepping program has reached a steady state solution.

(a)

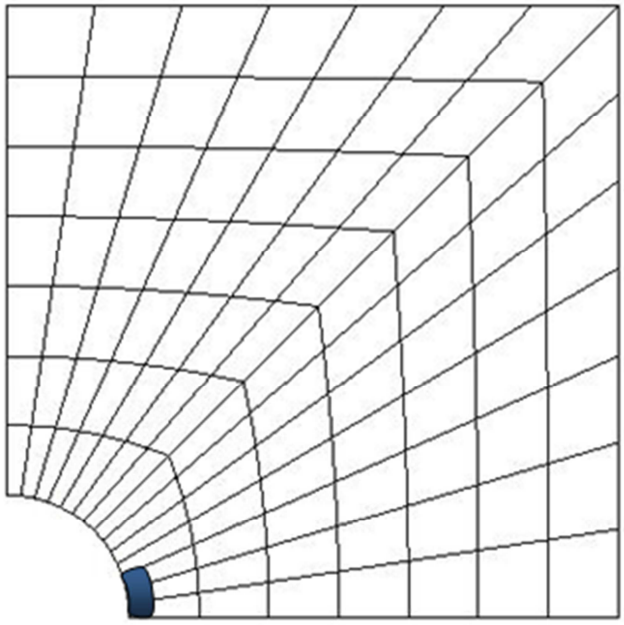

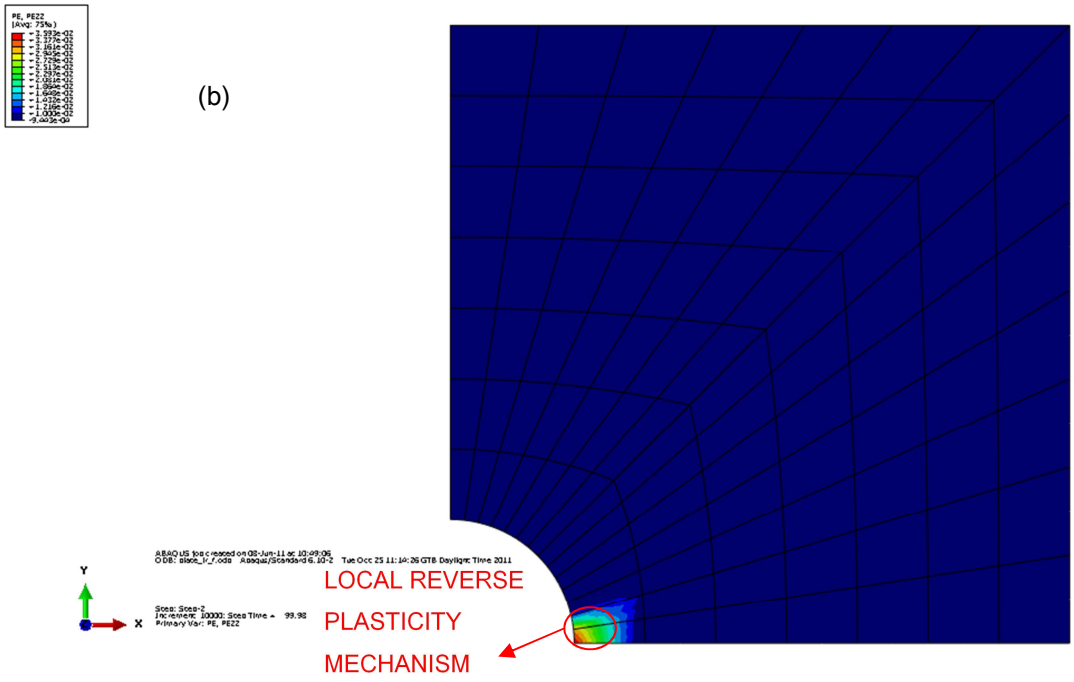

Figure 6.20 Local alternating plasticity mechanism for load case c. (a) RSDM (b) Abaqus

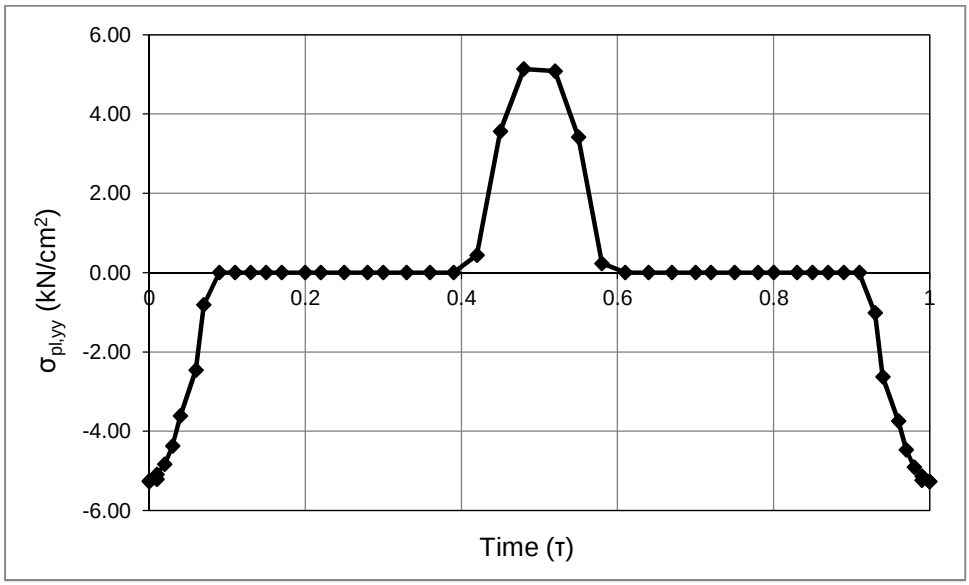

Figure 6.21 Predicted cyclic steady state distribution of the yy component of the stress vector $\boldsymbol{\sigma}_{pl}^{cs}(t)$ at GP2 (load case c – alternating plasticity)

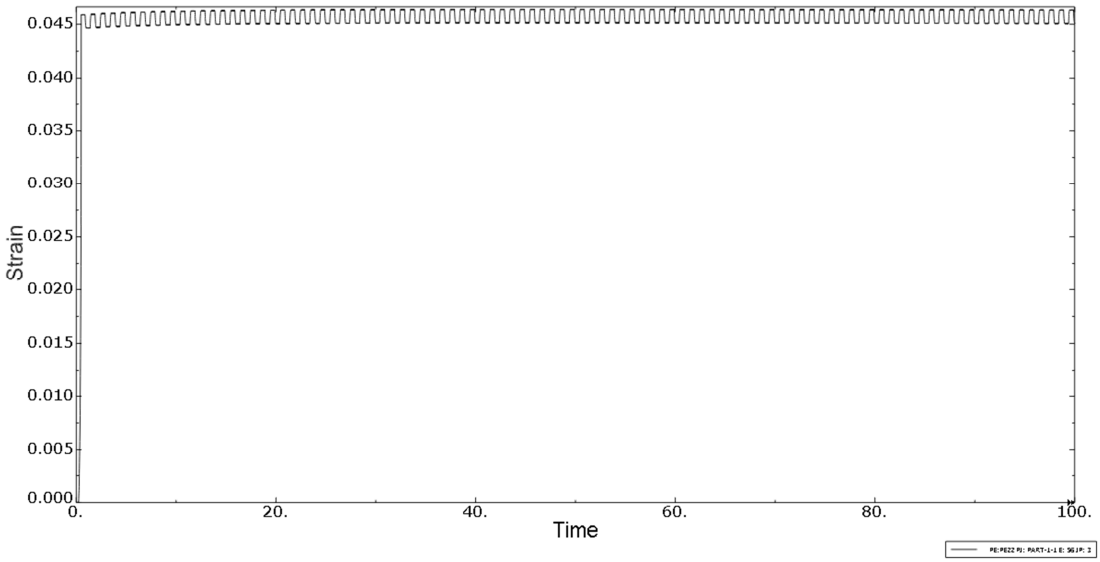

Figure 6.22 Abaqus yy-plastic strain variation at the GP2 over the first 100 cycles (load case c – alternating plasticity)

(d) The last cyclic loading case also involves two loads, one constant in time and one varying with time (Fig.6.23):

$$P_x(\tau) = 0.85\sigma_Y = const$$

$$P_y(\tau) = 0.5\sigma_Y \sin^2(\pi\tau)$$

As stated in (Chen and Ponter, 2001b), this loading is above the ratchet limit.

The most strained GP is GP1, along the xx direction. In Fig.6.24 the predicted cyclic state distributions of the xx component of the vector $\boldsymbol{\sigma}_{pl}^{cs}$ at GP1 is plotted. It may be observed that plastic straining is of the same positive sign inside the cycle intervals $[0, 0.22]$ and $[0.78, 1]$. This ratcheting behavior holds for quite a few GPs around the structure, with the higher straining (the GPs with the parameters a_i's having the bigger values, see eqn.5.27 of section 5.1.4) within the marked region in Fig.6.25(a), which definitely constitutes an incremental collapse mechanism. This mechanism is also validated by the time-stepping program (Abaqus) which diverges after the 47th cycle. At this point the most highly strained region of Abaqus matches closely the one predicted by the RSDM (see Fig.6.25(b)). The convergence of the RSDM for this last load case may be seen in Fig.6.26. The uniform convergence of

the RSDM is typical for all the loading cases that were tested before, with the present one requiring the biggest number of iterations.

The number of time points inside the cycle should be enough in order to represent the applied loading precisely. On the other hand, for an alternating plasticity case, it may be useful to increase the time points so that the values of the parameters a_i's (see section 5.1.4, eqn.5.27) approach zero within a small tolerance.

For all the examples considered above, fifty time points inside the cycle were used. For the cases of alternating plasticity, the use of two-hundred points decreased the values of the parameters a_i's by an order of magnitude.

The RSDM proved to be quite stable, no matter which asymptotic behavior was reached. Three terms of the Fourier series were found enough to represent the residual stress distribution. Computational efficiency, apart from the small number of the Fourier coefficients, is further enhanced due to the fact that the stiffness matrix needs to be decomposed only once in the beginning of the procedure. Thus, reviewing the examples considered herein, within the adopted tolerance, the number of the iterations ranged from a minimum of 20 for the case of ratcheting of the truss example, to a maximum of 570 for the case of ratcheting of the plate example. The amount of CPU-time required to solve this last case was just 136 s, for an Intel Core i7 at 2.93 Ghz with 4096 MB RAM.

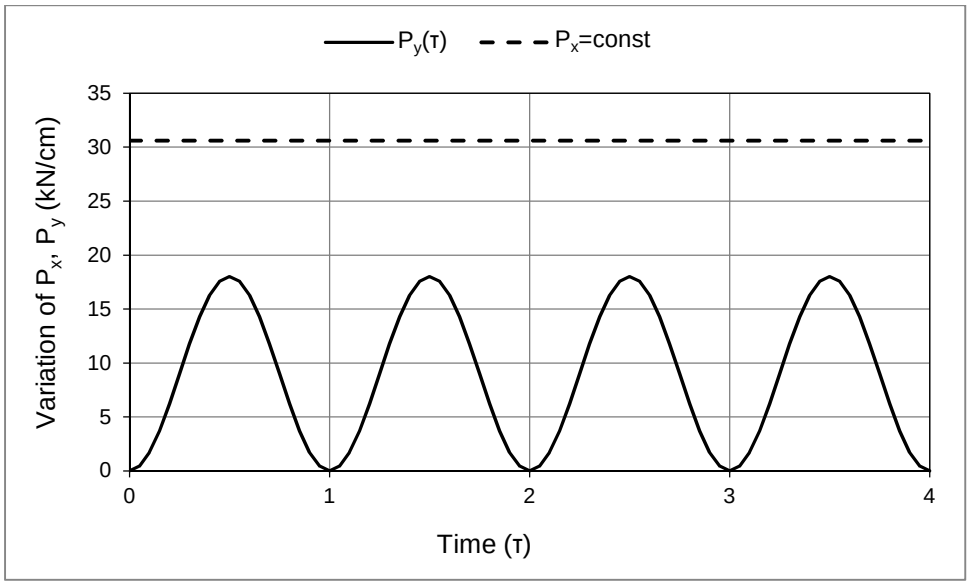

Figure 6.23 Load variation with time over four periods (load case d)

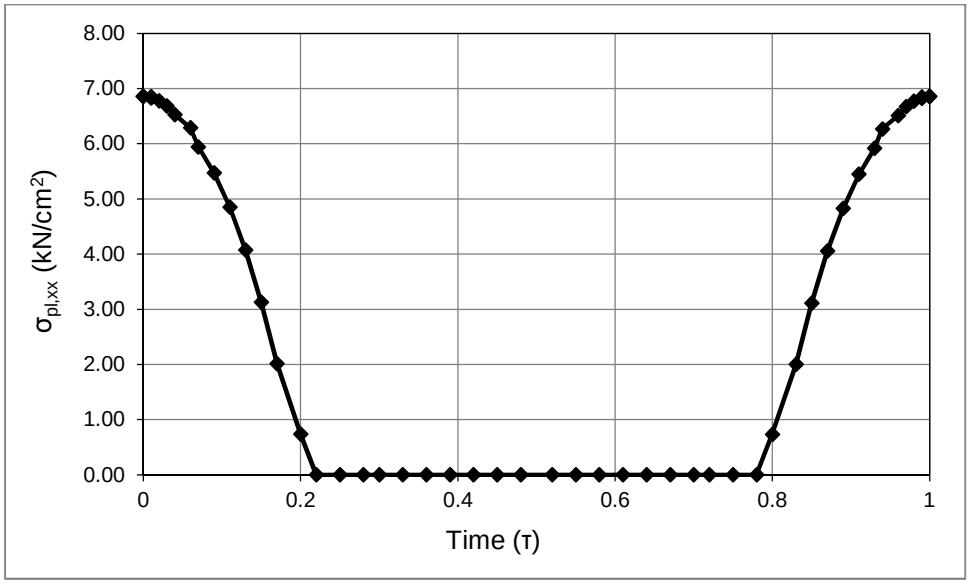

Figure 6.24 Predicted cyclic steady state distribution of the xx component of the stress vector $\boldsymbol{\sigma}_{pl}^{cs}(t)$ at GP2 (load case d – ratcheting)

(a)

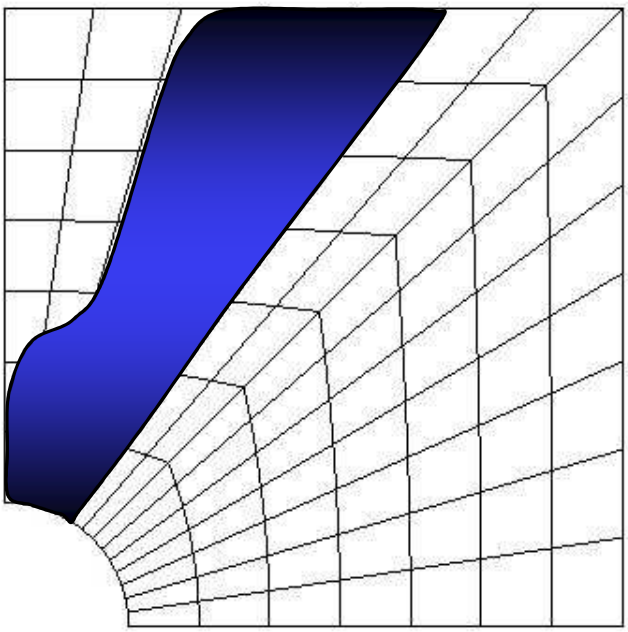

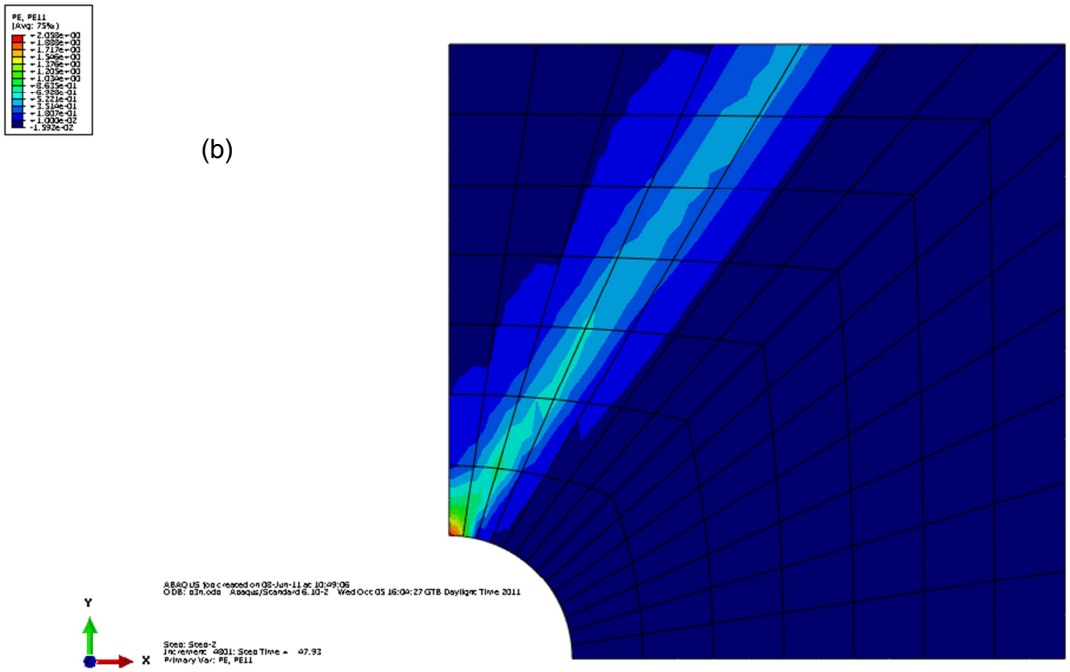

Figure 6.25 Ratcheting mechanism for load case d. (a) RSDM (b) Abaqus

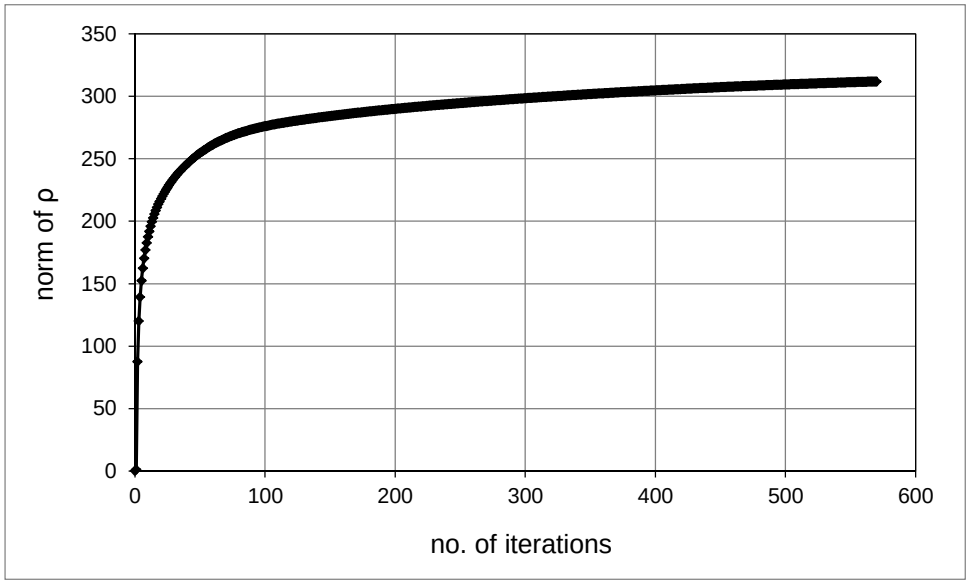

Figure 6.26 Convergence of the iterative procedure RSDM (load case d)

6.2. Shakedown analysis using RSDM-S

In this section the proposed procedure RSDM-S of Section 5.2, for the shakedown analysis of structures, is validated by analyzing a variety of examples which are available in the literature. The developed procedure RSDM-S is applied to different examples of increasing complexity with respect to its finite element modeling. Furthermore, the RSDM-S is applied to the shakedown analysis of structures under mechanical and thermal loadings.

6.2.1. Cylindrical tube under internal pressure

A simple example of a thick hollow cylinder is examined first (Fig.6.27). The cylinder is subjected to a single load, i.e. internal pressure. Plane strain conditions are assumed. Since both structure and loading are axisymmetric, ten axisymmetric finite elements were used to discretize a vertical section (a-a) of the cylinder. Eight-noded iso-parametric elements with 2x2 Gauss integrations point were used. The cylinder is assumed homogeneous, isotropic, elastic-perfectly plastic with the material data of Table 3.

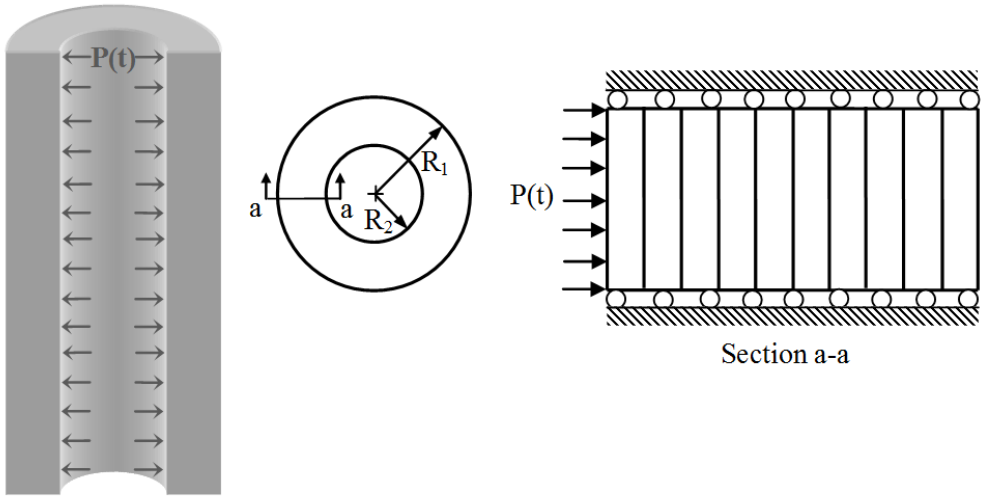

Figure 6.27 Geometry and finite element discretization of the cylinder

Description of the loading

The pressure P is assumed to vary between a minimum value of zero and a maximum value i.e. the load vary in the domain $P \in \left[0, P^*\right]$ where $P^* = 1$. A prescribed cyclic loading in the time domain, that passes through these two limits inside the cycle, may be established by using the following equation:

$$P(\tau) = P^* \alpha(\tau)$$

where the time function $\alpha(\tau)$ is a smooth fourth order polynomial (Fig.6.28):

$$\alpha(\tau) = 3,3334\tau^4 - 6,6667\tau^3 + 0,1667\tau^2 + 3,1667\tau, \quad \tau \in [0,1].$$

Different ratios of R_2 / R_1 were taken into account. In order to validate our results the predicted, by the procedure, shakedown pressures, were compared against analytical solutions (Lubliner, 1990). It may be seen that results agree quite well (Fig.6.29) (Spiliopoulos and Panagiotou, 2014(a)).

The initial value of $\omega = 1$ was sufficient for convergence.

A typical convergence of the procedure, for the ratio of $R_2 / R_1 = 0.5$ may be seen in Fig.6.30.

Young's modulus	E=210GPa
Poisson's ratio	v= 0,3
Yield stress	σ_Y=360MPa

Table 3. Material properties of the cylinder

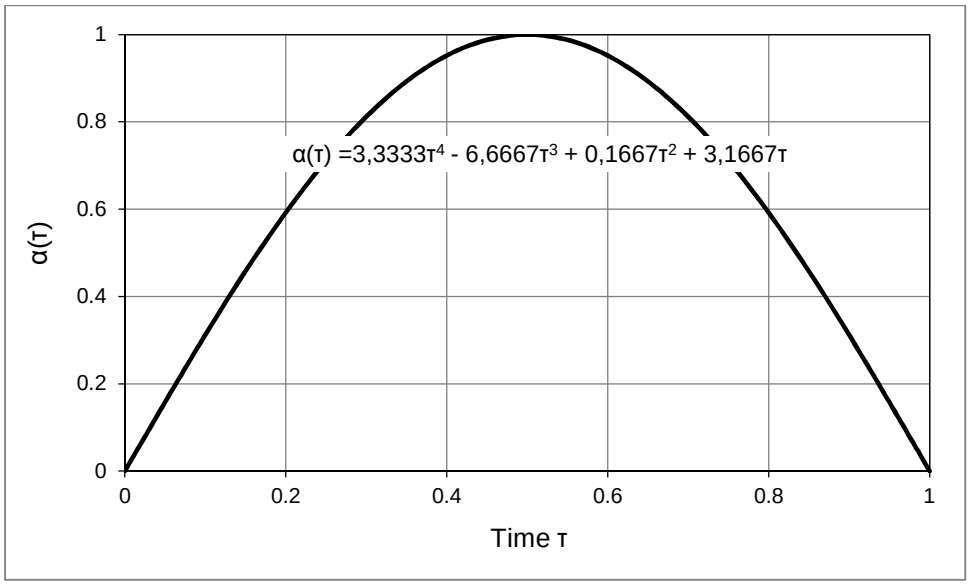

Figure 6.28 Time function variation over one period

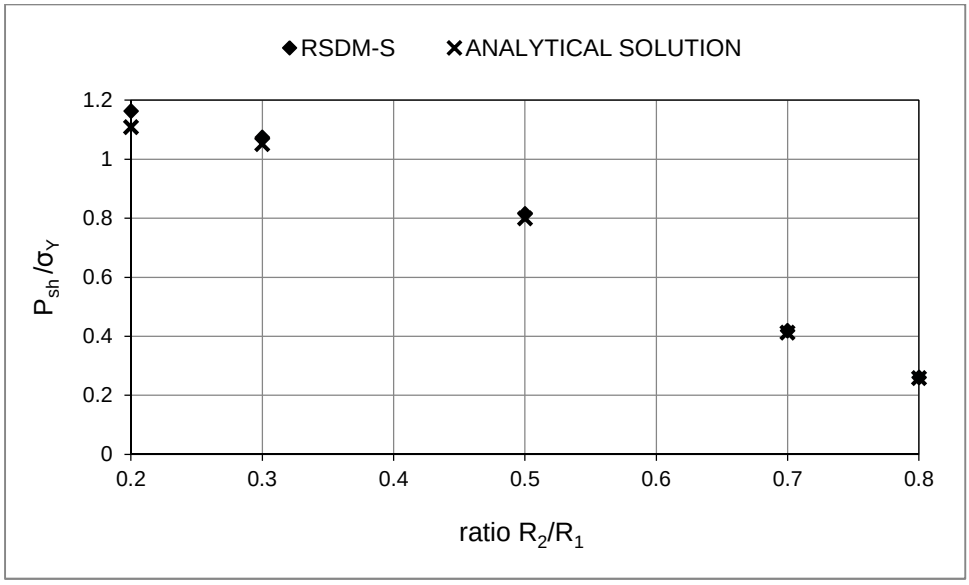

Figure 6.29 Shakedown pressures for different ratios of R_2/R_1 using the RSDM-S and its comparison with the analytical solution (Lubliner, 1990).

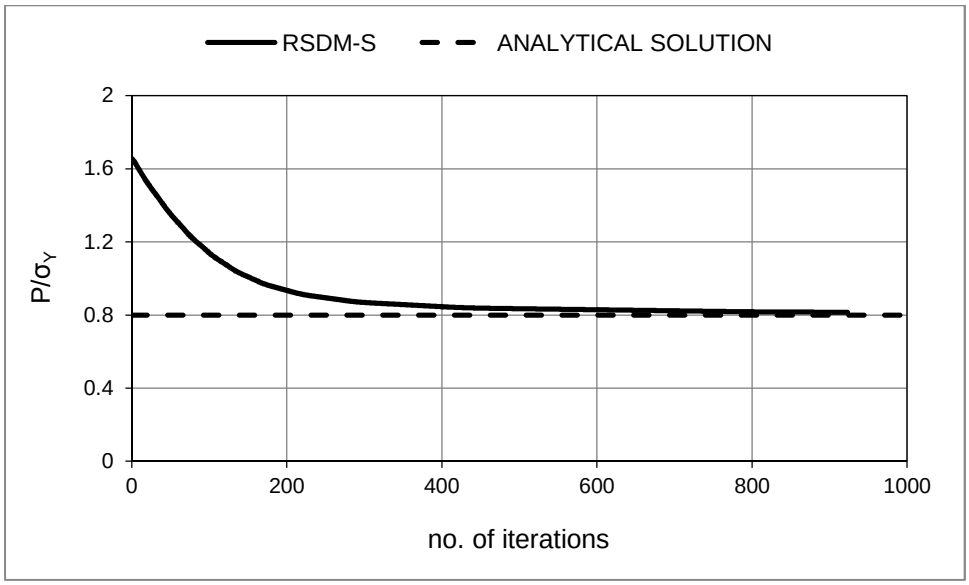

Figure 6.30 Convergence of the RSDM-S for the ratio R_2/R_1=0.5

6.2.2. Square plate with a circular hole

The second example of application is a square plate having a circular hole in its middle (Fig.6.31). This problem is frequently used as a benchmark in the shakedown analysis of structures. After Belytschko (1972) the case of the plate has been analyzed by various authors using different methods: Corradi and Zavelani (1974);

Gross-Weege (1997); Carvelli *et al*. (1999); Ponter and Engelhardt (2000); Chen and Ponter (2001a); Zhang and Raad (2002); Zouain *et al*. (2002); Garcea *et al*. (2005); Tran *et al*. (2010); and Simon and Weichert (2011) among others.

The plate is assumed homogeneous, isotropic, elastic-perfectly plastic with the material data of Table 2 (section 6.1.2). Concerning the geometrical characteristics of the plate, the ratio between the diameter D of the hole and the length L of the plate is equal to 0.2 and the ratio of the thickness d of the plate to its length is equal to 0.05. Specially, a case of $L = 20cm$ has been chosen herein.

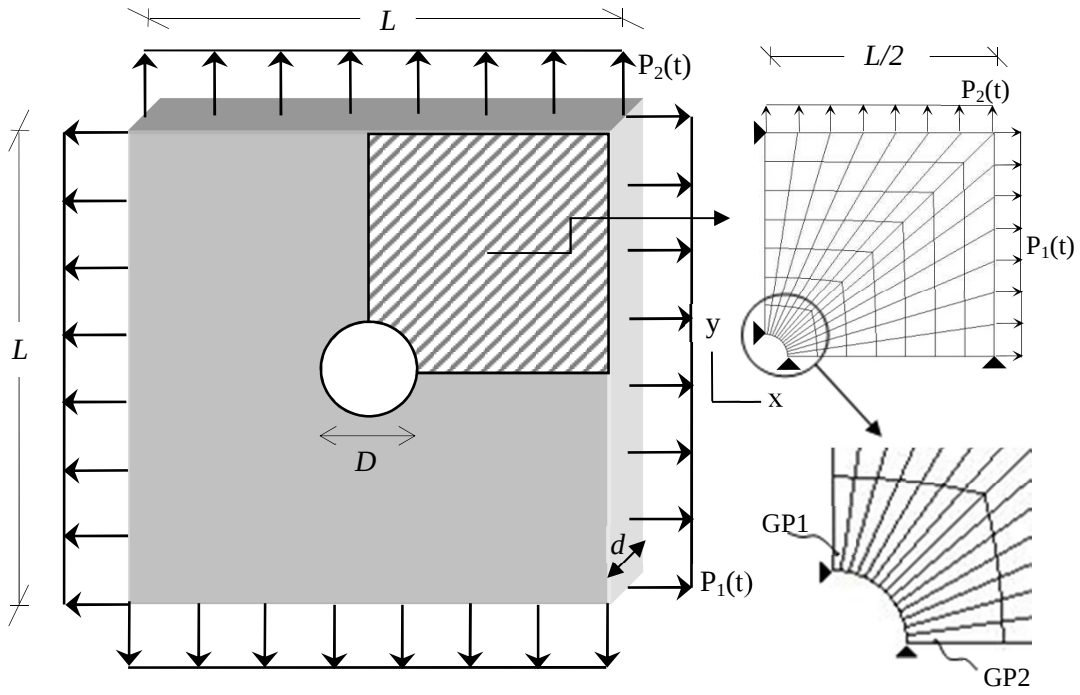

Figure 6.31 The geometry of the holed plate subjected to biaxial loading and its finite element mesh

The plate is subjected to two uniformly distributed loads (Fig.6.31), applied symmetrically at the edges of the plate. Due to the symmetry of the structure and the loading, only one quarter of the plate is analyzed. The finite element mesh discretization of the plate is also shown in Fig.6.31. Ninety-eight, eight-noded, iso-parametric elements with 3x3 Gauss integration points were used.

Both the cases of proportional and independent loading variations are examined. The resulting shakedown loads $P_{1,sh} = \gamma_{sh} P_1^*, P_{2,sh} = \gamma_{sh} P_2^*$ and the shakedown domain for each case are reported in the relevant figures (Spiliopoulos and Panagiotou, 2014(a)).

1. P_1 and P_2 vary proportionally

The proportional variation of the cyclic loading in the load domain may be described by the path $(0 \rightarrow (P_1^*, P_2^*) \rightarrow 0)$ (Fig.6.32).

A prescribed loading in the time domain may be defined with the use of (see Fig.6.32):

$$P(\tau) = \begin{Bmatrix} P_1^* \alpha(\tau) \\ P_2^* \alpha(\tau) \end{Bmatrix}$$

where $\alpha(\tau) = 3,3334\tau^4 - 6,6667\tau^3 + 0,1667\tau^2 + 3,1667\tau$.

The calculated shakedown domain for different ratios of (P_1^* / P_2^*) is presented in Fig.6.33. A good agreement with the literature results (Ponter and Engelhardt, 2000) may be seen. In Fig.6.34 one may see the convergence of the proposed procedure RSDM-S towards the value of the shakedown load for the case of $(P_1^* / P_2^*) = (1 / 0.5)$.

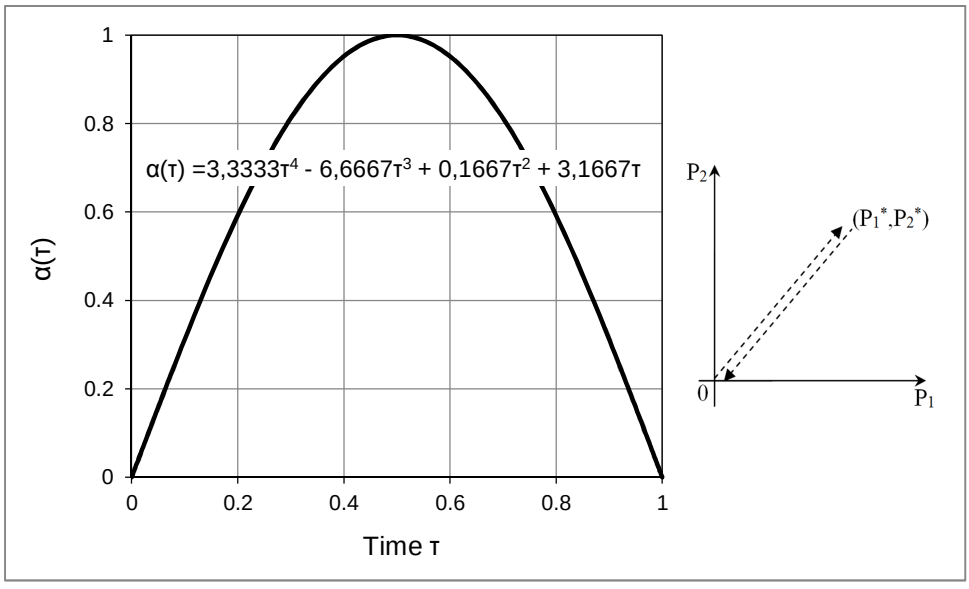

Figure 6.32 Time function variation over one period (proportional loading case)

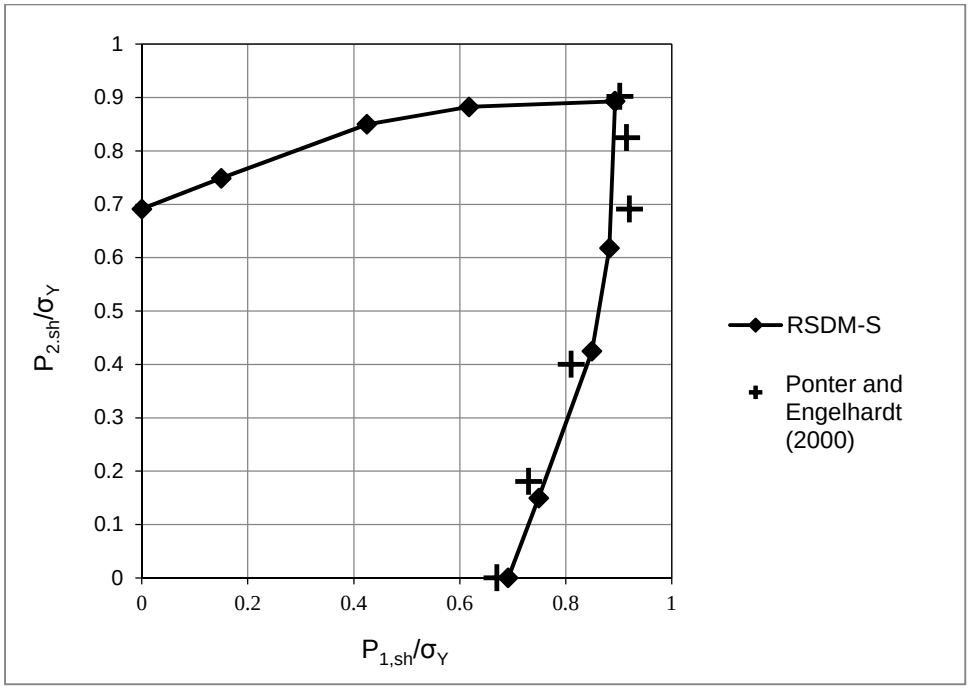

Figure 6.33 Shakedown domain produced by RSDM-S for the proportional loading case

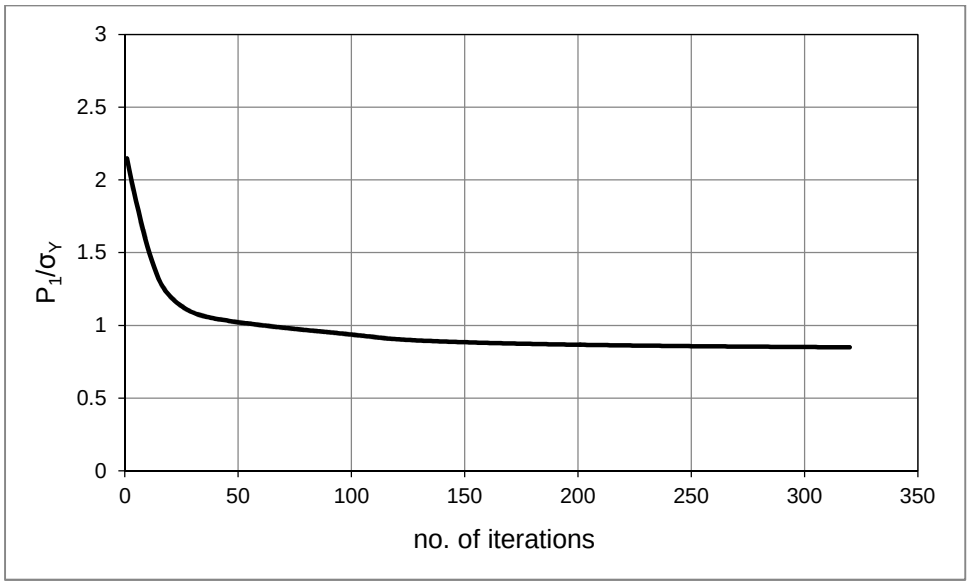

Figure 6.34 Convergence of the RSDM-S for proportional loading ($(P_1^*/P_2^*)=(1/0.5)$)

2. P_1 and P_2 vary independently

The RSDM-S is used to calculate the shakedown factor of the following three different loading domains:

i) The first domain under consideration is the triangular loading domain of Fig.6.35 that is described by the path $(0 \rightarrow (P_1^*,0) \rightarrow (P_1^*,P_2^*) \rightarrow 0)$. A

prescribed loading in time domain, that passes through the three vertices of the triangle, may be established by using the following equation (Fig.6.35):

$$P(\tau) = \begin{Bmatrix} P_1^* \alpha_1(\tau) \\ P_2^* \alpha_2(\tau) \end{Bmatrix}$$

where the time functions $\alpha_1(\tau), \alpha_2(\tau)$ are:

$$\alpha_1(\tau) = -9\tau^2 + 6\tau, \quad \alpha_2(\tau) = 0 \ , \ \tau \in [0, 1/3]$$
$$\alpha_1(\tau) = 1, \ \alpha_2(\tau) = -9\tau^2 + 12\tau - 3 \ , \ \tau \in (1/3, 2/3]$$
$$\alpha_1(\tau) = -9\tau^2 + 12\tau - 3, \quad \alpha_2(\tau) = -9\tau^2 + 12\tau - 3 \ , \ \tau \in (2/3, 1]$$

The proposed procedure predicts, for $P_1^* = P_2^*$ a shakedown load equal to $0.673\sigma_Y$, quite close to the result $0.667\sigma_Y$ reported in (Chen and Ponter, 2001a), using a different approach (LMM) as well as a different FE mesh.

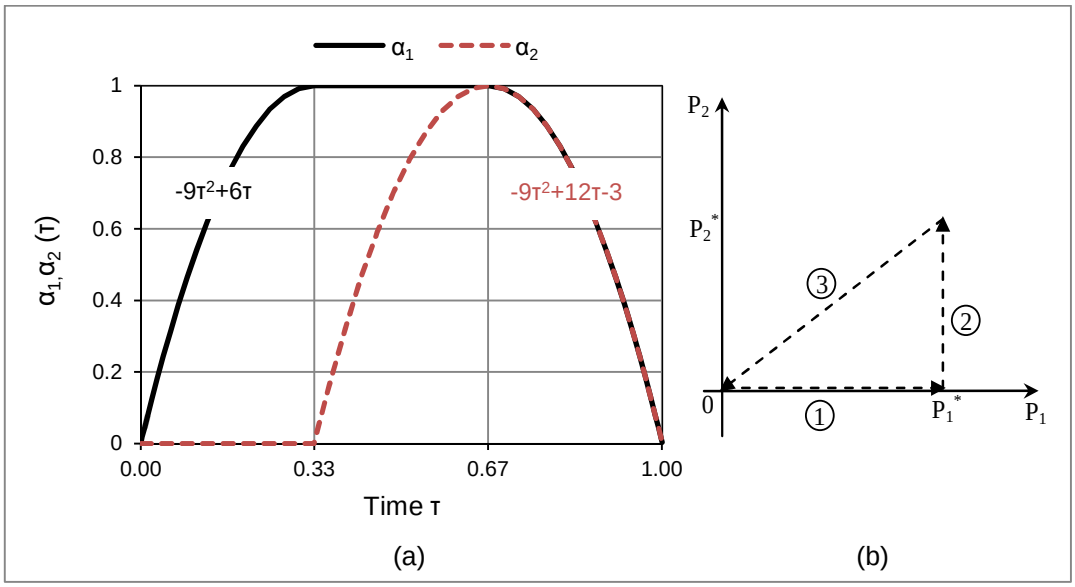

Figure 6.35 Independent cyclic loading variation over one time period in (a) time domain, (b) load domain

ii) Another type of triangular loading domain is studied next, having the path $(0 \rightarrow (P_1^*, 0) \rightarrow (0, P_2^*) \rightarrow 0)$ (see Fig.6.36). An analogous definition of the time functions for the triangular loading domain may be used:

$$\alpha_1(\tau) = -9\tau^2 + 6\tau, \quad \alpha_2(\tau) = 0 \ , \ \tau \in [0, 1/3]$$
$$\alpha_1(\tau) = -9\tau^2 + 6\tau, \ \alpha_2(\tau) = -9\tau^2 + 12\tau - 3 \ , \ \tau \in (1/3, 2/3]$$
$$\alpha_1(\tau) = 0 \ \ \alpha_2(\tau) = -9\tau^2 + 12\tau - 3 \ , \ \tau \in (2/3, 1]$$

This domain has been studied in (Ponter and Engelhardt, 2000) and the results of the RSDM-S are compared in Fig.6.38. The small discrepancy is attributed to the difference in the elastic solution, due to the different types of elements and orientation of the FE meshes. Thus, in (Ponter and Engelhardt, 2000) the limit of the elastic domain, for a single load, is $0.32\sigma_Y$, whereas with the FE mesh used here, it is $0.35\sigma_Y$.

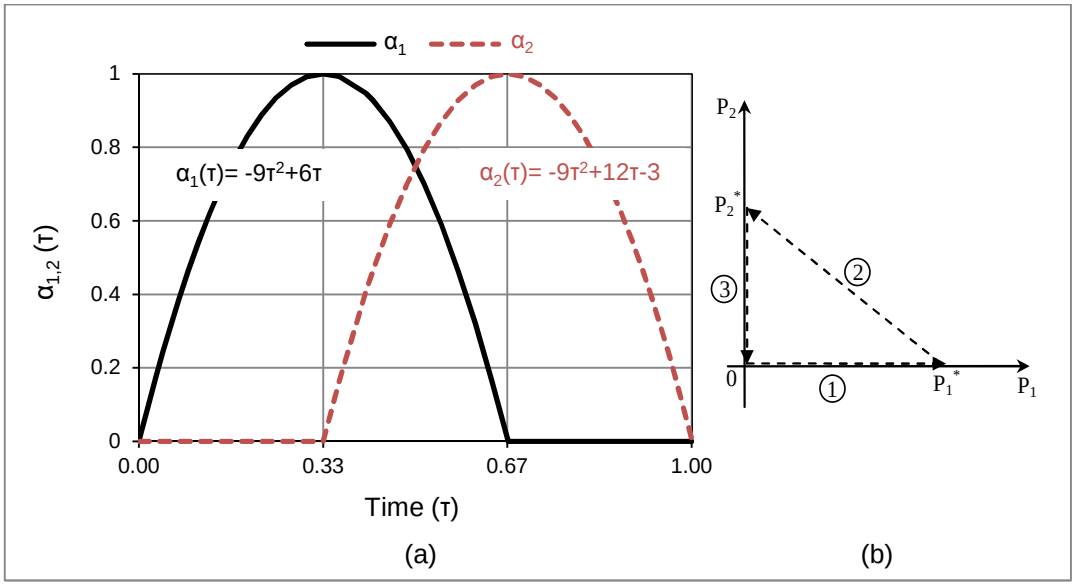

Figure 6.36 Independent cyclic loading variation over one time period in (a) time domain, (b) load domain

iii) The next loading domain under consideration is the more common rectangular loading domain (Fig.6.37(b)) in shakedown analysis. This particular case will be studied extensively. The shakedown loads of this loading case, coincides with the ones of the previous case. This loading domain may be expressed as: $(0 \rightarrow (P_1^*, 0) \rightarrow (P_1^*, P_2^*) \rightarrow (0, P_2^*) \rightarrow 0)$. The following time functions $\alpha_1(\tau), \alpha_2(\tau)$, shown in Fig.6.37(a), were used to establish a prescribed cyclic loading that passes through the four vertices of this domain:

$$\alpha_1(\tau) = -16\tau^2 + 8\tau, \quad \alpha_2(\tau) = 0 \quad , \quad \tau \in [0, 1/4]$$
$$\alpha_1(\tau) = 1, \quad \alpha_2(\tau) = -16\tau^2 + 16\tau - 3 \quad , \quad \tau \in (1/4, 1/2]$$
$$\alpha_1(\tau) = -16\tau^2 + 16\tau - 3, \quad \alpha_2(\tau) = 1 \quad , \quad \tau \in (1/2, 3/4]$$
$$\alpha_1(\tau) = 0, \quad \alpha_2(\tau) = -16\tau^2 + 24\tau - 8 \quad , \quad \tau \in (3/4, 1]$$

With the use of those equations the RSDM-S predicts the shakedown limit for various ratios of the applied loads i.e. P_1^* / P_2^*. In Fig.6.38 one may observe the coincidence of the results with the ones reported in (Carveli *et al.*, 1999), which were produced by using an algorithm based on the theory of mathematical programming. A similar FE mesh and element orientation is used both in (Carveli *et al.*, 1999) and herein.

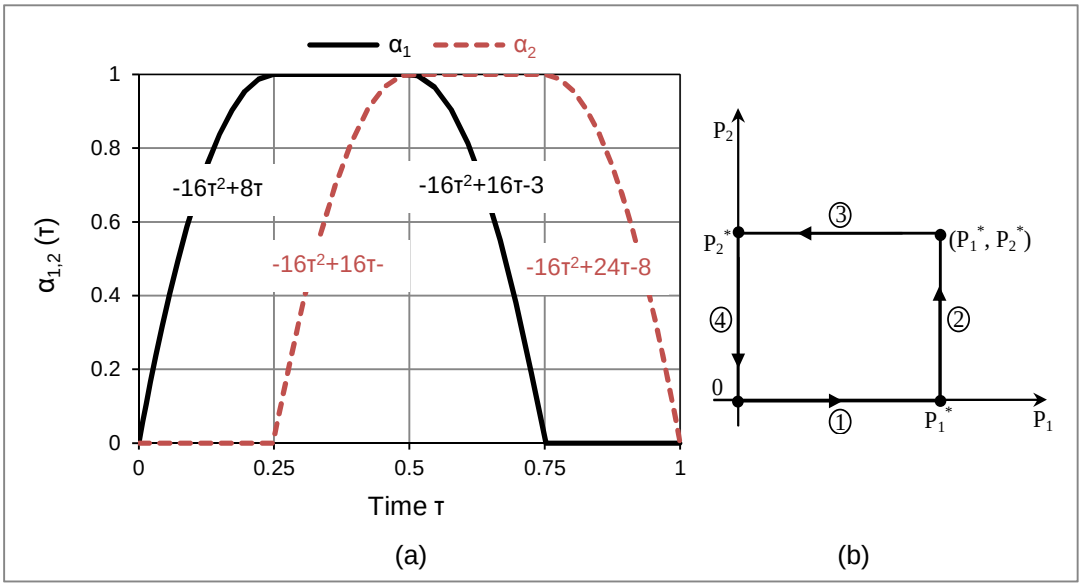

Figure 6.37 Independent cyclic loading variation over one time period in (a) time domain, (b) load domain

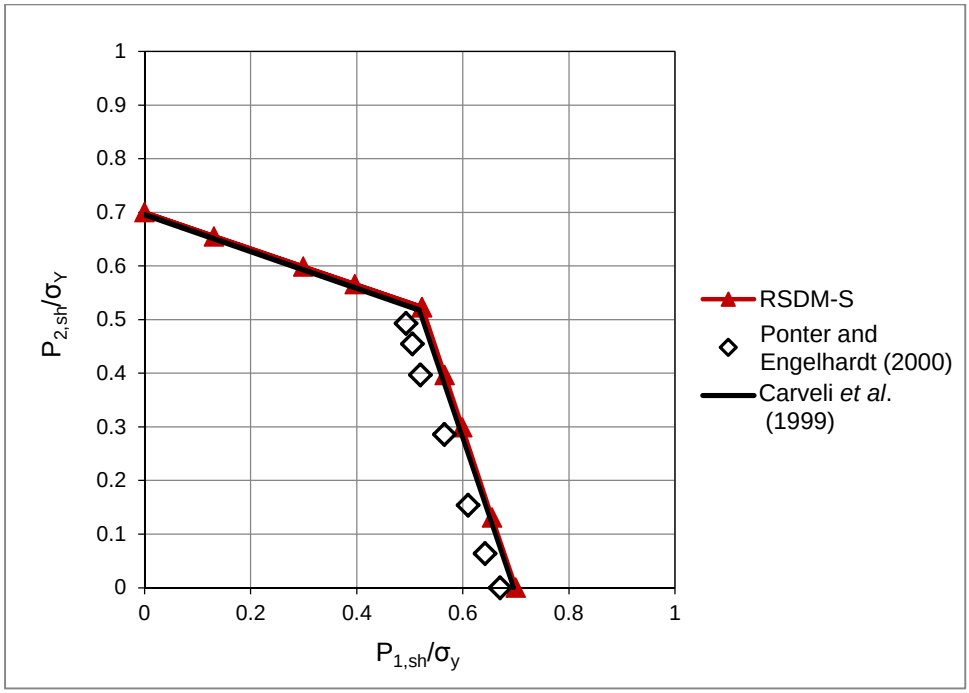

Figure 6.38 Shakedown domain produced by RSDM-S for either the triangular (Fig.6.36), or the rectangular loading domain (Fig.6.37)

A summary of the above results and the calculated shakedown factors for all the previous load cases may be seen in Table 4 (for $P_1^* / P_2^* = 1/1$).

Loading path	Shakedown load
Case 1	0,893σ_Y
Case 2i	0,673σ_Y
Case 2ii	0,522σ_Y
Case 2iii	0,522σ_Y

Table 4. Summary of the results

In Fig.6.39 one may see the convergence behavior of the RSDM-S procedure, for different loading ratios. The initial value of $\omega = 1$ was sufficient for convergence.

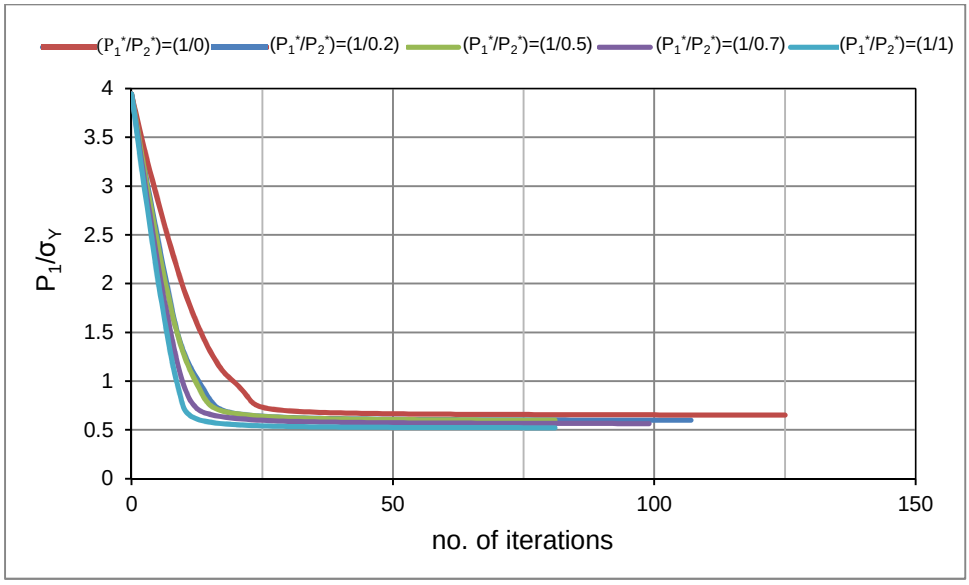

Figure 6.39 Convergence of the RSDM-S for various ratios (P_1^*/P_2^*) (rectangular load domain)

Another interesting issue concerns the plastic strain rates and their variation during the iterations of the procedure. As it has been already discussed in section 5.2.5 this may be portrayed through the variation of the plastic stress vector $\boldsymbol{\sigma}_{pl}$ at the various Gauss points in the discretized structure. One may see such a typical behavior, for example at the cycle time $3T/4$ and for $P_1^* = P_2^*$ in Figs.6.40, 6.41. In these two figures, the two largest components of the plastic stress vector at the two most strained points GPs 1 and 2, respectively (Fig.6.41) are plotted. It is shown that they converge to zero (within an accuracy of 10^{-2}) which is absolutely consistent with theory. It may be also seen that they converge at a different number of iterations.

The CPU time reported to reach a solution for an Intel Core i7 at 2.93 GHz with 4096 MB RAM was of the order of 40sec.

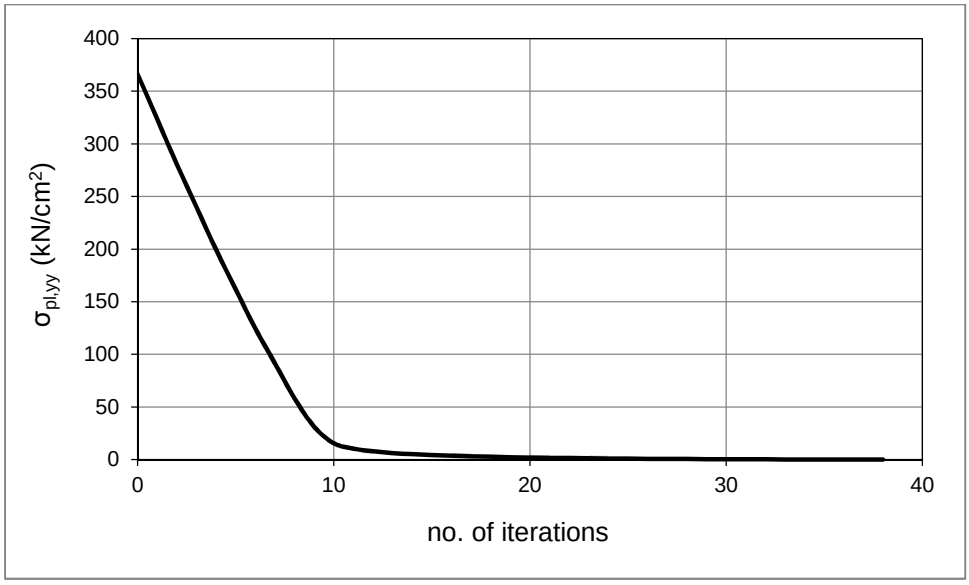

Figure 6.40 Evolution of the yy component of the plastic stress vector $\boldsymbol{\sigma}_{pl}^{cs}$ at GP2 (time 3T/4, $(P_1^*/P_2^*)=(1/1)$)

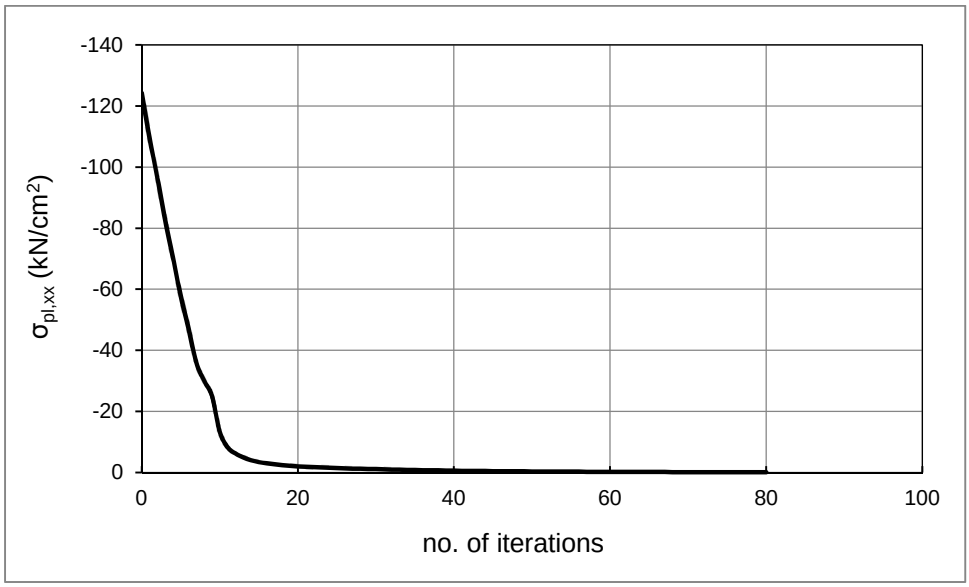

Figure 6.41 Evolution of the xx component of the plastic stress vector $\boldsymbol{\sigma}_{pl}^{cs}$ at GP1 (time 3T/4, $(P_1^*/P_2^*)=(1/1)$)

Why polynomial functions?

In all the examples, either the ones above, or the ones below, the time functions, used to connect the extreme load values inside a cycle, were polynomials of the order of two or four. The accuracy of the numerical integration, for the update of the Fourier coefficients used by the RSDM inside the inner loop, required, due to the

nonlinear nature of the functions involved, at least twenty points inside the cycle. Because of the smoother variation of the stresses inside the cycle in the case of the polynomials, the alternative time function of a linear type that was tried, judging from the example of the holed plate with the rectangular domain, required more time points to produce a solution of the same accuracy with the expense of more iterations (Fig.6.42) and greater computing time. In Table 5 one may see the shakedown loads by using either linear or polynomial time functions. It may be observed that the results almost coincide.

P_1^*/P_2^*	Polynomial time functions	Linear time functions
(1/0)	$0,7\sigma_Y$	$0,7\sigma_Y$
(1/0,2)	$0,665\sigma_Y$	$0,655\sigma_Y$
(1/0,5)	$0,598\ \sigma_Y$	$0,596\sigma_Y$
(1/0,7)	$0,566\sigma_Y$	$0,565\sigma_Y$
(1/1)	$0,522\sigma_Y$	$0,522\sigma_Y$

Table 5. Shakedown loads using either polynomial or linear time functions

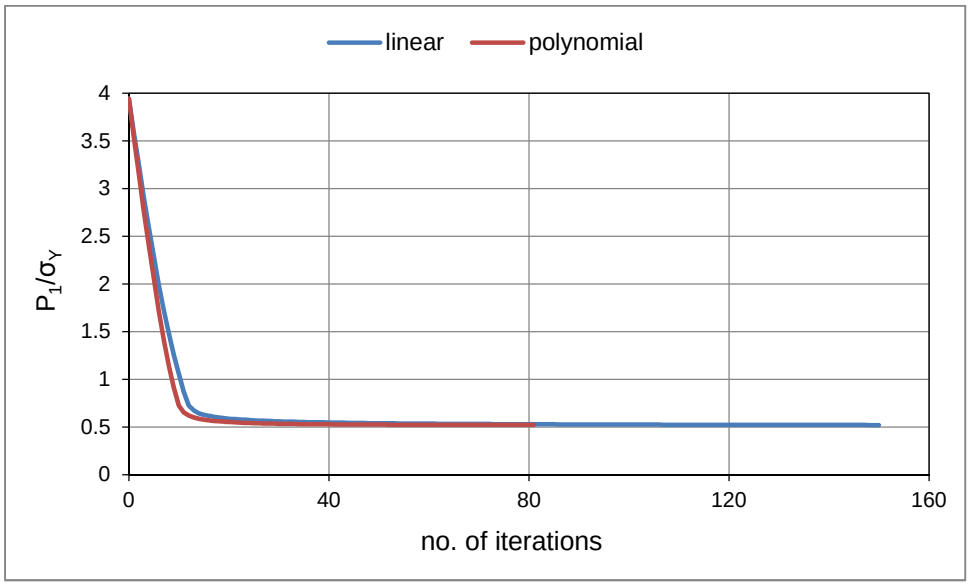

Figure 6.42 Comparison between linear and polynomial representation ($(P_1^*/P_2^*)=(1/1)$) (case of rectangular load domain)

6.2.3. Grooved rectangular plate under varying tension and bending

The next example of application consists of a grooved rectangle, which may form a part of a steel connection plate, subjected to an in plane tension $P_N(t)$ and a bending moment $P_M(t)$ along the boundaries of the plate (Fig.6.43). This example has been studied in (Tran *et al.*, 2010).

The structure has the following geometrical data: $R = 25cm$, $L = 2R$ and $H = 4R$.

The plate is assumed homogeneous, isotropic, elastic-perfectly plastic with the material data of the Table 6.

Due to the symmetrical geometry and loading, only half of the plate has been analyzed. The finite element mesh discretization of the structure is also shown in Fig.6.43. Two hundred and ninety-four, eight-noded, iso-parametric elements with 3x3 Gauss integration points were used herein.

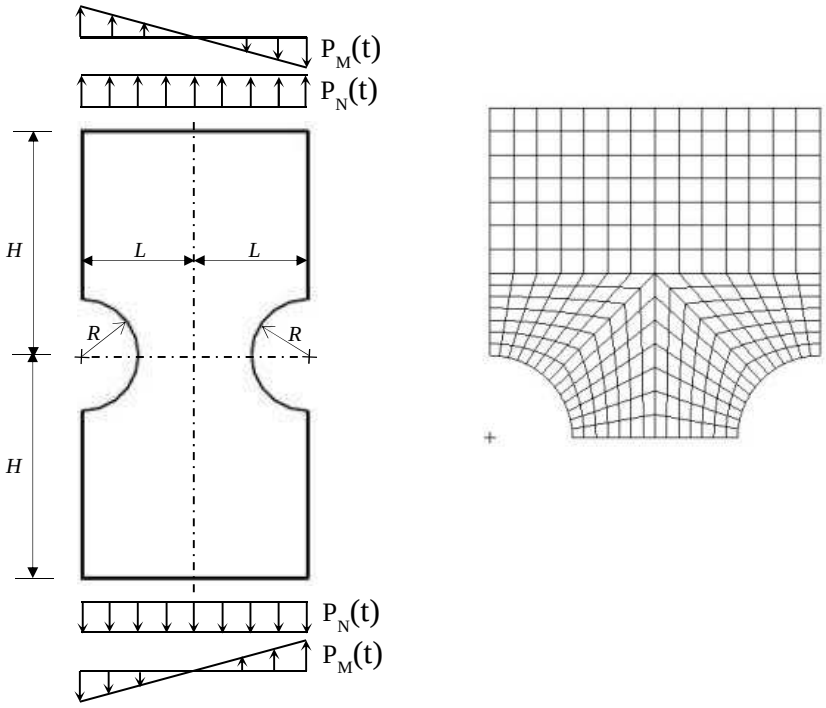

Figure 6.43 Geometry, loading and finite element discretization of the grooved plate

Young's modulus	E=210GPa
Poisson's ratio	v= 0,3
Yield stress	σ_Y=111,62MPa

Table 6. Material properties of the grooved plate

Description of the loading domain

A rectangular load domain is considered (Fig.6.44). The load domain is defined by: $P_N \in \left[0, P_N^*\right]$ and $P_M \in \left[0, P_M^*\right]$ having maximum values $P_N^* = P_M^* = 1$. A prescribed loading in time domain that passes through the four vertices of the rectangular, may be defined using the following equation:

$P(\tau) = \begin{Bmatrix} P_N^* \alpha_1(\tau) \\ P_M^* \alpha_2(\tau) \end{Bmatrix}$ where the time functions $\alpha_1(\tau), \alpha_2(\tau)$ are shown in Fig.6.44(a).

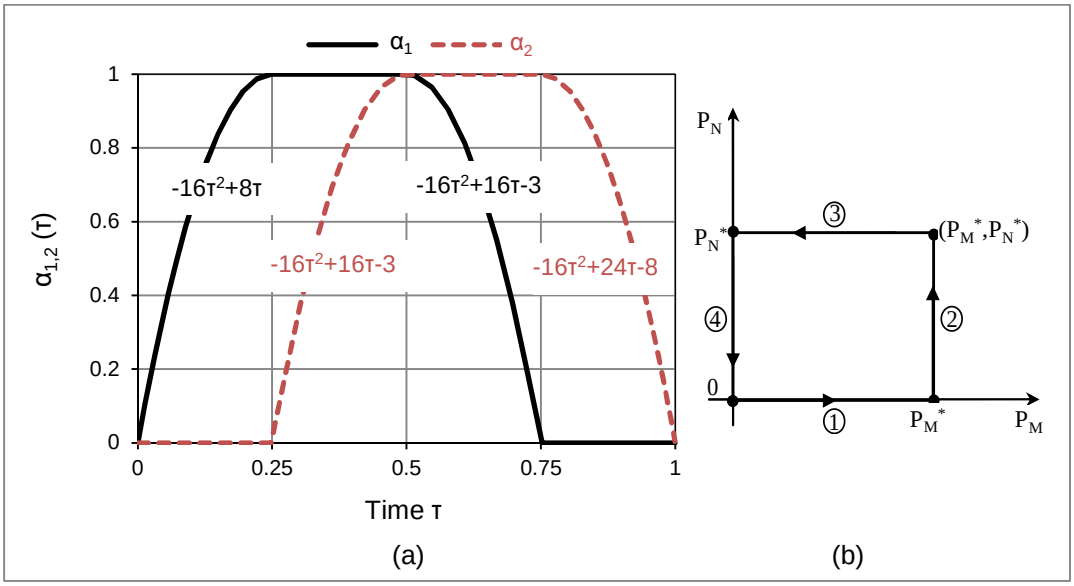

Figure 6.44 Independent cyclic loading variation over one time period in (a) time domain, (b) load domain

The shakedown domain obtained by the RSDM-S for various ratios of P_N^* / P_M^* is shown in Fig.6.45 (Spiliopoulos and Panagiotou, 2015). A good agreement with the existing in the literature results (Tran *et al.*, 2010) is observed.

Specifically, when we have both in-plane tension and bending with $P_N^* = P_M^* = 1$ the RSDM-S gives a shakedown factor equal to **0.227** which is quite close to the value 0.236 of (Tran *et al.*, 2010), where a different mesh and algorithm was used.

For this example, the initial convergence parameter $\omega = 1$, and in the process of the iterations, had to be halved twice due to an overshooting to a negative value of the calculated shakedown load, for the procedure to converge to the final shakedown factor.

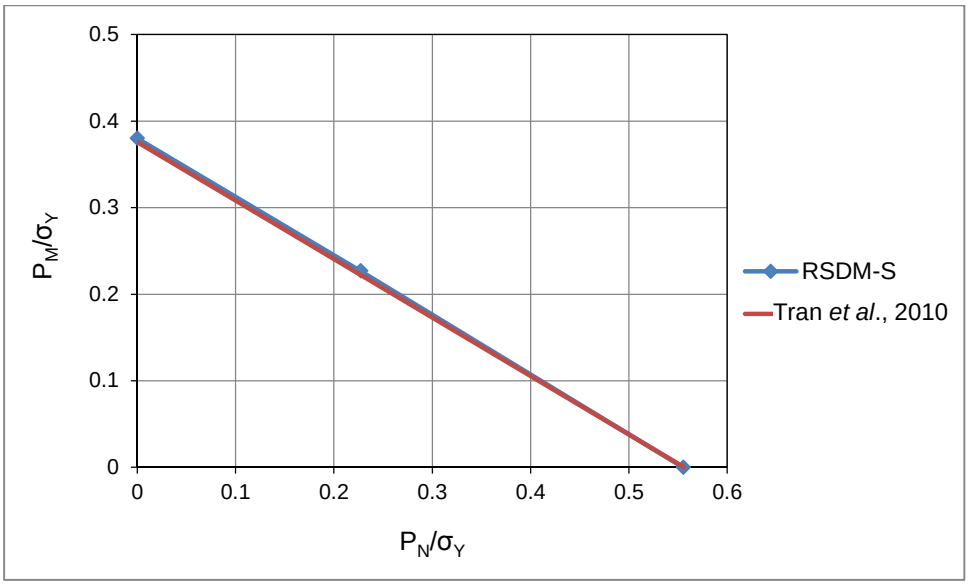

Figure 6.45 Shakedown domain produced by the RSDM-S for the grooved plate and its comparison with Tran *et al.* 2010

6.2.4. Bree problem

The first example that deals with the shakedown analysis of structures under thermo-mechanical loading is the classical Bree problem (Bree, 1967). This is a benchmark example in shakedown analysis, for this kind of loading. The structure is subjected to an uniaxial stress σ_P, constant in time, and a fluctuation of temperature difference $\Delta\theta(t)$ assumed to be linearly distributed along the width of the plate (Fig.6.46). The plate is assumed homogeneous, isotropic, elastic-perfectly plastic with the material data of the Table 7. The same geometrical data to discretize the problem as in (Ponter and Engelhardt, 2000) is used. The finite element mesh is shown in Fig.6.46, and consists of one hundred and twenty, eight-noded, iso-parametric elements with 3x3 Gauss integration points. We considered that the plate is constrained form in-plane bending, thus making the problem essentially one dimensional.

Description of the loading domain

A prescribed loading in time domain for the temperature may be established using a polynomial time function for the thermal load. (see also Fig.6.47). We consider:

$P(\tau) = \begin{Bmatrix} P^* \alpha_1(\tau) \\ \Delta\theta^* \alpha_2(\tau) \end{Bmatrix}$ where the time functions $\alpha_1(\tau), \alpha_2(\tau)$ are:

$\alpha_1(\tau) = const$

$\alpha_2(\tau) = 3,3334\tau^4 - 6,6667\tau^3 + 0,1667\tau^2 + 3,1667\tau$

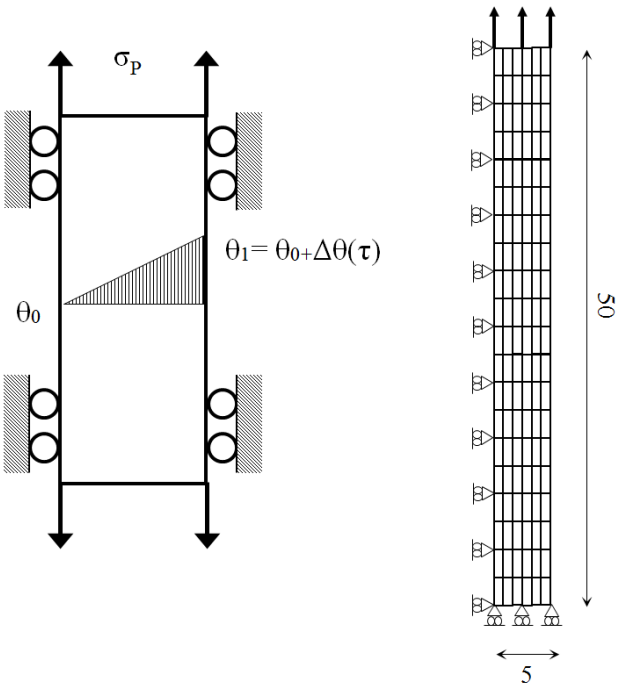

Figure 6.46 Geometry, loading and finite element mesh for the Bree problem

In Fig.6.48 one may see the calculated shakedown domain by the RSDM-S i.e. the maximum thermal elastic stress due to the fluctuating temperature σ_t plotted versus the axial stress σ_P both normalized against the yield stress σ_Y (Spiliopoulos and Panagiotou, 2014(b)). It may be observed that the solution is almost identical with the analytical solution (Bree, 1967).

Young's modulus	E=208GPa
Poisson's ratio	v= 0,3
Yield stress	σ_Y=360MPa
Coefficient of thermal expansion	$5x10^{-5}$ °C^{-1}

Table 7. Material properties of the Bree problem

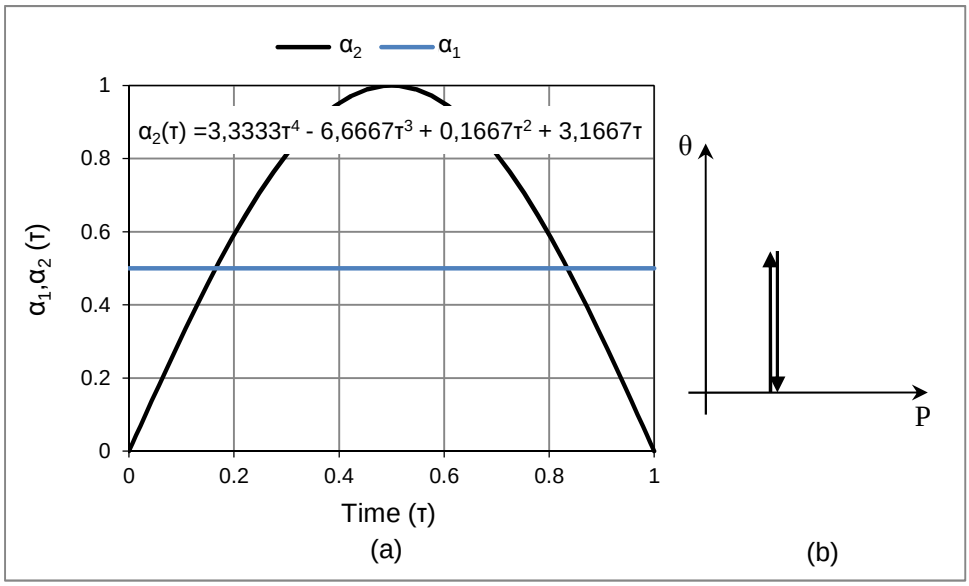

Figure 6.47 Cyclic loading variation over one time period in (a) time domain, (b) load domain

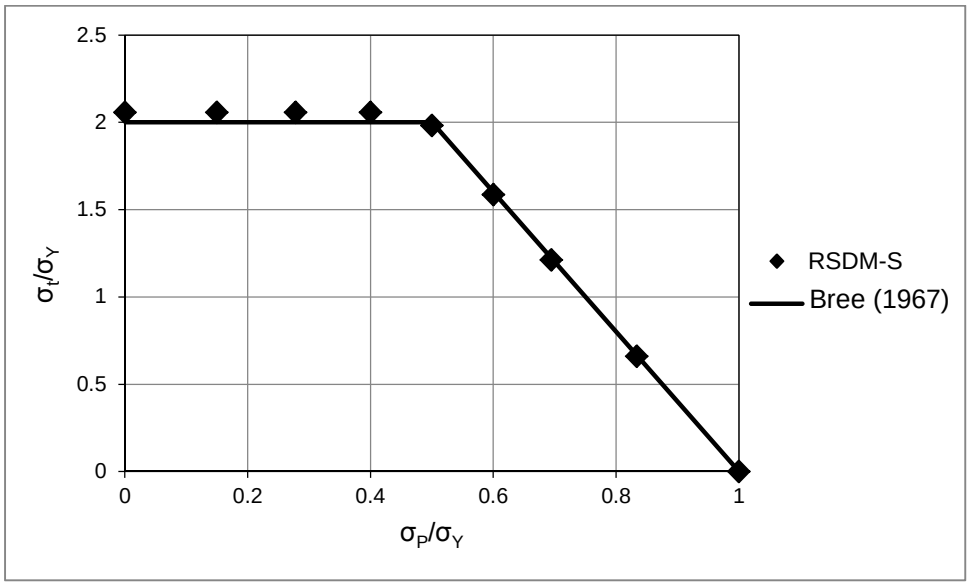

Figure 6.48 Shakedown domain produced by RSDM-S and its comparison with the analytical solution of Bree (1967)

6.2.5. Square plate with hole subjected to both mechanical and thermal loads

The next example of application is the holed plate subjected to a combination of mechanical and thermal loads (Fig.6.49). The geometrical data of the plate are the same as before (see section 6.2.2) and the material data are given in Table 8. The finite element mesh is also shown in Fig.6.49.

The plate is subjected to a temperature difference $\Delta\theta(t)$ between the edge of the hole and the edge of the plate, and a uniaxial tension $P(t)$ along the one side of the plate (Fig.6.49). A case of three loads acting on the plate, i.e. temperature difference $\Delta\theta(t)$ and uniform loads on both the two edges of the plate, will be presented later (see section 6.2.11). The variation of the temperature with radius r has the same logarithmic form as in (Chen and Ponter, 2001b):

$$\theta(r,\tau) = \theta_0 + \frac{\Delta\theta(\tau) * \ln\left(\frac{5\,D/2}{r}\right)}{\ln 5}$$

The above relation defines a good approximation of the temperature variation inside the plate giving a value of $\theta_1(\tau) = \theta_0 + \Delta\theta(\tau)$ around the edge of the hole $\left(r = D/2\right)$ and $\theta_1 = \theta_0$ at the outer edges of the plate $\left(r = 5D/2\right)$. The temperature θ_0 is assumed to be equal to zero. It should be noted that in the results σ_t denotes the maximum effective thermal elastic stress due to the fluctuating temperature.

The shakedown domain was calculated by the RSDM-S for two different load cases of thermo-mechanical loading. A first one, assuming constant axial load in time P and variable temperature difference $\Delta\theta(\tau)$, and a second one assuming an independent variation between the axial load $P(\tau)$ and the temperature difference $\Delta\theta(\tau)$ (Spiliopoulos and Panagiotou, 2014(b)).

Young's modulus	E=208GPa
Poisson's ratio	v= 0,3
Yield stress	σ_Y=360MPa
Coefficient of thermal expansion	$5x10^{-5}$ °C^{-1}

Table 8. Material properties of the plate

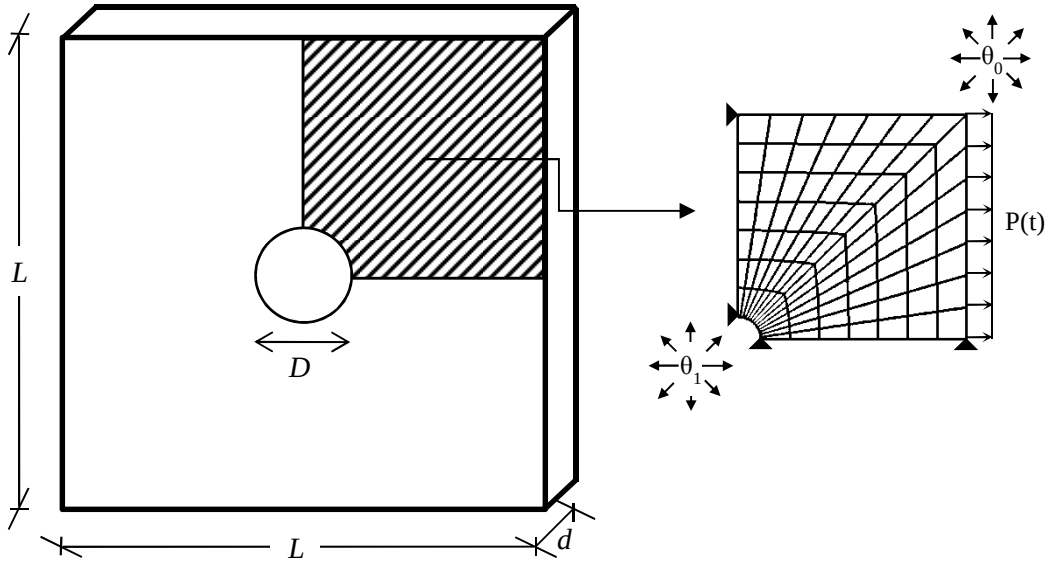

Figure 6.49 Geometry, and finite element discretization of the plate subjected to mechanical and thermal loading

1. Constant axial load P, variable temperature Δθ(τ)

A prescribed loading in time domain may be defined using a polynomial function for the thermal load (Fig.6.47). Specifically we have:

$P(\tau) = \begin{Bmatrix} P^* \alpha_1(\tau) \\ \Delta\theta^* \alpha_2(\tau) \end{Bmatrix}$ where the time functions $\alpha_1(\tau), \alpha_2(\tau)$ are:

$\alpha_1(\tau) = const$

$\alpha_2(\tau) = 3,3334\tau^4 - 6,6667\tau^3 + 0,1667\tau^2 + 3,1667\tau$

The calculated by the RSDM-S shakedown domain may be seen in Fig.6.50. It should be mentioned that the temperature axis is normalized against $2\sigma_Y$ as this is the value of σ_t at the reverse plasticity limit (Chen and Ponter, 2001b). It may be observed that the interaction diagram follows the classic Bree-like shape (Bree, 1967). Finally, the results are quite close with the ones in the literature (Chen and Ponter, 2001b).

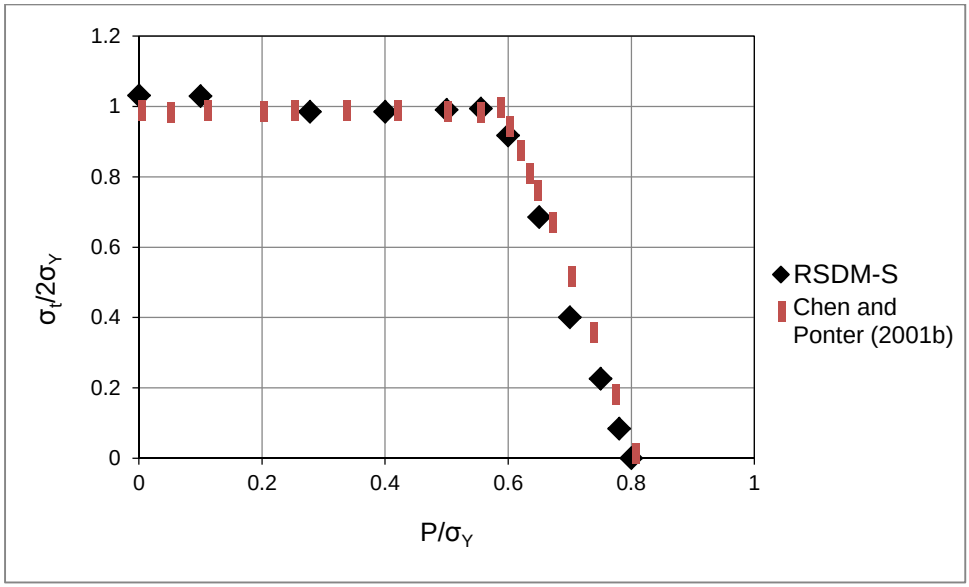

Figure 6.50 Shakedown domain produced by RSDM-S for loading case a (constant mechanical loading)

2. Independent variation of the axial load P(τ) and the temperature Δθ(τ)

The RSDM-S is used to find the shakedown loading for the rectangular loading domain (Fig.6.51(b)) where the two loads vary independently. A prescribed loading in time domain that passes through the four vertices of the domain may be defined by using the following equation:

$P(\tau) = \begin{Bmatrix} P^{*}\alpha_1(\tau) \\ \Delta\theta^{*}\alpha_2(\tau) \end{Bmatrix}$ where the time functions $\alpha_1(\tau), \alpha_2(\tau)$ are shown in Fig.6.51(a).

The computed, by the RSDM-S, shakedown domain is shown in Fig.6.52.

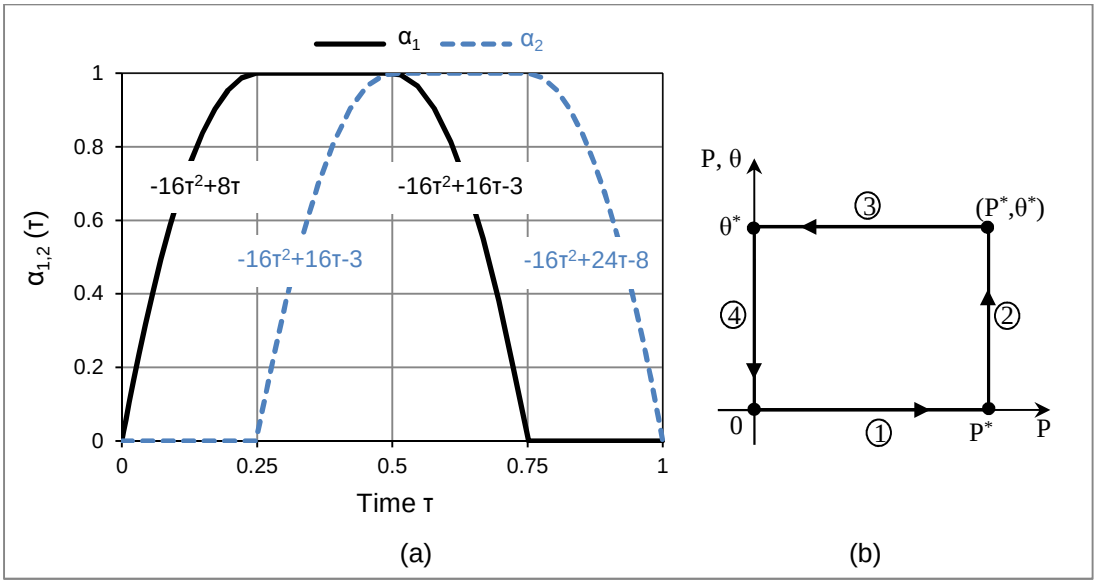

Figure 6.51 Independent cyclic loading variation over one time period in (a) time domain, (b) load domain (load case 2)

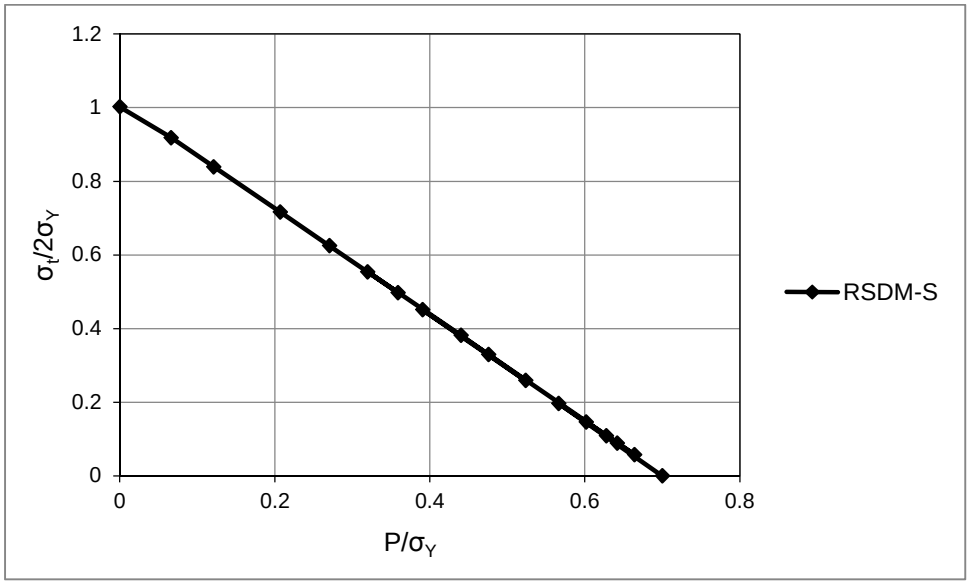

Figure 6.52 Shakedown domain produced by RSDM-S for loading case b (independent load case, rectangular loading domain)

6.2.6. Two-span beam

The next example of application is a continuous two-span steel beam (Fig.6.53). The beam has a rectangular cross-section characterized by the plastic moment M_{pl}. This problem has been analytically studied by (König, 1987). The geometry and the finite

element discretization of the beam are shown in Fig.6.53. A case of $L = 160cm$ has been chosen herein. The dimensions of the rectangular section is $h = 10cm$ and $b = 1cm$. The finite element mesh consists of ninety-six, eight noded, iso-parametric elements with 3x3 Gauss integration points (Fig.6.53). The beam is subjected to a cyclic loading of two vertical mechanical loads P_1, P_2. The beam is assumed homogeneous, isotropic, elastic-perfectly plastic having the material data shown in Table 9.

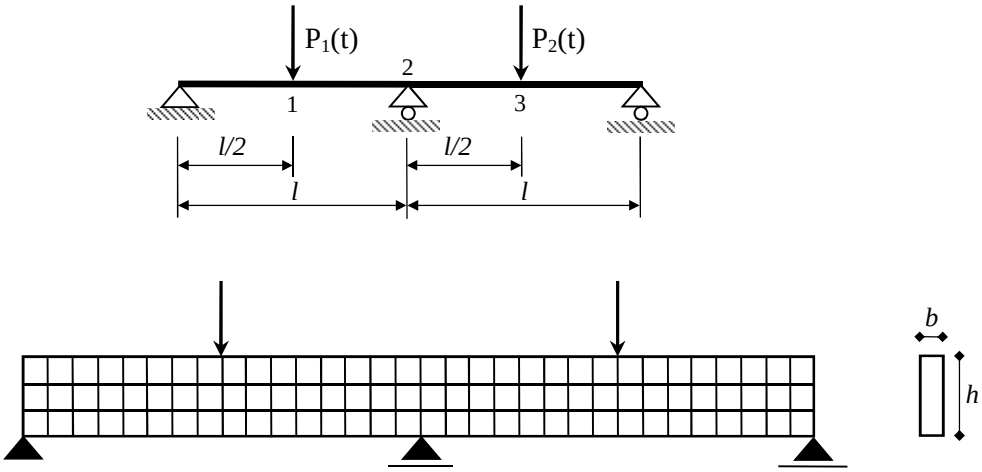

Figure 6.53 Geometry, loading and finite element mesh of the two-span beam

Young's modulus	E=210 GPa
Poisson's ratio	v= 0,3
Yield stress	σ_Y=360 MPa

Table 9. Material properties of the two-span beam

The following two different loading cases are examined:

1. *Constant P_1, variable load P_2*

   This first loading case consists of a constant load P_1 and a cyclical load P_2. Let the load vary cyclically in the following way:

   I $\quad P_1 = P, \quad P_2 = 0$

   II $\quad P_1 = P, \quad P_2 = P$

   III $\quad P_1 = P, \quad P_2 = 0$

A prescribed loading in time domain may be established with the use of the following polynomial function for the second load P_2 .

$$\alpha(\tau) = -4\tau^2 + 4\tau \quad , \quad \tau \in [0,1]$$

The calculated shakedown load using the RSDM-S is equal to $P_{SH} = 5.3\, M_{pl}/L$, which is close to the analytic solution $5.0526\, M_{pl}/L$ (König, 1987). This difference is acceptable as it is more or less related to the difference between the elastic solution of the problem using the two approaches i.e. one by using two dimensional finite elements and one using the classical beam theory.

2. *Independent variation of P_1, P_2*

   The next loading domain under consideration is the rectangular loading domain of Fig.6.55, with $P_1^* = P_2^* = 1$. This loading domain may be expressed as the path: $(0 \to (P_1^*, 0) \to (P_1^*, P_2^*) \to (0, P_2^*) \to 0)$. The time functions $\alpha_1(\tau), \alpha_2(\tau)$ of Fig.6.55 were used to establish a prescribed cyclic loading that passes through the four vertices of this domain.

   The shakedown load for this loading case is equal to $P_{SH} = 5.3\, M_{pl}/L$. It may be observed that the resulted shakedown load coincides with the one of the previous case.

The CPU time reported to reach a solution, for the last load case, for an Intel Core i7 at 2.93 GHz with 4096 MB RAM was of the order of 150sec.

6.2.7. Frame example

In the next example a simple frame, shown in Fig.6.54, is considered. This example has been investigated by Tran T.N. *et al*. (2010) using an edge-based smoothed finite element method (ES-FEM) and a primal-dual shakedown algorithm, and by Garcea *et al*. (2005) using a strain driven strategy. In those applications, however, the loading domains have one or both the minimum values different to zero unlike the loading domain used here, where the minimum values are both assumed zero. This more general kind of loading domain will be studied next, in Section 6.2.10.2.

The frame is assumed homogeneous, isotropic, elastic-perfectly plastic, having the material data shown in Table 10. The finite element mesh discretization of the frame, shown also in Fig.6.54, consists of 400 eight-noded, iso-parametric elements with 3x3 Gauss integration points.

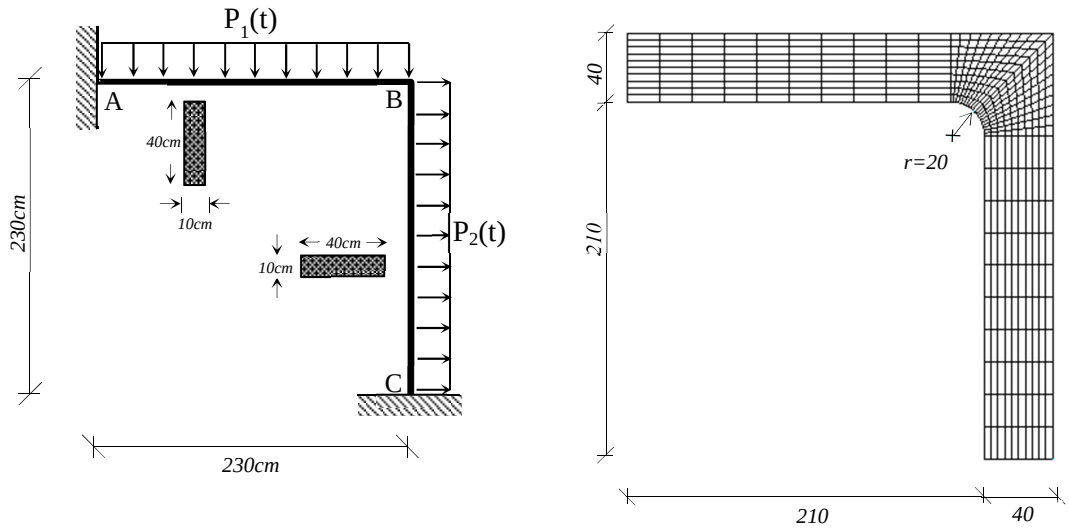

Figure 6.54 Geometry, loading and finite element mesh of the frame

Description of the loading domain

The frame is subjected to two uniform distributed loads $P_1(t)$ and $P_2(t)$, applied on the external faces of AB and BC respectively. A rectangular loading domain is considered (Fig.6.55) with the two loads varying independently, having maximum values $P_1^* = 3$ and $P_2^* = 1$, respectively.

A prescribed loading in time domain that passes through the four vertices of the rectangular, may be defined by using the time functions $\alpha_1(\tau), \alpha_2(\tau)$ of Fig.6.55.

Young's modulus	E=200GPa
Poisson's ratio	v= 0,3
Yield stress	σ_Y=100MPa

Table 10. Material properties of the frame

In this example the initial convergence parameter $\omega = 1$ had to be halved twice, for the procedure to converge to the final shakedown factor, which was found equal to **2.597** (Spiliopoulos and Panagiotou, 2014(a)). The CPU time was about 280s on the same, as above, processor.

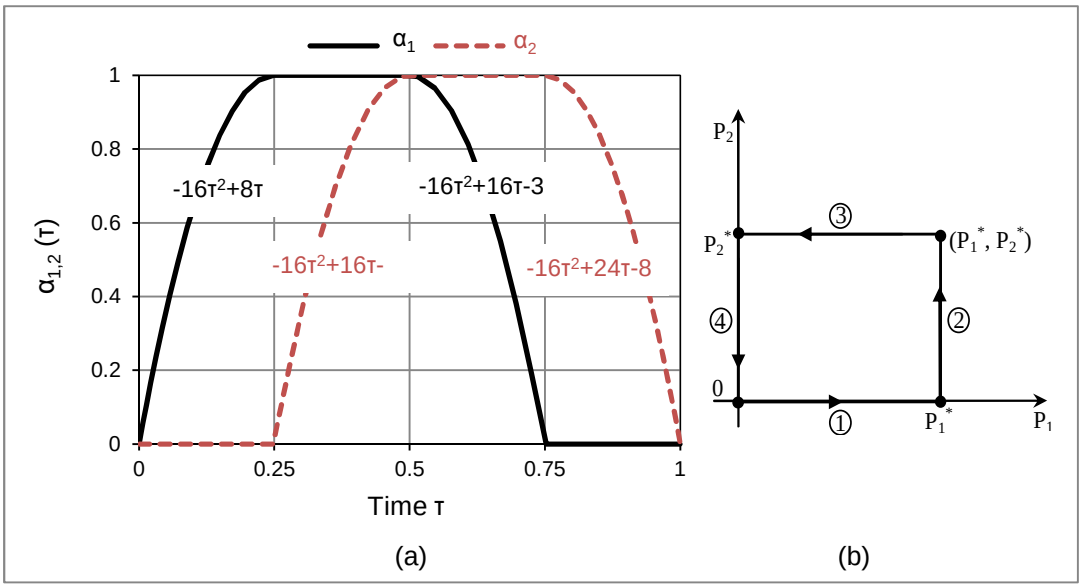

Figure 6.55 Independent cyclic loading variation over one time period in (a) time domain, (b) load domain

6.2.8. Symmetric continuous beam under distributed load

A symmetric three-span continuous beam under uniform loads is considered next. One may observe the finer discretization around the supports, in comparison with the beam of section 6.2.6, in order to have a better simulation of the boundary conditions. Due to symmetry, only a half of the beam is analyzed (Fig.6.56). This is a relatively large scale problem since its finite element discretization consisted of 800 eight-noded, iso-parametric elements with 3x3 Gauss integration points (Fig.6.56).

The beam is assumed homogeneous, isotropic, elastic-perfectly plastic, having the material data of Table 11.

This example has also been treated by Garcea *et al.* (2005) and Pham (2011), using a different loading domain, that has its origin different to zero, to the one employed here. However, a comparison could be made with Pham (2011) assuming

only the load P_1 acts on the structure. The RSDM-S gives a shakedown pressure equal to $3.1\,N/mm^2$ which is quite close to the value $3.3\,N/mm^2$ given by Pham that uses a different mesh and algorithm (IPM algorithm).

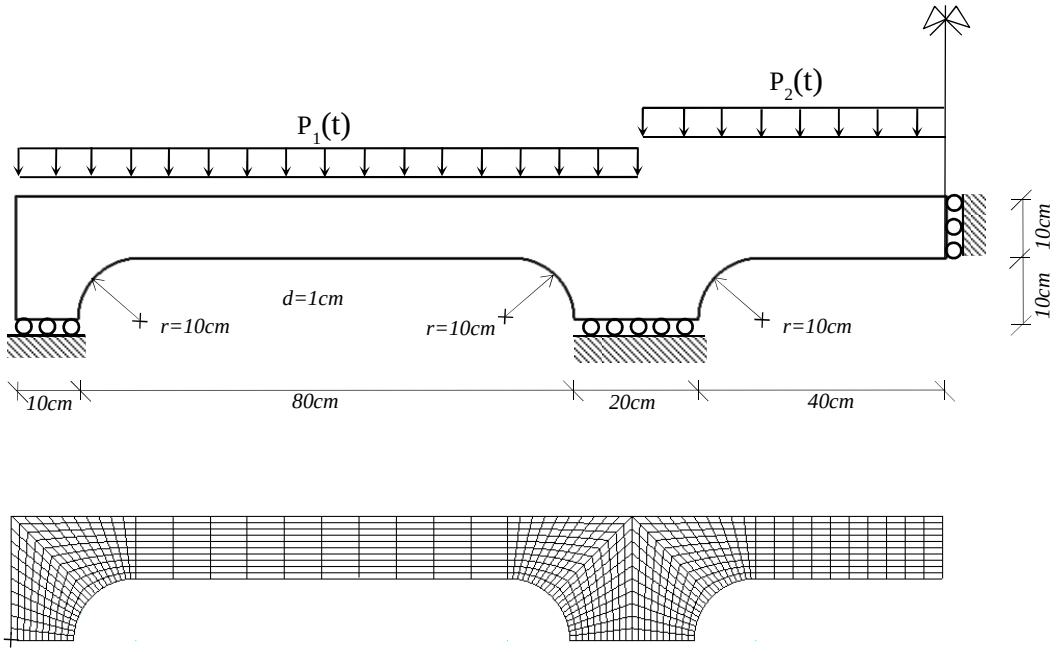

Figure 6.56 Geometry, loading and finite element mesh of the continuous beam

Young's modulus	E=180GPa
Poisson's ratio	v= 0,3
Yield stress	σ_Y=100MPa

Table 11. Material properties of the symmetric continuous beam

Description of the loading domain

The rectangular load domain of Fig.6.55(b) was tried next using the RSDM-S. The load varies in the domain $P_1 \in \left[0, P_1^*\right]$ and $P_2 \in \left[0, P_2^*\right]$ where $P_1^* = 1$ and $P_2^* = 2$.

A prescribed loading in time domain that passes through the four vertices of the rectangular, may be defined by using the following time functions $\alpha_1(\tau), \alpha_2(\tau)$:

$$\alpha_1(\tau) = -16\tau^2 + 8\tau, \quad \alpha_2(\tau) = 0 \quad , \quad \tau \in [0, 1/4]$$
$$\alpha_1(\tau) = 1, \quad \alpha_2(\tau) = -16\tau^2 + 16\tau - 3 \quad , \quad \tau \in (1/4, 1/2]$$
$$\alpha_1(\tau) = -16\tau^2 + 16\tau - 3, \quad \alpha_2(\tau) = 1 \quad , \quad \tau \in (1/2, 3/4]$$
$$\alpha_1(\tau) = 0, \quad \alpha_2(\tau) = -16\tau^2 + 24\tau - 8 \quad , \quad \tau \in (3/4, 1]$$

For this example the initial convergence parameter ω, in the process of the iterations, had to be halved three times, for the procedure to converge to the final shakedown factor which was found equal to **0.191**. Although the starting point was quite high as compared to the final result, the descent was rapid in 12 iterations, as shown in the Fig.6.57. In the insert of the figure, one may see, after the initial descent, the smooth convergence towards the shakedown value (Spiliopoulos and Panagiotou, 2014(a)).

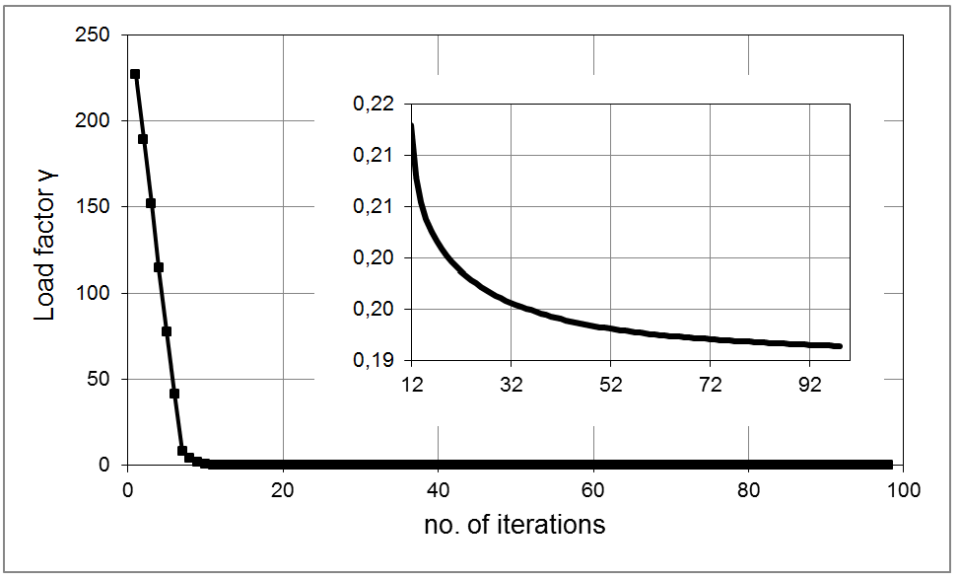

Figure 6.57 Convergence of the RSDM-S towards the shakedown factor for the continuous beam problem

In Fig.6.58 one may also see the evolution of the maximum, among all the time points, Euclidean norm of the plastic stress vector $\|\sigma_{pl}\|$. It may be that this norm ends up to zero which is consistent with theory (see section 5.2.5).

Less than 100 iterations were required to convergence. The amount of CPU time needed to solve this problem, on the same processor as above, was around 350s.

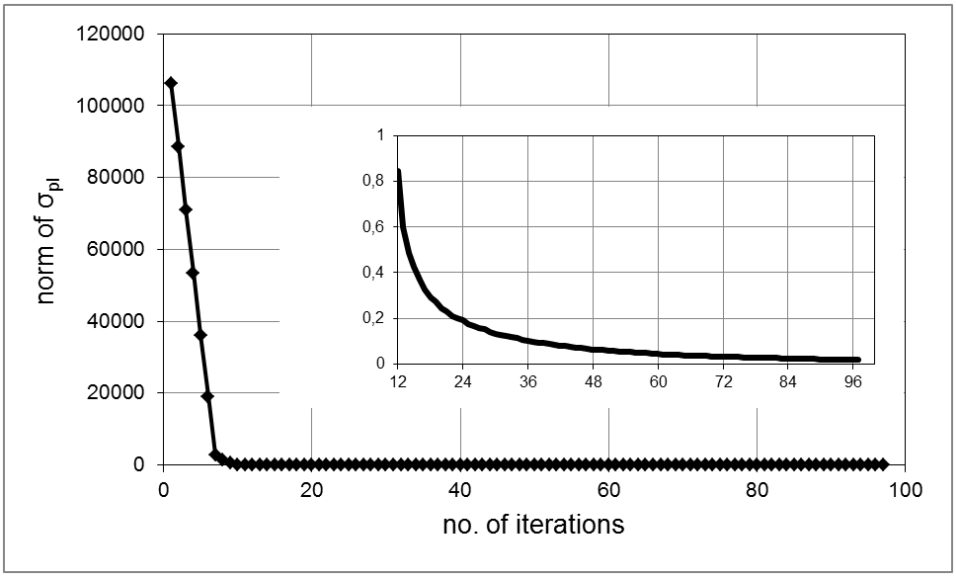

Figure 6.58 Evolution of the Euclidian norm of $\boldsymbol{\sigma}_{pl}^{cs}$ for the continuous beam problem (time 3T/4)

6.2.9. New convergence criterion

In this section, the updated convergence criterion, described in detail in section 5.2.6, is introduced. In order to prove the efficiency of this new criterion, the examples of the frame and the symmetric continuous beam, are solved by using the updated convergence parameters.

6.2.9.1. Frame example

The first example under consideration is the frame example of the previous section (Fig.6.54). The geometrical and material data as well as the mesh discretization are identical with the ones of the previous example. The common rectangular load domain of Fig.6.55 is considered with $P_1^* = 3$ and $P_1^* = 1$.

For this example the initial convergence parameter ω, in the process of the iterations, had to be halved twice, for the procedure to converge to the final shakedown factor which was found equal to **2.47**.

A number of 175 iterations were required to converge. The amount of CPU time needed to solve this problem, on the same processor as above, was around 160s.

As already mentioned above, using the old convergence criterion, convergence was succeeded after 280s (CPU time), with 354 iterations. Thus, it is pointed out that

there is a significant acceleration of the proposed procedure RSDM-S, using the improved convergence criterion.

The convergence of the RSDM-S based on the new criterion and its comparison with the old one may be seen in Fig.6.59. For a comparison to be better illustrated, the common 10 first iterations are not plotted.

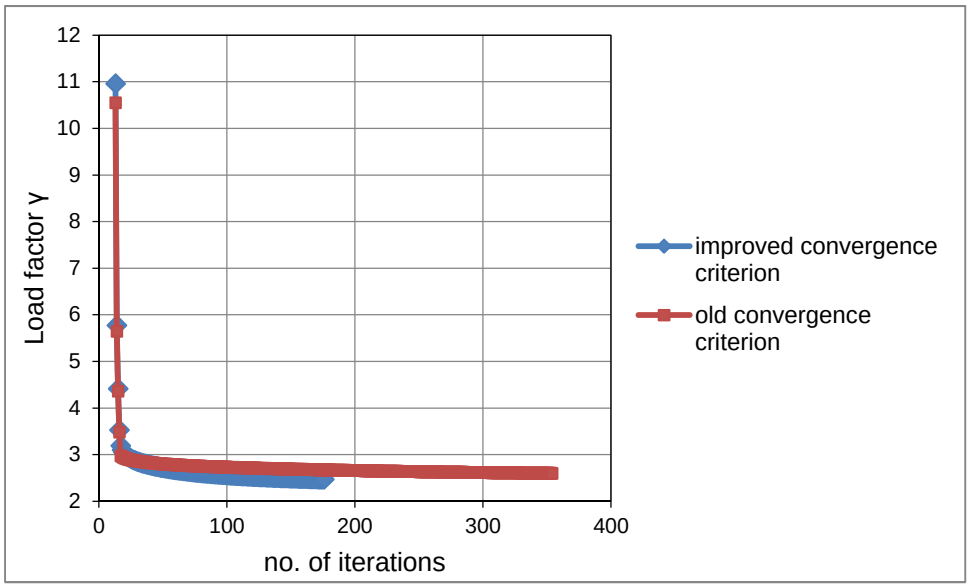

Figure 6.59 Comparison of the two convergence criteria for the frame example

6.2.9.2. Symmetric continuous beam under distributed load

The second example of validation is the symmetric beam example of the previous section (Fig.6.56). The geometrical and material data as well as the mesh discretization are the same with the ones of the previous example. The rectangular load domain of Fig.6.55 is considered again with $P_1^* = 1$ and $P_2^* = 2$.

For this example the initial convergence parameter ω, in the process of the iterations, had to be halved three times, for the procedure to converge to the final shakedown factor which was found equal to **0.191**. Once again although the starting point was quite high as compared to the final result, the descent was rapid in 12 iterations, as shown in the Fig.6.60. It is observed, that the load factors obtained by those two different criterions, coincide.

A number of 65 iterations were required to converge, less than the 100 iterations needed with the old convergence criterion. The amount of CPU time needed to solve

this problem was around 220s, **40% faster** than previously. In conclusion, the new convergence criterion proves to be more robust than the old one.

The convergence of the RSDM-S based on the new criterion and its comparison with the old one may be seen in Fig.6.60. For a better illustration of the comparison the first 10 iterations are not plotted.

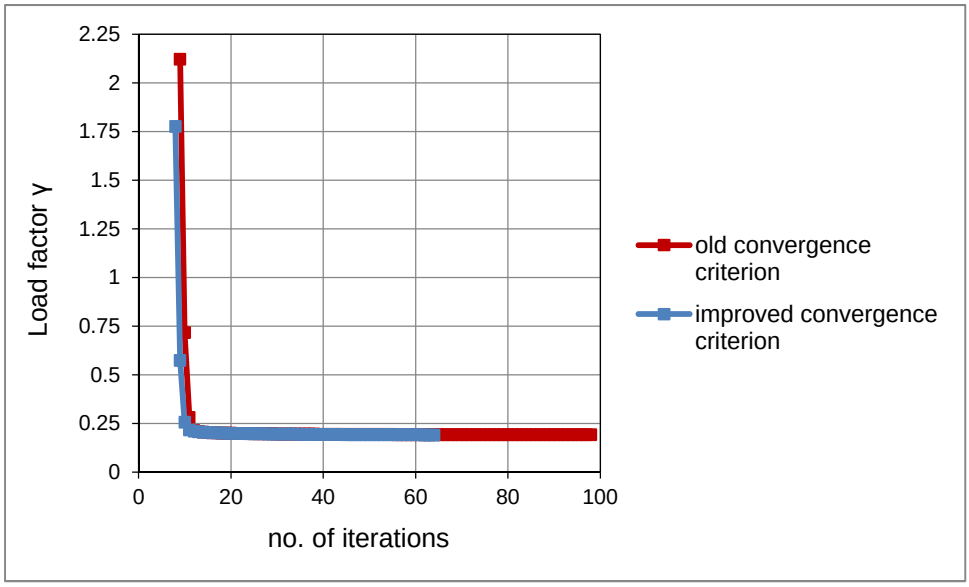

Figure 6.60 Comparison of the two convergence criteria for the beam example

6.2.10. General loading domain

In this section, examples of structures subjected to more general loading domain will be presented. The term general loading domain refers to loading domains that have one or more minimum values of P_i^* different to zero, i.e. the origin of the loading domain differs to zero (see section 5.2.3). It should be mentioned that all the following examples were solved using the new convergence criterion (see section 5.2.6).

6.2.10.1. Square plate under different load domains

Next we seek to find the shakedown limit of the plate of section 6.2.2 under some different loading cases that include a variation of the applied loads from minus to plus.

1. *Loading case a*

For the loading case (*a*) of Fig.6.61 the variable axial load P_2 is varying from negative to positive, i.e. in the domain $P_2 \in \left[-1,1\right]$, while the load P_1 is constant in time. Thus, we may choose any polynomial function $\alpha(\tau)$ that passes from the two points -1 and 1, in order to describe the variation of the load P_2. By setting different values to the constant load, the RSDM-S predicts the shakedown limits for the time varying load. The results are plotted in Fig.6.62. A good agreement with existing in the literature (Chen and Ponter, 2001b) may be seen.

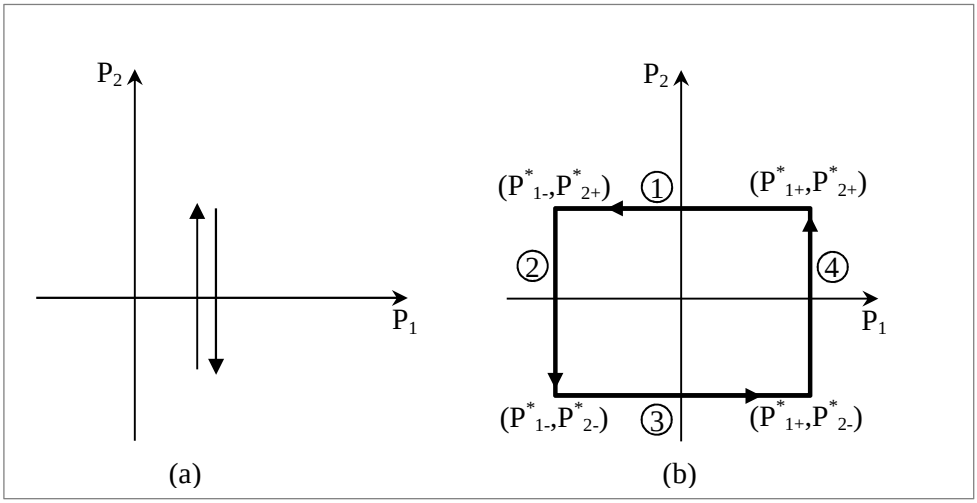

Figure 6.61 Loading case a, b

2. *Loading case b*

The second loading path assumes that $P_1(t)$ and $P_2(t)$ vary independently in the load domain of Fig.6.61(b).

A prescribed loading in time domain that passes through the four vertices of the rectangle may be defined by using the following equations (Fig.6.63):

$$P(\tau) = \begin{Bmatrix} P_1^* \alpha_1(\tau) \\ P_2^* \alpha_2(\tau) \end{Bmatrix} \text{ where } \begin{matrix} \alpha_1(\tau) \in \left[-1,1\right] \\ \alpha_2(\tau) \in \left[-1,1\right] \end{matrix}$$

$$\alpha_1(\tau) = 32\tau^2 - 16\tau + 1, \quad \alpha_2(\tau) = 1, \quad \tau \in [0, 1/4]$$
$$\alpha_1(\tau) = -1, \quad \alpha_2(\tau) = 32\tau^2 - 32\tau + 7, \quad \tau \in (1/4, 1/2]$$
$$\alpha_1(\tau) = 32\tau^2 - 32\tau + 7, \quad \alpha_2(\tau) = -1, \quad \tau \in (1/2, 3/4]$$
$$\alpha_1(\tau) = 1, \quad \alpha_2(\tau) = 32\tau^2 - 48\tau + 17, \quad \tau \in (3/4, 1]$$

The calculated shakedown domain and its comparison with the results of Gross-Weege (1997) may be seen in Fig.6.64.

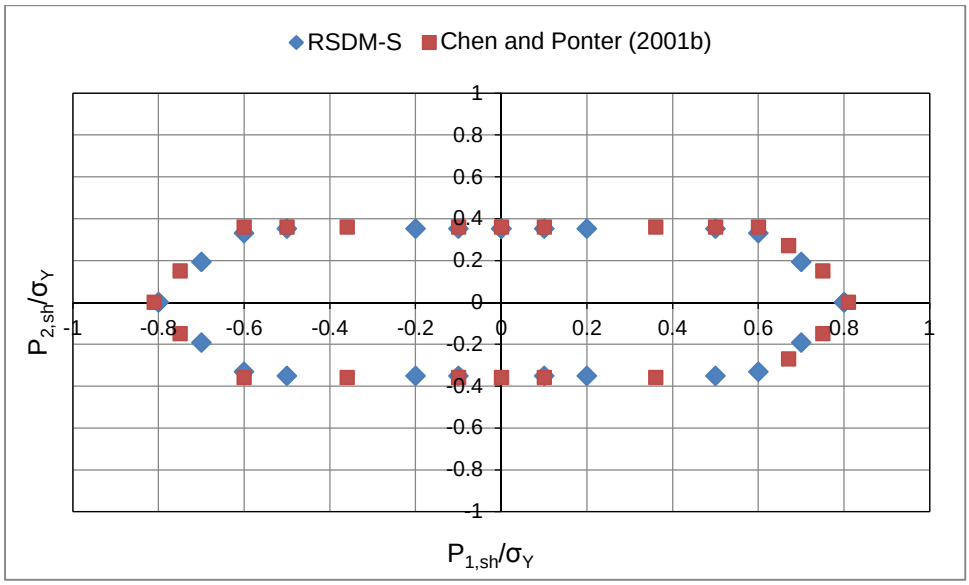

Figure 6.62 Shakedown domain produced by RSDM-S, and its comparison with Chen and Ponter (2001b), (loading case a)

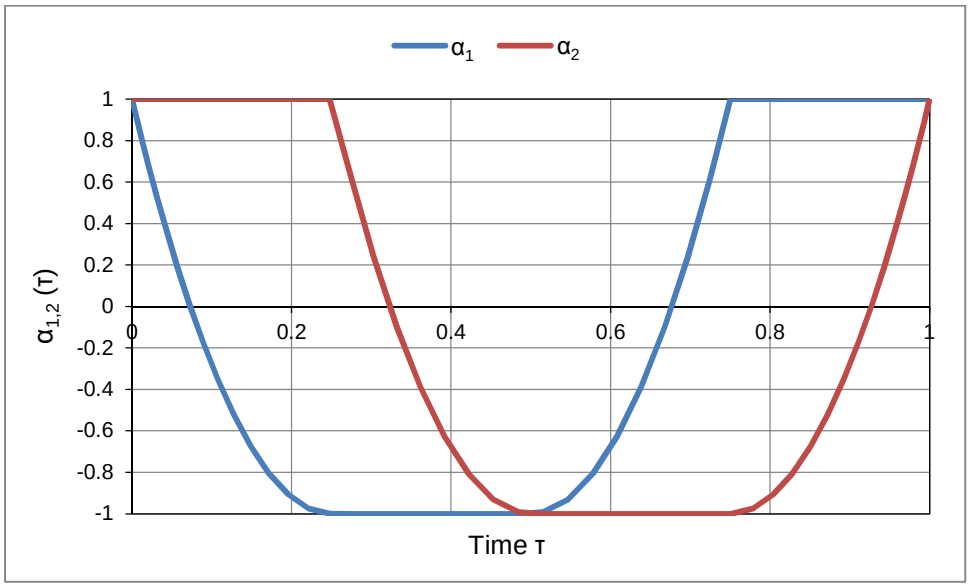

Figure 6.63 Time functions variation over one period (loading case b)

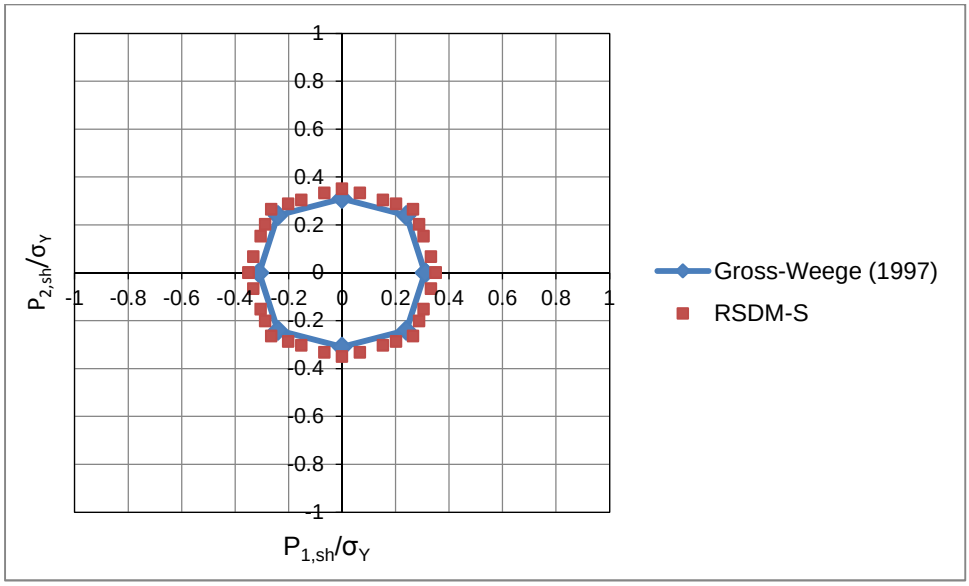

Figure 6.64 Shakedown domain produced by RSDM-S, and its comparison with Gross-Weege (1997), (loading case b)

6.2.10.2. Frame example

Let us consider the frame of Fig.6.54. The frame is subjected to two uniform distributed loads $P_1(t)$ and $P_2(t)$, applied on the external faces of AB and BC respectively. The geometry and the material of the structure are identical as previously (section 6.2.7).

Description of the loading domain

A general rectangular loading domain is considered (Fig.6.66) with the two loads $P_1(t)$ and $P_2(t)$ varying independently, between the values $[1.2,3]$ and $[0.4,1]$ respectively.

A prescribed loading in time domain that passes through the four vertices of the rectangle may be defined by using the following equations (Fig.6.65):

$P(\tau) = \begin{Bmatrix} P_1^* \alpha_1(\tau) \\ P_2^* \alpha_2(\tau) \end{Bmatrix}$ where the time functions $\alpha_1(\tau), \alpha_2(\tau)$ are:

$$\alpha_1(\tau) = -9.6\tau^2 + 4.8\tau + 0.4, \quad \alpha_2(\tau) = 0.4 \quad , \quad \tau \in [0, 1/4]$$
$$\alpha_1(\tau) = 1, \quad \alpha_2(\tau) = -9.6\tau^2 + 9.6\tau - 1.4 \quad , \quad \tau \in (1/4, 1/2]$$
$$\alpha_1(\tau) = -9.6\tau^2 + 9.6\tau - 1.4, \quad \alpha_2(\tau) = 1 \quad , \quad \tau \in (1/2, 3/4]$$
$$\alpha_1(\tau) = 0.4, \quad \alpha_2(\tau) = -9.6\tau^2 + 14.4\tau - 4.4 \quad , \quad \tau \in (3/4, 1]$$

In this case $P_1^* = 3$, $P_2^* = 1$ and $0.4 \le \alpha_1(\tau), \alpha_2(\tau) \le 1$ (see Figs.6.65,6.66).

For this example the initial convergence parameter ω, in the process of the iterations, had to be halved twice, for the RSDM-S to converge to the final shakedown limit which is equal to **3.91**.

The present results of RSDM-S, compared to those of different analysis methods in the literature, are shown in Table 12. It may be seen that they match quite well.

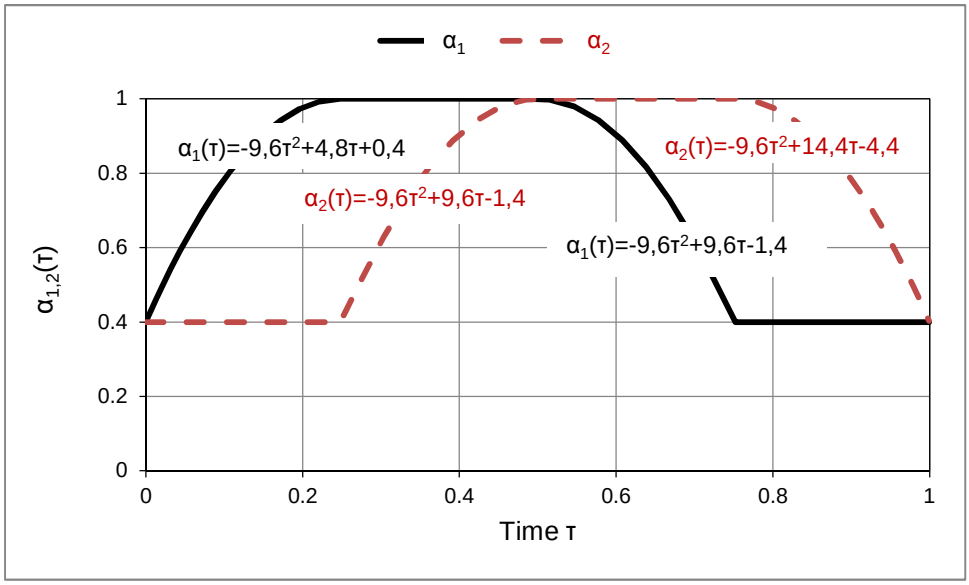

Figure 6.65 Time functions variation, over one period corresponding to the load domain of Fig.6.66

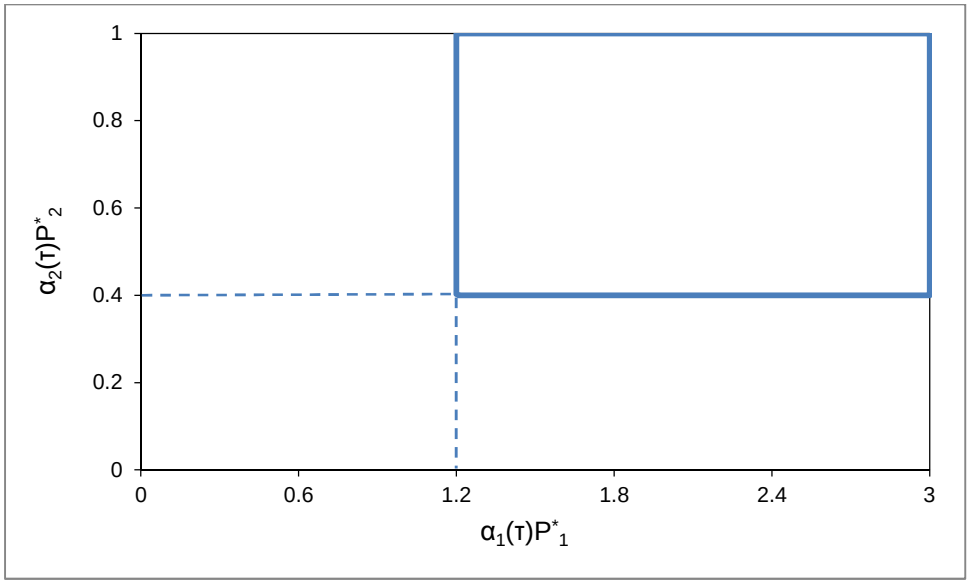

Figure 6.66 Loading domain of frame example

The amount of CPU time needed to solve this problem, on the same processor as above, was around 120s.

Author	Shakedown factor
Garcea *et al.* (2005)	3,925
Tran *et al.* (2010)	4,006
Pham (2011)	4,015
Present	**3,91**

Table 12. Comparison of numerical results of the frame

6.2.10.3. Symmetric continuous beam under distributed load

Let us consider the symmetric continuous beam of Fig.6.56. The beam is subjected to two uniform distributed loads $P_1(t)$ and $P_2(t)$, applied on each span. The geometry, the material as well as the mesh discretization of the beam are identical as previously (section 6.2.8).

Description of the loading domain

A general rectangular loading domain is considered (Fig.6.68) with the two loads varying independently, having the following amplitudes:

$P_1 \in [1.2,2]$

$P_2 \in [0,1]$

A prescribed loading in time domain that passes through the four vertices of the rectangular may be defined by using the following time functions $\alpha_1(\tau), \alpha_2(\tau)$ (Fig.6.67):

$$\alpha_1(\tau) = -6.4\tau^2 + 3.2\tau + 0.6, \quad \alpha_2(\tau) = 0, \quad \tau \in [0, 1/4]$$
$$\alpha_1(\tau) = 1, \quad \alpha_2(\tau) = -16\tau^2 + 16\tau - 3, \quad \tau \in (1/4, 1/2]$$
$$\alpha_1(\tau) = -6.4\tau^2 + 6.4\tau - 0.6, \quad \alpha_2(\tau) = 1, \quad \tau \in (1/2, 3/4]$$
$$\alpha_1(\tau) = 0.6, \quad \alpha_2(\tau) = -16\tau^2 + 24\tau - 8, \quad \tau \in (3/4, 1]$$

It is assumed that $P_1^* = 2$, $P_2^* = 1$ and $0.6 \le \alpha_1(\tau) \le 1, \quad 0 \le \alpha_2(\tau) \le 1$ (see Figs.6.67,6.68).

For this example the initial convergence parameter ω, in the process of the iterations, had to be halved three times, for the RSDM-S to converge to the final shakedown limit which is equal to **3.177.**

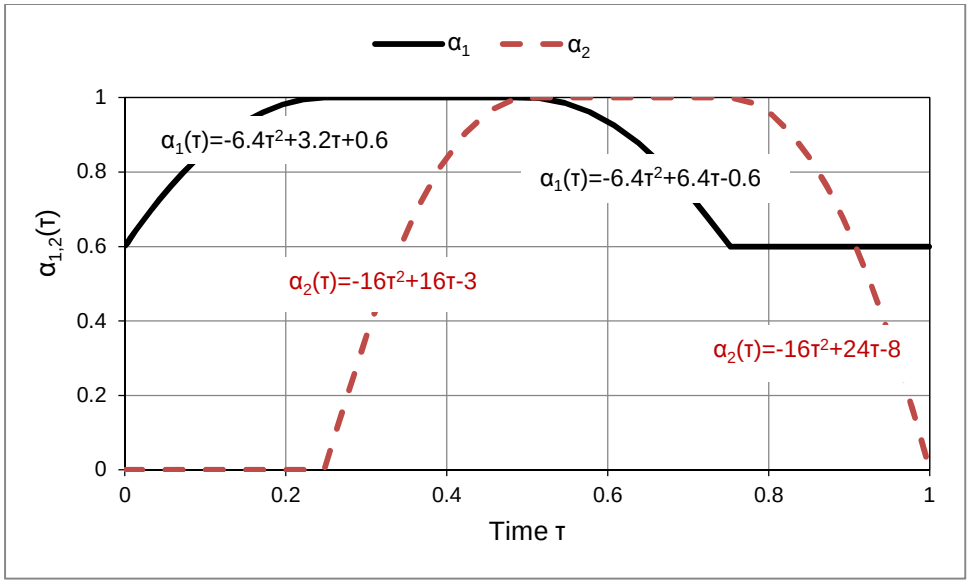

Figure 6.67 Time functions variation, over one period corresponding to the load domain of Fig.6.68

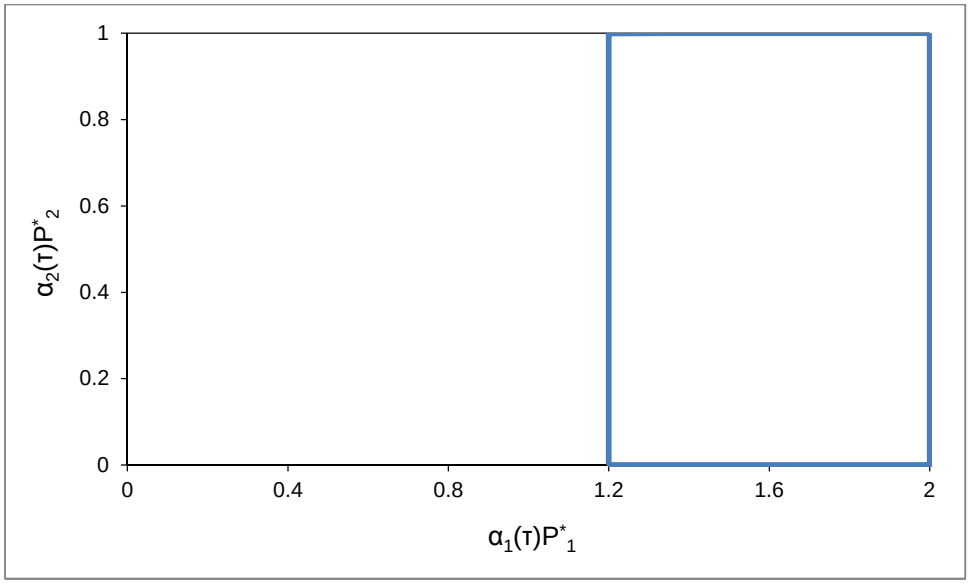

Figure 6.68 Loading domain of beam example

Less than 50 iterations were required for this problem to converge (Fig.6.69). The amount of CPU time needed to solve this problem, on the same processor as above, was around 300s.

The shakedown factor obtained by the RSDM-S, and its comparison with the results of different analysis methods, is shown in Table 13. It may be seen that there is a good agreement.

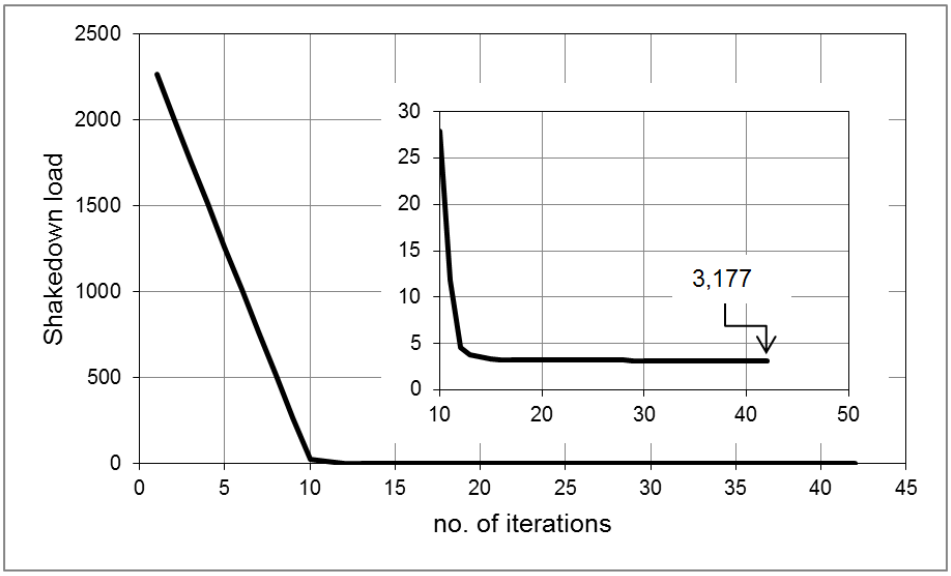

Figure 6.69 Convergence of the RSDM-S towards the shakedown factor for the continuous beam problem

Author	Shakedown limit
Garcea *et al.* (2005)	3,244
Tran *et al.* (2010)	3,377
Pham (2011)	3,264
Present	**3,177**

Table 13. Comparison of numerical results of the symmetric continuous beam

6.2.11. Three-dimensional loading space

Let us consider the holed square plate of the section 6.2.5. The plate is subjected herein (Fig.6.70), to a three-dimensional loading consisted of a) a thermal load, i.e a temperature difference $\Delta\theta(t)$ between the edge of the hole and the edge of the plate, b) a uniform distributed load $P_1(t)$ at the vertical edge of the plate and c) a uniform load $P_2(t)$ at the horizontal edge. The geometrical and material characteristics as well as the FE mesh discretization are the same with the ones of the example of sections 6.2.2 and 6.2.5. The variation of the temperature with radius r has the same logarithmic distribution as in the example of section 6.2.5:

$$\theta(r,\tau) = \theta_0 + \frac{\Delta\theta(\tau) * \ln\left(\frac{5\,D/2}{r}\right)}{\ln 5}$$

where $\theta_1(\tau) = \theta_0 + \Delta\theta(\tau)$ is the temperature around the edge of the hole $\left(r = D/2\right)$ and $\theta_1 = \theta_0$ at the outer edges of the plate $\left(r = 5D/2\right)$. The temperature θ_0 is chosen equal to zero. It should be noted that in the results σ_t denotes the maximum effective thermal elastic stress due to the fluctuating temperature.

Description of the loading domain

A three-dimensional load domain is assumed (Fig.6.71). The loads may vary independently in this domain having the following amplitudes:

$$P_1 \in \left[0, P_1^*\right]$$
$$P_2 \in \left[0, P_2^*\right]$$
$$\Delta\theta \in \left[0, \Delta\theta^*\right]$$

where the maximum values are $P_1^* = P_2^* = \Delta\theta^* = 1$.

A prescribed loading in the time domain that passes through the eight vertices of the load domain may be defined using the following equations (Fig.6.72):

$P(\tau) = \begin{Bmatrix} P_1^* \alpha_1(\tau) \\ P_2^* \alpha_2(\tau) \\ \Delta\theta^* \alpha_3(\tau) \end{Bmatrix}$ where the time functions $\alpha_1(\tau), \alpha_2(\tau), \alpha_3(\tau)$ are:

$$\alpha_1(\tau) = 0, \quad \alpha_2(\tau) = -16\tau^2 + 16\tau - 3, \quad \alpha_3(\tau) = 0, \quad \tau \in [0, 1/8]$$
$$\alpha_1(\tau) = 0, \quad \alpha_2(\tau) = 1, \quad \alpha_3(\tau) = -64\tau^2 + 32\tau - 3, \quad \tau \in (1/8, 2/8]$$
$$\alpha_1(\tau) = -64\tau^2 + 48\tau - 8, \quad \alpha_2(\tau) = 1, \quad \alpha_3(\tau) = 1, \quad \tau \in (2/8, 3/8]$$
$$\alpha_1(\tau) = 1, \quad \alpha_2(\tau) = 1, \quad \alpha_3(\tau) = -64\tau^2 + 48\tau - 8, \quad \tau \in (3/8, 4/8]$$
$$\alpha_1(\tau) = 1, \quad \alpha_2(\tau) = -64\tau^2 + 64\tau - 15, \quad \alpha_3(\tau) = 0, \quad \tau \in (4/8, 5/8]$$
$$\alpha_1(\tau) = 1, \quad \alpha_2(\tau) = 0, \quad \alpha_3(\tau) = -64\tau^2 + 96\tau - 35, \quad \tau \in (5/8, 6/8]$$
$$\alpha_1(\tau) = -64\tau^2 + 96\tau - 35, \quad \alpha_2(\tau) = 0, \quad \alpha_3(\tau) = 1, \quad \tau \in (6/8, 7/8]$$
$$\alpha_1(\tau) = 0, \quad \alpha_2(\tau) = 0, \quad \alpha_3(\tau) = -64\tau^2 + 112\tau - 48, \quad \tau \in (7/8, 1]$$

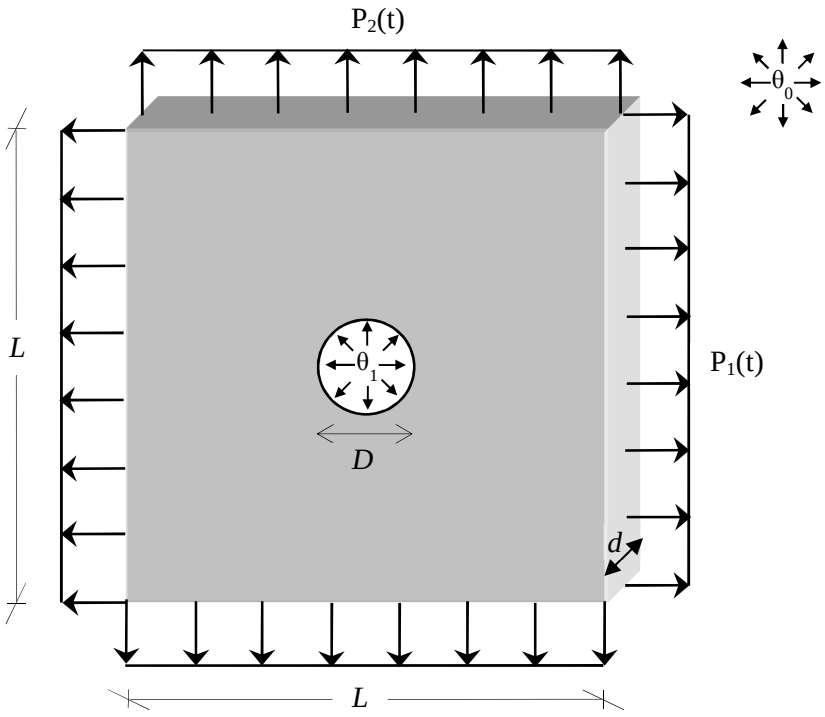

Figure 6.70 Geometry, and finite element discretization of the plate subjected to mechanical and thermal loading

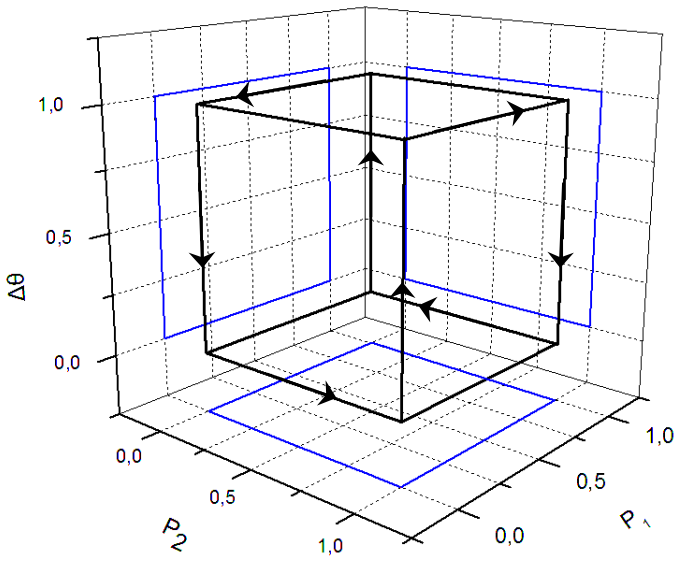

Figure 6.71 Three- dimensional load domain

In Table 14 one may see the resulted shakedown factor for some specific ratios of $P_1^* \,/\, P_2^* \,/\, \Delta\theta^*$. In Figs.6.73, 6.74 two-dimensional plots of the results obtained by RSDM-S, for different fixed ratios $P_1^* \,/\, P_2^*$, are presented.

Finally, the total 3D shakedown domain of the problem is shown in Fig.6.75. It should be mentioned that each solution for different fixed ratios $P_1^* \,/\, P_2^*$, represents a fixed angle φ in the $P_1 - P_2$-plane.

A good agreement with the results presented in (Simon and Weichert, 2012) was observed, even though a different algorithm (IPM) was used therein. For example for the case $P_1^* = P_2^* = \Delta\theta^* = 1$ the RSDM-S predicts a shakedown factor equal to **0.448** while the above authors predict a value equal to 0.426. In Table 14 the values in the parenthesis represents the results of (Simon and Weichert, 2012).

The CPU time needed for the RSDM-S to converge, for a typical case of $P_1^* = P_2^* = \Delta\theta^* = 1$, was about 50s on the same, as above, processor. A total number of 40 time points proved enough to describe the total 3D load domain. In Fig.6.76 one may see a typical convergence behavior of the RSDM-S i.e. for the fixed ratios $P_1^* \,/\, P_2^* \,/\, \Delta\theta^* = 1$. The initial value of $\omega = 1$ was sufficient for convergence.

An important observation is that both the CPU time and the total iterations were needed for the RSDM-S to converge in this case of a 3D loading domain, is of the same order with the one discussed in section 6.2.2 for a 2D case. On the contrary, Simon and Weichert (2012) mention that there is a significant increase of running time between the two cases, as the number of variables, for an IPM algorithm, in the three dimensional loading case is nearly twice the number in the two-dimensional case.

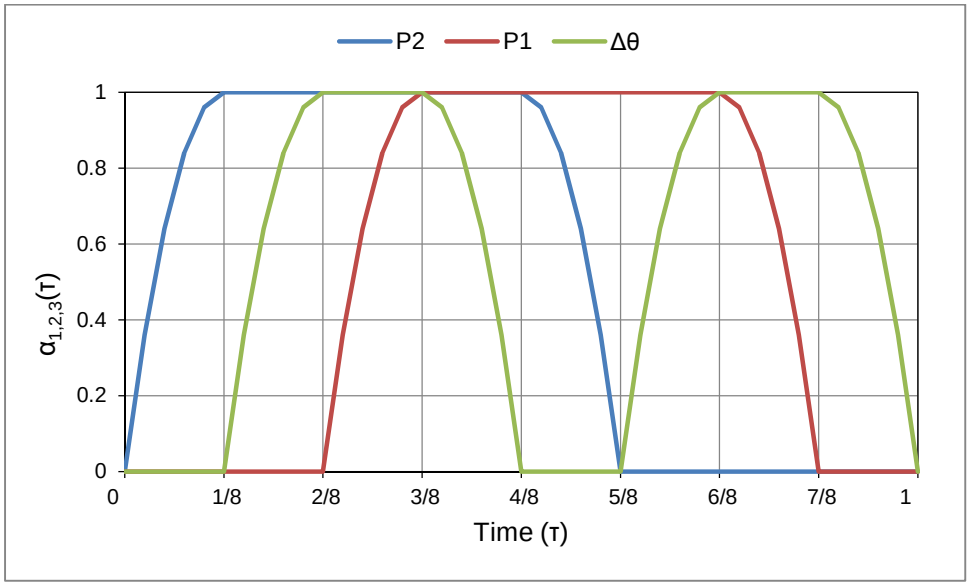

Figure 6.72 Time functions variation, over one period corresponding to the three- dimensional load domain of Fig.6.71

$(P_1^*,P_2^*,\Delta\theta^*)$	P_1/σ_Y	P_2/σ_Y	$\sigma_t/2\sigma_Y$
(1,0,0)	0,7 (0,619)	0	0
(0,1,0)	0	0,7 (0,611)	0
(0,0,1)	0	0	1,002
(1,1,0)	0,522 (0,454)	0,522 (0,454)	0
(1,0,1)	0,566 (0,568)	0	0,196
(1,1,1)	0,448 (0,426)	0,448 (0,426)	0,156
(1,0.5,1)	0,507 (0,489)	0,254 (0,244)	0,176

(1,0.5,0.5)	0,547 (0,508)	0,274 (0,254)	0,048
(1,1,0.5)	0,484 (0,44)	0,484 (0,44)	0,042
(0.5,0.5,1)	0,388 (0,402)	0,388 (0,402)	0,269
(0.5,1,0.5)	0,275 (0,254)	0,549 (0,508)	0,048

Table 14 Numerical results of shakedown analysis in three-dimensional loading space. Comparison with (Simon and Weichert, 2012)

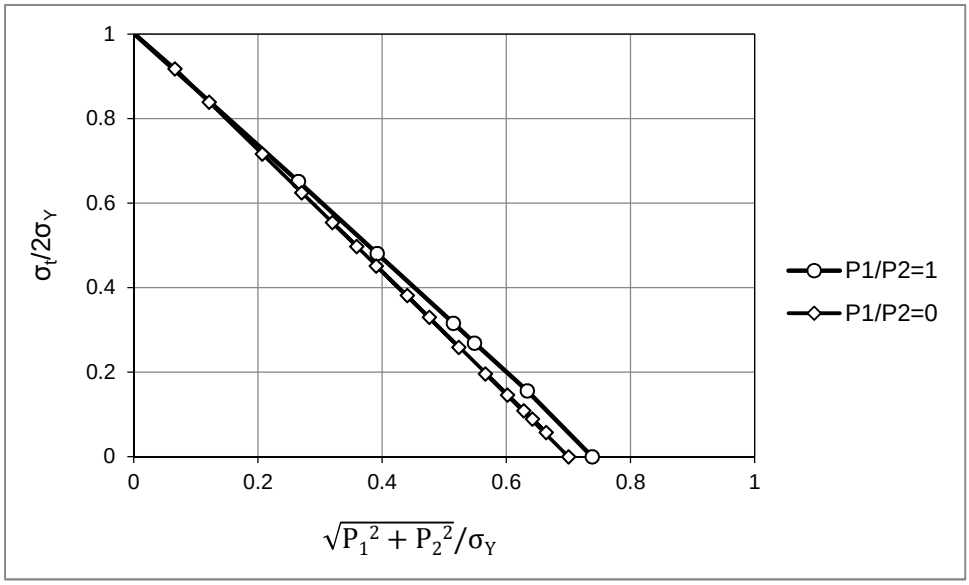

Figure 6.73 Shakedown domains in planes for fixed ratios (P_1^*/P_2^*)

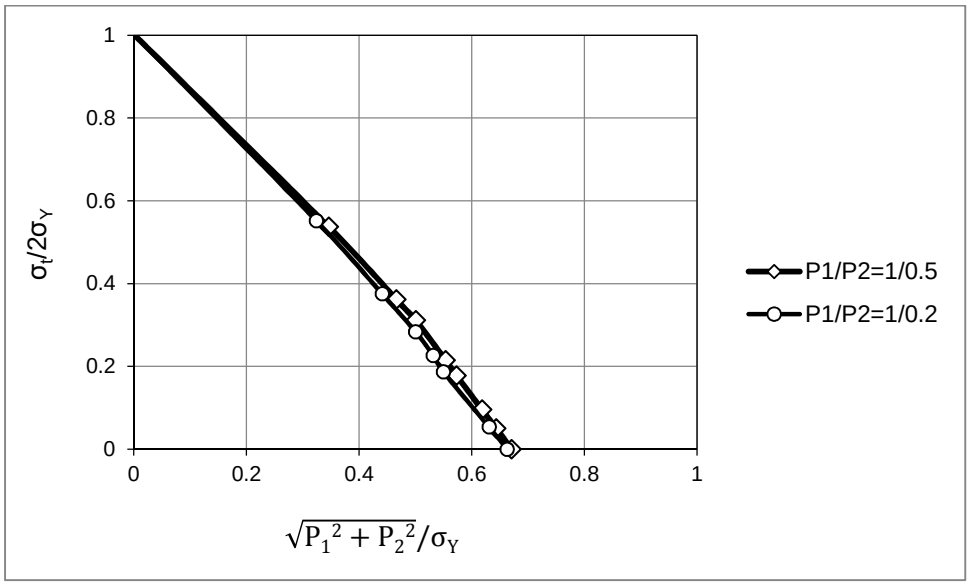

Figure 6.74 Shakedown domains in planes for fixed ratios (P_1^*/P_2^*)

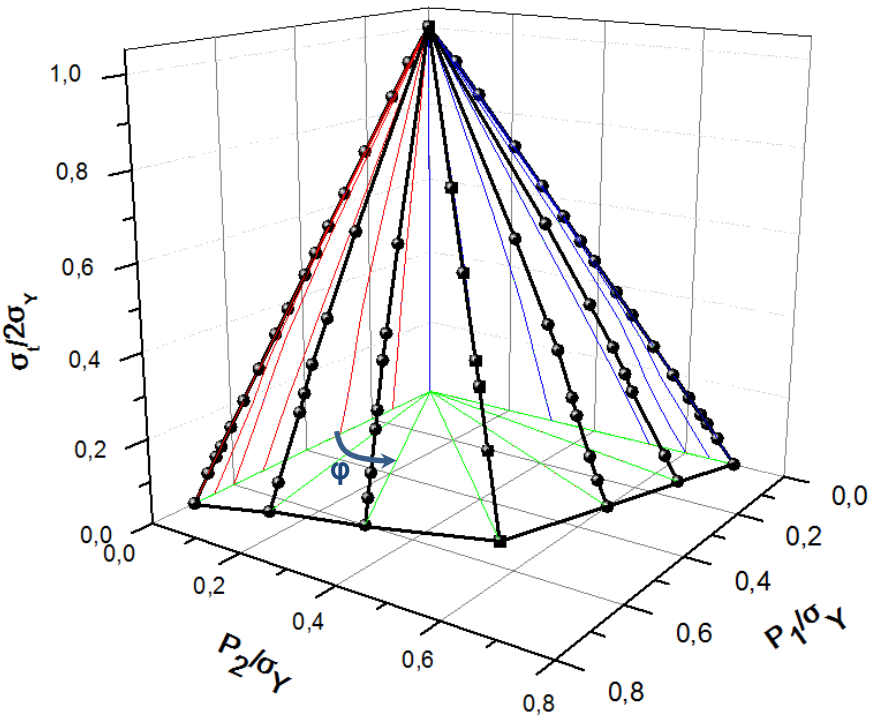

Figure 6.75 Shakedown domain in three-dimensional loading space

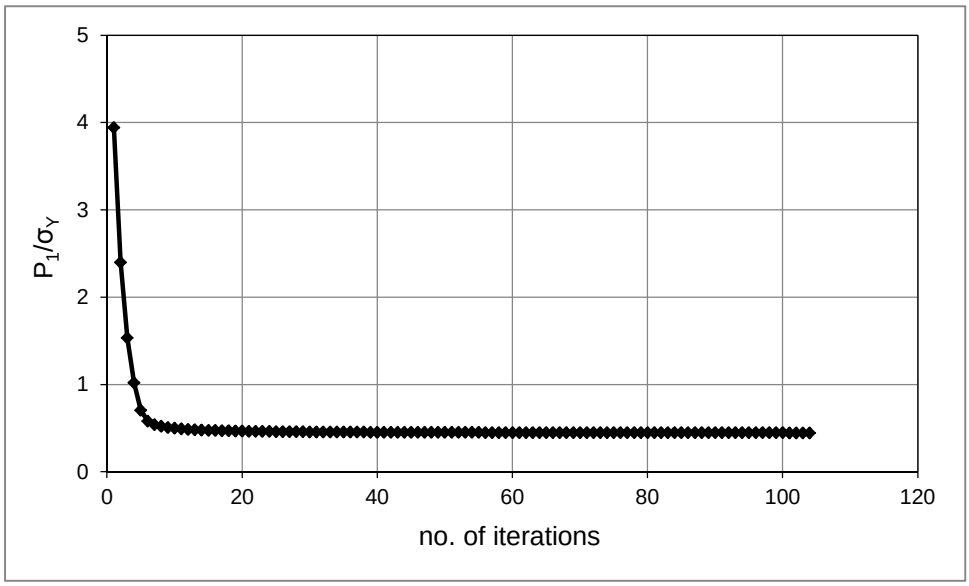

Figure 6.76 Convergence of the RSDM-S towards the shakedown factor for the three-dimensional loading case

6.2.12. Parametric studies

In this section a short description about the values of the parameters that were used in the developed procedure is presented. The examples of the plate of section 6.2.2 and the example of the symmetric continuous beam of Section 6.2.8 were chosen among others to study the influence of a) the number of the Fourier coefficients (NFC) and b) the number of time points (t.p.) that were necessary.

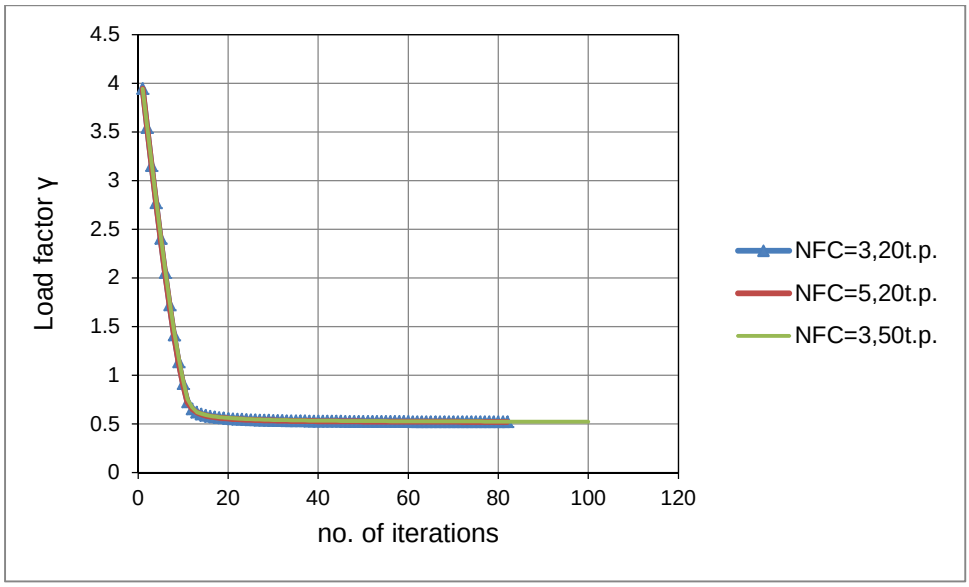

Figure 6.77 Convergence for different number of Fourier coefficients and time points (plate example of section 6.2.2)

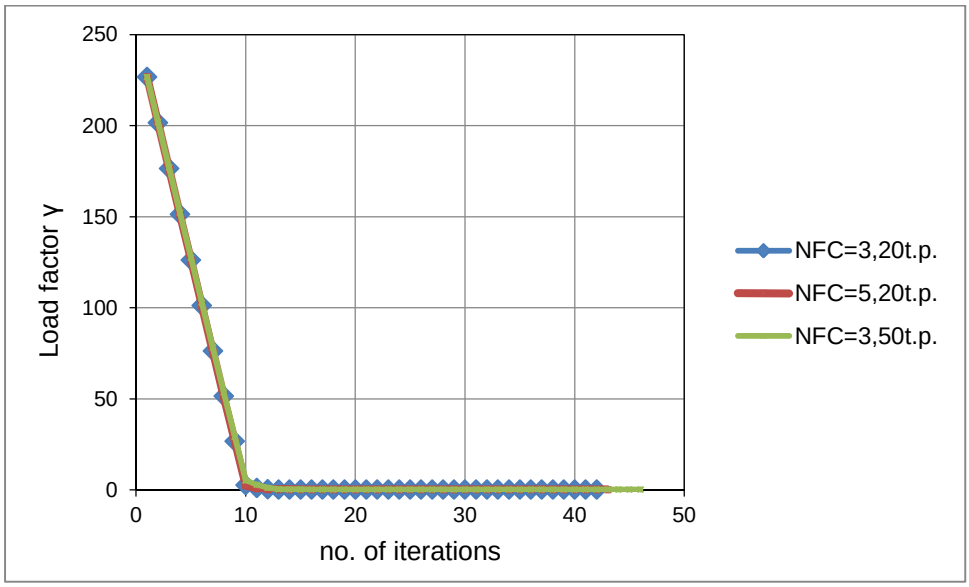

Figure 6.78 Convergence for different number of Fourier coefficients and time points (symmetric continuous beam example of section 6.2.8)

Judging from the numerical applications of the method, i.e., the convergence behavior as well as the computational time, one may say that it has proved to be very stable and efficient. A total number of 20 time points were proved enough for an accurate numerical integration of the residual stress rates. A big share to the efficiency of the method is the only three terms of the Fourier series that are needed to represent the residual stresses and the stiffness matrix which must be decomposed only once.

7.

Conclusions and future work

7.1. Conclusions

The first part of this work concerns the development of a numerical method, named RSDM, which predicts whether the continuous application of a given cyclic load would lead an elastoplastic structure either to safety or to low cycle fatigue or to excessive inelastic deformations, without having to perform cumbersome time-stepping calculations (Spiliopoulos and Panagiotou, 2012). The method can be classified as a Direct Method in the sense that it addresses, directly, the properties of the steady state cycle.

The basis of the method is the exploitation of the cyclic nature of the residual stress distribution in the steady cycle. Therefore, following its decomposition in Fourier series, the coefficients of these series are calculated in an iterative manner by satisfying equilibrium and compatibility. Plasticity effects may be easily implemented by a radial return on the yield surface along the total stress vector, which is the sum of the stresses obtained by a purely elastic solution and the residual stress. After convergence, if the applied loading is within the shakedown limit, the evaluated residual stress, constant in time inside the cycle, coincides with the actual residual stress. On the other hand, if the applied loading is above the shakedown boundary, the evaluated residual stress renders a steady state total stress, which is unsafe. The integral of the plastic straining over the cycle of loading, in the unsafe

regions, determines whether we have regions of alternating plasticity or ratcheting. In the latter case, the procedure predicts whether the structure itself will suffer incremental collapse. The whole procedure proved to be numerically stable and computationally efficient. This method assumes the complete knowledge of the loading history inside the cycle. Nevertheless, it seems to have the potential to provide also safety margins for any cyclic history in a given loading domain and further work has been done towards this direction.

Thus, the second major issue of this thesis concerns the shakedown analysis of structures. To this end, a new Direct Method to evaluate the shakedown factor of cyclically loaded elastoplastic structures has been developed. The method, which is in short called RSDM-S, is an iterative procedure and begins by converting the problem of loading margins to an equivalent loading of a prescribed time history multiplied by a load factor (Spiliopoulos and Panagiotou, 2014a, 2014b, 2015). Starting from a factor high above shakedown, at the end of each iteration a cyclic residual stress distribution is evaluated, through the RSDM, that is used to decrease this load factor. The procedure converges to the parameters of the limiting cycle, where the residual stresses become constant in time. The decomposition of the residual stresses into Fourier series proves to be well suited to represent mathematically, the procedure. The main advantage of the method is that the solution procedure provides a better understanding of the physics of the problem than any method based on MP algorithms. At the same time, the absence of such an algorithm makes it directly implementable into any existing FE software.

Both of the above procedures developed in this thesis are relatively simple methods, formulated within the FE method. The stiffness matrix of the structure needs to be formed and decomposed only once. Three terms of the Fourier series are enough for accurate results. These two factors guarantee the methods to be numerically efficient. The procedures were developed for an elastic-perfectly plastic material. It may be extended to account for different material behaviors (like hardening etc.). The methods may be implemented into any existing FE software.

7.2. Original contributions

The original contributions of this thesis may be synopsized in the following:

- a novel Direct Method (RSDM) has been developed to predict any steady state of cyclically loaded elastoplastic structures. This new method has a physical basis as it exploits the cyclic nature of the expected residual stress distribution at the steady state. The method is based on the decomposition of the residual stresses into Fourier series in time and any condition of shakedown, alternating plasticity or ratcheting may be realized (Spiliopoulos and Panagiotou, 2012, 2014c).
- a new Direct Method (RSDM-S) has been developed for the shakedown analysis of structures under any combination of cyclic thermomechanical loadings. The method is based on converting the problem of prescribed variations to a problem of prescribed time history and makes use of the RSDM method which assumes the decomposition of the residual stresses into Fourier series (Spiliopoulos and Panagiotou, 2014a, 2014b, 2015, Panagiotou and Spiliopoulos 2015).
- extension of the RSDM-S for the shakedown analysis of structures subjected to multidimensional loading space has been carried out.

7.3. Recommendations for future research

Following the research carried out in this thesis, the above extensions and future considerations that still remain open are proposed:

- Extension of the theoretical foundation of the RSDM & RSDM-S for limit states of cyclically loaded structures with different hardening laws.

The RSDM and RSDM-S have been currently developed and applied to structures made of elastic perfectly plastic material. However, many practical structures made of elastoplastic material exhibit hardening behavior. In order for the two methods to predict limit states like shakedown or ratcheting of such structures, the

implementation of various hardening laws like Prager's linear kinematic law and the Frederick Armstrong nonlinear kinematic hardening law could be attempted.

- A formulation of the method to examine the creep-fatigue behavior of structural components under cyclic thermos-mechanical loadings.

Based on the decomposition of the residual stress field at the cyclic state, a new direct numerical procedure for the estimation of creep fatigue life of structures, in the plastic range, under thermomechanical loadings could be constructed. An elastic-perfectly plastic behavior together with creep behavior could be assumed.

- A new approach for the evaluation of the ratchet limit of structures under cyclic thermomechanical loadings.

The RSDM-S has been currently developed in order to provide safety shakedown factors for cyclically loaded structures. Another major task in civil and mechanical structures under high levels of thermo-mechanical loadings is their response in excess of the shakedown region. Specifically the danger of occurrence or not of incremental collapse is highly important. To this direction a new direct method for the evaluation of the ratchet limit, in order to avoid incremental collapse mechanisms of cyclically loaded structures, may be developed. The new method could exploit the basic assumptions of the Residual Stress Decomposition Method.

7.4. List of publications

Part of the current work has been presented in the following publications:

a) Publications in referred international scientific journals

i) Spiliopoulos K.V., Panagiotou K.D., A direct method to predict cyclic steady states of elastoplastic structures. Comput. Methods Appl. Mech. Engrg. **223**, 186-198 (2012).

ii) Spiliopoulos K.V., Panagiotou K.D., A Residual Stress Decomposition Based Method for the Shakedown analysis of structures. Comput. Methods Appl. Mech. Engrg., **276**, 410-430 (2014a).

iii) Spiliopoulos K.V., K.D. Panagiotou K.D., A numerical procedure for the shakedown analysis of structures under thermomechanical loading. Arch. Appl. Mech., doi: 10.1007/s00419-014-0947-6 (2014b).

iv) Panagiotou K.D., Spiliopoulos K.V., Shakedown analysis of civil engineering structural elements. Engineering and Computational Mechanics, Proc. of the Institution of Civil Engineers, (accepted for publication) (2015).

b) Chapters in refereed books

i) Spiliopoulos K.V., Panagiotou K.D., The Residual Stress Decomposition Method (RSDM): A Novel Direct Method to Predict Cyclic Elastoplastic States. In: K. Spiliopoulos and D. Weichert (Eds.), Direct Methods for Limit States in Structures and Materials, Springer Science + Business Media, Dordrecht, 139-155 (2014c).

ii) Spiliopoulos K.V., Panagiotou K.D., RSDM-S: A Method for the Evaluation of the Shakedown Load of Elastoplastic Structures. In: P. Fuschi, A. Pisano and D. Weichert (Eds.), Direct Methods for Limit and Shakedown Analysis of Structures, Springer International Publishing, 159-175 (2015).

c) Publications in international scientific conferences and symposia

i) Spiliopoulos K.V., Panagiotou K.D., “A Direct Method for the Cyclic Elastoplastic Analysis of Simple Structures”, Proc. 3rd Intern. Conf. Nonlinear Dynamics, Kharkov, September 2010.

ii) Spiliopoulos K.V., Panagiotou K.D., “A Direct Method for the Cyclic Plasticity of Structures”, 4th Serbian-Greek Symposium on Recent Advances in Mechanics, Vlasina Lake, Serbia, 9 -10 September 2011.

iii) Spiliopoulos K.V., Panagiotou K.D., “A Computational Procedure for the Cyclic Steady State Elastoplastic Analysis of Structures”, Proc. COMPLAS XI, Barcelona, September 2011.

iv) Spiliopoulos K.V., Panagiotou K.V., “The Residual Stress Decomposition Method (RSDM): A Novel Direct Method to Predict Cyclic Elastoplastic States”, 3rd International Workshop on Direct Methods, Athens, 20-21 February 2012.

v) Spiliopoulos K.V., Panagiotou K.D., “A New Numerical Approach for the Evaluation of the Shakedown Load of Elastoplastic Structures”, 8th German-Greek-Polish Symposium on Recent Advances in Mechanics, Goslar, Germany, 9-13 September 2013.

vi) Spiliopoulos K.V., Panagiotou K.D., “A Computational Method for the Shakedown Analysis of Structures”, Euromech 548, Direct and Variational Methods for non smooth problems in Mechanics, Amboise, 2013.

vii) Spiliopoulos K.V., Panagiotou K.D., “Extension of the RSDM to the Shakedown Analysis of Structures”, 4th International Workshop on Direct Methods, Reggio di Calabria, Italy, 1-2 October 2013.

viii) Panagiotou K.D., Spiliopoulos K.V., “Shakedown analysis of structures under thermomechanical loading based on the RSDM”, WCCM-XI, Barcelona, 2014.

Appendix A

Fourier Series

A.1. Periodic functions

A function $f(x)$ is called *periodic* if there exists a constant T for which

$$f(x+T) = f(x) \tag{A1}$$

for any x in the domain of definition of $f(x)$. The constant T is called a period of the function $f(x)$ (Tolstov, 1962). The most common periodic functions are $\sin(x), \cos(x), \tan(x)$ etc. It is obvious that the sum, difference, product, or quotient of two functions of period T is again a function of period T. A typical graph of a periodic function may be seen in Fig.A.1.

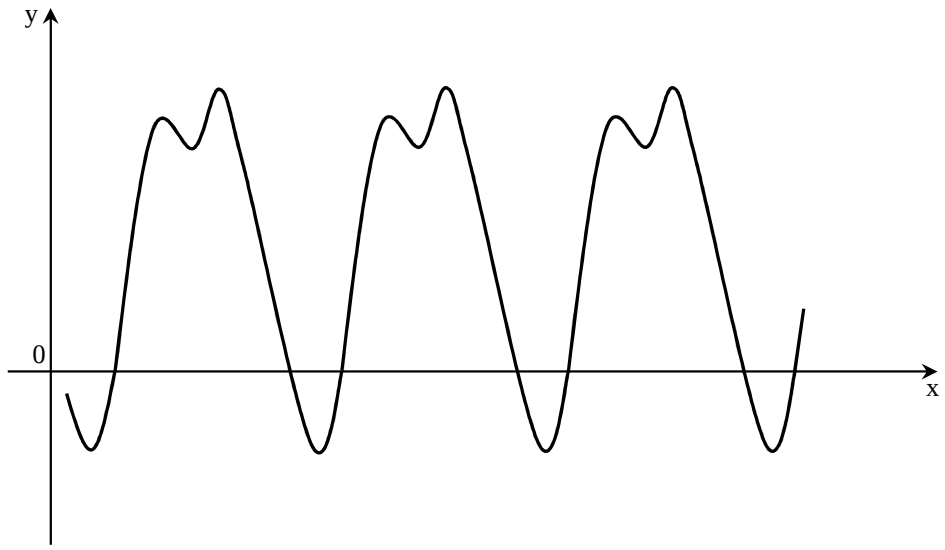

Figure A.1

If T is a period of the function $f(x)$, then the numbers $T, 2T, 3T...$ are also periods. This follows immediately from the series of equalities

$$f(x) = f(x+T) = f(x+2T) = f(x+3T) = ... = f(x+kT) \tag{A2}$$

where k is any positive integer.

If $f(x)$ is integrable on any interval of length T, then it is integrable on any other interval of the same length, and the value of the integral is the same i.e.,

$$\int_a^{a+T} f(x)dx = \int_b^{b+T} f(x)dx, \tag{A3}$$

for any a and b. This property is a consequence of the interpretation of an integral as an area (see Fig.A.2).

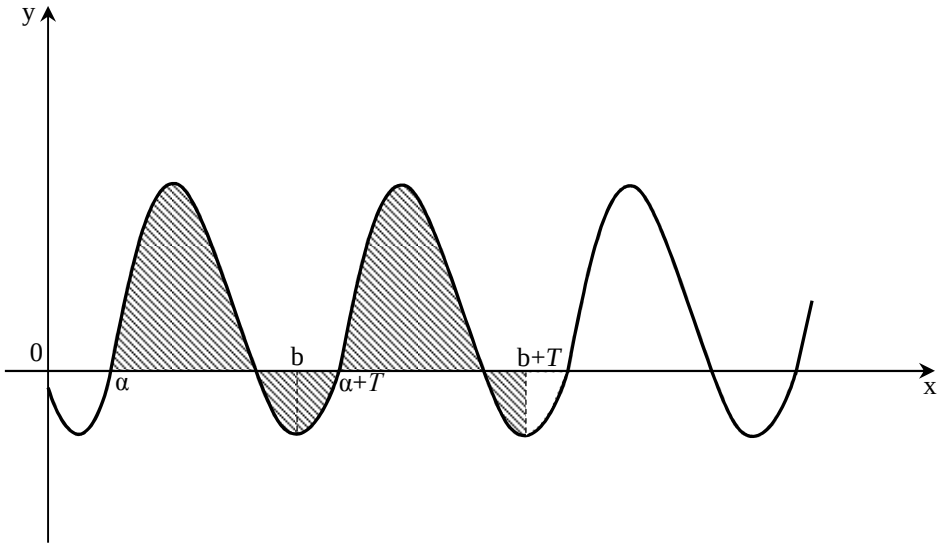

Figure A.2

A.2. Trigonometric polynomials and series

The simplest periodic function is

$$y = A\sin(\omega x + \varphi) \tag{A4}$$

This function is called harmonic of amplitude $|A|$ frequency ω and initial phase φ.

Using a well-known formula from trigonometry, we may write

$$A\sin(\omega x + \varphi) = A(\cos\omega x \sin\varphi + \sin\omega x \cos\varphi) \tag{A5}$$

Setting

$$a = A\sin\varphi, \quad b = A\cos\varphi \tag{A6}$$

every harmonic can be represented in the form

$$a\cos\omega x + b\sin\omega x \tag{A7}$$

If we introduce the period T and set $T = 2l$, then, since $T = 2\pi/\omega$, we may write eqn.A7 as

$$a\cos\frac{\pi x}{l} + b\sin\frac{\pi x}{l} \tag{A8}$$

Given the period $T = 2l$, let us consider the harmonics

$$a_k\cos\frac{\pi kx}{l} + b_k\sin\frac{\pi kx}{l} \qquad (k = 1,2,\ldots) \tag{A9}$$

with frequencies $\omega_k = \pi k/l$ and periods $T_k = 2\pi/\omega_k = 2l/k$. Since

$$T = 2l = kT_k \tag{A10}$$

the number $T = 2l$ is a period of all the harmonics (A9), for an integral multiple of a period is again a period. Therefore, every sum of the form

$$\rho_n(x) = A + \sum_{k=1}\left(a_k\cos\frac{\pi kx}{l} + b_k\sin\frac{\pi kx}{l}\right) \tag{A11}$$

where A is constant, is a function of period $2l$. The function $\rho_n(x)$ is called a *trigonometric polynomial of order* n.

A.3. The orthogonality of *sines* and *cosines*

Let us prove some auxiliary formulas

$$\begin{aligned}\int_{-\pi}^{\pi}\cos nx\,dx &= \left[\frac{\sin nx}{n}\right]_{-\pi}^{\pi} = 0,\\ \int_{-\pi}^{\pi}\sin nx\,dx &= \left[-\frac{\cos nx}{n}\right]_{-\pi}^{\pi} = 0,\end{aligned} \tag{A12}$$

and

$$\int_{-\pi}^{\pi} \cos^2 nxdx = \int_{-\pi}^{\pi} \frac{1+\cos 2nx}{2} dx = \pi,$$
$$\int_{-\pi}^{\pi} \sin^2 nxdx = \int_{-\pi}^{\pi} \frac{1-\cos 2nx}{2} dx = \pi. \tag{A13}$$

Using some basic trigonometric formulas we may write

$$\int_{-\pi}^{\pi} \cos nx \cos mxdx = \frac{1}{2}\int_{-\pi}^{\pi} \big[\cos(n+m)x + \cos(n-m)x\big]dx = 0,$$
$$\int_{-\pi}^{\pi} \sin nx \sin mxdx = \frac{1}{2}\int_{-\pi}^{\pi} \big[\cos(n-m)x - \cos(n+m)x\big]dx = 0 \tag{A14}$$

for any integers n and m $(n \neq m)$. Finally we may write that

$$\int_{-\pi}^{\pi} \sin nx \cos mxdx = \frac{1}{2}\int_{-\pi}^{\pi} \big[\sin(n+m)x + \sin(n-m)x\big]dx = 0 \tag{A15}$$

for any integers n and m. Equations A12, A14 and A15 show that the integral over the interval $\big[-\pi,\pi\big]$ of the product of any two different functions of the system (A12) vanishes.

We call that two functions $\varphi(x)$ and $\psi(x)$ are *orthogonal* on the interval $\big[a,b\big]$ if

$$\int_{a}^{b} \varphi(x)\psi(x)dx = 0 \tag{A16}$$

Thus the functions of the system (A12) are pairwise *orthogonal* on the interval $\big[-\pi,\pi\big]$. As we already mentioned, the integral of a periodic function is the same over any interval whose length equals the period. Thus, eqns.A12 to A15 are valid for any interval $\big[a,a+2\pi\big]$ (Tolstov, 1962).

A.4. Fourier series for functions of period 2π

Suppose the function $f(x)$ of period 2π has the following expansion

$$f(x) = \frac{a_0}{2} + \sum_{k=1}^{\infty} \left(a_k \cos kx + b_k \sin kx \right) \tag{A17}$$

where we denote the constant term by $a_0/2$. Let us now pose the problem of determining the coefficients a_0, a_k and b_k $(k = 1,2,...)$ from a knowledge of $f(x)$.

By integrating from $-\pi$ to π, we obtain

$$\int_{-\pi}^{\pi} f(x)dx = \frac{a_0}{2} \int_{-\pi}^{\pi} dx + \sum_{k=1}^{\infty} \left(a_k \int_{-\pi}^{\pi} \cos kx dx + b_k \int_{-\pi}^{\pi} \sin kx dx \right) \tag{A18}$$

According to eqn.A12 all the integrals in the sum vanish. Thus

$$a_0 = \frac{\int_{-\pi}^{\pi} f(x)dx}{\pi} \tag{A19}$$

If we multiply both sides of eqn.A18 by $\cos nx$ and integrate the result form π to $-\pi$, as before, we get

$$\int_{-\pi}^{\pi} f(x) \cos nx dx = \frac{a_0}{2} \int_{-\pi}^{\pi} \cos nx dx + \sum_{k=1}^{\infty} \left(a_k \int_{-\pi}^{\pi} \cos kx \cos nx dx + b_k \int_{-\pi}^{\pi} \sin kx \cos nx dx \right) \tag{A20}$$

By eqn.A12, the first integral on the r.h.s vanishes. Since the trigonometric functions of (A20) are orthogonal, all the integrals in the sum vanish, except one. The only integral remains is the coefficient of a_n:

$$\int_{-\pi}^{\pi} \cos^2 nx dx = \pi \tag{A21}$$

(see eqn.A13). Thus we get

$$\int_{-\pi}^{\pi} f(x) \cos nx dx = a_n \pi \tag{A22}$$

Similarly, we find that

$$\int_{-\pi}^{\pi} f(x)\sin nxdx = b_n\pi \tag{A23}$$

It follows from (A22) and (A23) that

$$\begin{aligned} a_n &= \frac{1}{\pi}\int_{-\pi}^{\pi} f(x)\cos nxdx \qquad (n = 0,1,2,...) \\ b_n &= \frac{1}{\pi}\int_{-\pi}^{\pi} f(x)\sin nxdx \qquad (n = 0,1,2,...) \end{aligned} \tag{A24}$$

The coefficients a_n and b_n calculated by the formulas A24 are called the *Fourier coefficients* of the function $f(x)$, and the trigonometric series with these coefficients is called the *Fourier series* of $f(x)$ (Tolstov, 1962).

The interval of integration $\left[-\pi,\pi\right]$ can be replaced by any other interval of length 2π and we have

$$\begin{aligned} a_n &= \frac{1}{\pi}\int_{a}^{a+2\pi} f(x)\cos nxdx \qquad (n = 0,1,2,...) \\ b_n &= \frac{1}{\pi}\int_{a}^{a+2\pi} f(x)\sin nxdx \qquad (n = 0,1,2,...) \end{aligned} \tag{A25}$$

Appendix B

Global convergence theorem of descent algorithms

The global convergence theorem (Luenberger and Yu, 2008) is used to establish convergence for the following general situation. Suppose there is a solution set Γ. Points are generated by the algorithm $\mathbf{x}_{k+1} \in \mathbf{A}(\mathbf{x}_k)$, and each new point always strictly decreases a descent function Z unless the solution set Γ is reached. Then, under appropriate conditions, it follows that the sequence converges to the solution set.

Global Convergence Theorem. *Let A be an algorithm on X, and suppose that, given $\mathbf{x}_0$ the sequence $\{\mathbf{x}_k\}_{k=0}^{\infty}$ is generated satisfying*

$$\mathbf{x}_{k+1} \in \mathbf{A}(\mathbf{x}_k).$$

Let a solution set $\Gamma \subset X$ be given, and suppose

a) all points $\mathbf{x}_k$ are contained in a compact set $R \subset X$

b) there is a continuous function Z on X such that

- *if $x \notin \Gamma$, then $Z(\mathbf{y}) < Z(\mathbf{x})$ for all $\mathbf{y} \in \mathbf{A}(\mathbf{x})$,*
- *if $x \in \Gamma$, then $Z(\mathbf{y}) \leq Z(\mathbf{x})$ for all $\mathbf{y} \in \mathbf{A}(\mathbf{x})$*

c) the mapping $\mathbf{A}$ is closed at points outside Γ.

Then the limit of any convergent subsequence of $\mathbf{x}_k$ is a solution.

Bibliography

Abaqus 6.10, Theory and user's manual, Dassault Systèmes (2010).

Akoa F., Hachemi A., An L., Mouhtamid S., Tao P., Application of lower bound direct method to engineering structures. J. Glob. Optim., **37**, 609–630 (2007).

Andersen E., Jensen B., Jensen J., Sandvik R., Worsøe U., MOSEK version 6. Technical Report TR-2009-3. MOSEK (2009).

Andersen E., Roos C., Terlaky T., On implementing a primal–dual interior-point method for conic quadratic optimization. Math. Program., **95**, 249–277 (2003).

Ardito R., Cocchetti G., Maier G., On structural safety assessment by load factor maximization in piecewise linear plasticity. Eur. J. Mech. A/Solids, **27**, 859–881 (2008).

Atkociunas J., Merkeviciute D., Venskus A., Optimal shakedown design of bar systems: strength, stiffness and stability constraints. Comput. Struct., **86**, 1757–1768 (2008).

Atkociunas J., Venskus A., Optimal shakedown design of frames under stability conditions according to standards. Comput. Struct., **89**, 435-443 (2011).

Barrera O., Ponter A.R.S., Cocks A.C.F., Extension of the Linear Matching Method to frame structures made from a material that exhibits softening. Eur. J. Mech. A\Solids, **30**, 783–793 (2011).

Belouchrani M.A., Weichert D., An extension of the static shakedown theorem to inelastic cracked structures. Int. J. Mech. Sci., **41**, 163–177 (1998).

Belytschko T., Plane stress shakedown analysis by finite elements. Int. J. Mech. Sci., **14**, 619–625 (1972).

Bisbos C.D, Ampatzis A.T., Shakedown analysis of spatial frames with parametrized load domain. Eng. Struct., **30**, 3119–3128 (2008).

Bisbos C.D., Makrodimopoulos A., Pardalos P., Second-order cone programming approaches to static shakedown analysis in steel plasticity. Optim. Meth. Soft., **20**, 25–52 (2005).

Bleich H., Über die Bemessung statisch unbestimmter Stahltragwerke unter Berücksichtigung des elastisch-plastischen Verhaltens des Baustoffes. Der Bauingenieur, **13**, 261–267 (1932).

Bodovillé G., de Saxcé G., Plasticity with nonlinear kinematic hardening: Modelling and shakedown analysis by the bipotential approach. Eur. J. Mech. A/Solids, **20**, 99–112 (2001).

Bouby C., de Saxcé G., Tritsch J.B., A comparison between analytical calculations of the shakedown load by the bipotential approach and step-by-step computations for elastoplastic materials with nonlinear kinematic hardening. Int. J. Solids Struct., **43**, 2670–2692 (2006).

Boulbibane M., Collins I.F., Ponter A.R.S. Weichert D., A Shakedown of Unbound Pavements. Road Materials and Pavement Design, **6**, 81–96 (2005).

Boulbibane M., Ponter A.R.S., A method for the evaluation of design limits for structural materials in a cyclic state of creep. European Journal of Mechanics, A/Solids, **21**, 899–914 (2003).

Boulbibane M., Ponter A.R.S., Extension of the linear matching method applicability to geotechnical problems. Comp. Meth. Appl. Mech. Eng., **194**, 4633–4650 (2005a).

Boulbibane M., Ponter A.R.S., Limit loads for multilayered half-space using the linear matching method. Computers and Geotechnics, **32**, 535–544 (2005b).

Boulbibane M., Weichert D., Application of shakedown theory to soils with nonassociated flow rules. Mech. Res. Comm., **24**, 513–519 (1997).

Bousshine L., Chaaba A., de Saxcé G., A new approach of shakedown analysis for non-standard elastoplastic materials by the bipotential theory. Euromech 385 Colloquium (1998).

Bousshine L., Chaaba A., de Saxcé G., A new approach to shakedown analysis for non-standard elastoplastic material by the bipotential. Int J. Plast., **19**, 583–598 (2003).

Bree J., Elastic-plastic behaviour of thin tubes subjected to internal pressure and intermittent high-heat fluxes with application to fast-nuclear-reactor fuel elements. J. Strain Anal., **2**, 226-238 (1967).

Bridgman P.W., Proc. Am. Acad. Arts Sci. 58, 163 (1923).

Bridgman P.W., Studies in large plastic flow and fracture. McGraw-Hill, New York (1952).

Carvelli V., Cen Z., Liu Y., Maier G., Shakedown analysis of defective pressure vessels by a kinematic approach. Arch. Appl. Mech., **69**, 751–764 (1999).

Casciaro R., Garcea G., Erratum to “An iterative method for shakedown analysis”. Comput. Methods Appl. Mech. Engrg., **191**, 5761–5792 (2002).

Ceradini G., Sull’sadattamento dei corpi elastoplastici soggetti ad azioni dinamiche. Giornale del Genio Civile, **415**, 239–258 (1969).

Ceradini G., Dynamic shakedown in elastic–plastic bodies. J. Eng. Mech. Div. Proc. ASCE, **106**, 481–499 (1980).

Chen H.F., Engelhardt M., Ponter A.R.S., Linear matching methods for creep rupture assessment. Int. J. Pressure Vessel and Piping, **80**, 213–220 (2003).

Chen H.F., Ponter A.R.S., Shakedown and limit analyses for 3-D structures using the linear matching method. Int. J. Press. Vess. and Piping, **78**, 443–451 (2001a).

Chen H. F, Ponter A.R.S., A method for the evaluation of a ratchet limit and the amplitude of plastic strain for bodies subjected to cyclic loading. Eur. J. Mech. A/Solids, **20**, 555–572 (2001b).

Chen H.F., Ponter A.R.S., A simplified creep-reverse plasticity solution method for bodies subjected to cyclic loading. European Journal of Mechanics, A/Solids, **81**, 651–577 (2004).

Chen H.F., Ponter A.R.S., Integrity assessment for a tubeplate using the linear matching method. International Journal of Pressure Vessel Technology, **81**, 327–336 (2004).

Chen H.F., Ponter A.R.S., Linear Matching Method on the evaluation of plastic and creep behaviours for bodies subjected to cyclic thermal and mechanical loading. Int. J. Num. Meth. Engng., **68**, 13–32 (2006).

Chen H.F., Ponter A.R.S., A Direct Method on the Evaluation of Ratchet Limit. Journal of Pressure Vessel Technology, **132**, (4), 041202 (8 pages) (2010).

Chen H.F., Ure J., Tipping D., Calculation of a lower bound ratchet limit part 1 – Theory, numerical implementation and verification. European Journal of Mechanics - A/Solids, **37**, 361–368 (2013).

Chen M., Zhang L.L., Weichert D., Tang W.C., Shakedown and limit analysis of periodic composites. Proc. Appl. Math. Mech., **9**, 415–416 (2009).

Christiansen E., Andersen K., Computation of collapse states with von Mises type yield condition. Int. J. Numer. Method Eng., **46**, 1185–1202 (1999).

Cocchetti G., Maier G., Elastic-plastic and limit-state analyses of frames with softening plastic-hinge models by mathematical programming. Int. J. Solids and Structures, **89**, 435-443 (2003).

Cohn M.Z., Maier G. (eds). Engineering Plasticity by Mathematical Programming. Proceedings of NATO Advanced Study Institute: Pergamon Press, New York (1977).

Collins I.F., Boulbibane M., The application of shakedown theory to pavement design. Metals and Materials, **4**, 832-837 (1998).

Comi C., Corigliano A., Dynamic shakedown in elastoplastic structures with general internal variable constitutive laws. Int. J. Plasticity, **7**, 679–692 (1991).

Cook R.D., Malkus D.S., Plesha M.E., Witt R.J., Concepts and applications of finite element analysis. J. Wiley & Sons (2002).

Corigliano A., Maier G., Pycko S., Dynamic shakedown analysis and bounds for elastoplastic structures with nonassociative, internal variable constitutive laws. Int. J. Sol. Struct., **32**, 3145–3166 (1995).

Corradi L., Maier G., Inadaptation theorems in the dynamics of elastic-work hardening structures. Ingenieur-Archiv, **43**, 44–57 (1973).

Corradi L., Maier G., Dynamic non-shakedown theorem for elastic perfectly-plastic continua. J. Mech. Phys. Sol., **22**, 401–413 (1974).

Corradi L., Zavelani A., A linear programming approach to shakedown analysis of structures. Comput. Methods Appl. Mech. Engrg., **3**, 37–53 (1974).

De Saxcè G., Bousshine L., Limit analysis theorems for implicit standard materials: application to the unilateral contact with dry friction and the nonassociated flow rules in soils and rocks. Int. J. Mech. Sci., **40**, 387–398 (1998).

De Souza Neto E.A., Peric D., Owen D.R.J, Computational methods for plasticity: Theory and applications. J. Wiley, (1996).

Dontato O. de, Second shakedown theorem allowing for cycles of both loads and temperature. 1st Lombardo Scienza Lettere (A), **104**, 265–277, (1970).

Drucker D.C., A definition of stable material. ASME J. Appl. Mech., **26**, 101-106 (1959).

Feng X.Q., Gross D., A global/local shakedown analysis method of elastoplastic cracked structures. Eng. Fract. Mech., **63**,179–192 (1999).

Frederick C.O., Armstrong P.J., Convergent internal stresses and steady cyclic states of stress. J. Strain Anal., Nr2 (1966).

Fuschi P., Structural shakedown for elastic–plastic materials with hardening saturation surface. Int. J. Solid Struct., **36**, 219–240 (1999).

Garcea G., Armentano G., Petrolo S., Casciaro R., Finite element shakedown analysis of two-dimensional structures. Int. J. Numer. Meth. Engng, **63**, 1174–1202 (2005).

Garcea G., Leonetti L., A unified mathematical programming formulation of strain driven and interior point algorithms for shakedown and limit analysis. Int. J. Numer. Meth. Engng., **88**, 1085–1111 (2011).

Giambanco G., Fuschi P., Rizzo S., Shakedown optimum design of reinforced concrete framed structures. Engineering Optimization, **23**, 141-154 (1994).

Gokhfeld D.A, Some problems of shakedown of plates and shells (in Russian), Proceed. VI-th Soviet Conf. Plates and Shells, Nauka, Moscow, 284–291 (1966).

Gokhfeld D.A, Cherniavsky O.F., Limit analysis of structures at thermal cycling. Sijthoff & Noordhoff (1980).

Gross-Weege J., A unified formulation of statical shakedown criteria for geometrically nonlinear problems. Int. J. Plasticity, **6**, 433–447 (1990).

Gross-Weege J., On the numerical assessment of the safety factor of elastic-plastic structures under variable loading, Int. J. Mech. Sc., **39**, 417–433 (1997).

Grüning M., Die Statik des ebenen Tragwerks. Springer, Berlin (1925).

Grüning M., Die Tragfähigkeit statisch unbestimmter Tragwerke aus Stahl bei beliebig häufig wiederholter Belastung. Springer, Berlin (1926).

Gvozdev A., Determination of the value of the collapse load for statically indeterminate systems undergoing plastic deformation. Proc. of the Conference on Plastic deformation. Izd. AN SSSR (1936).

Habibullah M.S., Ponter A.R.S., The Application of the Linear Matching Methods to Structural Problems with Cracks. Proc. 5th World Congress for Computational Mechanics, Springer-Verlag, (2004).

Habibullah M.S., Ponter A.R.S., Ratchetting Limits for Cracked Bodies subjected to cyclic loads and temperature. Engineering Fracture Mechanics, **72**, 1702–1716 (2005).

Hachemi A., Hamadouche M.A., Weichert D., Some nonclassical formulations of shakedown problems, in: Staat M., Heitzer M. (Eds.), Numerical Methods for limit and shakedown analysis, NIC Series, **15**, 57–84 (2003).

Hachemi A., Mouhtamid S., Nguyen A., Weichert D., Application of shakedown analysis to large-scale problems with selective algorithm, in: Weichert, D., Ponter, A. (Eds.), Limit States of Materials and Structures. Springer, 289– 305 (2009).

Hachemi A., Weichert D., An extension of the static shakedown theorem to a certain class of inelastic materials with damage. Arch. Mech., **44**, 491–498 (1992).

Hachemi A., Weichert D., Application of shakedown theory to damaging inelastic material under mechanical and thermal loads. Int. J. Mech. Sci., **39**, 1067–1076 (1997).

Hachemi A., Weichert D., Numerical shakedown analysis of damaged structures. Comp. Meth. Appl. Mech. Eng., **160**, 57–70 (1998).

Halphen B., Nguyen Q.S., Sur les materiaux standards gènèralizes (On generalized standard materials). J. Mèc., **14**, 39–63 (1975).

Heitzer M., Traglast- und Einspielanalyse zur Bewertung der Sicherheit passive Komponenten. Berichte des Forschungszentrums Jülich, Jül–3704 (1999).

Heitzer M., Pop G., Staat M., Basis reduction for the shakedown problem for bounded kinematic hardening material. J. Glob. Opt., **17**, 185–200 (2000).

Henky H., Z. angew. Math. Phys. **4**, 323 (1924).

Huang Y., Stein E., Shakedown of a cracked body consisting of kinematic hardening material. Eng. Fract. Mech., **54**, 107–112 (1996).

Isaakson E., Keller H.B., Analysis of numerical methods. J. Wiley (1966).

Ju J.W., On energy-based coupled elastoplastic damage theories: constitutive modeling and computational aspects. Int. J. Solids Struct., **25**, 803–833 (1989).

Koiter W.T., A new general theorem on shakedown of elastic-plastic structures. Proc. K. Ned. Ak. Wet. B59, 24–34 (1956).

Koiter W.T., General theorems for elastic-plastic structures, in: Sneddon I.N., Hill R. (Eds.), Progess in Solid Mechanics, North-Holland Publ. Co., Amsterdam, 165–221 (1960).

König J. A., Shakedown of elastic-plastic structures. Amsterdam, Elsevier (1987).

König J.A., Kleiber M., On a new method of shakedown analysis. Bull. Acad. Polon. Sci. Ser. Sci. Tech. **26**, 165-171 (1978).

König J.A., Maier G., Shakedown analysis of elastoplastic structures: a review of recent developments. Nucl. Eng. Des., **66**, 81–95 (1981).

König J.A., Siemaszko A., Strainhardening effects in shakedown processes. Ingenieur-Archiv, **58**, 58–66 (1988).

Krabbenhøft K., Lyamin A., Sloan S., Formulation and solution of some plasticity problems as conic programs. Int. J. Solid Struct., **44**, 1533–1549 (2007a).

Krabbenhøft K., Lyamin A., Sloan S., Shakedown of a cohesive-frictional half-space subjected to rolling and sliding contact. Int. J. Solid Struct., **44**, 3998-4008 (2007b).

Krabbenhøft K., Lyamin A., Sloan S., Wriggers P., An interior-point algorithm for elastoplasticity. Int. J. Numer. Method Eng., **69**, 592–626 (2007c).

Le C.V., Nguyen-Xuan H., Askes H., Bordas S., Rabczuk T., Nguyen-Vinh H., A cell-based smoothed finite element method for kinematic limit analysis. Int. J. Numer. Methods Eng., **83**, 1651–1674 (2010).

Lemaitre J.A., Chaboche L. (eds.), 1985, Mècanique des matèriaux solides. Dunod, Paris (1985).

Liu Y.H, Zhang X.F, Cen Z.Z., Lower bound shakedown analysis by the symmetric Galerkin boundary element method. Int. J. Plast, **21**, 21–42 (2005).

Long V.L., Nguyen D.H., Limit and shakedown analysis of 3-D steel frames. Engineering and Structures, **30**, 1895-1904 (2008).

Lubliner J., Plasticity theory. MacMilan publisher, New York (1990).

Luenberger D.G., Ye Y., Linear and nonlinear programming. New York, Springer, (2008).

Lyamin A., Sloan S., Lower bound limit analysis using nonlinear programing. Int. J. Numer. Meth. Engng., **55**, 573–611 (2002).

Mackenzie D., Boyle J.T., A method of estimating limit loads by iterative elastic analysis. I – Simple examples. Int. J. Press. Vess. and Piping, **53**, 77–95 (1993).

Mackenzie D., Boyle J.T., Hamilton R., The elastic compensation method for limit and shakedown analysis: a review. J. Strain Analysis., 35, 171–188 (2000).

Mackenzie D., Shi J., Boyle J.T., Finite element modelling for limit analysis by the elastic compensation method. Comp. Struct., **51**, 403–410 (1994).

Maier G., Shakedown theory in perfect elastoplasticity with associated and nonassociated flow-laws: a finite element, linear programming approach. Meccanica, **4**, 1–11, (1969).

Maier G., A matrix structural theory of piecewise-linear plasticity with interacting yield planes. Meccanica, **7**, 51–66 (1970).

Maier G., Shakedown of plastic structures with unstable parts. Proc. ASCE, J. Eng. Mech. Div., **98**, 1322–1327 (1972).

Maier G., A shakedown matrix theory allowing for workhardening and second order geometric effects. In: ‘‘Foundations of Plasticity,’’ ed. A. Sawczuk, Noordoff, Leyden, 1, 417–433 (1973a).

Maier G., Upper bounds on deformations of elastic-workhardening structures in the presence of dynamic and second-order geometric effects. J. Struct. Mech., **2**, 265–280 (1973b).

Maier G., Carvelli V., etti G., On direct methods for shakedown and limit analysis. Eur. J. Mech. A/Solids (Special issue), **19**, S79–S100 (2000).

Maier G., Novati G., Dynamic shakedown and bounding theory for a class of nonlinear hardening discrete structural models. Int. J. Plasticity, **6**, 551–572 (1990).

Maier G., Pastor J., Ponter A.R.S., Weichert D., Direct methods of limit and shakedown analysis, in: de Borst R., Mang H.A. (Eds.), Comprehensive structural integrity – fracture of materials from nano to macro. Numerical and computational methods. Elsevier, Amsterdam, 3, 637–684 (2003).

Maitournam M.H., Pommier B., Thomas J., Determination of the asymptotic response of a structure under cyclic thermomechanical loading. Comptes Rendus Mecanique, **330**, 703–708 (2002).

Makrodimopoulos A., Computational formulation of shakedown analysis as a conic quadratic optimization problem. Mech. Res. Commun., **33**, 72–83 (2006).

Makrodimopoulos A., Bisbos C.D. Shakedown analysis of plane stress problems via SOCP, in: Staat M. and Heitzer M. (Eds.), Numerical Methods for Limit and Shakedown Analysis. Publication Series of the John von Neumann Institute for Computing (NIC), Germany, 185-216 (2003).

Malena M., Casciaro, R., Finite element shakedown analysis of reinforced concrete 3D frames. Comput. Struct., **86**, 1176-1188 (2008).

Mandel J., Adaptation d'une structure plastique ècrouissable et approximations. Mech. Res. Comm., **3**, 483–488 (1976).

Martin J.B., Plasticity. MIT Press, USA, 1975.

Melan E., Theorie unbestimmter Systeme aus idealplastischem Baustoff. Sitzungsberichte, Akademie der Wissenschaften 145, 195–218 (1936).

Melan E., Der Spannungszustand eines Mises-Hencky'schen Kontinuums bei veränderlicher Belastung. Sitzungsberichte. Akademie der Wissenschaften, Wien, 147, 73–87 (1938a).

Melan E., Zur plastizität des raümlichen Kontinuums. Ingenieur Archiv, **9**, 116-126 (1938b).

Mises R. v., Göttinger Nachr. Math.-Phys. Kl. 582 (1913).

Morelle P., Structural shakedown analysis by dual finite-element formulations. Eng. Struct., **6**, 70–79 (1984).

Munoz J., Bonet J., Huerta A., Peraire J., Upper and lower bounds in limit analysis: adaptive meshing strategies and discontinuous loading. Int. J. Numer. Method Eng., **77**, 471–501 (2009).

Neal B.G., Plastic-Collapse and Shake-Down Theorems for Structures of Strain Hardening Material. J. Aero. Sci., **17**, 297–307 (1950).

Neal B.G., Symonds P.S., A Method for Calculating the Failure Load for a Framed Structure Subjected to Fluctuating Loads. J. Inst. Civil Engrs., **35**, 186 (1951).

Nesterov Y., Nemirovskii A., Interior-Point Polynomial Algorithms in Convex Programming. SIAM, Philadelphia (1994).

Ngo N.S., Tin-Loi F., Shakedown analysis using the p-adaptive finite element method and linear programming. Eng. Struct., **29**, 46–56 (2007).

Owen D.R.J., Hinton E., Finite elements in plasticity: Theory and practice. Pineridge Press Limited, Swansea U.K. (1980).

Panagiotou K.D., Spiliopoulos K.V., Shakedown analysis of civil engineering structural elements. Engineering and Computational Mechanics, Proc. of the Institution of Civil Engineers, (accepted for publication) (2015).

Pastor F., Loute E., Solving limit analysis problems: an interior-point method. Commun. Numer. Meth. Engrg., **21**, 631–642 (2005).

Pastor F., Thoré P., Loute E., Pastor J., Trillat M., Convex optimization and limit analysis: application to Gurson and porous Drucker–Prager materials. Eng. Fract. Mech., **75**, 1367–1383 (2008).

Pham D., Shakedown theory for elastic plastic kinematic hardening bodies. Int. J. Plast., **23**, 1240–1259 (2007).

Pham D., On shakedown theory for elastic–plastic materials and extensions. J. Mech. Phys. Solid, **56**, 1905–1915 (2008).

Pham P.T., Upper bound limit and shakedown analysis of elastic-plastic bounded linearly kinematic hardening structure. PhD thesis, RWTH University, Aachen (2011).

Pham P.T., Vu D., Tran T., Staat M., An upper bound algorithm for shakedown analysis of elastic–plastic bounded linearly kinematic hardening bodies. In: Proc ECCM 2010.

Pham D., Weichert D., Shakedown analysis for elastic–plastic bodies with limited kinematical hardening. Proc. R. Soc. Lond. A 457, 1097–1110 (2001).

Polizzotto C., A convergent bounding principle for a class of elasto-plastic strain-hardening solids. Int. J. Plast., **2**, 359–370 (1986).

Polizzotto C., Shakedown analysis for a class of strengthening materials within the framework of gradient plasticity. Int. J. Plast., **26**, 1050–1069 (2010).

Polizzotto C., Borino G., Shakedown and steady state responses of elastic–plastic solids in large displacements. Int. J. Sol. Struct., **33**, 3415–3437 (1996).

Polizzotto C., Borino G., Caddemi S., Fuschi P., Theorems of restricted dynamic shakedown. Int. J. Mech. Sci., **35**, 787–801 (1993).

Polizzotto C., Borino G., Farinello F., Shakedown analysis by elastic simulation, in: Weichert D., Maier G. (Eds.), Inelastic Analysis of structures under variable loads. Kluwer Academic Publishers, Dodrecht, 335–364 (2000).

Polizzotto C., Borino G., Fuschi P., An extended shakedown theory for elastic–plastic-damage material models. Euro. J. Mech. A/Solids, **15**, 825–858 (1996).

Ponter A.R.S., General displacement and work bounds for dynamically loaded bodies. J. Mech. Phy. Solids, **23**, 151–163 (1975a).

Ponter A.R.S., A general shakedown theorem for inelastic materials. Proc. SMiRT-3, London, paper L5/2 (1975b).

Ponter A.R.S., A minimum theorem for the cyclic behavior of creeping bodies. Meccanica, **36**, 37–47 (2001).

Ponter A.R.S, A linear matching method for shakedown analysis, in: Weichert D., Ponter A.R.S. (Eds.), Inelastic behavior of structures under variable repeated loads – Direct analysis methods, CISM, Springer, 267–318 (2002).

Ponter A.R.S., Boulbibane M., Minimum theorems and the linear matching method for bodies in a cyclic state of creep. European Journal of Mechanics, A/Solids, **21**, 915–925 (2003).

Ponter A.R.S., Carter K.F., Limit state solutions, based upon linear elastic solutions with a spatially varying elastic modulus. Comput. Methods Appl. Mech Engng. **140**, 237–258 (1997a).

Ponter A.R.S., Carter K.F., Shakedown state simulation techniques based on linear elastic solutions. Comput. Methods Appl. Mech Engng. **140**, 259–279 (1997b).

Ponter A.R.S., Chen H.F., A minimum theorem for cyclic loading in excess of shakedown, with applications to the evaluation of a ratchet limit. Eur. J. Mech. A/Solids, **20**, 539–554 (2001).

Ponter A.R.S., Chen H.F., Ciavarella M., Specchia G., Shakedown analyses for rolling and sliding contact problems. Int. J. Solids and Structures, **43**, 4201–4219 (2006).

Ponter A.R.S., Engelhardt M., Shakedown limits for a general yield condition: implementation and application for a von Mises yield condition. Eur. J. Mech. A/Solids **19**, 423–445 (2000).

Ponter A.R.S., Fuschi P., Engelhardt M., Limit analysis for a general class of yield conditions. Eur. J. Mech. A/Solids **19**, 401–421 (2000).

Prager W., Problem Types in the Theory of Perfectly Plastic Materials. Journal of the Aeronautical Sciences, **15**, 337–341 (1948).

Prager W., Shakedown in elastic-plastic media subjected to cycles of load and temperature, Proc. Symp. Plasticita nella Scienza delle Construzioni, Bologna, 239–244 (1956).

Pycko S., König J.A., Steady plastic cycles on reference configuration in the resence of secondorder geometric effects. Eur. J. Mech. A/Solids, **10**, 563–574 (1991).

Pycko S., Maier G., Shakedown theorems for some classes of nonassociative hardening elastic–plastic material models. Int. J. Plast., **11**, 367–395 (1995).

Rozenblum V.I., On shakedown analysis of nonuniformly heated elastic-plastic bodies. Izw. Akad. Nauk SSR, No 7, 136–138 (1957).

Rozenblum V.I., On shakedown analysis of nonuniformly heated elastic-plastic bodies. PMTF, Russia, No 5, 98–101 (1965).

Sawczuk A., On incremental collapse of shells under cyclic loading. IUTAM Symp. Theory of Thin Shells, Copenhagen 1967, Springer, Berlin, 328–340(1969).

Shen W., Traglast- und Anpassungsanalyse von Konstructionen aus elastisch, ideal plastischem Material. PhD. thesis, Universität Stuttgart (1986).

Siemaszko A., König J.A., Analysis of stability of incremental collapse of skeletal structures. J. Struct. Mech., **13**, 301–321 (1985).

Simon J.W, Direct evaluation of the limit states of engineering structures exhibited limited, nonlinear kinematical hardening. Int. J. Plast., **42**, 141–167, (2013).

Simon J.W., Kreimeier M., Weichert D., A selective strategy for shakedown analysis of engineering structures. Int. J. Numer. Meth. Engrg., **94**, 985–1014 (2013).

Simon J.W., Weichert D., Numerical lower bound shakedown analysis of engineering structures. Comp. Methods Appl. Mech. Engrg., **200**, 2828–2839 (2011).

Simon J.W., Weichert D., Shakedown analysis with multidimensional loading spaces. Comput. Mech., **49**, 477–485 (2012).

Skordeli M., Shakedown analysis of metal structures, subjected to ellipsoidal variable repeated loading via robust optimization techniques. PhD thesis, AUTH, Thessaloniki (2010).

Skordeli M., Bisbos C.D, Limit and shakedown analysis of 3D steel frames via approximate ellipsoidal yield surfaces. Eng. Struct., **32**, 1556–1567 (2010).

Spiliopoulos K.V., A simplified method to predict the steady cyclic stress state of creeping structures. ASME J. Applied Mechanics, **69**, 149–153 (2002).

Spiliopoulos K.V., Panagiotou K.D., A direct method to predict cyclic steady states of elastoplastic structures. Comp. Methods Appl. Mech. Engrg., **223**, 186-198 (2012).

Spiliopoulos K.V., Panagiotou K.D., A residual stress decomposition based method for the Shakedown Analysis of Structures. Comp. Methods Appl. Mech. Engrg., **276**, 410-430 (2014a).

Spiliopoulos K.V., Panagiotou K.D., A Numerical Procedure for the Shakedown Analysis of Structures Under Thermomechanical Loading. Arch. Appl. Mech., doi: 10.1007/s00419-014-0947-6 (2014b).

Spiliopoulos K.V., Panagiotou K.D., The Residual Stress Decomposition Method (RSDM): A Novel Direct Method to Predict Cyclic Elastoplastic States. In: K. Spiliopoulos and D. Weichert (Eds.), Direct Methods for Limit States in Structures and Materials, Springer Science + Business Media, Dordrecht, 139-155 (2014c).

Spiliopoulos K.V., Panagiotou K.D., RSDM-S: A Method for the Evaluation of the Shakedown Load of Elastoplastic Structures. In: P. Fuschi, A. Pisano and D. Weichert (Eds.), Direct Methods for Limit and Shakedown Analysis of Structures, Springer International Publishing, 159-175 (2015).

Staat M., Heitzer M., Limit and shakedown analysis for plastic safety of complex structures. Transactions of SMiRT 14, B02/2 (1997).

Stein E., Zhang G., Huang Y., Modeling and computation of shakedown problems for nonlinear hardening materials. Comput. Meth. Appl. Mech. Eng., **103**, 247–272 (1993).

Stein E., Zhang G., König J.A., Shakedown with nonlinear strain-hardening including structural computation using finite element method. Int. J. Plast., **8**, 1–31 (1992).

Stumpf H., Schieck B., Shakedown at finite elasto-plastic strains, in: Weichert D., Maier G. (Eds.), Inelastic Analysis of Structures under Variable Loads. Kluwer Academic Publishers, 31–47 (2000).

Symonds P.S., Basic Theorems in the Plastic Theory of Structures. J. Aero. Sci. **17**, 669–670 (1950).

Symonds P.S., Shakedown in Continuous Media. J. Appl. Mech. **17**, 85–89 (1951).

Symonds P.S., Neal B.G., Recent progress in the plastic methods of structural analysis. J. Franklin Inst. 252(6), 469–492 (1951a)

Symonds P.S., Neal B.G., The Calculation of Failure Loads on Plane Frames under Arbitrary Loading Programs. J. Inst. Civil Engrs. **35**, 41–61 (1951b)

Symonds P.S., Prager W.: Elastic-plastic analysis of structures subjected to loads varying arbitrarily between prescribed limits. J. Appl. Mech. **17**, 315–324 (1950).

Tolstov G.P., Fourier series. Dover, New York (1962).

Tran T.N., A dual algorithm for shakedown analysis of plate bending. Int. J. Numer. Meth. Eng., **86**, 862-875 (2011).

Tran T.N., R. Kreißig R., Staat M., Probabilistic limit and shakedown analysis of thin plates and shells. Structural Safety, **31**, 1-18 (2009).

Tran T.N., R. Kreißig R., Vu D.K., Staat M., Upper bound limit and shakedown analysis of shells using the exact Ilyushin yield surface. Comput. Struct., **86**, 1683–1695 (2008).

Tran T.N., Liu G.R., Nguyen-Xuan H., Nguyen-Thoi T., An edge-based smoothed finite element method for primal-dual shakedown analysis of structures. Int. J. Numer. Meth. Engrg., **82**, 917–938 (2010).

Ure J., Chen H.F., Tipping D., Calculation of a lower bound ratchet limit part 2 – Application to a pipe intersection with dissimilar material join. European Journal of Mechanics - A/Solids, **37**, 369–378 (2013).

Vanderbei R. J., Linear programming: Foundations and extensions, International Series in Operations Research & Management Science, 4th ed., Springer (2014).

Vu D., Staat M., Analysis of pressure equipment by application of the primal–dual theory of shakedown. Commun. Numer. Method Eng., **23**, 213–225 (2007).

Vu D., Yan A., Nguyen-Dang H., A dual form for discretized kinematic formulation in shakedown analysis. Int. J. Solid Struct., **41**, 267–277 (2004).

Weichert D., Shakedown at finite displacements; note on Melan's theorem. Mech. Res. Comm., **11**, 121–127 (1984).

Weichert D., On the influence of geometrical nonlinearities on the shakedown of elastic–plastic structures. Int. J. Plasticity, **2**, 135–148 (1986).

Weichert D., Gross-Weege J., The numerical assessment of elastic–plastic sheets under variable mechanical and thermal loads using a simplified two-surface yield condition. Int. J. Mech. Sci., **30**, 757–767 (1988).

Weichert D., Hachemi A., Schwabe F., Application of shakedown analysis in the plastic design of composites. Arch. Appl. Mech., **69**, 623–633 (1999).

Weichert D., Ponter A.R.S., A historical view on shakedown theory, in: Stein E. (Eds.), The history of theoretical, material and computational mechanics – Mathematics meets mechanics and engineering. Springer, 169–193 (2014).

Zarka J., Direct analysis of elastic–plastic structures with overlay materials during cyclic loading. International Journal for Numerical Methods in Engineering, **15**, 225–235 (1980).

Zarka J., Casier J., Elastic plastic response of a structure to cyclic loading, practical rules. In Mechanics Today, vol. 6, Nemat S (Eds.), Pergamon Press, Oxford (1981).

Zarka J., Frelat J., Inglebert G., Kasmai-Navidi P., A new approach in inelastic analysis of structures. CADLM, Laboratoire de Mécanique des Solides de l'Ecole Polytechnique, France (1990).

Zhang G., Einspielen und dessen numerische Behandlung von Flächentragwerken aus ideal plastischem bzw. kinematisch verfestigendem Material. Phd. thesis, Universität Hannover (1991).

Zhang T., Raad L., An eigen-mode method in kinematic shakedown analysis. Int. J. Plasticity, **18**, 71–90 (2002).

Zouain N., Borges L., Silveira J.L., An algorithm for shakedown analysis with nonlinear yield function. Comp. Methods Appl. Mech. Engrg., **191**, 2463–2481 (2002).